A STUDY ON NON-PERTURBATIVE AND OUT-OF-EQUILIBRIUM ASPECTS OF THE QUARK-GLUON PLASMA

By

MANAS DEBNATH

PHYS11202104013

National Institute of Science Education and Research, Bhubaneswar

A thesis submitted to the

Board of Studies in Physical Sciences

In partial fulfillment of requirements

For the Degree of

DOCTOR OF PHILOSOPHY

of

HOMI BHABHA NATIONAL INSTITUTE

June, 2026

Homi Bhabha National Institute

Recommendations of the Viva Voce Committee

As members of the Viva Voce Committee, we certify that we have read the dissertation prepared by **Manas Debnath** entitled **"A study on Non-perturbative and Out-of-equilibrium Aspects of the Quark-gluon plasma"** and recommend that it maybe accepted as fulfilling the thesis requirement for the award of Degree of Doctor of Philosophy.

______________________________ Date: 10/6/2026

Chairman - Professor Bedangadas Mohanty

______________________________ Date: 10.06.2026

Guide / Convener - Dr. Najmul Haque

______________________________ Date: 10/06/2026

Examiner - Prof. Vinod Chandra

______________________________ Date:

Member 1 - Dr. Amaresh Kumar Jaiswal 10/06/2026

______________________________ Date:

Member 2 - Dr. Victor Roy

______________________________ Date: 10.06.2026

Member 3 - Dr. Sandeep Chatterjee 10.06.2026

____

Final approval and acceptance of this thesis is contingent upon the candidate's submission of the final copies of the thesis to HBNI.

I/We hereby certify that I/we have read this thesis prepared under my/our direction and recommend that it may be accepted as fulfilling the thesis requirement.

Date: 10.06.2026

Place: Jatni, NISER

Guide: ______________________________

STATEMENT BY AUTHOR

This dissertation has been submitted in partial fulfillment of requirements for an advanced degree at Homi Bhabha National Institute (HBNI) and is deposited in the Library to be made available to borrowers under rules of the HBNI.

Brief quotations from this dissertation are allowable without special permission, provided that accurate acknowledgment of source is made. Requests for permission for extended quotation from or reproduction of this manuscript in whole or in part may be granted by the Competent Authority of HBNI when in his or her judgment the proposed use of the material is in the interests of scholarship. In all other instances, however, permission must be obtained from the author.

Manas Debnath

Manas Debnath
10/06/2026

DECLARATION

I hereby declare that the investigation presented in the thesis has been carried out by me. The work is original and has not been submitted earlier as a whole or in part for a degree / diploma at this or any other Institution / University.

Manas Debnath

Manas Debnath
10/06/2026

Dedication

I dedicate the thesis to my family for unconditional support and love in every moment.

Manas Debnath
10/06/2026

CERTIFICATION ON ACADEMIC INTEGRITY

Undertaking by the Student:

1. I, **Manas Debnath**, HBNI Enrolment No. **PHYS11202104013**, hereby undertake that the thesis titled "**A study on Non-perturbative and Out-of-equilibrium Aspects of the Quark-gluon plasma**" is prepared by me and is the original work undertaken by me.

2. I also hereby undertake that this document has been duly checked through a plagiarism detection tool and is found to be plagiarism-free as per the guidelines of the Institute/UGC.

3. I am aware and undertake that if plagiarism is detected in my thesis at any stage in the future, suitable penalty will be imposed as applicable according to the guidelines of the Institute/UGC.

Signature of the Student with date

Manas Debnath, 10.06.2026

Endorsed by the Thesis Supervisor:

I certify that the thesis written by the Researcher is plagiarism-free as stated above by the student.

Signature of the Thesis Supervisor with date Haque, 10.06.2026

Name:	Dr. Najmul Haque
Designation:	Associate Professor
Department/Centre:	School of Physical Sciences
Name of the CI/OCC:	National Institute of Science Education and Research, Bhubaneswar

LIST OF PUBLICATIONS

Publications included in the thesis

Journal:

1. **The complex heavy quarkonium potential with the Gribov–Zwanziger action**

   Manas Debnath, Ritesh Ghosh, Najmul Haque, ***Eur. Phys. J.C* 84** (2024) 313, [arXiv:2305.16250 [hep-ph]].

2. **Energy loss of a fast moving parton in Gribov-Zwanziger plasma**

   Manas Debnath, Ritesh Ghosh, Mohammad Yousuf Jamal, Manu Kurian, Jai Prakash, ***Phys. Rev. D* 109** (2024) 1, L011503, [arXiv:2311.16005 [hep-ph]].

3. **Shear and bulk viscosity for a pure glue theory using an effective matrix model**

   Manas Debnath, Ritesh Ghosh, Najmul Haque, Yoshimasa Hidaka, Robert D. Pisarski, ***Phys. Rev. D* 112** (2025) 1, 014040, [arXiv: 2504.20138 [hep-ph]].

4. **Complex Heavy Quarkonium Potential in an Anisotropic Collisional Quark-Gluon Plasma**

   Manas Debnath, Lata Thakur, Najmul Haque, [arXiv:2504.02802 [hep-ph]].

Conference papers:

1. **Shear viscosity for a pure glue theory using an effective matrix model**

   Manas Debnath, Ritesh Ghosh, Najmul Haque, Yoshimasa Hidaka,

   Robert D. Pisarski, ***J.Subatomic Part.Cosmol.*** **4** (2025), 100129.

Manas Debnath

Manas Debnath

10/06/2026

ACKNOWLEDGMENTS

First and foremost, I would like to express my deepest gratitude to my Guru, Najmul sir, for his unwavering guidance, invaluable advice, and constant motivation. His mentorship and relentless push for excellence have shaped not only this thesis but also my growth as a researcher. Whenever, I almost have given up during my phd tenure, I wonder how this man always comes with unique direction to proceed further, which made me realize one simple but elegant motto of life - there is always a way, I just have to give enough effort. I also thank my distinguished collaborators Rob, Yoshimasa, Ritesh da, Manu, Jai, Yousuf and Lata di. I feel really fortunate to meet these really brilliant people throughout my PhD tenure. A special thanks to Rob for taking the time to teach us about matrix model himself. I acknowledge my doctoral committee members - Prof. Bedangadas Mohanty, Dr. Amaresh Kumar Jaiswal, Dr. Victor Roy, Dr. Sandeep Chatterjee and Prof. Hiranmaya Mishra - for their invaluable guidance and constructive feedback, which significantly shaped and strengthened my PhD work. After Najmul sir, the person I consider my co-guide, my mentor - is Ritesh da. Sometime I feel I should apologize for calling him frequently at middle of night or at very early in the morning for doubts. He was my chatgpt in my phd tenure, even before chatgpt was a thing. I wonder, how could I finish my phd if he wasn't there- from helping me writing papers, correcting my calculations, motivating me to do independent calculations even when he had already done it way before me, helping me in-front of senior and eminent scientists, like I could not finish counting. He was like my elder brother here at NISER. Arghya da is the person who first inspired me in my research field. During the early days of my PhD, when I had little understanding of the subject and felt completely lost, the papers I was asked to study seemed almost incomprehensible. At that crucial moment, Arghya da entered my life and provided the much-needed bird's-eye view of the field. His explanations and perspective helped me connect the dots and understand the broader structure of the problems I would eventually work on. I acknowledge Pracheta di for all the physics discussions to having tea in the evening to smashing opponents on the badminton court, her presence transformed her from a senior into an elder sister. I also wish to thank Samapan da for his help during my early years at NISER especially for guiding me in preparing presentations, sitting through long mock-talk sessions, and helping me overcome my fear of speaking on stage.

I am grateful to the NISER community as a whole for providing an environment where I could walk freely even in the middle of the night without any concern, and for amenities such as the night canteen, which faithfully catered to my midnight cravings. I acknowledge DAE, HBNI and NISER for funding me for five years during my phd tenure. I also acknowledge ANRF for funding my conference travel.

I want to thank Sadaf, my immediate senior, for many helps. From him, I was able to navigate do's and dont's during presentations. I want to thank friends, without whom I would not survive this long five years at NISER. The quarantine days during my first year at NISER, was blessings in disguise for me, otherwise I would wonder how I could find all these amazing people. When life felt hopeless, I am indebted to the late night banters with Sourav, Soham, Sagnik, Amit, Debopam. I will miss our 'club-house' in Amit's and Sagnik's room where I would go to chill and listening to Sagnik, Amit and Debopam's adventurous travel stories and taking our frustrations out load. I will miss the badminton matches and late night walks with Soham. I will miss the love-hate fights of Akash and Sayan. I will miss the discussions on philosophies- Advaita Vedanta, Upanishad, ancient culture etc - with Sourav and Abhishek. I will miss the tea time 'adda' with Ayan, Tanya, Soham. I acknowledge Sourav, Debopam and Soham for lending me their scooty or giving me frequent ride here and there whenever I needed.

I would also like to acknowledge the wonderful seniors I had the privilege of meeting during my time at NISER - Kallol da, Sabir da, Deeptak da, Aritra da, Srijita di, Tushar Adhri di, Sabiar da, and Sukanya di. I am equally grateful for the close friends I made along the way - Reghukrishnan, Ankit, Mahadev, Tousif, Bhubaneswari, Jaffri, Habib, Dinesh, and Sumit - whose companionship made this journey far more meaningful.

I acknowledge my juniors - Tanmay, Gourab, Diwakar, Krishanu, Shashank, Prasanjit, Pritha, and Arya - whose questions encouraged me to revisit and deepen my understanding of several topics during my PhD. I remain deeply thankful to my childhood friend Gourab (Nandi), and to my friends from my B.Sc. days - Sudeepan, Sayan, Vicky, Ankush, Souvik, Sujas -for motivating me to continue pursuing physics when the path seemed uncertain.

I also feel fortunate to have worked with Dr. Ayan Mukhopadhyay during my master's thesis at IIT Madras; his guidance gave me an early and invaluable exposure to high-energy physics. I acknowledge with gratitude my B.Sc. professor, Dr. Sovon Sounda, whose teaching and encouragement played a decisive role in shaping my academic path. I was truly fortunate to have been his student at RKMRC, Narendrapur.

Finally, I express my heartfelt gratitude to my family - my mother, father, younger sister, and my chhoto mama - whose unwavering belief in me has been my greatest source of strength. This PhD was once their dream for me, and making them proud brings me immense joy. A special note of appreciation goes to the most important person in my life who has been supporting me day and night, for believing in me more than I do on myself - Dr. Alokananda Roy.

Manas Debnath

Manas Debnath

10/06/2026

Abstract

This thesis examines the quark-gluon plasma (QGP) through non-perturbative effective theories and kinetic theory approaches, focusing on transport properties, heavy quark dynamics, and collective behavior relevant to RHIC and LHC experiments. Using the effective matrix model of QCD, the first part evaluates shear and bulk viscosities of a pure glue plasma, revealing a minimum in η/s near the deconfinement temperature and a pronounced peak in ζ/s. These feature capture near-critical dynamics that lie beyond the reach of perturbation treatments. The second part applies the Gribov-Zwanziger formalism to heavy quarkonium physics. The modified gluon propagator leads to a stronger screening, reducing quarkonium stability. This framework is further used to study collisional energy loss of fast partons, where the infrared dynamics amplify the parton energy loss. The final component analyzes the heavy quark potential in an anisotropic and collisional QGP. Incorporating a Bhatnagar-Gross-Krook collision kernel shows that collisions significantly enhance the imaginary part of the potential, increasing quarkonium decay widths, however the real potential is hardly affected by collision. Together, these studies link the non-perturbative structure of QCD with experimentally measurable signatures in heavy-ion collisions.

Contents

SUMMARY

The study of the quark-gluon plasma (QGP) remains a central attraction in high-energy nuclear physics, driven primarily by the RHIC and the LHC's experimental programs. When QCD matter is subjected to sufficient high temperatures and energy densities, the confined hadronic phase can no longer persist and transforms into a deconfined state composed of quarks and gluons, commonly referred to as the quark-gluon plasma, as predicted by Quantum Chromodynamics (QCD), due to the asymptotic freedom of the coupling constant. Understanding heavy-quark interactions, the transport properties and collective behavior of this Quark-gluon plasma medium in perturbative and non-perturbative regime of QCD is essential for reconstructing the dynamical evolution of the fireball created in heavy-ion collision experiments. In this thesis, I addressed these fundamental questions using a combination of non-perturbative effective theories based on resummed thermal field theory, and kinetic-theory methods.

The first part of this thesis is devoted to the computation of trasnport coefficient, such as the shear and the bulk viscosities of a pure glue plasma within the framework of the effective matrix model of QCD. This model, developed by Pisarski, Hidaka and collaborators, describes the semi-QGP region by promoting the Polyakov loop eigenvalues to

dynamical variables governed by an effective potential. Using kinetic theory with collision terms derived from the scattering matrix, the shear and the bulk viscosities are evaluated across the semi-QGP region. The results reveal a pronounced minimum of η/s near T_d and a sharp peak in ζ/s, illustrating how matrix models provide a controlled bridge between perturbative high-temperature plasma and non-perturbative confinement physics. These results demonstrate the capability of the matrix model to describe near-critical transport phenomena in a manner inaccessible to purely perturbative approaches.

The second major component of the thesis investigates heavy-quark physics through the medium modification of the heavy-quarkonium potential in the Gribov-Zwanziger (GZ) prescription. The GZ approach incorporates the effects of the Gribov horizon, resulting in a modified gluon propagator that naturally suppresses long-wavelength modes. Using this framework within thermal field theory, the real part and the imaginary part of the potential are computed. The Gribov parameter introduces enhanced screening and magnified Landau damping relative to hard thermal loop (HTL) predictions, leading to a more suppressed real part and a significantly larger imaginary part. These findings indicate that the infrared structure implied by the Gribov horizon shortens quarkonium lifetimes, thereby demonstrating the crucial role of non-perturbative IR physics in heavy-quark suppression.

This thesis also extends the Gribov-Zwanziger analysis to the energy loss of energetic partons traversing the QGP. The presence of the Gribov parameter increases the effective screening scale of the medium, thereby amplifying the collisional energy-loss rate compared to conventional perturbative expectations. The resulting enhancement highlights the sensitivity of jet quenching to confinement-related infrared dynamics and provides a qualitative mechanism by which non-perturbative correlations can influence high-energy probes in relativistic nuclear collisions.

The final part of this thesis investigates the complex heavy-quark potential in a momentum-space anisotropic and collisional quark-gluon plasma. Anisotropy is a key feature of the early time QGP, where rapid longitudinal expansion drives the momentum distribution away from equilibrium. Collisions, incorporated via the Bhatnagar-Gross-Krook (BGK) collisional kernel, regulate the Weibel instabilities inherent in the collisionless theory. The resulting gluon propagator and dielectric function allow a consistent determination of the real and imaginary parts of the heavy-quark potential for arbitrary anisotropy and finite collision rate. The analysis shows that while the real part remains largely insensitive to collisional effects, the modulus of the imaginary part shows larger values with increase of collision parameter, leading to an increased decay width for quarkonia such as the J/ψ. These results highlight the importance of collisional damping in refining theoretical predictions for quarkonium suppression in out-of-equilibrium QGP.

Collectively, this thesis provides a unified investigation of non-perturbative and near-critical QCD physics through three complementary frameworks: the effective matrix model, the Gribov-Zwanziger formalism, and anisotropic thermal field theory with collisions. By analyzing transport coefficients, heavy-quark potentials, and parton energy loss within these frameworks, the work highlights some aspects of the microscopic non-perturbative structure of QCD and the macroscopic observables measured in heavy-ion experiments. The findings enrich our understanding of the QGP near and above the deconfinement transition and offer predictions with direct implications for current and future collider programs.

ABBREVIATIONS

BNL	Brookhaven National Laboratory
EoS	Equation of State
HIC	Heavy ion collisions
HQ	Heavy Quark
HTL	Hard Thermal Loop
LHC	Large Hadron Collider
GZ	Gribov-Zwanziger
QCD	Quantum Chromodynamics
QED	Quantum Electrodynamics
QGP	Quark Gluon Plasma
RHIC	Relativistic Heavy ion collider
HHTL	Holonomous Hard Thermal Loop

List of Figures

CHAPTER 1

INTRODUCTION

> " I am just a child who has never grown up. I still keep asking these 'how' and 'why' questions. Occasionally, I find an answer."
>
> - *Stephen Hawking, From 'A Brief History of Time'*

It is estimated that, the Big Bang, which created this known observable universe, happened almost 13.8 billion years ago, and yet we are trying to understand how did matter form after the Big Bang. Many indirect pieces of evidence and theoretical predictions shows that there might be a plasma phase after the Big Bang and from that matters was formed. This plasma is primarily made up of quarks and gluon which interact with each other strongly. The plasma medium's temperature is around ~ 200 MeV (or 10^{12} K). This strong interaction is studied through the Quantum Chromodynamics (QCD). High energy heavy-ion facilities -most notably RHIC at Brookhaven and the LHC at CERN - were designed to reproduce, in a controlled experimental setting, the extreme temperatures and densities thought to characterize the early universe. This thesis aim to study that Quark-gluon plasma phase for extreme temperatures.

1.1 Quantum Chromodynamics

The theory that governs the strong interactions among the quarks and gluons, carrying color charges, is described by the Quantum Chromodynamics (QCD), also called the theory of colors [1–3].The QCD theory with gauge degrees of freedom only, is a non-abelian gauge theory of $SU(3)$ gauge group. Hence, it has $(3^2 - 1) = 8$ generators, as a result 8 types of color gauge fields, denoted as $A^{\rm a}_\mu$, where color index 'a' that runs from 1 to 8. In QCD, the dynamical matter fields are incorporated by the quarks- the spin$-\frac{1}{2}$ Dirac fermions and these transform under the fundamental representation of the $SU(3)$ gauge group. In nature, six flavors of quarks are known along with their anti-particles : up (u), down (d), strange (s), top (t), bottom (b), and charm (c) - each appears with three color state : red, blue and green. These quarks interact by exchanging gluons, the color-charged gauge bosons of $SU(3)$, which themselves carry colors and mediate strong force. The QCD Lagrangian thus describes the dynamics of color carrying fields- both gluons and quarks.

The QCD Lagrangian is analogous to that of QED (Quantum Electrodynamics), with extra color structure along with it, comes due to non-abelian nature of the theory. This QCD Lagrangian density is given by,

$$\mathcal{L} = \bar{\psi}_i\bigg(i\gamma^\mu(D_\mu)_{ij} - m\delta_{ij}\bigg)\psi_j - \frac{1}{4}F^{\rm a}_{\mu\nu}F^{\mu\nu}_{\rm a} + \mathcal{L}_{\rm GF} + \mathcal{L}_{\rm Ghost}, \tag{1.1}$$

where ψ_i is a three component quark field in the fundamental representation of the $SU(3)$ group, where $i, j = 1, 2, 3$. γ^μ is the Dirac matrices and 'm' indicates the quark mass and

D_μ represents the gauge covariant derivative, given by

$$(D_\mu)_{ij} = \partial_\mu \delta_{ij} - ig(T_{\rm a})_{ij} A^{\rm a}_\mu \tag{1.2}$$

$F^{\rm a}_{\mu\nu}$ is the gluon field strength obtained from the gluon field $A^{\rm a}_\mu(x)$, which is in adjoint representation of the $SU(3)$ group. $T_{\rm a}$'s are the generators of the local $SU(3)$ symmetry. The generators are given by $T_{\rm a} = \lambda_{\rm a}/2$, where $\lambda_{\rm a}$'s ($\rm a = 1, \cdots, 8$) are the Gell-Mann matrices. The gluon field strength is given by,

$$F^{\rm a}_{\mu\nu} = \partial_\mu A^{\rm a}_\nu - \partial_\nu A^{\rm a}_\mu + g\, f^{\rm abc} A^{\rm b}_\mu A^{\rm c}_\nu \tag{1.3}$$

where $\rm a, b, c = 1, \cdots, 8$, and $f^{\rm abc}$ denotes the structure constants of the $SU(3)$ group. It should be noted that $g = \sqrt{4\pi\, \alpha_s(Q)}$.

In Eq. (1.1), the other two terms : $\mathcal{L}_{\rm GF}, \mathcal{L}_{\rm Ghost}$ appears solely due to choosing a fixed gauge.

One of the striking feature of the QCD is asymptotic freedom of QCD coupling constant, $\alpha_s(Q)$ first discussed in [4] - which dictates the strength of the strong interaction, ever increasing with decrease of energy and decreasing with increase of energy. This is due to the QCD β-function is negative at one loop order, implying the coupling $\alpha_s(Q)$ decreases logarithmically with increasing momentum transfer, Q^2. Consequently, at very high energies (or temperatures), quarks and gluons behaves as if they almost free - justifying perturbative treatments of QCD in this regime. Conversely, the coupling grows large at low energy, leading to confinement, where quarks and gluons are bound inside a hadron. Thus, asymptotic freedom, not only describes the success of perturbative QCD at high energies, but also provides the limitations of perturbative QCD of quarks and gluons at confined state within the hadrons, indicating a change of phase from confined hadrons to deconfined quark-gluon plasma phase at extreme conditions. In Fig. 1.1, the variation

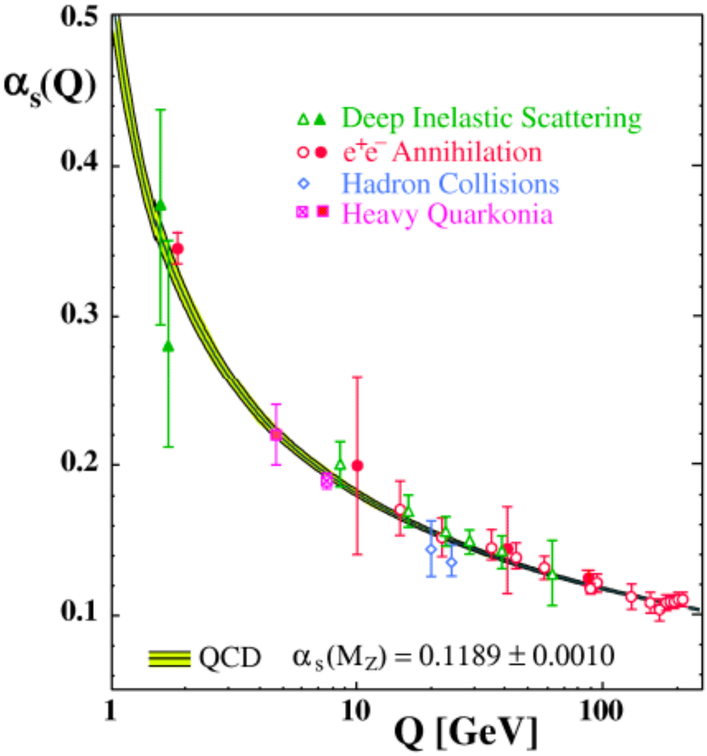

Figure 1.1: QCD running coupling as a function of energy scale. (Figure from Ref [5].)

of QCD running coupling constant as a function of energy scale Q is shown ([5]), at one loop this can be expressed as

$$\alpha_s(Q^2) = \frac{g^2(Q^2)}{4\pi} = \frac{4\pi}{(11 - \frac{2}{3}N_f)\ln\left(\frac{Q^2}{\Lambda^2_{\rm QCD}}\right)}, \tag{1.4}$$

where N_f and Q^2 represent the number of quark flavors and the four momentum transfer respectively. $\Lambda_{\rm QCD}$ is the typical QCD scale parameter. The running coupling decreases with increasing momentum transfer.

While asymptotic freedom enables us to use perturbative QCD (pQCD) at high energies, it also highlights the limitations of pQCD at low energies, where $\alpha_s(Q)$ becomes strong and color-charged particles becomes confined inside the hadrons. This nature of QCD implies that the strength of the interaction depends primarily on energy scale, or equivalently on temperature of the system. As temperature or density increases, the coupling weakens and a transition from the confined hadronic phase to a deconfined phase of quarks and gluons is expected to occur. The study of this phase transition region nearer the transition temperature, which is non-perturbative in nature, is the core theme of this current thesis.

1.2 Quark-gluon Plasma

In Relativistic Heavy Ion Colliders, when two heavy ions collide with each other at ultra-relativistic energies, the energy density at the overlap region becomes so large that nucleons lose their individual identities and their constituent quarks and gluons form a deconfined, strongly interacting medium known as quark-gluon plasma(QGP) phase, the same QGP state which can be found at the inside the core of highly dense neutron stars and is believed to exist after the few microseconds of the Big Bang at the early universe. In Fig. 1.2, (adapted from Chun Shen [6]), it is illustrated how two heavy nuclei collide at ultra-relativistic energy, then a non-equilibrium phase is created, from then the medium thermalizes and QGP is formed. At later time, QGP then cools off and a phase transition (or crossover) occur to form hadron gas, a confined state of quarks and gluons and followed by hadronic interactions leading to kinetic freeze-out, after which only color-neutral hadrons are being detected in the detectors.

Experimental evidences at RHIC (Ref. [7–10]) and CERN (Ref. [11–14]) through the studies of energy loss of transverse momentum and strangeness enhancement hints the

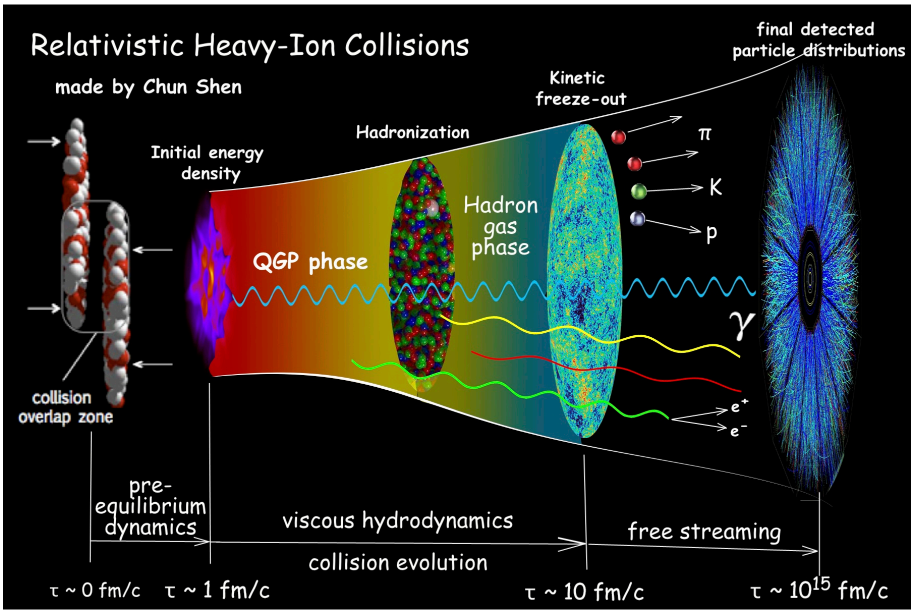

Figure 1.2: Illustration of QGP formation in heavy-ion collisions and its hadronization (Figure from Ref. [6]).

existence of QGP medium. And some rigorous numerical studies through Lattice QCD also confirms the existence of a QGP phase by studying the QCD phase structure (Ref. [15–17]). Another key evidence which arises from collective flow phenomena, particularly the large elliptic flow coefficient (v_2), which indicates that medium behaves nearly like a perfect fluid with extremely low shear viscosity to entropy density ratio (η/s) [18–21]. So, the key observables that scientists look for to study the properties of QGP medium are

- *Collective flow* ([21–23]) , specially elliptic flow (v_2) indicates about the anisotropic expansion caused by initial asymmetry of the nucleons overlapping and also indicated about the fluidity of QGP medium after the heavy-ion collision, which implies that a strongly interacting deconfined medium of quarks and gluons are formed inside the collider, and it also indicated that the formed QGP is behaves as a perfect fluid.

- *Jet quenching* ([24–27]) phenomena is the suppression of high-energy jets in the heavy-ion collision that indicates that constituent fast partons lose significant energy while traversing through the QGP medium, which hints at existence of QGP medium in the heavy-ion collision

- *Quarkonium suppression* ([28]) is the observation of reduced yields of the heavy quarkonium states (J/ψ and Υ) in the detectors, which hints that this quarkonium pair must have melted inside some hot medium, a signature of QGP existence.

- *Strangeness enhancement*: In heavy ion collision, there is a increased production of strange hadrons compared to proton-proton collision which indicates a rapid chemical equilibration, which is possible if a QGP medium is formed ([11, 29]).

- *Direct photon and dilepton emission*- In heavy-ion collision photons and dileptons are emitted and detected in detectors. Since, photons and dileptons don't interact strongly, so they escapes the QGP medium and indicates about the temperature of the medium ([30–32]).

These diverse theoretical and experimental studies have established the existence of quark-gluon plasma and provided significant insights into its properties. However, a complete understanding of QCD matter requires mapping its various possible phases under different conditions of temperature (T) and baryon chemical potential (μ_B). This is also one of the key goals of modern particle colliders in heavy-ion collision program, that is - being able to map the whole QCD phase diagram with precision.

Various Lattice calculation and experimental evidences (Ref. [33–35]) shows that for small or vanishing baryon chemical potential (μ_B), the transition from confined hadronic phase to deconfined quark-gluon plasma phase is a smooth cross-over. This implies that the thermodynamic quantities such as energy density or pressure shows a continuous change over the transition temperature, which is estimated to be $T \approx 154 \pm 9$ MeV (Ref. [34]).

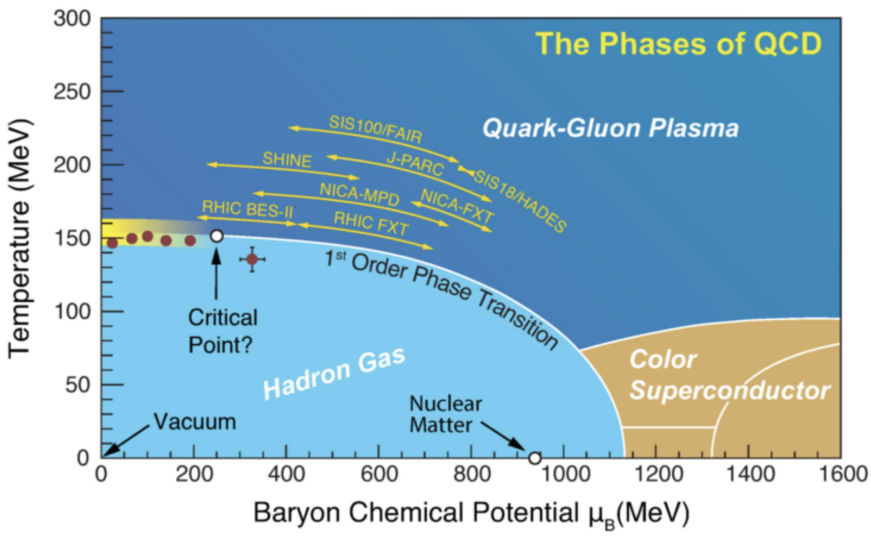

Figure 1.3: A schematic sketch of QCD phase diagram in $T - \mu_B$ plane, locating the QGP phase and Hadronic phase, and also the color superconducting phase. The actual location of critical point and order of the phase transition curve is yet to be determined. Figure taken from [36].

Figure 1.3 shows the QCD phase diagram in temperature (T) versus baryon chemical potential (μ_B) plane,(taken from [36]), which gives a approximate picture of the various phases of QCD matter. Ongoing experimental programs such as the Beam Energy Scan (BES) at RHIC, NICA in Russia, and FAIR in Germany aim to explore this high-density region and search for possible signatures of the critical point, providing a direct link between heavy-ion phenomenology and the thermodynamics of QCD.

1.3 Perturbative QCD at finite temperature

Experimental and theoretical studies together establish the formation of a strongly interacting quark–gluon plasma in heavy-ion collisions and highlight the need to understand its dynamical and thermodynamic behavior from first principles. A complete description of this medium requires Quantum Chromodynamics formulated at finite temperature and density, so that macroscopic observables of the QGP can be related to its underlying microscopic degrees of freedom. In particular, quantities such as the temperature-dependent pressure, energy density, heavy-quark interaction potential, and transport coefficients (including shear and bulk viscosities) encode essential information about the coupling strength, collective evolution, and non-perturbative structure of the QGP near the transition region. The evaluation of these thermal QCD quantities therefore plays a crucial role in constraining phenomenological models and in extracting properties of the strongly coupled plasma created in modern collider experiments. Incorporating temperature in conventional quantum field theory has been extensively discussed in Ref. [37–44].

As previously mention, in Eq. 1.1, we will use the same Lagrangian. In Eq. 1.1, we generally choose a covariant gauge for $\mathcal{L}_{\rm GF}$, with ξ a arbitrary gauge parameter, such that,

$$\mathcal{L}_{\rm GF} = -\frac{1}{\xi}\,{\rm Tr}[(\partial_\mu A^\mu)^2] \tag{1.5}$$

and so the ghost term becomes, also called the Fadeev-Popov ghost term due to Fadeev-Popov ghost fields,

$$\mathcal{L}_{\rm Ghost} = -\bar{\eta}^{\rm a}\partial^2\eta^{\rm a} + g\, f^{\rm abc}\bar{\eta}^{\rm a}\partial^\mu(A^{\rm b}_\mu\eta^{\rm c}) \tag{1.6}$$

where η and $\bar{\eta}$ are Fadeev-Popov ghost and anti-ghost field respectively.

In the current thesis, I have considered the finite temperature by considering the system

is in equilibrium, cause that's when temperature (T) is defined thermodynamically. So in equilibrium system, we wick rotate the temporal axis, by substituting $t = i\tau$, with t being the Minkowski time and τ being the Euclidean time. So, for finite temperature all the fields are either periodic (for bosons) or anti-periodic (for fermions) in $\tau = \beta = 1/T$. So, the bosonic field follows the periodic boundary condition, $\phi(0, \mathbf{x}) = \phi(\beta, \mathbf{x})$ and fermionic fields follows anti-periodic boundary condition, $\phi(0, \mathbf{x}) = -\phi(\beta, \mathbf{x})$.
The Euclidean partition function becomes

$$Z = \int \mathcal{D}A_\mu \, \mathcal{D}\bar{\psi} \, \mathcal{D}\psi \, \mathcal{D}\bar{\eta} \, \mathcal{D}\eta \, \exp\left[- \int_0^{1/T} d\tau \int d^3x \, \mathcal{L}^E_{QCD} \right] \tag{1.7}$$

with $\mathcal{L}^E_{QCD}$ being the Wick-rotated QCD Lagrangian density. The consequence of this periodic (or anti-periodic) boundary is that, in going from co-ordinate space $(\tau, \mathbf{x})$ to momentum space $(\omega, \mathbf{p})$, the ω becomes discrete and imaginary, and these discrete frequencies is called the Matsubara frequency. Hence the momentum integrals become,

$$\int \frac{d^4P}{(2\pi)^4} \to T \sum_{\omega_n} \int \frac{d^3P}{(2\pi)^3} \tag{1.8}$$

where,

$$\omega_n = 2n\pi T \qquad \text{for bosons,} \tag{1.9a}$$

$$= (2n+1)\pi T \qquad \text{for fermions} \tag{1.9b}$$

Analogous to perturbative methods in zero temperature quantum field theory, in thermal perturbation theory as well, we expand the partition function Eq. 1.7 and do the perturbative computation (see Ref. [43, 45]).

Suppose, we have a set of fields, denoted by Φ, then the partition function should look like,

$$Z = N' \int [\mathcal{D}\Phi] \mathrm{e}^{S}, \tag{1.10}$$

where S denotes the total action, which can be decomposed as free part (S_0) and interaction part (S_I),

$$S = S_0 + S_I. \tag{1.11}$$

Here, S_0 is at most quadratic in the field, and S_I is the part that appears due to interaction and this can be of higher order in fields. In perturbative approach, we expand Eq. 1.10 in a power series in the interaction part, S_I,

$$Z = N' \int [\mathcal{D}\Phi] \mathrm{e}^{S_0} \sum_{l=0}^{\infty} \frac{1}{l!} S_I^l \tag{1.12}$$

Taking log on Eq. 1.12, we can get,

$$\begin{aligned} \log\, Z &= \log \left(N' \int [\mathcal{D}\Phi] \mathrm{e}^{S_0}\right) + \log \left(1 + \sum_{l=1}^{\infty} \frac{1}{l!} \frac{\int [\mathcal{D}\Phi] \mathrm{e}^{S_0} S_I^l}{\int [\mathcal{D}\Phi] \mathrm{e}^{S_0}}\right) \\ &= \log\, Z_0 + \log\, Z_I \end{aligned} \tag{1.13}$$

Eq. 1.13 which separates the tree-level (free) contribution, $\log Z_0$, from the higher-order interaction corrections, $\log Z_I$. The logarithm of the partition function, or equivalently the free energy, is the central quantity in thermal field theory. In thermal QCD, the interaction term S_I consists of gluon self-interactions (three- and four-gluon vertices), quark–gluon interactions, and ghost–gluon couplings. These vertices generate loop corrections to physical observables such as the free energy density, the heavy-quark potential, and various transport coefficients. The Feynman rules at finite temperature follow the same structure as at zero temperature, with the modification that energy integrals are replaced by discrete

Matsubara sums. It is important to emphasize, however, that perturbation theory is reliable only when the contributions from higher-order diagrams are progressively smaller than those from the preceding orders. This condition is naturally satisfied at high temperatures or baryon densities due to asymptotic freedom, which ensures that the strong coupling α_s becomes small. Consequently, each succeeding term in the perturbative expansion of the partition function is suppressed, making the perturbative approach valid in this regime. At lower temperatures, where the coupling grows large, perturbation theory breaks down, and non-perturbative methods such as lattice QCD or effective models become essential for describing QCD matter.

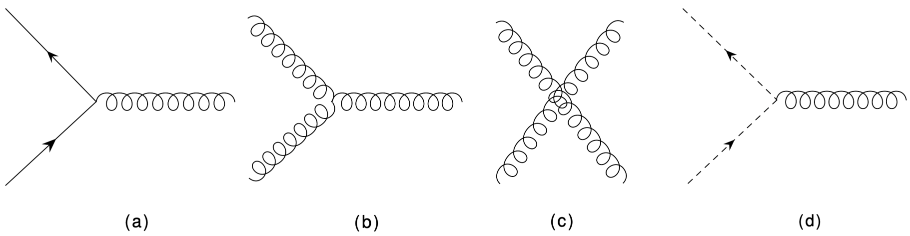

Figure 1.4: The QCD vertices, (a) quark-gluon vertex, (b) three gluon vertex, (c) four gluon vertex, (d) ghost-gluon vertex.

At finite temperature, the bare gluon propagator in momentum space in the covariant gauge is given by,

$$D^0_{\mu\nu}(K) = \frac{1}{K^2}\left(\delta_{\mu\nu} - (1-\xi)\frac{K_\mu K_\nu}{K^2}\right), \tag{1.14}$$

where $K^2 = k_0^2 - k^2$. Similarly, the bare quark and ghost propagator is given by respectively,

$$S^0(K) = \frac{1}{-i\gamma \cdot K + m}, \qquad \text{and} \qquad G^0(K) = \frac{1}{K^2} \tag{1.15}$$

1.3.1 Frequency sum

Bosonic field:

A general form of a frequency sum for bosonic fields can be written as,

$$T \sum_{n=-\infty}^{n=+\infty} f(k_0 = i\omega_n = i\,2n\pi T). \tag{1.16}$$

Here k_0 is the temporal component in momentum space in Minkowski configuration, and f is some meromorphic function.

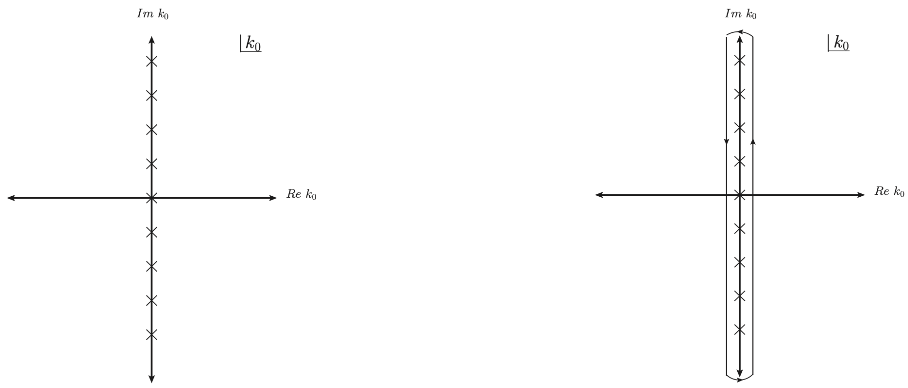

Figure 1.5: Poles of $\coth(\beta k_0/2)$ at $k_0 = i2n\pi T$ for $n = -\infty, \cdots, 0, \cdots, \infty$ in complex k_0 plane. Figure taken from [37].

The above bosonic frequency sum can be written as a sum of residues of a hyperbolic cotangent function, so Eq. 1.16 can be rewritten as,

$$\frac{1}{\beta} \sum_{n=-\infty}^{n=+\infty} f(k_0 = i\omega_n = i\,2n\pi T)\,\mathrm{Res}\left[\frac{\beta}{2}\coth\left(\frac{\beta\,k_0}{2}\right)\right] = \frac{1}{2\pi i}\oint\limits_C dk_0 \frac{1}{2} f(k_0)\coth\left(\frac{\beta k_0}{2}\right) \tag{1.17}$$

Now, one should note some important points in Eq. 1.17 :

- $\coth(\beta k_0/2)$ has countably infinite poles at the imaginary axis in complex-k_0 plane at $k_0 = i\omega_n = i2n\pi T$, and is a bounded and analytic function everywhere except at the poles.

- $f(k_0)$ is a meromorphic function which implies that it may have simple poles but it has no essential singularities or any branch cut.

- The function $f(k_0)$ does not have a pole on imaginary axis.

Now the contour which encloses the poles of $\coth(\beta k_0/2)$, can be deformed into two contours C_1 and C_2 with shape of half-circle (see FIg. 1.6), now enclosing the simple poles of $f(k_0)$ function only, leaving the poles of $\coth(\beta k_0/2)$, provided that $f(k_0)$ is a fast decreasing function.

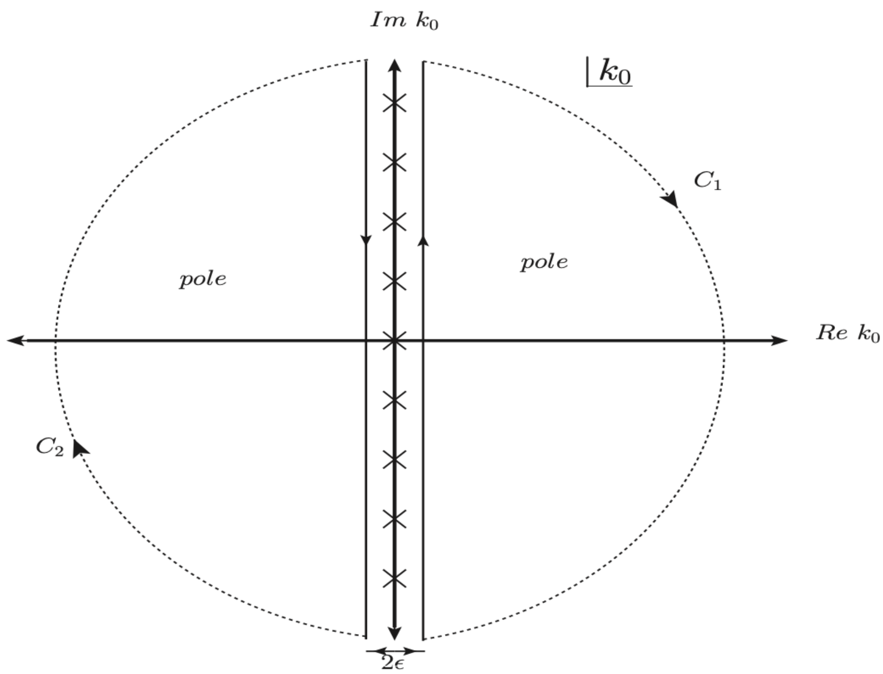

Figure 1.6: Contour C_1 and C_2 is obtained by deforming the original contour, which now enclode only the poles of the meromorphic function $f(k_0)$.([37]).

So the Matsubara sum can be written as,

$$T \sum_{n=-\infty}^{\infty} f(k_0 = i\omega_n) \;=\; \frac{1}{2\pi i} \oint_{C_1 \cup C_2} dk_0 f(k_0 = i\omega_n) \left[\frac{1}{2} + \frac{1}{\exp(\beta k_0) - 1}\right], \quad (1.18)$$

where we used the fact that $\coth\left(\frac{\beta k_0}{2}\right) = 1 + \frac{2}{\exp(\beta k_0)-1}$, and the constant term 1, represents the vacuum term (or $T = 0$ contribution) and the term with $n_B(k_0) = (\exp(\beta k_0) - 1)^{-1}$ represents the thermal term (or $T \neq 0$ contribution). After some calculations this Matsubara sum becomes,

$$\begin{aligned} T\sum_{n=-\infty}^{\infty} f(k_0 = i\omega_n) &= \frac{1}{2\pi i}\int_{-i\infty}^{i\infty} dk_0 \frac{1}{2}[f(k_0) + f(-k_0)] \\ &+ \frac{1}{2\pi i}\int_{-i\infty+\epsilon}^{i\infty+\epsilon} dk_0 [f(k_0) + f(-k_0)] n_B(k_0). \end{aligned} \tag{1.19}$$

Fermionic field:

For the fermionic field, we have to consider the following frequency sum,

$$T\sum_{n=-\infty}^{n=\infty} f(k_0 = i\omega_n = i(2n+1)\pi T), \tag{1.20}$$

and we note that $\tanh\left(\frac{\beta k_0}{2}\right)$ has poles at $k_0 = i\omega_n = i(2n+1)\pi T$. So with the similar technique as bosonic Matsubara sum, we get,

$$\begin{aligned} T\sum_{n=-\infty}^{n=+\infty} f\left(k_0 = i\omega_n\right) &= \frac{1}{2\pi i}\int_{-i\infty}^{+i\infty} d\left(k_0\right)\frac{1}{2}\left[f\left(k_0\right) + f\left(-k_0\right)\right] \\ &+ \frac{1}{2\pi i}\int_{\epsilon-i\infty}^{\epsilon+i\infty} d\left(k_0\right)\left[f\left(k_0\right) + f\left(-k_0\right)\right]\frac{1}{\exp\left(\beta k_0\right)+1}. \end{aligned} \tag{1.21}$$

This bosonic and fermionic Matsubara sums will be used to calculate various thermodynamical quantities which involve various loop calculations whether it is perturbative calculation or effective field theory calculation , like gluon loop, quark loop etc.

1.3.2 Few Results: Frequency Sum

We know the general form of the bosonic propagator

$$\Delta_B(K) = 1/(K^2 - m^2) = 1/(k_0^2 - k^2 - m^2),$$

in momentum space, which can be re-written by

$$\Delta_B(K) = -\int_0^\infty d\tau\, e^{k_0\tau}\, \Delta_B(\tau, E_k), \tag{1.22}$$

where

$$\begin{aligned}\Delta_B(\tau, E_k) &= -T \sum_{k_0 = i2n\pi T} e^{-k_0\,\tau} \Delta_B(K) \\ &= \frac{1}{2E_k}\left[(1 + n_B(E_k))e^{-E_k\tau} + n_B(E_k)e^{E_k\tau}\right] \\ &= \sum_{s=\pm} \frac{s}{2E_k}(1 + n_B(sE_k))e^{-sE_k\tau}.\end{aligned} \tag{1.23}$$

Equation 1.23 can also be obtained using the contour method from Eq. 1.19, with $E_k = \sqrt{k^2 + m^2}$ is the particle energy and $n_B(E_k) = \frac{1}{e^{\beta E_k} - 1}$ denotes Bose-Einstein (BE) distribution.

The fermion propagator is written as,

$$S(K) = (\gamma \cdot K + m)\Delta_F(K). \tag{1.24}$$

Analogous to Eq. 1.22, $\Delta_F(K)$ can be written as,

$$\Delta_F(K) = -\int_0^\beta d\tau\, e^{k_0\tau} \Delta_F(\tau, E_k), \tag{1.25}$$

where

$$\Delta_F(\tau, E_k) = -T \sum_{k_0 = i(2n+1)\pi T} e^{-k_0 \tau} \Delta_F(K) = \sum_{s=\pm} \frac{s}{2E_k}(1 - n_F(sE_k))e^{-sE_k \tau}, \quad (1.26)$$

with $n_F(E_k) = \frac{1}{e^{\beta E_k}+1}$, is called the Fermi-Dirac (FD) distribution.

One of the useful result using the Matsubara sum techniques, that needed in the current thesis, is

$$T \sum_{k_0 = i(2n+1)\pi T} \Delta_F(K)\, \Delta_F(Q = P - K) = -\sum_{s_1, s_2} \frac{s_1 s_2}{4E_k E_q} \frac{1 - n_F(s_1 E_k) - n_F(s_2 E_q)}{p_0 - s_1 E_k - s_2 E_q}. \quad (1.27)$$

1.4 Non-perturbative Region of QCD

Till now, it is well understood that, perturbative QCD calculation provides a reliable description at high temperature or density, but it is not reliable at lower temperature near the confinement-deconfinement transition. In this region, the coupling constant, α_s, grows large, and the perturbative expansion doesn't converge. At zero chemical potential, this region is around $T \sim 154 \pm 9$ MeV, as can be seen in Fig. 1.3, is intrinsically non-perturbative and understanding the behaviour of QCD matter in this region remains one of the central challenge in contemporary theoretical QCD community.

A variety of approaches have been attempted to fill the gap between non-perturbative and perturbative. One of the successful and widely used theoretical framework is the Hard Thermal Loop (HTL) perturbation theory, developed by Braaten and Pisarski (Ref. [46–49]). The HTL formalism systematically resums an infinite subset of one-particle-irreducible (1PI) diagrams in the soft momentum limit, effectively using a dressed propagators and vertices to include collective medium effects such as Debye screening and Landau damping. This resummation restores the consistency of perturbation theory in the high-temperature plasma and allows for a realistic description of quasiparticle excitations, spectral functions, and transport coefficients. The quantitative success of the HTL framework is exemplified by the three-loop computation of the QCD pressure by Haque, Mustafa, and Strickland [50, 51], a technically demanding calculation that established the reliability of HTLpt in describing high-temperature QCD thermodynamics.

Despite its success, the HTL framework remains quantitatively reliable only at temperatures well above the critical temperature T_c. As the system approaches T_c, where the coupling becomes strong and non-perturbative effects dominate, even HTL-resummed perturbation theory loses accuracy - necessitating more effective and genuinely non-perturbative approaches to describe the QGP near the phase transition.

In this strongly coupled regime, effective models have proven particularly useful in capturing the essential features of QCD thermodynamics. In this thesis, I have used the effective matrix model, which was specifically constructed to describe the thermodynamics of QCD matter in the vicinity of transition region ([52–60]). This model effectively encodes confinement deconfinement dynamics through an order parameter, called the Polyakov loop. The matrix model introduces an effective potential for the Polyakov loop - a gauge-invariant order parameter for confinement and thereby captures the transition from color confinement to deconfinement. At the same time, the model retains key features of the gluonic self-interactions and color structure inherent to QCD. This model serves pretty well from the deconfinement temperature, T_d to almost $4T_d$, also known as semi-QGP region. This model uses the techniques of HTLpt, but with additional background field due to the Polyakov loop, that is why sometimes it is referred as Holonomous HTL (HHTL in short).

Another important non-perturbative framework is the Gribov-Zwanziger (GZ) approach

[61, 62], which provides a confinement mechanism from first principles. By restricting the gauge field configurations to the so-called Gribov region in field space, this formalism introduces an infrared mass scale- the Gribov parameter - that modifies the gluon propagator to vanish at zero momentum. This behavior is a clear signature of confinement and has important consequences for infrared QCD dynamics. Extensions of the GZ framework to finite temperature have been developed to study how such confinement features manifest in the deconfined phase, influencing screening, collective modes, and the free energy of the QGP. The Gribov-type corrections can also be combined with other effective models, forming hybrid frameworks that capture both infrared confinement and realistic thermodynamics near the phase boundary.

In this thesis, these theoretical frameworks are utilized as complementary approaches to explore different aspects of the quark-gluon plasma in regimes where standard perturbative methods fail. The Effective Matrix Model serves as the central framework for studying the equilibrium thermodynamics of QCD matter near the deconfinement transition. Within this model, we compute the shear and bulk viscosities for a pure glue theory [63], providing non-perturbative insight into the transport properties of the strongly coupled plasma. In parallel, we employ the Gribov-Zwanziger framework to investigate confinement-related effects on medium observables. Using the Gribov-modified gluon propagator, we study both the complex heavy-quark potential [64] and the energy loss of fast-moving partons [65] within a hot QCD medium. These analyses reveal how the infrared modifications introduced by the Gribov parameter influence color screening, damping, and partonic interactions, thereby connecting confinement dynamics to finite-temperature observables. Finally, to probe the early, out-of-equilibrium stage of QGP evolution, we extend the analysis to an anisotropic collisional plasma using the Hard Thermal Loop formalism. In this context, we examine the behavior of the complex heavy-quarkonium potential under momentum-space anisotropy [66], providing insight into the pre-equilibrium suppression dynamics of heavy quark bound states. Taken together, these works establish a coherent picture of QCD matter across its different dynamical regimes - ranging from the non-perturbative equilibrium phase near the transition temperature to the transient anisotropic stage following heavy-ion collisions; thereby contributing toward a unified understanding of the quark-gluon plasma.

CHAPTER 2

SHEAR AND BULK VISCOSITY IN PURE GLUONIC SYSTEM

In this chapter transport coefficient such as shear and bulk viscosity has been computed for a pure gluonic system using the matrix model. This chapter is based on the work presented in the following paper: ***Shear and bulk viscosity for a pure glue theory using an effective matrix model***

Manas Debnath, Ritesh Ghosh, Najmul Haque, Yoshimasa Hidaka, Robert D. Pisarski
Phys.Rev.D 112 (2025) 1, 014040 [arXiv:2504.20138].

2.1 Introduction

The behavior of gauge theories at nonzero temperature is a question of fundamental importance, affecting both the behavior of the collisions of heavy ions at high energies and the evolution of the early universe. While quantities in thermal equilibrium can be computed from numerical simulations on the lattice, quantities near equilibrium are not easy to measure. Notably, this includes the transport coefficients, for which, at present, the lattice can only provide rough estimates, (However, in recent years for the heavy quark momentum diffusion constant, results with much more quantitative control have been obtained [67].).

In a $SU(N_c)$ gauge theory without dynamical quarks, the simplest way to measure the deconfining phase transition is through the Polyakov loop, ℓ, which is the trace of the Wilson line in the direction of imaginary time, $\ell = \mathrm{tr}\,\mathbf{L}/N_c$. When $N_c > 2$, the trace of higher powers of the Wilson line, $\ell_j = \mathrm{tr}\,\mathbf{L}^j/N_c$, $j = 1 \ldots (N_c - 1)$ are also independent, gauge invariant quantities, and so should be included for a complete description of deconfinement. Alternatively, one can consider the $N_c - 1$ eigenvalues of the thermal Wilson line. These are gauge-invariant and measure the holonomy of the Wilson line in imaginary time. They can naturally be used to construct a matrix model for deconfinement.

If the deconfining phase transition occurs at a temperature T_d, the Polyakov loops, or equivalently the holonomy, is non-trivial from T_d to a couple of times T_d. This region can be described as a semi-quark gluon plasma (semi-QGP), where the effects of partial deconfinement play a dominant role.

In this paper we use an effective matrix model, which describes a partially deconfined phase with nonzero holonomy [53, 54, 68–79]. Since we compute scattering processes, we need the generalization of hard thermal loops (HTL's) [38, 42, 46, 49, 50, 80–85] to nonzero holonomy [31, 55–60, 86–97]. The computation of the shear [98, 99] and bulk [100] viscosities follows the computation to leading logarithmic order in ordinary perturbation theory, at zero holonomy.

Besides using a model with nonzero holonomy, our principal assumption is that the gauge coupling is of moderate strength, even down to $T \sim T_d$. For example, in an effective three-dimensional theory, the coupling constant runs not as $\alpha_s(T_d)$, but from two loop calculations, closer to $\alpha_s(2\pi T_d)$ [101, 102]. We then assume that both gluons and teen fields act like well defined quasiparticles, even down to temperatures $\sim T_d$.

At nonzero holonomy, besides the usual gluons, it is also necessary to add new, fictional degrees of freedom, which we call "teens". We denote this by the Bengali character ৩ [103], which is pronounced teen, and represents the number three. This is because our theory has gluons, Faddeev-Popov ghosts, and teens. For future reference, we also use the Bengali characters ব, pronounced "baw", and দ, as "daw".

At large N_c, in the deconfined phase, the pressure is $\sim N_c^2$, while it is $\sim N_c^0$ in the confined phase. Thus, to model the theory as $T \to T_d$, it is necessary to add something so that the leading term in the pressure vanishes. We take the teen fields to lie in the adjoint representation, so their pressure is $\sim N_c^2$. For the term in the pressure $\sim N_c^2$ to vanish, these teen fields must be ghosts, with negative pressure. Because the leading nonperturbative term in the pressure is $\sim T^2$ [79], we take the teens as two-dimensional fields, isotropically embedded in four dimensions.

The outline of this chapter is as follows. In Sec. 2.2, we discuss how to characterize non-trivial holonomy. In Sec. 2.3 we review the solution of the matrix model at large N_c [60, 91, 96, 104, 105]. We describe how the previous solution can be modified to give close agreement to lattice values for the Polyakov loop. In Sec. 2.4, we describe how to compute in perturbation theory at nonzero holonomy. In Secs. 2.5 and 2.6, we calculate the shear viscosity and bulk viscosities respectively, considering $2 \to 2$ scattering involving gluon and teen, computing to leading logarithmic order in weak coupling. In Sec. 5.6, we summarize the results.

2.2 The thermal Wilson line and non-trivial holonomy

At a nonzero temperature T, the thermal Wilson line is

$$\mathbf{L}(\boldsymbol{x}) = \mathcal{P} \exp \left(ig \int_0^{1/T} A_0(\boldsymbol{x}, \tau) d\tau \right) , \tag{2.1}$$

where $\mathcal{P}$ refers to path, which is here time ordering, and the Euclidean time $\tau : 0 \to 1/T$. Under a gauge transformation $\Omega(\boldsymbol{x}, \tau)$ this transforms as

$$\mathbf{L}(\boldsymbol{x}) \to \Omega^\dagger(\boldsymbol{x}, 1/T)\, \mathbf{L}(\boldsymbol{x})\, \Omega(\boldsymbol{x}, 0) \ . \tag{2.2}$$

We can define local gauge transformations as those which fall off at spatial infinity, $\Omega(\boldsymbol{x}, \tau) \to \mathbf{1}$ as $\boldsymbol{x} \to \infty$. There are also global gauge rotations, which are constant in space. Normally these are innocuous, as they just rotate the gauge fields. However, in a pure gauge theory, we can take a global gauge rotation in the center of the gauge group. For $SU(N_c)$ these are elements of $Z(N_c)$, where $\Omega_k = \mathrm{e}^{2\pi i k/N_c}\mathbf{1}$, with $k = 1 \ldots N_c$. Since the Ω_k commute with all group elements, the gluons remain unchanged. Thus we can take the gauge transformation at $\tau = 1/T$ equal to that at $\tau = 0$, times an element of $Z(N_c)$: and thus, the traced Polyakov loop, $\mathrm{tr}\ \mathbf{L}(\boldsymbol{x})$, is a gauge invariant operator. The gauge transformations can be generalized into aperiodic transformations up to a constant element in the center of the gauge group.

$$\Omega(\boldsymbol{x}, 1/T) = \mathrm{e}^{2\pi i k/N_c}\, \Omega(\boldsymbol{x}, 0) \ ; \ k = 1, \ldots, (N_c - 1) \ . \tag{2.3}$$

While locally, the gluons are insensitive to the Ω_k, the thermal Wilson line is not:

$$\mathbf{L}(\boldsymbol{x}) \to \mathrm{e}^{2\pi i k/N_c} \Omega^\dagger(\boldsymbol{x}, 0)\, \mathbf{L}(\boldsymbol{x})\, \Omega(\boldsymbol{x}, 0) \ . \tag{2.4}$$

From this form, we can take traces of the powers of the thermal Wilson line,

$$\ell_j(\boldsymbol{x}) = \frac{1}{N_c} \ \mathrm{tr}\ \mathbf{L}(\boldsymbol{x})^j \ . \tag{2.5}$$

These are all invariant under gauge transformations, but transform under global $Z(N_c)$ rotations as

$$\ell_j(\boldsymbol{x}) \to \mathrm{e}^{2\pi i j k/N_c}\, \ell_j(\boldsymbol{x}) \ . \tag{2.6}$$

This global $Z(N_c)$ symmetry is related to a one-form $Z(N_c)$ symmetry [106], with the thermal Wilson line the one-form operator. For the propagation of an infinitely massive test quark, the thermal Wilson line describes the evolution of the color charge through the thermal medium. The Polyakov loops ℓ_j represent the trace of this propagator, as it winds around in imaginary time j times.

Test quarks do not propagate in the confined phase of a gauge theory, and so the expectation value of $Z(N_c)$ charged Polyakov loops, where $j = 1, \ldots, (N_c - 1)$, vanish. Of course, ℓ_{N_c} is a singlet under $Z(N_c)$, and has a nonzero expectation value at any $T \neq 0$. Conversely, the expectation values of $Z(N_c)$ charged loops are nonzero in the deconfined phase, above the temperature for the deconfining phase transition, at T_d.

Numerical simulations on the lattice typically measure the expectation value of the loop with unit charge, ℓ_1 [107]. To measure loops with higher charge, it is necessary to measure loops in an irreducible representation of the gauge group. After the fundamental representation, given by ℓ_1, the next simplest is the adjoint, which is $Z(N_c)$ neutral, and representations with two indices [53], which carry charge two under $Z(N_c)$. See, *e.g.*, Eq. (21) of Ref. [53]. Polyakov loops with higher charge play an essential role in the effective theory we construct. Models employing just the first Polyakov loop were first proposed by Fukushima [108], and are extremely useful. Since only the first loop is included, however, they cannot be completed.

An alternate approach is to notice that since the thermal Wilson line transforms homogeneously under (periodic) gauge transformations, then, we can always rotate it to a diagonal form:

$$\mathbf{L}(\boldsymbol{x}) = \exp(2\pi i\, \boldsymbol{q}/N_c)\,, \tag{2.7}$$

where $\boldsymbol{q}$ is a diagonal matrix. As an element of $SU(N_c)$, $\boldsymbol{q}$ is traceless, with $N_c - 1$ independent elements. The form of Eq. (2.7) can be described by expanding about a constant value of the timelike component of the gauge field,

$$A_0^{ab}(\boldsymbol{x}, \tau) = \frac{2\pi i T}{g}\; q_a\; \delta^{ab}\;, \tag{2.8}$$

where $a, b = 1, \ldots, N_c$ refer to color indices in the fundamental representation. We note that at the leading order, the q_a are automatically gauge invariant; beyond the leading loop order, the gauge-invariant quantities are related to the "bare" q_a through finite terms [72]. We only compute the potential for the $\boldsymbol{q}$ at one-loop order, so this will not arise in our analysis. We simply mention it to stress that the eigenvalues of the thermal Wilson line form gauge invariant quantities. At the tree level, a constant value for the gauge potential has zero action. A potential for $\boldsymbol{q}$ is generated at one-loop order [68, 69],

$$\mathcal{V}_4 = \frac{2\pi^2 T^4}{3} \sum_{a,b=1}^{N_c} \mathcal{P}^{ab,ba}\; B_4(q_a - q_b)\;. \tag{2.9}$$

We introduce the color projection operator

$$\mathcal{P}^{ab,cd} = \delta^{ad}\delta^{bc} - \frac{1}{N_c}\,\delta^{ab}\delta^{cd}\ . \tag{2.10}$$

This operator is transverse in the color indices, $\sum_a \mathcal{P}^{aa,cd} = 0$. It is convenient to introduce in Eq. (2.9), so that we sum only over the $N_c^2 - 1$ degrees of freedom for $SU(N_c)$, and not those of $U(N_c)$. It also enters frequently later. Also,

$$B_4(q) = -\frac{1}{30} + q^2(1-q)^2\ ;\ q \equiv |q|_{\mathrm{mod}1} \tag{2.11}$$

is the fourth Bernoulli polynomial. The potential $\mathcal{V}_4$ is elementary to compute, using a constant background field for A_0. Because the q_a's enter through the adjoint covariant derivative, the quantities $q_a - q_b$ enter automatically. Since the q_a's only enter into $\mathbf{L}$ through an exponential, the potential is periodic, so the q's enter as $|q|$, modulo unity.

This potential is minimized at $q_a = 0$, which is the usual perturbative vacuum, or at $Z(N_c)$ transforms thereof [71, 72]. This potential can then be used to compute the $Z(N_c)$ interface tension, which is equivalent to a 't Hooft loop around a spatial boundary [109]. Thus, while this one-loop potential is useful at high temperatures, it manifestly cannot describe the transition to a confining phase. This behavior is manifestly non-perturbative. To describe this, we add the following term:

$$\mathcal{V}_2 = c\,T^2 T_d^2 \sum_{a,b=1}^{N_c} \mathcal{P}^{ab,ba}\ B_2(q_a - q_b)\ , \tag{2.12}$$

where B_2 is the second Bernoulli polynomial,

$$B_2(q) = \frac{1}{6} - q(1-q)\ ;\ q \equiv |q|_{\mathrm{mod}\,1}\ , \tag{2.13}$$

and the constant c is adjusted so that the transition occurs at T_d. This is non-perturbative, as it is proportional to T_d, the temperature for deconfinement.

This term is certainly not unique. It is motivated on two grounds. First, from $\approx 1.2\, T_d$ to $\approx 4\, T_d$, the leading correction to the pressure in a pure gauge theory is $\sim T^2$. This is not exact, however, only approximate. Secondly, it is necessary to ensure that the non-perturbative part of the potential is such that there is no first-order transition from a truly perturbative phase, where all $q_a = 0$, to the semi-QGP, where $q_a \neq 0$. The second Bernoulli polynomial is particularly useful to ensure this, since $B_2 \sim q$ at small q.

2.3 Matrix solution at large N_c

In Refs. [57, 59], matrix models were analyzed by fitting to the pressure. In computing the shear and bulk viscosity, however, we found it convenient to simply take the limit of large N_c. This is simply because, at finite N_c, one has to take into account that the generators of $SU(N_c)$ are traceless, and this rather complicates the analysis. Since the model, as we discuss, has obvious limitations, we ease our computational burden by considering the limit of large N_c. Thus, in this section, we review the solution at large N_c [60]; see, also, Refs. [91, 96, 104, 105].

At large N_c, the sum over the color indices can be replaced by an integral,

$$\sum_{a=1}^{N_c} \to N_c \int_{-q_0}^{+q_0} dq\ \rho(q)\ . \tag{2.14}$$

Here we introduce $y = a/N_c$, with $q_a \to q(y)$. Instead of integrating over y, however, we can introduce the spectral density, $\rho(q) = dy/dq$. The solution at large N_c involves a spectral density that has a finite range, $-q_0 \to q_0$.

At large N_c, we then need to minimize the potential

$$\mathcal{V}_{\text{eff}}(q) = d_2(T)V_2(q) - d_1(T)V_1(q) \ , \tag{2.15}$$

where

$$V_n(q) = \int_{-q_0}^{+q_0} dq \int_{-q_0}^{+q_0} dq' \rho(q)\, \rho(q')\, |q-q'|^n (1-|q-q'|)^n \ . \tag{2.16}$$

To one-loop order, $d_2 = (2\pi^2/3)\, T^4$. Previously [60, 91, 96, 104, 105], it was assumed that $d_1 \sim T^2 T_d^2$. In this work, in order to fit the Polyakov loop, we adopt a more general ansatz. By taking derivatives of the equation of motion, the solution is found to be the following. The temperature dependence only enters through the ratio of the coefficients of the Bernoulli polynomials,

$$d(T)^2 = \frac{12 d_2(T)}{d_1(T)} \ . \tag{2.17}$$

The eigenvalue density has an elementary form,

$$\rho(q) = 1 + b(T)\cos(d(T)\, q) \ ; \ q : -q_0(T) \to q_0(T) \ . \tag{2.18}$$

This eigenvalue density must also satisfy the normalization condition,

$$\int_{-q_0}^{+q_0} dq\ \rho(q) = 1 \ . \tag{2.19}$$

The solution is

$$\cot\left(d(T)q_0(T)\right) = \frac{d(T)}{3}\left(\frac{1}{2} - q_0(T)\right) - \frac{2}{d(T)(1-2q_0(T))} \ , \tag{2.20}$$

and

$$b(T)^2 = \frac{d(T)^4}{9}\left(\frac{1}{2} - q_0(T)\right)^4 + \frac{d(T)^2}{3}\left(\frac{1}{2} - q_0(T)\right)^2 + 1 \; . \tag{2.21}$$

The properties of this solution are roughly in accord with the numerical simulations from the lattice. The loop with charge k is given by

$$\ell_k = \int_{-q_0}^{+q_0} dq \; \rho(q) \cos(2\pi k q) \; . \tag{2.22}$$

Notably, at the deconfining phase transition, $d(T_d) = 2\pi$, and the value of the first loop is

$$\ell_1(T_d) = \frac{1}{2} \; . \tag{2.23}$$

Unexpectedly, the values of all higher loops vanish at this point,

$$\ell_k(T_d) = 0 \; ; \; k \geq 2 \; . \tag{2.24}$$

This follows directly from the form of the solution at T_d, Eq.(2.18), which equals

$$\rho(q) = 1 + \cos(2\pi q) \; ; \; T = T_d \; . \tag{2.25}$$

We do not see a general reason why all loops with charge two and higher should vanish at T_d, Eq. (2.24), but it obviously follows from the simple form of the eigenvalue density at the transition.

Away from the transition, plots of the charged loops are shown in Fig. 2.1, plotted versus $d/(2\pi)$. Loops with charge two or greater vanish at the transition, where $d/(2\pi) = 1$, but they also begin to oscillate in sign. Again, this is presumably a detailed feature of the model.

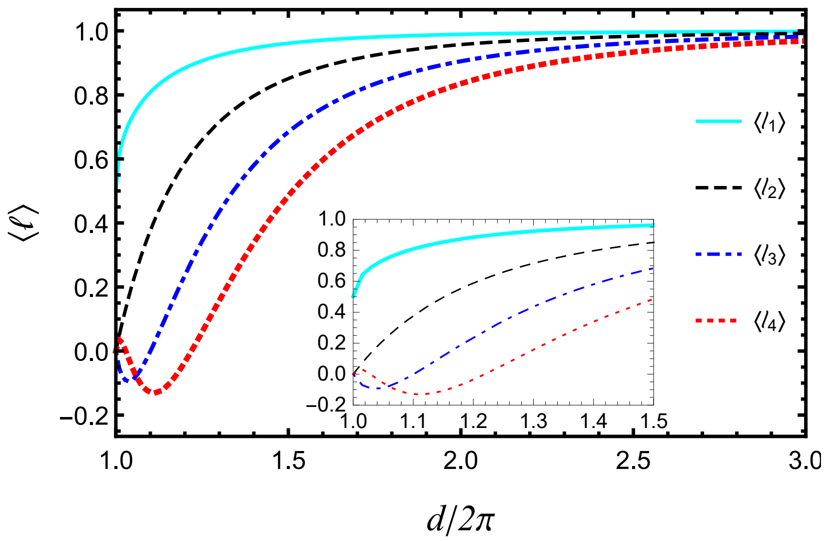

Figure 2.1: Plots of the first four Polyakov loops as a function of $d/(2\pi)$ in the matrix model.

In Fig. 2.2, we show a plot of the value of the first Polyakov loop, $\ell_1(T)$, versus results from the lattice. If we require that the transition take place at T_d, then we must fix $d(T) = 2\pi T/T_d$, as the transition occurs when $d(T) = 2\pi$. Results for the renormalized Polyakov loop are available for $N_c = 3$ [107] and higher N_c [110]. The results are similar, if not identical. For $N_c = 3$, the value of the renormalized loop is smaller at T_d, $\ell_1(T_d) \approx 0.4$. For $N_c = 5$, $\ell_1(T_d) \approx 0.5$. The potential is proportional to the pressure, so one can also immediately compute the entropy density, $s(T) = \partial\mathscr{P}(T)/\partial T$, and from that, the energy density, $\mathscr{E}(T) = Ts(T) - \mathscr{P}(T)$. The deviation from conformality is most easily measured through the "interaction measure", which is

$$\frac{\mathscr{E} - 3\mathscr{P}}{T^4} = T\frac{\partial}{\partial T}\left(\frac{\mathscr{P}}{T^4}\right) . \tag{2.26}$$

This is plotted in Fig. 2.3. The pressure from the matrix model is compared to the lattice

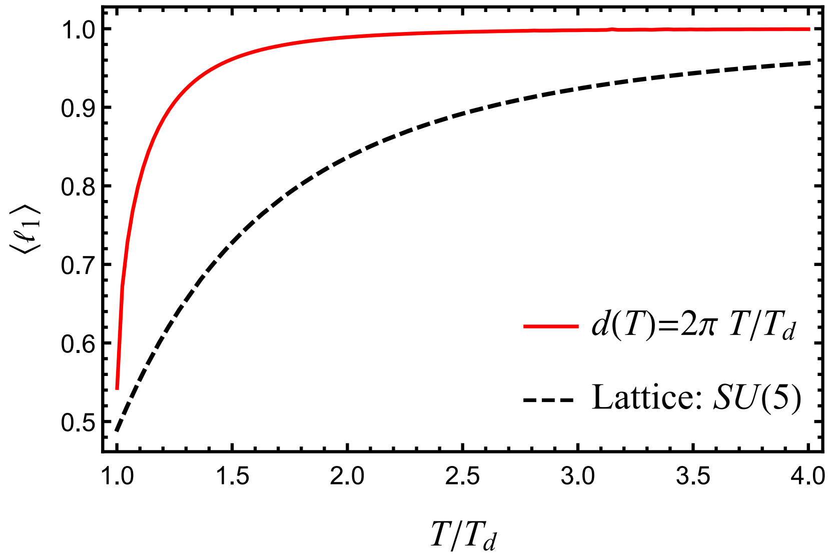

Figure 2.2: Plot of the Polyakov loop using the solution $d(T) = 2\pi T/T_d$, versus that for $N_c = 5$.

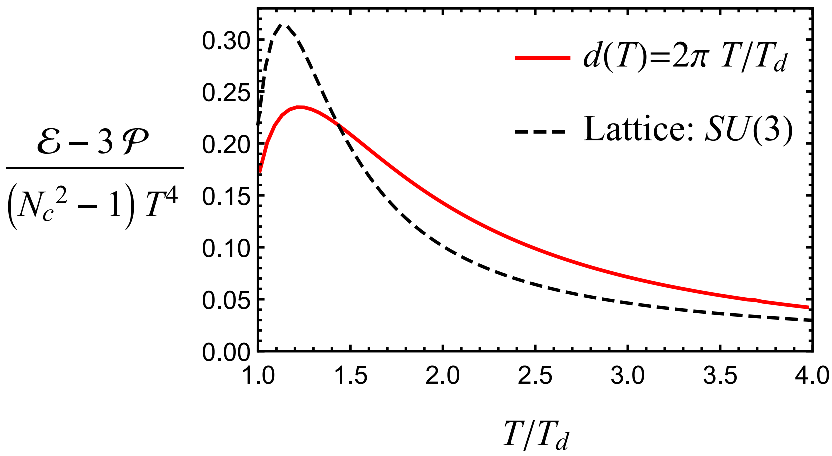

Figure 2.3: Plot of the interaction measure, divided by the number of gluons, $N_c^2 - 1$, using the solution $d(T) = 2\pi T/T_d$, versus that for $N_c = 3$.

results for $N_c = 3$ [111], as that is the most accurate. From Ref. [111], for three colors the pressure can be fit by the function

$$\mathscr{P}_{\text{lat}}(T) = 8\,T^4\,\frac{p_1 + p_2\ln(t) + p_3\ln^2(t)}{8(1 + p_4\ln(t) + p_5\ln^2(t))}\,,\quad t = \frac{T}{T_d}\,, \tag{2.27}$$

where $p_1 = 0.0045$, $p_2 = 1.76$, $p_3 = 10.6$, $p_4 = 2.07$, and $p_5 = 5.8$. The overall factor of 8 on the right-hand side is for the number of gluons. We comment that there are results for the pressure from the lattice for higher N_c, but the results do not differ significantly from $N_c = 3$ [112], at least to the accuracy at which we work. We note that very recent work [113] computes thermodynamic quantities across the $SU(3)$ deconfinement transition and presents an improved equation of state, with a similar fit function for the pressure in Eq. (2.27). We mention that in the analysis for three colors, the pressure was fit to rather good accuracy but at the expense of adding further terms to the pressure [57, 59]. In any case, while the fit to the pressure is approximate, as is obvious from Fig. 2.2, there is a sharp discrepancy between the Polyakov loop in the matrix model versus the renormalized Polyakov loop from the lattice for $N_c = 5$. In particular, the Polyakov loop on the lattice approaches unity *much* slower than in the matrix model. This is not an artifact of large N_c, and is present in the solution of the matrix model for three colors [57, 59]. This is a serious deficiency of the matrix model, for which we do not have an explanation. Since we

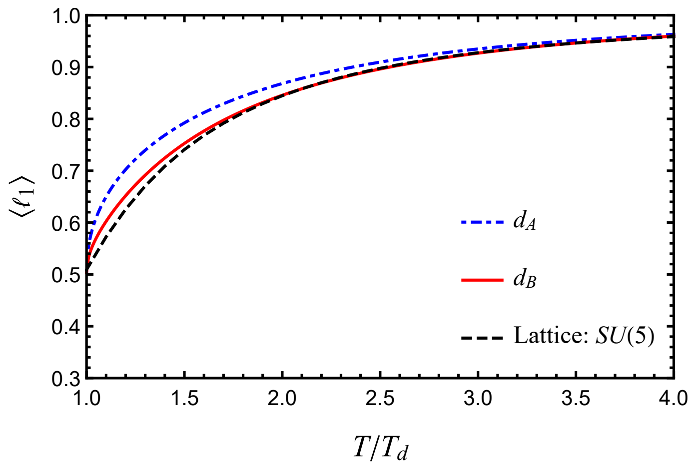

Figure 2.4: Results for the Polyakov loop with the ansatz of Eq. (2.28) versus the lattice for $N_c = 5$.

can compute using the matrix model, however, we adopt the following approach. This is admittedly a heuristic approach until said time that a better matrix model can be developed.

We take the solution of the matrix model and adjust $d(T)$ so that the Polyakov loop agrees with the values from the lattice. Accordingly, the terms for the pressure also need to be adapted. We take two ansatzes:

$$
\begin{aligned}
d_A(T) &= 1.08\, t + 5.2032\ , \\
d_B(T) &= \frac{0.26}{t^3} + 1.105\, t + 4.9182\ ,\ t = \frac{T}{T_d}\ .
\end{aligned}
\tag{2.28}
$$

We take $d_2(T) \sim T^4$, as for an ideal gas, and define $d_1(T)$ from the definition of $d(T)$ in Eq. (2.17).

The results for the first Polyakov loop are plotted in Fig. 2.4, where they are compared to the lattice Polyakov loop for $N_c = 5$. The first form, $d_A(T)$, is relatively close to the lattice loop. Given the definition of $d(T)$, $d_1(T) \sim d_2(T)/d_A(T)^2$, and so while at large T, $d_1(T) \sim T^2$, as expected from the matrix model, near the transition, the form of $d_1(T)$ cannot be motivated except by the fit to the loop. This is even more true for the second form, $d_B(T)$, which contains a somewhat arbitrary coefficient $\sim 1/t^3$, which is chosen so that there is close agreement with the lattice value of ℓ_1. The results for the interaction measure are shown in Fig. 2.5. The agreement is satisfactory, although the matrix model does not describe the a sharp peak in the interaction measure at $\sim 1.1 T_d$.

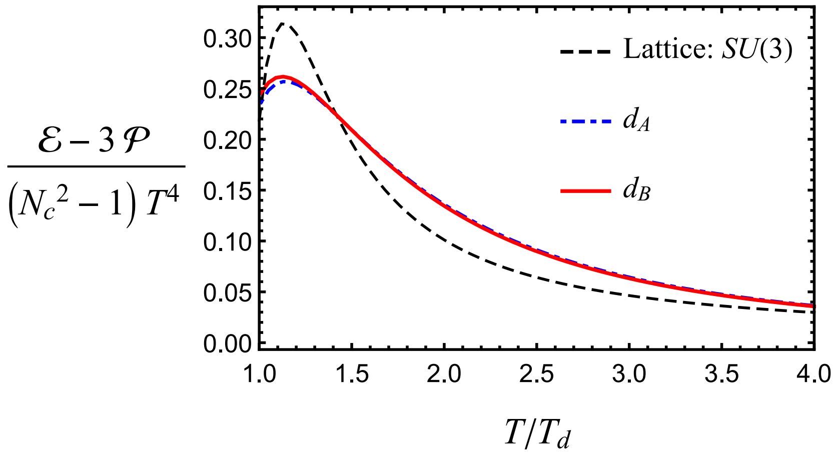

Figure 2.5: Results for the interaction measure, divided by the number of degrees of freedom, $N_c^2 - 1$, with the ansatz of Eq. (2.28) versus that, from the lattice, for $N_c = 3$, Eq. (2.27).

2.4 Perturbation theory at nonzero holonomy

It is straightforward to compute at nonzero holonomy by expanding about the background field of Eq. (2.8). For a detailed discussion, see Ref. [56]. The computation for the gluons is standard so that here we simply establish notation.

We compute at nonzero temperature in Euclidean spacetime, where

$$\int \frac{d^4K}{(2\pi)^4} = T \sum_{n=-\infty}^{+\infty} \frac{d^3k}{(2\pi)^3} \; ; \; K_\mu = (k_0, \boldsymbol{k}) \; ; \; k_0 = 2\pi n T \; . \tag{2.29}$$

In the background field of Eq. (2.8), for a gluon the time-like component of the momentum is

$$K_\mu^{ab} = (k_0^{ab}, \boldsymbol{k}) \; , \; k_0^{ab} = k_0 + Q^{ab} = k_0 + Q^a - Q^b = 2\pi T(n + q_a - q_b) \; . \tag{2.30}$$

The difference $q_a - q_b$ enters because the adjoint covariant derivative involves a commutator of the background field, $A_0^{\rm cl}$. This only happens for the quantum fluctuations with color components that are off-diagonal. For fluctuations that are color diagonal, the background field is not entered. This is the principal reason why computations at nonzero holonomy are more complicated at finite N_c than at infinite N_c.

In the Landau choice of background field gauge, the gluon propagator is

$$D^{\mu\nu}(K^{ab}) = \left(\delta^{\mu\nu} - \frac{K^{ab}_\mu K^{ab}_\nu}{(K^{ab})^2} \right) \frac{1}{(K^{ab})^2} \, \mathcal{P}^{ab,cd} \, . \tag{2.31}$$

This involves the color projection operator, $\mathcal{P}^{ab,cd}$, Eq. (2.10). The three and four-gluon vertices, and the coupling to Faddeev-Popov ghosts, follow directly by replacing the momentum with color flow momenta.

2.4.1 Teen fields

We concentrate on the effective theory for the two-dimensional ghost fields [97], which we denote as ৩. This is the Bengali character for three, pronounced teen. We chose this because it is simple to write, and it is the third field after gluons and Faddeev-Popov ghosts. We introduce a unit spatial vector $\hat{l}$, and to respect rotational invariance, integrate over all directions of $\hat{l}$. The longitudinal and transverse coordinates with respect to $\hat{l}$ are

$$x^i = (x_\parallel, \boldsymbol{x}_\perp) \quad , \quad x_\parallel = \boldsymbol{x} \cdot \hat{l} \quad , \quad \boldsymbol{x}_\perp \cdot \hat{l} = 0 \, . \tag{2.32}$$

We then introduce gauge covariant derivatives for the fermionic field, ϕ:

$$S_{\text{৩}} = \int_0^{1/T} d\tau \int \frac{d\Omega_{\hat{l}}}{4\pi} \int_{-\infty}^{\infty} dx_\parallel \int_{|x_\perp^2| > 1/T_d^2} d^2 x_\perp \, \mathcal{L}_{\text{৩}} \, , \tag{2.33}$$

where the Lagrangian associated with the 2D ghost field, i.e.,"teen" field is given by

$$\mathcal{L}_{\circlearrowleft} = \; 2 \;\operatorname{tr}\left((D_0\bar{\phi})(D_0\phi) + (D_\parallel\bar{\phi})(D_\parallel\phi) + (\boldsymbol{D}_\perp\bar{\phi})\cdot(\boldsymbol{D}_\perp\phi)\right) \;, \tag{2.34}$$

and ϕ and $\bar{\phi}$ are taken to lie in the adjoint representation. The overall factor of 2 is because we use generators normalized such that $\operatorname{tr} t^{ab}t^{cd} = \mathcal{P}^{ab,cd}/2$. The integral over transverse momenta is explicitly the cutoff at T_d, and so is manifestly non-perturbative.

In practice, we do not evaluate the effective Lagrangian of Eq. (2.33) exactly, but directly in momentum space, putting a cutoff on the transverse directions $= T_d$. This violates gauge invariance. We show that at one-loop order, this violation does not appear in the teen contribution to the gluon self-energy, but does in the teen self-energy. However, the teen self-energy does not contribute to either the shear or bulk viscosities to leading logarithmic order in weak coupling, and so for now, we ignore how to implement the teen fields in a more consistent manner.

Now, the teen propagator is

$$D^{ab,cd}_{\circlearrowleft}(K) = \frac{1}{(K^{ab})^2}\,\mathcal{P}^{ab,cd} \;. \tag{2.35}$$

As for the gluons, the interactions follow directly using color flow momenta. The three-point vertex connecting a teen, an anti-teen, and one gluon is

$$-\frac{\delta S_{\circlearrowleft}}{\delta\phi^{fe}(R)\,\delta B^{dc}_\mu(Q)\,\delta\bar{\phi}^{ba}(P)} = igf^{ab,cd,ef}\;\left(P^{ab}_\mu - R^{ef}_\mu\right) \;. \tag{2.36}$$

Here, $f^{ab,cd,ef} = i(\delta^{ad}\delta^{cf}\delta^{eb} - \delta^{af}\delta^{cb}\delta^{ed})/\sqrt{2}$ is the structure constant. Now, the four-point vertex connecting two gluons and two teen fields is

$$-\frac{\delta S_{\circlearrowleft}}{\delta B_\mu^{hg}(S)\,\delta B_\mu^{fe}(R)\,\delta\bar{\phi}^{dc}(Q)\delta\phi^{ba}(P)} = -g^2\sum_{ij}(f^{ab,ef,ij}f^{cd,gh,ji} + f^{ab,gh,ij}f^{cd,ef,ji})\,\delta_{\mu\nu}. \tag{2.37}$$

2.4.2 Teen contribution to gluon self-energy

The two contributions to the gluon self-energy from teen fields are illustrated in Fig. 2.6. As usual, there is a tadpole term, and a term involving two teen fields. From Fig. 2.6a, the

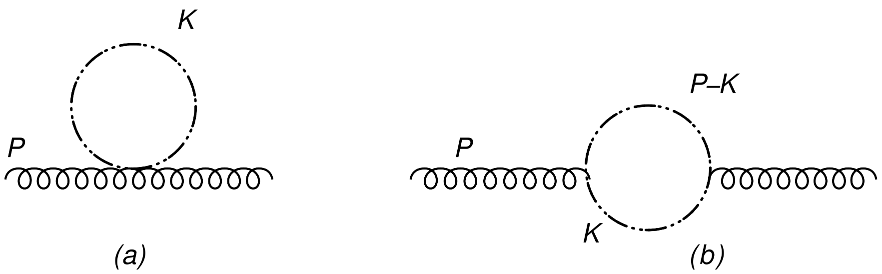

Figure 2.6: Teen ($\circlearrowleft$) contribution to the gluon self-energy

tadpole diagram contributes

$$\begin{aligned} J_1^{\mu\nu} &= f^{ab,ef,gh}f^{cd,fe,hg}X_1^{\mu\nu}\,, \\ X_1^{\mu\nu} &= -2g^2\int_{\circlearrowleft}\frac{d^4k}{(2\pi)^4}\frac{\delta^{\mu\nu}}{(K^{fe})^2}\,. \end{aligned} \tag{2.38}$$

The projection operators $\mathcal{P}^{ab,cd}$ are multiplied with traceless generators t^{ab}, so the second term $\sim -\delta^{ab}\delta^{cd}/N_c$ drops out, and we can take $\mathcal{P}^{ab,cd} \to \delta^{ac}\delta^{bd}/N_c$.

The momentum integral for the teen field is

$$\int_{\circlearrowleft}\frac{d^4K}{(2\pi)^4} = T\sum_{n=-\infty}^{+\infty}\int_{\circlearrowleft}\frac{d^3k}{(2\pi)^3}\,,\quad \int_{\circlearrowleft}\frac{d^3k}{(2\pi)^3} = \int_{-\infty}^{+\infty}\frac{dk_\parallel}{2\pi}\int_{|k_\perp|<T_d}\frac{d^2k_\perp}{(2\pi)^2}\,. \tag{2.39}$$

Here $k_\parallel = \boldsymbol{k}\cdot\hat{l}$, and $\boldsymbol{k}_\perp = \boldsymbol{k} - \hat{l}(\boldsymbol{k}\cdot\hat{l})$ for a given $\hat{l}$, with $\hat{l}^2 = 1$. The integration over all directions of $\hat{l}$ then restores rotational invariance. To simplify the integral over the teen momenta, we will usually assume that $T \gg T_d$. This allows us to separate the sum over n, with momenta $\sim 2\pi nT$, and $k_\parallel$, from the two-dimensional integral over $k_\perp$.

The contribution to the self-energy from the self-energy diagram can be written from Fig. 2.6b as

$$
\begin{aligned}
J_2^{\mu\nu} &= f^{ab,ef,gh} f^{cd,fe,hg}\, X_2^{\mu\nu}\,, \\
X_2^{\mu\nu} &= g^2 \int_{\circlearrowleft} \frac{d^4K}{(2\pi)^4} \frac{(2K^{fe}-P^{ab})^\mu (2K^{fe}-P^{ab})^\nu}{(K^{fe})^2 (P^{ab}-K^{fe})^2}\,.
\end{aligned}
\tag{2.40}
$$

The combined contribution to the gluon self-energy from the two diagrams becomes

$$
\begin{aligned}
X^{\mu\nu} &= X_1^{\mu\nu} + X_2^{\mu\nu} \\
&= -g^2 \int_{\circlearrowleft} \frac{d^4K}{(2\pi)^4} \left\{ \frac{2\delta^{\mu\nu}}{(K^{fe})^2} - \frac{4(K^{fe})^\mu (K^{fe})^\nu}{(K^{fe})^2 (P^{ab}-K^{fe})^2} \right\}.
\end{aligned}
\tag{2.41}
$$

Here, we neglected the external momentum in the numerator, as the calculation is performed using the HTL approximation in the following. We start with the spatial component of $X_2^{\mu\nu}$

$$
X_2^{ij}(P^{12}, Q_1, Q_2) = \frac{1}{2}\, g^2 \int_{\circlearrowleft} \frac{d^3k}{(2\pi)^3} \frac{4k^i k^j}{4E_k E_{p-k}} \left[(\mathcal{I}_1 + \mathcal{I}_2 + \mathcal{I}_3 + \mathcal{I}_4) + (Q_1 \leftrightarrow Q_2) \right] \tag{2.42}
$$

Here, $E_k = |\boldsymbol{k}|$, and $E_{p-k} = |\boldsymbol{p}-\boldsymbol{k}|$. We have symmetrized with respect to Q_1 and Q_2, which accounts for the overall factor of $1/2$. In detail,

$$
\mathcal{I}_1 = \frac{-1}{ip_0^{12} - E_k - E_{p-k}} \Big(1 + n(E_k - iQ_1) + n(E_{p-k} - iQ_2) \Big)\,, \tag{2.43}
$$

$$\mathcal{I}_2 = \frac{1}{ip_0^{12} - E_k + E_{p-k}}\Big(n(E_k - iQ_1) - n(E_{p-k} + iQ_2)\Big)\ , \tag{2.44}$$

$$\mathcal{I}_3 = \frac{-1}{ip_0^{12} + E_k - E_{p-k}}\Big(n(E_k + iQ_1) - n(E_{p-k} - iQ_2)\Big)\ , \tag{2.45}$$

$$\mathcal{I}_4 = \frac{1}{ip_0^{12} + E_k + E_{p-k}}\Big(1 + n(E_k + iQ_1) + n(E_{p-k} + iQ_2)\Big)\ . \tag{2.46}$$

To simplify things we write $Q_1 = Q^f - Q^e$ and $Q_2 = Q^a - Q^b + Q^f - Q^e$, with $p_0^{12} = p_0 - Q_1 + Q_2$.

The terms that do not involve Landau-damping, and so are due to quasi-particle (QP), can be written as

$$\begin{aligned} X^{ij}_{2,\mathrm{QP}}(P^{12}, Q_1, Q_2) &= \frac{1}{2}g^2 \int_{\circlearrowleft} \frac{d^3k}{(2\pi)^3}\frac{4k^ik^j}{4E_kE_{p-k}}\left[(\mathcal{I}_1 + \mathcal{I}_4) + (Q_1 \leftrightarrow Q_2)\right] \\ = \quad g^2 \int_{\circlearrowleft} \frac{d^3k}{(2\pi)^3}\frac{2\delta^{ij}}{4E_k}\frac{\boldsymbol{v}_k^2}{3}&\Big[n(E_k - iQ_1) + n(E_k + iQ_1) + n(E_k - iQ_2) + n(E_k + iQ_2)\Big]\ , \end{aligned} \tag{2.47}$$

where $\boldsymbol{v}_k = \boldsymbol{k}/E_k$. Now, the terms involving Landau damping (LD) are

$$\begin{aligned} X^{ij}_{2,\mathrm{LD}}(P^{12}, Q_1, Q_2) &= \frac{1}{2}g^2 \int_{\circlearrowleft} \frac{d^3k}{(2\pi)^3}\frac{4k^ik^j}{4E_kE_{p-k}}\left[(\mathcal{I}_2 + \mathcal{I}_3) + (Q_1 \leftrightarrow Q_2)\right] \\ = \quad \frac{1}{2}g^2 \int_{\circlearrowleft} \frac{d^3k}{(2\pi)^3} v_k^i v_k^j &\Bigg[\frac{2}{ip_0^{12} + \boldsymbol{p}\cdot\hat{l}}\big\{n(E_k - iQ_1) - n(E_k + iQ_1) + n(E_k - iQ_2) \\ &\qquad -n(E_k + iQ_2)\big\} \\ - \quad \frac{\boldsymbol{p}\cdot\hat{l}}{ip_0^{12} + \boldsymbol{p}\cdot\hat{l}}\frac{\partial}{\partial E_k}&\big\{n(E_k - iQ_1) + n(E_k + iQ_1) + n(E_k - iQ_2) + n(E_k + iQ_2)\big\}\Bigg]\ . \end{aligned} \tag{2.48}$$

The second line of Eq. (2.48) can be simplified as

$$
\begin{aligned}
- & \frac{g^2}{2}\int_{\wp}\frac{d^3k}{(2\pi)^3}\Bigg[v_k^i v_k^j\frac{-ip_0^{12}}{ip_0^{12}+\boldsymbol{p}\cdot\hat{l}}\left\{n'(E_k-iQ_1)+n'(E_k+iQ_1)+n'(E_k-iQ_2)\right.\\
&\qquad\qquad\qquad\qquad\qquad\qquad\qquad\qquad\left.+n'(E_k+iQ_2)\right\}\\
&\qquad\quad+v_k^i v_k^j\left\{n'(E_k-iQ_1)+n'(E_k+iQ_1)+n'(E_k-iQ_2)+n'(E_k+iQ_2)\right\}\Bigg]\\
= & -\frac{g^2}{2}\int_{\wp}\frac{d^3k}{(2\pi)^3}\Bigg[v_k^i v_k^j\frac{-ip_0^{12}}{ip_0^{12}+\boldsymbol{p}\cdot\hat{l}}\left\{n'(E_k-iQ_1)+n'(E_k+iQ_1)+n'(E_k-iQ_2)\right.\\
&\qquad\qquad\qquad\qquad\qquad\qquad\qquad\qquad\left.+n'(E_k+iQ_2)\right\}\\
&\quad-\delta^{ij}\left(\frac{1}{E_k}-\frac{v_k^2}{3E_k}\right)\left\{n(E_k-iQ_1)+n(E_k+iQ_1)+n(E_k-iQ_2)+n(E_k+iQ_2)\right\}\Bigg]\,,
\end{aligned}
\tag{2.49}
$$

where $n'(E-iQ_1)=\partial n(E-iQ_1)/\partial E$, *etc.*

Now, the spatial components of the tadpole term are

$$
\begin{aligned}
X_1^{ij} &= -g^2\int\frac{d^4K}{(2\pi)^4}\delta^{ij}\left[\frac{1}{K_1^2}+\frac{1}{K_2^2}\right]\\
&= -g^2\int\frac{d^3k}{(2\pi)^3}\delta^{ij}\frac{1}{2E_k}\Big[n(E_k-iQ_1)+n(E_k+iQ_1)+n(E_k-iQ_2)+n(E_k+iQ_2)\Big].
\end{aligned}
\tag{2.50}
$$

If we add Eqs. (2.47), (2.49), and (2.50), the terms $\sim\delta^{ij}$ vanish.

Collecting the non-vanishing terms, the spatial components of $X^{\mu\nu}$ become

$$
\begin{aligned}
X^{ij} = g^2 & \int_0^{T_d}\frac{k_\perp\,dk_\perp}{2\pi}\int_0^\infty\frac{2dk_\parallel}{2\pi}\int\frac{d\Omega_{\hat{l}}}{4\pi}\,\frac{\hat{k}^i\hat{k}^j}{ip_0^{12}+\boldsymbol{p}\cdot\hat{l}}\\
&\times\Big[\left\{n(E_k-iQ_1)-n(E_k+iQ_1)+n(E_k-iQ_2)-n(E_k+iQ_2)\right\}
\end{aligned}
$$

$$+\,ip_0^{12}\frac{1}{2}\Big\{n'(E_k-iQ_1)+n'(E_k+iQ_1)+n'(E_k-iQ_2)+n'(E_k+iQ_2)\Big\}\Big]\,. \tag{2.51}$$

Now, the temporal component of $X^{\mu\nu}$ is

$$\begin{aligned} X^{00} &= -g^2\int\frac{d^4K}{(2\pi)^4}\left[\frac{1}{K_1^2}+\frac{1}{K_2^2}\right]+\frac{1}{2}g^2\int\frac{d^4K}{(2\pi)^4}\left[\frac{4(k_1^0)^2}{K_1^2(P^{12}-K_1)^2}+\frac{4(k_2^0)^2}{K_2^2(P^{12}-K_2)^2}\right] \\ &= g^2\int\frac{d^4K}{(2\pi)^4}\left[\frac{1}{K_1^2}+\frac{1}{K_2^2}\right]-\frac{1}{2}g^2\int\frac{d^4K}{(2\pi)^4}\left[\frac{4(\boldsymbol{k}_1)^2}{K_1^2(P^{12}-K_1)^2}+\frac{4(\boldsymbol{k}_2)^2}{K_2^2(P^{12}-K_2)^2}\right]. \end{aligned} \tag{2.52}$$

Collecting the temporal and spatial components, the total $X^{\mu\nu}$ defined in Eq. (2.42) becomes

$$\begin{aligned} X^{\mu\nu} &= \frac{g^2}{2}\int_0^{T_d}\frac{k_\perp\,dk_\perp}{2\pi^2}\int_0^\infty 2dk_\parallel\int\frac{d\Omega_{\hat{l}}}{4\pi} \\ &\times\ \Bigg[\frac{\bar{K}^\mu\bar{K}^\nu}{ip_0^{12}+\boldsymbol{p}\cdot\hat{l}}\big\{n(E_{k_\parallel}-iQ_1)-n(E_{k_\parallel}+iQ_1)+n(E_{k_\parallel}-iQ_2)-n(E_{k_\parallel}+iQ_2)\big\} \\ &+\ \frac{1}{2}\left(u^\mu u^\nu+\frac{ip_0^{12}\bar{K}^\mu\bar{K}^\nu}{ip_0^{12}+\boldsymbol{p}\cdot\hat{l}}\right)\big\{n'(E_{k_\parallel}-iQ_1)+n'(E_{k_\parallel}+iQ_1) \\ &\qquad\qquad +n'(E_{k_\parallel}-iQ_2)+n'(E_{k_\parallel}+iQ_2)\big\}\Bigg] \\ &= \frac{g^2}{2\pi^2}\frac{T_d^2}{2}\left[-2\pi i\big(B_1(q_1)+B_1(q_2)\big)T\int\frac{d\Omega_{\hat{l}}}{4\pi}\frac{\bar{K}^\mu\bar{K}^\nu}{\bar{K}\cdot P^{12}}\right] \\ &\quad+\frac{g^2}{2\pi^2}\frac{T_d^2}{2}\left[u^\mu u^\nu+ip_0^{12}\int\frac{d\Omega_{\hat{l}}}{4\pi}\frac{\bar{K}^\mu\bar{K}^\nu}{\bar{K}\cdot P^{12}}\right] \\ &= \frac{g^2}{2\pi^2}\frac{T\,T_d^2}{2}\Big[-2\pi i\big(B_1(q_1)+B_1(q_2)\big)\Big]\delta\Gamma^{\mu\nu}(P^{12})-\frac{g^2}{2\pi^2}\frac{T_d^2}{2}\delta\Pi^{\mu\nu}(P^{12})\,. \end{aligned} \tag{2.53}$$

This involves the functions $\delta\Gamma$ and $\delta\Pi$. $\delta\Pi$ is the usual hard thermal loop function,

$$\delta\Pi^{\mu\nu}(P) = -u^\mu u^\nu - ip_0 \int \frac{d\Omega_{\hat{l}}}{4\pi} \frac{\bar{K}^\mu \bar{K}^\nu}{P \cdot \bar{K}} \;, \tag{2.54}$$

where $u^\mu = \delta^{\mu 0}$ is a vector in the rest frame of the medium. The other function is

$$\delta\Gamma^{\mu\nu}(P) = -\frac{1}{ip_0} \left(\delta\Pi^{\mu\nu}(P) + u^\mu u^\nu \right) \;. \tag{2.55}$$

The null vector $\bar{K}^\mu \equiv (i, \hat{l})$, and B_1 is the first Bernoulli polynomial,

$$B_1(q) = |q|_{\mathrm{mod}\, 1} - \frac{1}{2} \;. \tag{2.56}$$

So, the teen contribution to the gluon self-energy becomes

$$\begin{aligned} \Pi_{\circlearrowleft}^{\mu\nu;ab,cd}(P^{ab}) &= J_1^{\mu\nu}(P^{ab}) + J_2^{\mu\nu}(P^{ab}) \\ &\overset{\mathrm{HTL}}{\approx} f^{ab,ef,gh} f^{cd,fe,hg} X^{\mu\nu}(P^{ab}, Q^{fe}, Q^{hg}) \\ &= \delta^{ad,bc} X^{\mu\nu}(P^{ab}, Q^{ae}, Q^{eb}) - \delta^{ab,cd} X^{\mu\nu}(P^{ab}, Q^{ca}, Q^{ac}) \;. \end{aligned} \tag{2.57}$$

For the gluon self-energy, the largest terms are $\sim g^2T^3$ times $\delta\Gamma$, and $\sim g^2T^2$ times $\delta\Pi$. For soft momenta $P_\mu \sim gT$, the term $\sim g^2T^2$ is as large as the term at the tree level. Remember that after analytic continuation, this holds as well for the time-like component, $p_0^{12} = -i\omega + \epsilon$, with $|\omega| \sim gT$.

For the teen loop in the gluon self-energy, we keep the largest terms, which are $\sim TT_d^2$ times $\delta\Gamma$, and $\sim T_d^2$ times $\delta\Pi$. We show shortly when *both* the gluon and teen contributions are included, that the terms $\sim \delta\Gamma$ cancel [56, 97], as a consequence of the equations of motion. The term $\sim \delta\Pi$ contributes to the gluon self-energy. In keeping the largest terms, we write $\overset{\text{HTL}}{\approx}$ in Eq. (2.57) to represent that only the largest terms for soft momenta have been kept. The contribution to the gluon self-energy from a gluon loop at non-zero holonomy is given in Ref. [56]. The total is

$$\begin{aligned}\Pi^{\mu\nu;ab,cd}_{\text{total}}(P^{ab}) &= \Pi^{\mu\nu;ab,cd}_{\text{gl}}(P^{ab}) + \Pi^{\mu\nu;ab,cd}_{\varsigma}(P^{ab}) \\ &= -\mathcal{K}^{ab,cd}\delta\Gamma^{\mu\nu}(P^{ab}) - (m^2)^{ab,cd}\delta\Pi^{\mu\nu}(P^{ab}) \ . \end{aligned} \tag{2.58}$$

Now, $\mathcal{K}^{ab,cd}$ in Eq. (2.58) is

$$\begin{aligned}\mathcal{K}^{ab,cd} &= \frac{2\pi i g^2}{3}\,\delta^{ad}\delta^{bc}\left[\sum_{e=1}^{N_c}\Big(\mathcal{A}_0(Q^{ae}) + \mathcal{A}_0(Q^{eb})\Big)T^3\right. \\ &\quad \left. + 3\sum_{e=1}^{N_c}\frac{1}{8\pi^3}\left\{\big(B_1(q_a - q_e) + B_1(q_e - q_b)\big)\right\}T_d^2 T\right] , \end{aligned} \tag{2.59}$$

where

$$\mathcal{A}_0(Q) = \frac{3}{2\pi i T^3}\int \frac{d^3k}{(2\pi)^3}\left(n(E_k - iQ) - n(E_k + iQ)\right) \ . \tag{2.60}$$

It is direct to show that Eq. (2.59) vanishes by the equations of motion [97]. Physically, the sum of the currents induced by the gluon and teen field cancel [97]. This is an essential check on the consistency of the model.

The second term in Eq. (2.58) involves the usual hard thermal loop in the gluon self-energy, $\delta\Pi(P)$, times the Debye mass squared [56, 97]. The latter includes contributions from the gluons and teen fields,

$$(m^2)^{ab,cd} = (m^2_{\text{gl}})^{ab,cd} + \frac{g^2 T_d^2}{4\pi^2}\mathcal{P}^{ab,cd} \ , \tag{2.61}$$

where

$$(m_{\rm gl}^2)^{ab,cd} = \frac{g^2T^2}{6}\left(\delta^{ad}\delta^{bc}\sum_{f=1}^{N_c}\left\{\mathcal{A}(Q^{af})+\mathcal{A}(Q^{fb})\right\} - 2\delta^{ab}\delta^{cd}\mathcal{A}(Q^{ac})\right) , \tag{2.62}$$

with

$$\mathcal{A}(Q) = \frac{12}{T^2}\int\frac{d^3k}{(2\pi)^3}\frac{1}{2E_k}\left(n(E_k-iQ)+n(E_k+iQ)\right) . \tag{2.63}$$

2.4.3 Teen self-energy

The diagrams which contribute to the teen self-energy are those of Fig. 2.7. There is a tadpole diagram, plus a diagram with a virtual gluon teen pair. As for the usual scalar self-

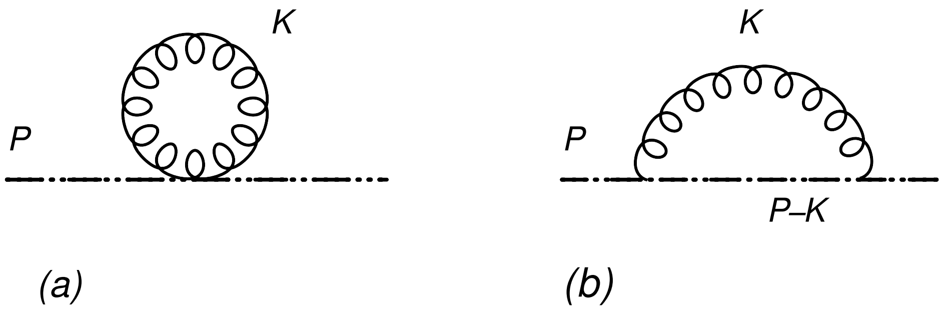

Figure 2.7: Teen self-energy diagrams

energy, the teen self-energy is gauge-dependent. Thus we content ourselves with power counting. The tadpole diagram, Fig. 2.7a, only involves a virtual gluon, and so is proportional to $\sim g^2T^2$. The diagram with a gluon-teen pair involves a virtual teen field, Fig. 2.7b involves an integral over a teen field, and so is automatically $\sim g^2T_d^2$. We shall see, however, that the teen self-energy does not enter into the computation of the shear and bulk viscosities at leading logarithmic order. As we demonstrate in the following, this is not obvious, and due to which the diagrams in detail contribute at leading logarithmic order.

2.5 Shear viscosity

2.5.1 Scattering amplitude

We follow the perturbative computation of the shear viscosity following Arnold, Moore, and Yaffe [98, 99, 114–119], modified to the case of nonzero holonomy [55, 87]. At leading logarithmic order, what contributes is the scattering of two to two scattering: two incident particles, with momenta P_1 and P_2, go into fields with momenta P_3 and P_4. The particles can be either gluon or teen fields. For $2 \to 2$ scattering, the Mandelstam variables are

$$s = (P_1 + P_2)^2 \ , \ t = (P_1 - P_3)^2 \ , \ u = (P_1 - P_4)^2 \ . \tag{2.64}$$

While we begin with Euclidean momenta, when evaluating the matrix elements, and quantities such as the Mandelstam variables, we blithely analytically continue to Minkowski momenta.

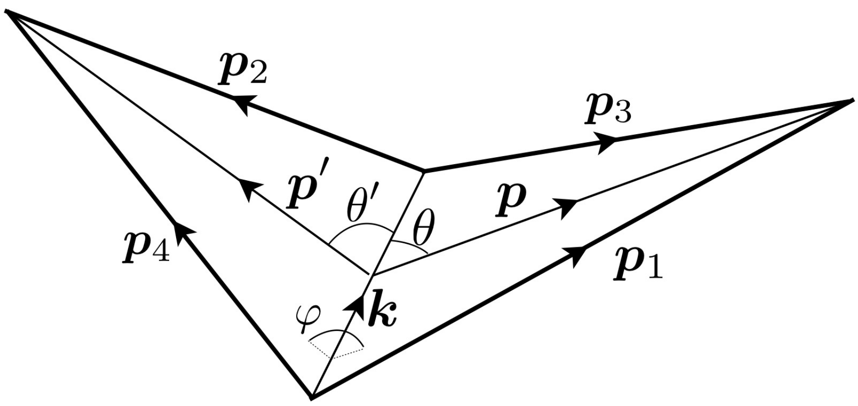

Figure 2.8: Kinematics of 2-2 scattering, from Ref. [86]

It is convenient to parametrize these momenta as

$$P_1 = P + \frac{K}{2}\ , \ P_2 = P' - \frac{K}{2}\ , P_3 = P - \frac{K}{2}\ , P_4 = P' + \frac{K}{2}\ . \tag{2.65}$$

The dominant contribution to the shear and bulk viscosities is forward scattering. The momenta P_1 and P_2, and P_3 and P_4, are hard, with the components of the momenta on the order of the temperature, T. The exchanged momentum in the t-channel, K, is soft, on the order of gT.

We introduce the angles θ and θ'

$$\cos\theta = \hat{\boldsymbol{k}} \cdot \hat{\boldsymbol{p}}\ , \qquad\qquad \cos\theta' = \hat{\boldsymbol{k}} \cdot \hat{\boldsymbol{p}}'\ , \tag{2.66}$$

as illustrated in Fig. 2.8. We define the unit vector $\hat{\boldsymbol{k}} = \boldsymbol{k}/k$, where $k = |\boldsymbol{k}|$, and ϕ as the angle between two planes spanned by vectors $(\boldsymbol{p}_1, \boldsymbol{p}_3)$ and $(\boldsymbol{p}_2, \boldsymbol{p}_4)$.

For forward scattering,

$$\cos\theta \simeq x \equiv \frac{k_0}{k}\ , \tag{2.67}$$

and $\theta \approx \theta'$, with

$$\cos\phi \simeq \frac{\hat{\boldsymbol{p}} \cdot \hat{\boldsymbol{p}}' - x^2}{1 - x^2}\ . \tag{2.68}$$

The Mandelstam variables become

$$\begin{aligned} s &\simeq 2pp'(1-x^2)(1-\cos\phi)\ , \\ u &\simeq -2pp'(1-x^2)(1-\cos\phi)\ , \\ t &\simeq -k^2(1-x^2)\ . \end{aligned} \tag{2.69}$$

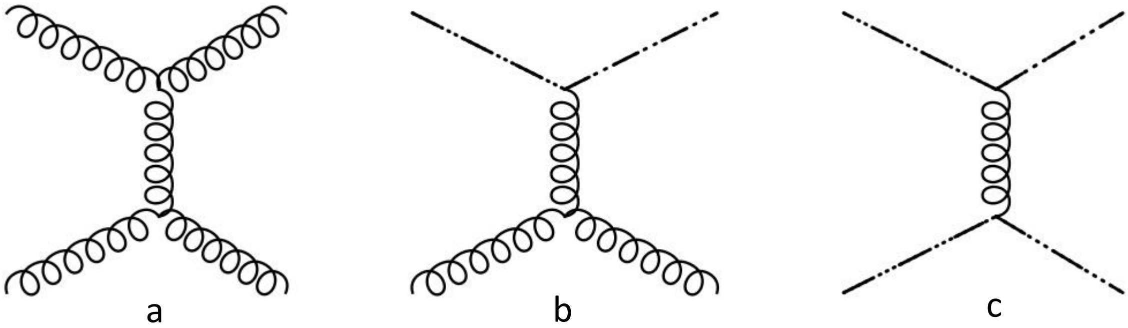

Figure 2.9: The diagrams involving the exchange of a virtual soft gluon: gluon-gluon scattering (a), gluon-teen scattering (b), and teen-teen scattering (c).

We only consider the diagrams that contribute to leading logarithmic order for the shear and bulk viscosity. These are the t- and u-channels, where a soft field is exchanged in the t-channel; the u-channel is related to the t-channel by exchanging $P_3 \leftrightarrow P_4$. All diagrams in the t- and u-channels were taken into account in computing the full result. Thus, we neglect diagrams where soft fields are exchanged in other channels, and diagrams with four-point interactions, which include those between four gluons, or two gluons and two teens.

The diagrams that contribute to leading logarithmic order are of two types. There are those involving the exchange of a soft gluon, illustrated in Figs. 2.9a-c, and those involving the exchange of a soft teen field, illustrated in Figs. 2.10a,b.

Exchange of a soft, virtual gluon

The amplitude for two gluons scattering into two gluons, Fig. 2.9a, is

$$\mathcal{M}_{\mathrm{gg}\to\mathrm{gg}} = \epsilon_1^{\mu_1}(P_1^{a_1b_1})\,\epsilon_3^{*\mu_3}(P_3^{a_3b_3})\,J^{\mu,ab}_{\mathrm{g},\mu_1\mu_3}(P_1^{a_1b_1},P_3^{a_3b_3})\,D^{ba,dc}_{\mu\nu}(K^{ba}) \\ \times\; J^{\nu,cd}_{\mathrm{g},\mu_2\mu_4}(P_2^{a_2b_2},P_4^{a_4b_4})\,\epsilon_2^{\mu_2}(P_2^{a_2b_2})\,\epsilon_4^{*\mu_4}(P_4^{a_4b_4})\,. \tag{2.70}$$

Here P_i^{μ,a_i,b_i} are the momenta for particles $i = 1, \ldots, 4$. The polarization tensor are $\epsilon^{\mu}_{1,2}$ for incoming particles, and $\epsilon^{*\mu}_{3,4}$ for outgoing fields. They satisfy

$$\epsilon_i^{\mu}(P_i^{a_ib_i})\, P^{a_ib_i}_{\mu,i} = \epsilon_i^{*\mu}(P_i^{a_ib_i})\, P^{a_ib_i}_{\mu,i} = 0\ . \tag{2.71}$$

In these expressions, we keep the color indices because especially Eq. (2.70) makes it clear how the color flow works. They really are not necessary in Eq. (2.71), though, since the on-shell condition only applies after analytic continuation to Minkowski momenta, $p_0^{ab} \to -i\omega$.

In Eq. (2.70), $D^{ba,dc}_{\mu\nu}(K^{ba})$ is the gluon propagator of Eq. (2.31). Now, the color current for a gluon is

$$J^{\mu,ab}_{\mathrm{g},\mu_1\mu_3}(P_1^{a_1b_1}, P_3^{a_3b_3}) = 2igP^{\mu,ab}\, \delta^{\mu_1\mu_3}\, t^{ab}_{a_1b_1,a_3b_3}\ . \tag{2.72}$$

We suppress the two spin indices for a spin-one gluon since that is just an overall degeneracy. The generator in the adjoint representation is

$$t^{ab}_{cd,ef} = i\, f^{(ab,cd,ef)} = \frac{i}{\sqrt{2}}\left(\delta^{ad}\delta^{cf}\delta^{be} - \delta^{af}\delta^{bc}\delta^{de}\right)\ , \tag{2.73}$$

as defined in Eq. (24) of Ref. [56]. In the matrix element, we only consider forward scattering, where $P_1^{a_1b_1} \simeq P_3^{a_3b_3} \simeq P^{ab}$. All of the external gluon momenta are hard, $P^{a_ib_i} \sim T$.

The scattering for a teen plus gluon scattering into the same is shown in Fig. 2.9b. The teen field has spin-zero, and so no spin degeneracy. The scattering amplitude in the t-channel is

$$\mathcal{M}_{\mathfrak{t}\mathrm{g}\to\mathfrak{t}\mathrm{g}} = J^{\mu,ab}_{\mathfrak{t}}(P_1^{a_1b_1}, P_3^{a_3b_3})\, D^{ba,dc}_{\mu\nu}(K^{ba})\, J^{\nu,cd}_{\mathrm{g},\mu_2\mu_4}(P_2^{a_2b_2}, P_4^{a_4b_4})\, \epsilon^{\mu_2}(P_2^{a_2b_2})\, \epsilon^{*\mu_4}(P_4^{a_4b_4})\ ,$$

(2.74)

where $J^{\mu;ab}_{\circlearrowleft}$ is the color current associated with teen ($\circlearrowleft$)-gluon vertex,

$$J^{\mu,ab}_{\circlearrowleft}(P_1^{a_1b_1}, P_3^{a_3b_3}) = 2igP^{\mu,ab}\, t^{ab}_{a_1b_1,a_3b_3} \,. \tag{2.75}$$

The color structure is identical to that of the gluon, Eq. (2.72), as both lie in the adjoint representation. Since the teen particle is a scalar, though, there is no factor of $\delta^{\mu_1\mu_3}$, as in the gluon current of Eq. (2.72).

There is another implicit difference: the perpendicular component of the teen momenta $P_1^{a_1b_1}$ and $P_2^{a_2b_2}$ are of the order of T_d. Thus, when a soft gluon is exchanged with $K \sim gT$, $k_\perp$ is also restricted to be $\sim T_d$.

The scattering amplitude for teen plus teen scattering into the same, Fig. 2.9c, is

$$\mathcal{M}_{\circlearrowleft\circlearrowleft\to\circlearrowleft\circlearrowleft} = J^{\mu;ab}_{\circlearrowleft}(P_1^{a_1b_1}, P_3^{a_3b_3})\, D^{ba,dc}_{\mu\nu}(K^{ba})\, J^{\nu;cd}_{\circlearrowleft}(P_2^{a_2b_2}, P_4^{a_4b_4}) \,. \tag{2.76}$$

Exchange of a soft teen field

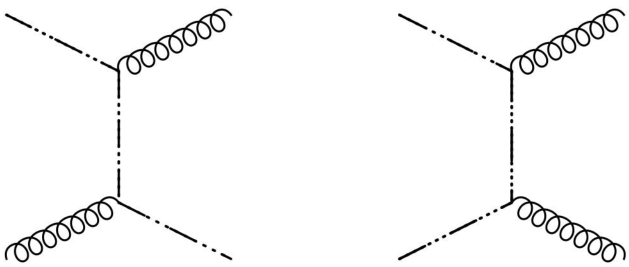

a b

Figure 2.10: The diagrams involving the exchange of a soft, virtual teen particle: Compton scattering (a) and teen-teen annihilation (b).

There are two diagrams involving the exchange of a teen particle. One contribution is where a teen plus a gluon scatters into a gluon plus a teen, Fig. 2.10a. This is analogous to Compton scattering. The amplitude is

$$\mathcal{M}_{\circlearrowleft g \to g \circlearrowleft} = \epsilon^{\mu}(P_1^{a_1 b_1})\, J_{\circlearrowleft}^{\mu,ab}(P_1^{a_1 b_1}, P_3^{a_3 b_3})\, D_{\circlearrowleft}^{ba,dc}(K^{ba})\, J_{\circlearrowleft}^{\nu,cd}(P_2^{a_2 b_2}, P_4^{a_4 b_4})\, \epsilon^{*\nu}(P_4^{a_4 b_4}) \; . \tag{2.77}$$

Lastly, there is the scattering of two teens into two gluons, illustrated in Fig. 2.10b. The amplitude is

$$\mathcal{M}_{\circlearrowleft\circlearrowleft \to gg} = J_{\circlearrowleft}^{\mu,ab}(P_1^{a_1 b_1}, P_3^{a_3 b_3})\, D_{\circlearrowleft}^{ba,dc}(K^{ba})\, J_{\circlearrowleft}^{\nu,cd}(P_2^{a_2 b_2}, P_4^{a_4 b_4}) \epsilon^{*\mu}(P_3^{a_3 b_3})\, \epsilon^{*\nu}(P_4^{a_4 b_4}) \; . \tag{2.78}$$

These are identical to the diagrams involving gluon exchange, with the replacement of the gluon by the teen particle.

The matrix elements for the teen particle, however, simplify significantly. Consider the factors of the polarization tensor for the scattering of two gluons into two gluons, Eq. (2.70). This involves

$$\mathcal{M}_{gg \to gg} \sim g^2 \; \left(\epsilon^{\mu_1}(P_1^{a_1 b_1})\epsilon^*_{\mu_1}(P_3^{a_3 b_3})\right) \; \left(\epsilon^{\mu_2}(P_2^{a_2 b_2})\epsilon^*_{\mu_2}(P_4^{a_4 b_4})\right) \; \ldots \; , \tag{2.79}$$

where for simplicity, we drop the other factors. For all of the other diagrams involving gluon exchange, the polarization tensors are contracted with one another, and so give contributions to leading order in the coupling constant, $\sim g^2$.

In contrast, consider the scattering of a teen plus gluon into a gluon plus teen, Fig. 2.10a.

Including just the factors of the polarization tensor, which is

$$\mathcal{M}_{\circlearrowleft \mathrm{g} \to \mathrm{g} \circlearrowright} \sim \; g^2 \; \left(\epsilon^{\mu} (P_1^{a_1 b_1}) P^{ab}_{\mu}\right) \; \left(\epsilon^{*\nu} (P_4^{a_4 b_4}) P^{ab}_{\nu}\right) \; \sim g^4 \; . \tag{2.80}$$

Each of the polarization vectors dotted into the momentum of that field vanishes, such as $\epsilon_1^{\mu} P_{1\mu}^{a_1 b_1} = 0$, *etc.*, Eq. (2.71). Then the momentum that appears in the current, $\sim P^{ab}_{\mu}$, is approximately equal to the external momenta, such as $P^{a_1 b_1}_{1\mu}$, up to soft corrections, $\sim K^{ba}_{\mu}$. These terms are, by assumption, suppressed by $\sim g$. Thus in all, the matrix elements involving the exchange of a teen particle, Fig. 2.10, are only $\sim g^4$, relative to those involving gluon exchange, Fig. 2.9, which are $\sim g^2$.

This cancellation for the scattering of the scalar field is well known. As discussed in Sec. 2.4.3, this is most fortunate, and these subtleties associated with constructing a complete, and gauge invariant description of the teen fields can thus be overlooked to leading logarithmic order.

2.5.2 Collision integrals

To evaluate the transport coefficients, we use kinetic theory. The Boltzmann equation described the evolution of the particle distribution function $f_{ab}(\boldsymbol{r}, \boldsymbol{p}, t)$ in phase space. The Boltzmann equation accounts for advection due to motion, external forces, and collisions among particles.

The Boltzmann equation is evaluated using the Chapman-Enskog method. The distribution function $f_{ab}(\boldsymbol{r}, \boldsymbol{p}, t)$ is expanded in a series in powers of the Knudsen number ϵ, which quantifies the ratio of the mean free path to the characteristic length scale of the system. This expansion assumes that the system is close to local equilibrium, allowing for the separation of equilibrium and non-equilibrium contributions to the distribution function.

At zeroth order ϵ^0, the collisions among particles are neglected, and the equilibrium distribution function f^0_{ab} is obtained. Deviations from equilibrium enter at ϵ^1. By substituting the zeroth-order solution into the Boltzmann equation and retaining terms linear in ϵ, a linearized Boltzmann equation is obtained. Solving this equation iteratively yields the first-order correction to the distribution function f^1_{ab}, capturing the effects of collisions on the distribution of particles.

The shear viscosity η is then extracted from the correction at first order, f^1_{ab}. This involves calculating the momentum flux tensor and comparing it to the gradient of the velocity field, quantifying the resistance to shear flow in the plasma.

Finally, the obtained expression for shear viscosity undergoes various consistency checks to ensure its physical validity. These checks may involve verifying that η is positive, and exhibits the correct behavior in the limit of a small Knudsen number.

The energy-momentum tensor for the gluon is given by

$$T^{\mu\nu}_{\mathrm{g}}(\boldsymbol{r},t) = 2\int_{\mathrm{g}} d\Gamma_{ab}\; P^{\mu,ab}P^{\nu,ab}\; f_{\mathrm{g},ab}(\boldsymbol{r},\boldsymbol{p},t)\;, \tag{2.81}$$

where $f_{\mathrm{g},ab}(\boldsymbol{r},\boldsymbol{p},t)$ is the statistical distribution function for the gluon. In thermal equilibrium, this is the Bose-Einstein distribution function in a background field $Q^a - Q^b$,

$$f^0_{\mathrm{g},ab} = f^0_{ab}(E_p) \equiv \frac{1}{\mathrm{e}^{(E_p - i(Q^a - Q^b))/T} - 1}\;, \tag{2.82}$$

with $E_p = \sqrt{\boldsymbol{p}^2}$ the energy. The phase space integral is

$$\int_{\mathrm{g}} d\Gamma_{ab} = \sum_s \sum_{a,b=1}^{N_c} \mathcal{P}^{ab,ba} \int \frac{d^3p}{(2\pi)^3 2E_p}\;. \tag{2.83}$$

This includes a sum over the colors a, b, and the helicity s. The factor $\mathcal{P}^{ab,ba}$ ensures that the overall number of degrees of freedom is $N_c^2 - 1$, as appropriate for $SU(N_c)$.

The teen field is analogous to a Faddeev-Popov ghost field and is an anti-commuting field in the adjoint representation. An anti-commuting field is normally a fermion. Fermions, however, are anti-periodic in the imaginary time, τ, under the shift $\tau \to \tau + 1/T$. Instead, in thermal equilibrium, the teen field should be periodic in τ, like a gluons. Consequently, for the teen field, we start with the statistical distribution function for a fermion, after shifting $(Q^a - Q^b)$ by πT:

$$\frac{1}{\mathrm{e}^{(E_p - i(Q^a - Q^b + \pi T))/T} + 1} = (-) f^0_{ab}(E) \; . \tag{2.84}$$

Thus absorption of a teen field from a thermal bath produces a relative minus sign, versus that of a gluon. This shows that the teen field is a ghost. To keep track of the signs, we introduce a sign function, which $= +1$ for gluons, and $= -1$ for teens,

$$\mathcal{S}_{\mathrm{g}} = +1 \quad ; \quad \mathcal{S}_{\circlearrowleft} = -1 \; . \tag{2.85}$$

In equilibrium, we find it useful to take the statistical distribution function for the teen equal to that for the gluon,

$$f^0_{\circlearrowleft,ab}(E_p) = (+) f^0_{\mathrm{g},ab}(E_p) \; . \tag{2.86}$$

If we take the distribution functions to be the same, then because there is a $(-)$ sign on the right hand side of Eq. (2.84), whenever a single factor of a statistical distribution function enters for absorption from the medium, $= f^0_{ab}(E)$, we have to multiply that by the sign function: $\mathcal{S}_{\circlearrowleft} = -1$ for a teen field, and $\mathcal{S}_{\mathrm{g}} = +1$ for a gluon.

This is *not* true for emission into the medium, however. For a fermion with a statistical distribution function $f^0_{\mathrm{ferm},ab}(E)$, emission is associated with the factor $1 - f^0_{\mathrm{ferm},ab}(E)$. In this case, the minus sign reflects the Pauli exclusion principle. For a teen field, then, by Eq. (2.84) this becomes $1 + f^0_{\mathrm{g},ab}(E)$. Thus for a teen field, there is *no* sign function, which arises when it is emitted into the medium. This is why we prefer to keep the signs of the teen and gluon distribution functions the same, Eq. (2.86), and instead introduce the sign functions $\mathcal{S}_{\text{ব}}$, *etc.*, for absorption.

It is useful to compare these signs to the case where gluons scatter off of physical fermions, which we do in Appendix A.1. Because they are physical, fermions do not have a $(-)$ sign when they are absorbed from the medium, while teen particles, which are ghosts, do.

The teen contribution to the stress-energy tensor is

$$T^{\mu\nu}_{\text{৩}} = 2 \int_{\text{৩}} d\Gamma_{ab}\; P^{\mu,ab} P^{\nu,ab}\; \mathcal{S}_{\text{৩}}\; f_{\text{৩},ab} \; . \tag{2.87}$$

This contributes to the pressure with a negative sign, which is what is expected for a ghost field. As explained previously, we need a ghost to decrease the pressure as the temperature is lowered, and the confined phase is approached.

While the gluon and teen distribution functions are equal in equilibrium, they differ away from equilibrium. Thus, there is a Boltzmann equation describing the evolution of each distribution function.

In the absence of collisions, for a system in the background gauge fields A_μ and with total color charge $\mathcal{Q}$, the gluon statistical distribution function satisfies the Vlasov equation [49, 84, 85],

$$P^\mu \left(\frac{\partial}{\partial x^\mu} - g \; \mathrm{tr}\left(\mathcal{Q} G_{\mu\nu}\right) \frac{\partial}{\partial p_\nu} - ig \left[\mathcal{Q}, \frac{\partial}{\partial \mathcal{Q}} \right] \right) f(x,p,\mathcal{Q}) = 0 \; . \tag{2.88}$$

In the semi-QGP, however, since $A_0^{\rm cl}$ is constant, the field strength vanishes, $G_{\mu\nu} = 0$. Further, as shown by Eq. (2.59), the total color charge vanishes $\mathcal{Q} = 0$. Thus, only the first term on the left hand side of Eq. (2.88) contributes, and we must consider the effect of collisions in the Boltzmann equation.

For collisions, we include the scattering of $2 \to 2$ particles to lowest order,

$$1_{\text{ব}}\, 2_{\text{দ}} \to 3_{\text{ব}'}\ 4_{\text{দ}'}\ . \tag{2.89}$$

The associated momenta are P_1^{μ,a_1b_1}, *etc.* We introduce the symbols ব, দ, ব$'$, and দ$'$ to denote that these particles can be either gluon or teen fields. The Boltzmann equation is

$$\mathcal{S}_{\text{ব}}\, 2P^{\mu,a_1b_1}\partial_\mu f_{\text{ব},a_1b_1}(\boldsymbol{x},\boldsymbol{p},t) = -\mathcal{C}_{\text{ব},a_1b_1}[f_{\text{ব}}]\ , \tag{2.90}$$

where the collisional kernel is

$$\begin{aligned}\mathcal{C}_{\text{ব},a_1b_1}[f_{\text{ব}}] = \frac{1}{2}\sum_{\text{দ},\text{ব}',\text{দ}'} &\mathcal{S}_{\text{ব}}\mathcal{S}_{\text{দ}}\int_{\text{দ}} d\Gamma_{a_2b_2}\int_{\text{ব}'} d\Gamma_{a_3b_3}\int_{\text{দ}'} d\Gamma_{a_4b_4}\,(2\pi)^4 \\ &\times \delta^{(4)}(P_1^{a_1b_1}+P_2^{a_2b_2}-P_3^{a_3b_3}-P_4^{a_4b_4})\,|\mathcal{M}_{\text{বদ}\to\text{ব}'\text{দ}'}|^2 \\ &\times \Big[f_{\text{ব},a_1b_1}f_{\text{দ},a_2b_2}\Big(1+f_{\text{ব}',a_3b_3}\Big)\Big(1+f_{\text{দ}',a_4b_4}\Big) \\ &\qquad -f_{\text{ব}',a_3b_3}f_{\text{দ}',a_4b_4}\Big(1+f_{\text{ব},a_1b_1}\Big)\Big(1+f_{\text{দ},a_2b_2}\Big)\Big]\ .\end{aligned} \tag{2.91}$$

The only subtlety is the sign factors. The sign factor $\mathcal{S}_{\text{ব}}$ enters on the left hand side of Eq. (2.90), as that describes the distribution function for the initial particle, $1_{\text{ব}}$.

On the right-hand side, in the collision term of Eq. (2.91), there are only symmetry factors for particles absorbed from the medium. This is $\mathcal{S}_{\text{ব}}\mathcal{S}_{\text{দ}}$ for the first term, and $\mathcal{S}_{\text{ব}'}\mathcal{S}_{\text{দ}'}$

for the second. Since teen number is conserved, however, the sign factors satisfy

$$\mathcal{S}_{ব}\,\mathcal{S}_{দ} = \mathcal{S}_{ব'}\,\mathcal{S}_{দ'}\ . \tag{2.92}$$

It is easy to convince oneself by working out all of the examples, such as ঙg $\to$ ঙg, *etc.* Because of this, in Eq. (2.91) we can write the sign factors of both terms as a common prefactor, $= \mathcal{S}_{ব}\,\mathcal{S}_{দ}$.

With the Chapman-Enskog method, the time derivative is expanded in the power of ϵ

$$\partial_t = \sum_{n=1}^{\infty} \epsilon^n \partial_t^{(n)}. \tag{2.93}$$

We expand the distribution function around the distribution function in thermal equilibrium, f^0_{ab},

$$f_{ব,ab} = f^0_{ab} + \epsilon f^1_{ব,ab} + \epsilon^2 f^2_{ব,ab} + \cdots\ . \tag{2.94}$$

Notice that the index ব does not enter into the distribution function as lowest order, because in equilibrium the gluon and teen distribution functions are the same as given in Eq. (2.86). Thus we generally replace $f^0_{ব,ab}(E)$ by $f^0_{ab}(E)$. We parametrize $f^n_{ব,ab}$ as

$$f^n_{ব,ab} = f^0_{ab}(1 + f^0_{ab})\phi^{(n)}_{ব,ab}\ . \tag{2.95}$$

Because we introduced the sign functions above, there is no need to introduce a sign function in the definition of $\phi^{(n)}_{ব,ab}$.

To ϵ^n order, the Boltzmann equation is

$$\mathcal{S}_{\text{ব}}\, 2P^{\mu,a_1b_1}\partial_\mu^{(n)} f_{\text{ব},a_1b_1} = -(\mathcal{L}\phi^{(n)})_{\text{ব},a_1b_1} + K^{(n)}_{\text{ব},a_1b_1}\ , \ K^{(n)}_{\text{ব},a_1b_1} = -\mathcal{C}^{(n)}_{\text{ব},a_1b_1} + (\mathcal{L}\phi^{(n)})_{\text{ব},a_1b_1}\ . \tag{2.96}$$

The linearized operator $\mathcal{L}$ is

$$\begin{aligned}(\mathcal{L}\phi^{(n)})_{\text{ব},a_1b_1} = \frac{1}{2}\sum_{\text{দ},\text{ব}',\text{দ}'} \mathcal{S}_{\text{ব}}\mathcal{S}_{\text{দ}} \int_{\text{দ}} d\Gamma_{a_2b_2} \int_{\text{ব}'} d\Gamma_{a_3b_3} \int_{\text{দ}'} d\Gamma_{a_4b_4} \\ \times\ (2\pi)^4\delta^{(4)}(P_1^{a_1b_1} + P_2^{a_2b_2} - P_3^{a_3b_3} - P_4^{a_4b_4})|\mathcal{M}_{\text{বদ}\to\text{ব}'\text{দ}'}|^2 \\ \times\ \left[f^0_{a_1b_1} f^0_{a_2b_2}(1+f^0_{a_3b_3})(1+f^0_{a_4b_4})\right]\left(\phi^{(n)}_{\text{ব},a_1b_1} + \phi^{(n)}_{\text{দ},a_2b_2} - \phi^{(n)}_{\text{ব}',a_3b_3} - \phi^{(n)}_{\text{দ}',a_4b_4}\right).\end{aligned} \tag{2.97}$$

The right-hand side includes a sum over both gluons and teens. To order ϵ^n,

$$P^{\mu,a_1b_1}\partial_\mu^{(n)} f_{\text{ব},a_1b_1} = p^{0,a_1b_1}\sum_{k=1}^{n}\partial_t^{(k)} f^{n-k}_{\text{ব},t,a_1b_1} + p^i\partial_i f^{n-1}_{\text{ব},t,a_1b_1}\ . \tag{2.98}$$

To leading logarithmic order in weak coupling , the viscosities are computed from

$$\mathcal{S}_{\text{ব}}\ 2P^{\mu,a_1,b_1}\partial_\mu^{(1)} f_{\text{ব},a_1b_1} = -(\mathcal{L}\phi^{(1)})_{\text{ব},a_1b_1}\ . \tag{2.99}$$

We set $K^1 = 0$, so that the right hand side of Eq. (2.99) is just the collision kernel, $(\mathcal{L}\phi^{(1)})_{\text{ব},a_1b_1} = \mathcal{C}^{(1)}_{\text{ব},a_1b_1}$.

We assume that near equilibrium, that the four velocity of the medium is βu^μ, where $\beta = 1/T$ is the temperature, and $u^\mu = (1,\boldsymbol{u})/\sqrt{1-\boldsymbol{u}^2}$ the velocity. It suffices to work to linear order in $|\boldsymbol{u}|$. Then, except for an overall factor of $\mathcal{S}_{\text{ব}}$, the left-hand side of the

Boltzmann equation is

$$
\begin{aligned}
2P^{\mu,a_1b_1}\partial_\mu^{(1)} f^0_{\text{ব},a_1b_1} &= -2P^{\mu,a_1b_1} f^0_{a_1b_1}(1+f^0_{a_1b_1})(P^{\nu,a_1b_1}\partial_\mu^{(1)}(\beta u_\nu) - i\partial_\mu^{(1)}\nu^{a_1b_1}) \\
&= -f^0_{a_1b_1}(1+f^0_{a_1b_1})\Big[2(P^{0,a_1b_1})^2\partial_t^{(1)}\beta + 2p^iP^{0,a_1b_1}(\partial_i\beta + \beta\partial_t^{(1)}u_i) \\
&\quad + p^jp^i\beta\sigma_{ij} - \frac{2}{3}p^2\beta\partial_k u^k - 2P^{\mu,a_1b_1}i\partial_\mu^{(1)}\nu^{a_1b_1}\Big] \ , \qquad (2.100)
\end{aligned}
$$

where

$$
\sigma_{ij} = \partial_i u_j + \partial_j u_i - \frac{2}{3}\,\delta^{ij}\,\partial_k u_k \ , \qquad (2.101)
$$

and $\nu^{ab} = \beta(Q^a - Q^b) = 2\pi(q_a - q_b)$.

Using energy-momentum conservation or hydrodynamic equations to leading order,

$$
\partial_t^{(1)}\beta \;=\; \beta v_s^2 \partial_i u^i \ , \qquad (2.102a)
$$

$$
\beta\partial_t^{(1)} u_i \;=\; -\partial_i\beta \ , \qquad (2.102b)
$$

where the speed of sound, squared, is

$$
v_s^2 = \frac{\partial \mathscr{P}}{\partial \mathscr{E}} \ , \qquad (2.103)
$$

we obtain

$$
2P^{\mu,a_1b_1}\partial_\mu^{(1)} f_{\text{ব},a_1b_1} = f^0_{a_1b_1}(1+f^0_{a_1b_1})\Big[2p^2\left(\frac{1}{3} - v_s^2\right)\beta\partial_i u^i - p^ip^j\beta\sigma_{ij}\Big] \ . \qquad (2.104)
$$

To obtain this expression, we have analytically continued $P^{0,a_1b_1} \to E_p = p$.

We have also dropped a term $\sim \partial_\mu^{(1)}\nu^{ab} = 2\pi\partial_\mu^{(1)}(q_a - q_b)$. By Eq. (2.102) this term is $\sim \partial_i u^i$ times $i\partial_T q_{a_1b_1} f^0_{a_1b_1}(1+f^0_{a_1b_1})$. As it is proportional to $\sim \partial_i u_i$, it only contributes to the bulk viscosity. Since $f^0_{a_1b_1}(1+f^0_{a_1b_1})$, and all other terms which contribute, are even under $a_1 \leftrightarrow b_1$, since $q_{a_1b_1} = -q_{b_1a_1}$ is odd, this cancels after summing over a_1 and b_1.

We also neglected the contribution of the thermal mass to the bulk viscosity. This contribution becomes non-negligible at high temperatures where $v_s^2 \sim 1/3$; however, near T_d, as discussed in Sec. 2.6, the deviation of v_s^2 from $1/3$ provides the dominant contribution in our model.

For the shear viscosity, we can drop the term $\sim \partial_i u^i$, and we are left with

$$2P^{\mu,a_1b_1}\partial^{(1)}_{\mu} f_{\text{ব},a_1b_1} \;\;=\;\; -\beta f^0_{a_1b_1}(1+f^0_{a_1b_1})p^ip^j\sigma_{ij}\ . \tag{2.105}$$

The term $\sim \partial_i u^i$ does contribute to the bulk viscosity, which we compute in the next section.

The Boltzmann equation becomes

$$\beta f^0_{a_1b_1}(1+f^0_{a_1b_1})p^ip^j\sigma_{ij} = \mathcal{S}_{\text{ব}}(\mathcal{L}\phi^{(1)})_{\text{ব},a_1b_1}\ . \tag{2.106}$$

Now, $\phi^{(1)}_{\text{ব},ab}$ can be parameterized as

$$\phi^{(1)}_{\text{ব},ab} = \sigma_{ij}\left(p^ip^j - \frac{1}{3}p^2\delta^{ij}\right)\chi_{\text{ব},ab}(p) = \sigma_{ij}\chi^{ij}_{\text{ব},ab}(p)\ , \tag{2.107}$$

and so we can write

$$\beta\left(p^ip^j - \frac{1}{3}p^2\delta^{ij}\right)f^0_{a_1b_1}(1+f^0_{a_1b_1}) = \mathcal{S}_{\text{ব}}(\mathcal{L}\chi^{ij})_{\text{ব},a_1b_1}\ . \tag{2.108}$$

The dissipative part of the energy-momentum tensor becomes

$$
\begin{aligned}
\delta T^{ij} &= \sum_{\text{ব}} 2\mathcal{S}_{\text{ব}} \int_{\text{ব}} d\Gamma_{ab}\, p^i p^j f^{(1)}_{\text{ব},ab} = \sum_{\text{ব}} 2\mathcal{S}_{\text{ব}} \int_{\text{ব}} d\Gamma_{ab}\, p^i p^j f^0_{ab} \Big(1 + f^0_{ab}\Big) \phi^{(1)}_{\text{ব},ab} \\
&= \sigma^{ij} \sum_{\text{ব}} \mathcal{S}_{\text{ব}}\, \frac{2}{5} \int_{\text{ব}} d\Gamma_{ab}\, \chi^{kl}_{\text{ব},ab} \left(p^k p^l - \frac{1}{3} p^2 \delta^{kl} \right) f^0_{ab} (1 + f^0_{ab}) \; . \qquad (2.109)
\end{aligned}
$$

Using Eq. (2.108) in the last equation, we can write

$$
\delta T^{ij} = \sigma^{ij} \frac{2T}{5} \sum_{\text{ব}} \int_{\text{ব}} d\Gamma_{ab} \chi^{kl}_{\text{ব},ab} (\mathcal{L}\chi^{kl})_{\text{ব},ab} \; . \qquad (2.110)
$$

The expression for the shear viscosity then reduces from $\delta T^{ij} = \eta \sigma^{ij}$ to

$$
\eta = \frac{2T}{5} \sum_{\text{ব}} \int_{\text{ব}} d\Gamma_{ab}\, \chi^{ij}_{\text{ব},ab} (\mathcal{L}\chi^{ij})_{\text{ব},ab} \; . \qquad (2.111)
$$

Thus we need to determine the functions $\chi^{ij}_{\text{ব},ab}$ for both gluons and teens. The case of gluons is familiar [120, 121]. Expanding $\chi_{\mathrm{g},ab}$ in orthogonal polynomials,

$$
\chi_{\mathrm{g},ab} = \sum_{n=0}^{\infty} c^{\mathrm{g}}_n\, \chi^{\mathrm{g}}_n(p) \; . \qquad (2.112)
$$

We define the d^{g}_n's as

$$
d^{\mathrm{g}}_n\, \delta_{mn} = \frac{1}{T^6} \sum_{ab,s} \mathcal{P}^{ab,ba} \int \frac{d^3 p}{(2\pi)^3 2E_p} f^0_{ab} (1 + f^0_{ab}) p^4\, \chi^{\mathrm{g}}_m(p)\, \chi^{\mathrm{g}}_n(p) \; . \qquad (2.113)
$$

Using Gram-Schmidt orthogonalization, we can then solve for the χ^{g}_n's. We choose

$$
\chi^{\mathrm{g}}_n = \sum_{m=0}^{n} b^{\mathrm{g}}_{nm} \left(\frac{p}{T} \right)^m \; , \qquad (2.114)
$$

with leading coefficients $b^{\rm g}_{nn} = 1$. The first few terms are

$$\chi^{\rm g}_0 = 1 \,, \tag{2.115a}$$

$$\chi^{\rm g}_1 = \frac{p}{T} + b^{\rm g}_{10} \,, \tag{2.115b}$$

$$\chi^{\rm g}_2 = \left(\frac{p}{T}\right)^2 + \left(\frac{p}{T}\right) \, b^{\rm g}_{21} + b^{\rm g}_{20} \,. \tag{2.115c}$$

This involves the dimensionless constants,

$$b^{\rm g}_{10} = -\frac{h_1}{h_0} \,, \tag{2.116a}$$

$$b^{\rm g}_{20} = \frac{h_1 h_3 - h_2^2}{h_0 h_2 - h_1^2} \,, \tag{2.116b}$$

$$b^{\rm g}_{21} = \frac{h_1 h_2 - h_0 h_3}{h_0 h_2 - h_1^2} \,. \tag{2.116c}$$

The h_n's are then

$$\begin{aligned} h_n &= \frac{1}{T^{6+n}} \sum_{ab,s} \mathcal{P}^{ab,ba} \int \frac{d^3p}{(2\pi)^3 2E_p} f^0_{ab}(1 + f^0_{ab}) p^{4+n} \\ &= \frac{1}{T^{6+n}} \sum_{ab,s} \mathcal{P}^{ab,ba} \int \frac{d^3p}{(2\pi)^3 2E_p} \frac{{\rm e}^{-(E_p - iQ^{ab})/T}}{(1 - {\rm e}^{(E_p - iQ^{ab})/T})^2} p^{4+n} \\ &= \frac{\Gamma(6+n)}{2\pi^2} \sum_{k=1}^{\infty} \frac{1}{k^{5+n}} \left(|{\rm Tr}\mathbf{L}^{\rm k}|^2 - 1 \right) \,. \end{aligned} \tag{2.117}$$

$\mathbf{L}$ is the thermal Wilson line, Eq. (2.1) of Sec. 2.2. The lowest $d^{\rm g}_n$ can be written in terms of h_n as

$$d^{\rm g}_0 = h_0 \,, \tag{2.118a}$$

$$d^{\rm g}_1 = h_2 + b_{10} h_1 \,, \tag{2.118b}$$

$$d_2^{\mathrm{g}} \;=\; h_4 + h_3 b_{21}^{\mathrm{g}} + h_2 b_{20}^{\mathrm{g}} \; . \tag{2.118c}$$

For the teen field, we proceed similarly. We expand $\chi_{\circlearrowleft,ab}$ in orthogonal polynomials,

$$\chi_{\circlearrowleft,ab} = \sum_{n=0}^{\infty} c_n^{\circlearrowleft} \, \chi_n^{\circlearrowleft}(p) \; , \tag{2.119}$$

and define

$$d_n^{\circlearrowleft} \, \delta_{mn} = \frac{1}{T^4 T_d^2} \sum_{a,b} \mathcal{P}^{ab,ba} \int_{\circlearrowleft} \frac{d^3p}{(2\pi)^3 2E_p} f_{ab}^0 (1 + f_{ab}^0) \, p^4 \; \chi_m^{\circlearrowleft}(p) \; \chi_n^{\circlearrowleft}(p) \; . \tag{2.120}$$

The momentum integral is that for a teen field, Eq. (2.39). Again by using Gram-Schmidt orthogonalization,

$$\chi_0^{\circlearrowleft} \;=\; 1 \; , \tag{2.121a}$$

$$\chi_1^{\circlearrowleft} \;=\; \frac{p}{T} + b_{10}^{\circlearrowleft} \; , \tag{2.121b}$$

$$\chi_2^{\circlearrowleft} \;=\; \left(\frac{p}{T}\right)^2 + \left(\frac{p}{T}\right) \, b_{21}^{\circlearrowleft} + b_{20}^{\circlearrowleft} \; , \tag{2.121c}$$

and

$$\begin{aligned} b_{10}^{\circlearrowleft} &= -\frac{t_1}{t_0} \; , \\ b_{20}^{\circlearrowleft} &= \frac{t_1 t_3 - t_2^2}{t_0 t_2 - t_1^2} \; , \\ b_{21}^{\circlearrowleft} &= \frac{t_1 t_2 - t_0 t_3}{t_0 t_2 - t_1^2} \; , \end{aligned} \tag{2.122}$$

where

$$
\begin{aligned}
t_n &= \frac{1}{T_d^2 T^{4+n}} \sum_{a,b} \mathcal{P}^{ab,ba} \int_{\text{ব}} \frac{d^3p}{(2\pi)^3 2E_p} f_{ab}(1+f_{ab}) p^{4+n} \\
&= \frac{1}{T_d^2 T^{4+n}} \sum_{a,b} \mathcal{P}^{ab,ba} \int \frac{p_\perp dp_\perp dp_\parallel}{(2\pi)^2 2E_{p_\parallel}} f_{ab}(1+f_{ab}) p_\parallel^{4+n} \\
&\approx \frac{\Gamma(4+n)}{8\pi^2} \sum_{k=1}^{\infty} \frac{1}{k^{3+n}} \left(|\mathrm{Tr}\mathbf{L}^{\mathrm{k}}|^2 - 1 \right) \ .
\end{aligned} \tag{2.123}
$$

The normalization constants $d_n^{\text{ঁ}}$ are obtained similarly as Eq. (2.118c). We have used the approximation $p_\parallel(\sim T) \gg p_\perp(\sim T_d)$ for the teen field.

Here one should note that for the integration over the teen field momentum we have used,

$$
\int_0^\infty dp\, p^2 = \int_0^{T_d} p_\perp\, dp_\perp \int_0^\infty dp_\parallel = \frac{T_d^2}{2} \int_0^\infty dp_\parallel \, . \tag{2.124}
$$

Using the Boltzmann equation,

$$
S_n^{\text{ব}} = (\mathcal{L}\, c)_n^{\text{ব}} \ , \tag{2.125}
$$

where

$$
S_n^{\text{ব}} = \mathcal{S}_{\text{ব}}\, \beta \int_{\text{ব}} d\Gamma_{ab}\, \chi^{ij}_{\text{ব},n} f^0_{ab}(1+f^0_{ab}) \left(p^i p^j - \frac{1}{3} p^2 \delta^{ij} \right) \ , \tag{2.126}
$$

and

$$
\begin{aligned}
(\mathcal{L}\, c)_n^{\text{ব}} &= \int_{\text{ব}} d\Gamma_{a_1 b_1}\, \chi^{ij}_{\text{ব},n} (\mathcal{L}\chi^{ij})_{\text{ব},a_1 b_1} \\
&= \frac{1}{2} \sum_{m=0}^{\infty} \sum_{\text{দ},\text{ব}',\text{দ}'} \mathcal{S}_{\text{ব}}\, \mathcal{S}_{\text{দ}} \int_{\text{ব}} d\Gamma_{a_1 b_1} \int_{\text{দ}} d\Gamma_{a_2 b_2} \int_{\text{ব}'} d\Gamma_{a_3 b_3} \int_{\text{দ}'} d\Gamma_{a_4 b_4} (2\pi)^4
\end{aligned}
$$

$$
\times \quad \delta^{(4)}(P_1^{a_1b_1} + P_2^{a_2b_2} - P_3^{a_3b_3} - P_4^{a_4b_4}) \;\left[f^0_{a_1b_1} f^0_{a_2b_2}(1 + f^0_{a_3b_3})(1 + f^0_{a_4b_4})\right]
$$

$$
\times \quad |\mathcal{M}_{\text{বদ}\to\text{ব}'\text{দ}'}|^2 \, \chi^{ij}_{\text{ব},n}\left(\chi^{ij}_{\text{ব},m} c^{\text{ব}}_m + \chi^{ij}_{\text{দ},m} c^{\text{দ}}_m - \chi^{ij}_{\text{ব}',m} c^{\text{ব}'}_m - \chi^{ij}_{\text{দ}',m} c^{\text{দ}'}_m\right) . \tag{2.127}
$$

The shear viscosity is then

$$
\eta = \frac{2T}{5} \sum_{\text{ব}} \sum_{n=0}^{\infty} c^{\text{ব}}_n (\mathcal{L}c)^{\text{ব}}_n = \frac{2T}{5} \sum_{\text{ব}} \sum_{n=0}^{\infty} S^{\text{ব}}_n (\mathcal{L}^{-1}S)^{\text{ব}}_n . \tag{2.128}
$$

To simplify the computation, we only take the lowest elements,

$$
S^{\mathrm{g}}_n = \frac{2T^5}{3} \, d^{\mathrm{g}}_0 \, \delta_{n,0} \;, \tag{2.129a}
$$

$$
S^{\text{ঁ}}_n = -\frac{2T_d^2 T^3}{3} \, d^{\text{ঁ}}_0 \, \delta_{n,0} \;. \tag{2.129b}
$$

This approximation is valid to a few percent for the theory with pure glue [98, 99] and with non-zero holonomy [56]. Given the coarseness of our approximations, we assume the same here.

2.5.3 Kinematics

We consider the scattering of two to two particles, বদ $\to$ বদ processes in Fig. 2.9. In Eq. (2.128) we can symmetrize between the $c^{\text{ব}}_n$'s, and rewrite

$$
\sum_{n,\text{ব}} c^{\text{ব}}_n (\mathcal{L}c)^{\text{ব}}_n = \sum_{n,m,\text{ব},\text{দ}} \Lambda^{\text{ব},\text{দ}}_{nm} \;, \tag{2.130}
$$

where

$$
\Lambda^{\text{ব},\text{দ}}_{nm} = \left(2\,\frac{1}{4}\right) \frac{1}{2} \, \mathcal{S}_{\text{ব}} \, \mathcal{S}_{\text{দ}} \int_{\text{ব}} d\Gamma_{a_1b_1} \int_{\text{দ}} d\Gamma_{a_2b_2} \int_{\text{ব}} d\Gamma_{a_3b_3} \int_{\text{দ}} d\Gamma_{a_4b_4} (2\pi)^4
$$

$$
\begin{aligned}
&\times\delta^{(4)}(P_1^{a_1b_1}+P_2^{a_2b_2}-P_3^{a_3b_3}-P_4^{a_4b_4})\ f^0_{a_1b_1}f^0_{a_2b_2}\big(1+f^0_{a_3b_3}\big)\big(1+f^0_{a_4b_4}\big)\\
&\times|\mathcal{M}_{\text{বদ}\to\text{বদ}}|^2\ \Big[\big(\chi^{ij}_{\text{ব},n}(p_1)-\chi^{ij}_{\text{ব},n}(p_3)\big)c_n^{\text{ব}}+\big(\chi^{ij}_{\text{দ},n}(p_2)-\chi^{ij}_{\text{দ},n}(p_4)\big)c_n^{\text{দ}}\Big]\\
&\times\Big[\big(\chi^{ij}_{\text{ব},m}(p_1)-\chi^{ij}_{\text{ব},m}(p_3)\big)c_m^{\text{ব}}+\big(\chi^{ij}_{\text{দ},m}(p_2)-\chi^{ij}_{\text{দ},m}(p_4)\big)c_m^{\text{দ}}\Big]\ . \qquad (2.131)
\end{aligned}
$$

In these expressions, the first factor of 2 is because $\text{বদ}\to\text{দব}$ gives the same contribution as $\text{বদ}\to\text{বদ}$ to leading logarithmic order [98]. The factor of $1/4$ is because we have symmetrized with respect to the $c_n^{\text{ব}}$'s.

Assuming that the dominant scattering is in the forward direction, with the momenta in the t-channel small,

$$
\begin{aligned}
\Lambda^{\text{ব},\text{দ}}_{nm} \ \simeq\ & \frac{1}{4}\mathcal{S}_{\text{ব}}\,\mathcal{S}_{\text{দ}}\int_{\text{ব}}d\Gamma_{a_1b_1}\int_{\text{দ}}d\Gamma_{a_2b_2}\int_{\text{ব}}d\Gamma_{a_3b_3}\int_{\text{দ}}d\Gamma_{a_4b_4}\\
&\times(2\pi)^4\delta^{(4)}(P_1^{a_1b_1}+P_2^{a_2b_2}-P_3^{a_3b_3}-P_4^{a_4b_4})|\mathcal{M}_{\text{বদ}\to\text{বদ}}|^2\\
&\times f^0_{a_1b_1}f^0_{a_2b_2}\big(1+f^0_{a_3b_3}\big)\big(1+f^0_{a_4b_4}\big)k^2(F^{\text{ব}}_{nm}(p,x)c_n^{\text{ব}}c_m^{\text{ব}}+F^{\text{দ}}_{nm}(p',x)c_n^{\text{দ}}c_m^{\text{দ}})\ ,
\end{aligned}
\qquad (2.132)
$$

with

$$
F^{\text{ব}}_{nm}(p,x)=2(1-x^2)p^2\chi^{\text{ব}}_n(p)\chi^{\text{ব}}_m(p)+\frac{2x^2}{3}(p^2\chi^{\text{ব}}_n(p))'(p^2\chi^{\text{ব}}_m(p))'\ , \qquad (2.133)
$$

where $x=k_0/k$ as defined in Eq. (2.67). In the limit of $k_0\to 0$, we can write

$$
\begin{aligned}
f^0_{a_1b_1}f^0_{a_2b_2}\big(1+f^0_{a_3b_3}\big)\big(1+f^0_{a_4b_4}\big) &= \sum_{n_4=0}^{\infty}\sum_{n_3=0}^{\infty}\sum_{n_2=1}^{\infty}\sum_{n_1=1}^{\infty}\exp\Big[-\beta\sum_{j=1}^{4}n_j(E_j-iQ^{a_jb_j})\Big]\\
\simeq \sum_{n_3,n_4=0}^{\infty}\sum_{n_1,n_2=1}^{\infty}&\mathcal{G}(Q,n_1,\ldots,n_4)\exp\big[-\beta\{(n_1+n_3)p+(n_2+n_4)p'\}\big]\ , \qquad (2.134)
\end{aligned}
$$

where

$$\mathcal{G}(Q, n_1, \ldots, n_4) = \exp\left[i\beta \sum_{j=1}^{4} n_j Q^{a_j b_j}\right] , \tag{2.135}$$

and we employed the expansion of the distribution function,

$$f^0_{ab}(E) = \sum_{n=1}^{\infty} \mathrm{e}^{-\beta n(E - iQ^{ab})} . \tag{2.136}$$

The form in Eq. (2.134) is useful, as we have factored the dependence upon the momenta from that upon the color charge.

Gluon-gluon scattering

At nonzero holonomy, first of all we consider the matrix elements for gluon-gluon (gg $\to$ gg) scatterings, that is given by

$$\begin{aligned}
\Lambda^{\mathrm{gg}}_{nm} &= 2\frac{g^4}{(2\pi)^5} \prod_{i=1}^{4} \sum_{a_i b_i} \sum_{n_1,n_2=1}^{\infty} \sum_{n_3,n_4=0}^{\infty} \mathcal{G}(Q, n_1, \ldots, n_4)\, t^{ab}_{13}\, t^{ba}_{24}\, t^{cd}_{13}\, t^{dc}_{24} \int_0^{\infty} dp\, p^2 e^{-\beta p(n_1+n_3)} \\
&\times \int_0^{\infty} dp' p'^2 e^{-\beta p'(n_2+n_4)} \int_{-1}^{1} dx\, (F^{\mathrm{g}}_{nm}(p,x) + F^{\mathrm{g}}_{nm}(p',x)) c^{\mathrm{g}}_n c^{\mathrm{g}}_m \int_{-\pi}^{\pi} \frac{d\phi}{2\pi} \int_0^{\infty} dk\, k^3 \\
&\times \Big\{ D^{ab}_L(K) + (1-x^2)\cos\phi D^{ab}_T(K) \Big\} \Big\{ D^{cd}_L(K) + (1-x^2)\cos\phi D^{cd}_T(K) \Big\}^* .
\end{aligned} \tag{2.137}$$

The detailed definitions of the longitudinal and transverse propagators, $D^{ab}_L(K)$ and $D^{ab}_T(K)$, are not required, since to leading logarithmic order [42],

$$\int dk\, k^3\, |D^{ab}_L(K) + (1-x^2)\cos\phi D^{ab}_T(K)|^2 \simeq \frac{1}{2}(1-\cos\phi)^2 \ln\left(\frac{\kappa}{g^2 N_c}\right) , \tag{2.138}$$

where $x = \cos(\theta)$ is defined in Eq. (2.67).

In Eq. (2.138), we introduce the parameter κ. This represents the uncertainty in our computation, which is only done to leading logarithmic order in weak coupling. Perturbatively, it can be computed by including effects at next to leading logarithmic order, following Ref. [99].

The angular integration becomes

$$\int_{-1}^{1} dx \int \frac{d\phi}{2\pi} \left[F^{\rm g}_{nm}(p,x) + F^{\rm g}_{nm}(p',x)\right](1-\cos\phi)^2 = \frac{20}{3}\sum_{l=0}^{n+m} C^{\rm g}_{nm,l}\left[p^2\left(\frac{p}{T}\right)^l + p'^2\left(\frac{p'}{T}\right)^l\right], \tag{2.139}$$

where

$$C^{\rm g}_{nm,l} = \sum_{r=0}^{n}\sum_{s=0}^{m} b^{\rm g}_{nr} b^{\rm g}_{ms}\left(1+\frac{1}{10}(rs+2l)\right)\delta_{r+s,l}\ . \tag{2.140}$$

Integrating over p and p', we obtain

$$\int dp\, p^2 e^{-\beta p(n_1+n_3)} \int dp' p'^{4+l}\beta^l e^{-\beta p'(n_2+n_4)} = \frac{2T^8\,\Gamma(5+l)}{(n_1+n_3)^3(n_2+n_4)^{5+l}}\ . \tag{2.141}$$

The matrix element becomes

$$\begin{aligned}\Lambda^{\rm gg}_{nm} \;&=\; 20g^4\frac{T^8}{\pi^5}\ln\left(\frac{\kappa}{g^2N_c}\right)\prod_{i=1}^{4}\sum_{a_ib_i}\sum_{n_1,n_2=1}^{\infty}\sum_{n_3,n_4=0}^{\infty}\mathcal{G}(Q,n_1,\ldots,n_4)\,t^{ab}_{13}\,t^{ba}_{24}\,t^{cd}_{13}\,t^{dc}_{24}\\ &\quad\times\frac{1}{(n_1+n_3)^3}\sum_{l=0}^{m+n}\frac{C^{\rm g}_{nm,l}}{(n_2+n_4)^{5+l}}\frac{\Gamma(5+l)}{24}c^{\rm g}_n c^{\rm g}_m\ .\end{aligned} \tag{2.142}$$

At large-N_c, this simplifies to

$$\Lambda^{\rm gg}_{nm} \;=\; \frac{10T^8(g^2N_c)^2N_c^2}{\pi^5}\ln\left(\frac{\kappa}{g^2N_c}\right)\mathcal{X}^{\rm gg}_{nm}c^{\rm g}_n c^{\rm g}_m\ , \tag{2.143}$$

with

$$\mathcal{X}^{\mathrm{gg}}_{nm} \;=\; \sum_{m_1=1}^{\infty}\sum_{m_2=1}^{\infty}\sum_{m_3=1}^{m_1}\sum_{m_4=1}^{m_2}\sum_{l=0}^{m+n}\frac{\ell_{m_1}}{m_1^3}\frac{\ell_{m_2}}{m_2^{5+l}}\,C^{\mathrm{g}}_{nm,l}\frac{\Gamma(5+l)}{\Gamma(5)}\ell_{m_1,m_2,m_3,m_4}\;, \tag{2.144}$$

where we define

$$\ell_{m_1,m_2,m_3,m_4} = \ell_{m_4-m_3}\ell_{m_2+m_3-m_1-m_4} + \ell_{m_1-m_3+m_4}\ell_{m_2+m_3-m_4}\;. \tag{2.145}$$

Gluon-teen scattering

For gluon-teen scattering, Fig. 2.9b,

$$\begin{aligned}\Lambda^{\mathrm{g}\circlearrowright}_{nm} = &-\frac{1}{2}2\frac{g^4}{(2\pi)^5}\prod_{i=1}^{4}\sum_{a_ib_i}\sum_{n_1,n_2=1}^{\infty}\sum_{n_3,n_4=0}^{\infty}\mathcal{G}(Q,n_1,\ldots,n_4)\,t^{ab}_{13}\,t^{ba}_{24}\,t^{cd}_{13}\,t^{dc}_{24}\int_0^{T_d}p_\perp dp_\perp\int_0^{\infty}dp_\parallel\\ &\times\; e^{-\beta p(n_1+n_3)}\int_0^{\infty}dp'p'^2e^{-\beta p'(n_2+n_4)}\int_{-1}^{1}dx\,(F^{\circlearrowright}_{nm}(p,x)c^{\circlearrowright}_nc^{\circlearrowright}_m + F^{\mathrm{g}}_{nm}(p',x)c^{\mathrm{g}}_nc^{\mathrm{g}}_m)\int_{-\pi}^{\pi}\frac{d\phi}{2\pi}\\ &\times\int_0^{\infty}dk\,k^3\left[D^{ab}_L(K)+(1-x^2)\cos\phi D^{ab}_T(K)\right]\left[D^{cd}_L(K)+(1-x^2)\cos\phi D^{cd}_T(K)\right]^*.\end{aligned} \tag{2.146}$$

We put $-1/2$ factor in the above equation because the teen has the negative sign, $\mathcal{S}_{\circlearrowright}=-1$, and has no spin. The k integration is the same as in Eq. (2.138). The angular integration becomes

$$\begin{aligned}\int dx\int\frac{d\phi}{2\pi}&\left[F^{\circlearrowright}_{nm}(p,x)+F^{\mathrm{g}}_{nm}(p',x)\right](1-\cos\phi)^2\\ &=\frac{20}{3}\sum_{l=0}^{n+m}\left[C^{\circlearrowright}_{nm,l}\left(\frac{p}{T}\right)^l p^2 + C^{\mathrm{g}}_{nm,l}\left(\frac{p'}{T}\right)^l p'^2\right]\,,\end{aligned} \tag{2.147}$$

where $C^{\mathrm{g}}_{nm,l}$ is given in Eq. (2.140) and

$$C^{\circlearrowleft}_{nm,l} = \sum_{r=0}^{n}\sum_{s=0}^{m} b^{\circlearrowleft}_{nr} b^{\circlearrowleft}_{ms}\left(1 + \frac{1}{10}(rs + 2l)\right)\delta_{r+s,l} \ . \tag{2.148}$$

Integrating over p and p', we get

$$\int p_\perp dp_\perp \int dp_\parallel e^{-\beta p_\parallel (n_1+n_3)} \int dp' p'^{4+l} \beta^l e^{-\beta p'(n_2+n_4)} = \frac{T^6\, T_d^2\, \Gamma(5+l)}{2(n_1+n_3)(n_2+n_4)^{5+l}} \ . \tag{2.149}$$

In this expression we approximate $p \approx p_\parallel$. We also require

$$\int p_\perp dp_\perp \int dp_\parallel\, p_\parallel^{2+l} e^{-\beta p (n_1+n_3)} \int dp' p'^2 \beta^l e^{-\beta p'(n_2+n_4)} = \frac{T^6\, T_d^2\, \Gamma(3+l)}{(n_1+n_3)^{3+l}(n_2+n_4)^3} \ . \tag{2.150}$$

The matrix element becomes

$$\begin{aligned}\Lambda^{\mathrm{g}\circlearrowleft}_{nm} = &-\frac{1}{2} 20 g^4 \frac{T_d^2\, T^6}{\pi^5} \ln\left(\frac{\kappa}{g^2 N_c}\right) \prod_{i=1}^{4} \sum_{a_i b_i} \sum_{n_1,n_2=1}^{\infty} \sum_{n_3,n_4=0}^{\infty} \mathcal{G}(Q, n_1, \ldots, n_4)\, t^{ab}_{13}\, t^{ba}_{24}\, t^{cd}_{13}\, t^{dc}_{24} \\ &\times \left[\frac{1}{n_1+n_3} \sum_{l=0}^{m+n} \frac{C^{\mathrm{g}}_{nm,l} c^{\mathrm{g}}_n c^{\mathrm{g}}_m}{(n_2+n_4)^{5+l}} \frac{\Gamma(5+l)}{8\Gamma(5)} + \frac{1}{(n_2+n_4)^3} \sum_{l=0}^{m+n} \frac{C^{\circlearrowleft}_{nm,l} c^{\circlearrowleft}_n c^{\circlearrowleft}_m}{(n_1+n_3)^{3+l}} \frac{\Gamma(3+l)}{48\Gamma(3)}\right] \ .\end{aligned} \tag{2.151}$$

Equation (2.151) further simplifies to

$$\Lambda^{\mathrm{g}\circlearrowleft}_{nm} \quad = \quad \frac{10 T_d^2 T^6 (g^2 N_c)^2 N_c^2}{\pi^5} \ln\left(\frac{\kappa}{g^2 N_c}\right) \left(\mathcal{X}'^{\mathrm{gg}}_{nm} c^{\mathrm{g}}_n c^{\mathrm{g}}_m + \mathcal{X}'^{\circlearrowleft\circlearrowleft}_{nm} c^{\circlearrowleft}_n c^{\circlearrowleft}_m\right) \ , \tag{2.152}$$

with

$$\mathcal{X}'^{\text{gg}}_{nm} = -\frac{1}{2}\sum_{m_1,m_2=1}^{\infty}\sum_{m_3=1}^{m_1}\sum_{m_4=1}^{m_2}\sum_{l=0}^{m+n}\frac{\ell_{m_1}}{m_1}\frac{\ell_{m_2}}{m_2^{5+l}}\frac{\Gamma(5+l)}{8\Gamma(5)}\,C^{\text{g}}_{nm,l}\;\ell_{m_1,m_2,m_3,m_4}\;, \tag{2.153a}$$

$$\mathcal{X}'^{\text{♋♋}}_{nm} = -\frac{1}{2}\sum_{m_1,m_2=1}^{\infty}\sum_{m_3=1}^{m_1}\sum_{m_4=1}^{m_2}\sum_{l=0}^{m+n}\frac{\ell_{m_1}}{m_1^{3+l}}\frac{\ell_{m_2}}{m_2^{3}}\frac{\Gamma(3+l)}{48\Gamma(3)}\,C^{\text{♋}}_{nm,l}\;\ell_{m_1,m_2,m_3,m_4}\;. \tag{2.153b}$$

Teen-teen scattering

We next turn to teen-teen scattering. The matrix elements in this case is

$$\begin{aligned}
\Lambda^{\text{♋♋}}_{nm} &= 2\frac{1}{4}\frac{g^4}{(2\pi)^5}\prod_{i=1}^{4}\sum_{a_ib_i}\sum_{n_1,n_2=1}^{\infty}\sum_{n_3,n_4=0}^{\infty}\mathcal{G}(Q,n_1,\ldots,n_4)\,t^{ab}_{13}\,t^{ba}_{24}\,t^{cd}_{13}\,t^{dc}_{24}\\
&\times \int_0^{T_d}p_\perp dp_\perp\int_0^\infty dp_\parallel\, e^{-\beta p(n_1+n_3)}\int_0^{T_d}p'_\perp dp'_\perp\int_0^\infty dp'_\parallel\, e^{-\beta p'(n_2+n_4)}\int_{-1}^{1}dx\\
&\times (F^{\text{♋}}_{nm}(p,x)+F^{\text{♋}}_{nm}(p',x))c^{\text{♋}}_n c^{\text{♋}}_m\int_{-\pi}^{\pi}\frac{d\phi}{2\pi}\int_0^\infty dk\,k^3\\
&\times \left\{D^{ab}_L(K)+(1-x^2)\cos\phi D^{ab}_T(K)\right\}\left\{D^{cd}_L(K)+(1-x^2)\cos\phi D^{cd}_T(K)\right\}^*.
\end{aligned} \tag{2.154}$$

We put the $1/4$ factor in front of the above equation because teen ghosts have no spin. Now, integrating over p and p',

$$\int p_\perp dp_\perp\int p'_\perp dp'_\perp\int dp_\parallel e^{-\beta p(n_1+n_3)}\int dp' p'^{2+l}\beta^l e^{-\beta p'(n_2+n_4)} = \frac{T^4\,T_d^4\,\Gamma(3+l)}{4(n_1+n_3)(n_2+n_4)^{3+l}}\;. \tag{2.155}$$

The matrix element becomes

$$\Lambda_{nm}^{\text{৩৩}} = 20\frac{1}{4}g^4\frac{T^4\,T_d^4}{\pi^5}\ln\left(\frac{\kappa}{g^2N_c}\right)\prod_{i=1}^{4}\sum_{a_ib_i}\sum_{n_1,n_2=1}^{\infty}\sum_{n_3,n_4=0}^{\infty}\mathcal{G}(Q,n_1,\ldots,n_4)\,t_{13}^{ab}\,t_{24}^{ba}\,t_{13}^{cd}\,t_{24}^{dc}$$
$$\times\frac{1}{(n_1+n_3)}\sum_{l=0}^{m+n}\frac{C_{nm,l}^{\text{৩}}c_n^{\text{৩}}c_m^{\text{৩}}}{(n_2+n_4)^{3+l}}\frac{\Gamma(3+l)}{96\,\Gamma(3)}\,. \tag{2.156}$$

Equation (2.156) simplifies as

$$\Lambda_{mn}^{\text{৩৩}} = \frac{10T^4\,T_d^4(g^2N_c)^2N_c^2}{\pi^5}\ln\left(\frac{\kappa}{g^2N_c}\right)\mathcal{X}_{nm}^{\text{৩৩}}c_n^{\text{৩}}c_m^{\text{৩}}\,, \tag{2.157}$$

with

$$\mathcal{X}_{nm}^{\text{৩৩}} = \frac{1}{4}\sum_{m_1,m_2=1}^{\infty}\sum_{m_3=1}^{m_1}\sum_{m_4=1}^{m_2}\sum_{l=0}^{m+n}\frac{\ell_{m_1}}{m_1}\frac{\ell_{m_2}}{m_2^{3+l}}C_{nm,l}^{\text{৩}}\frac{\Gamma(3+l)}{96\Gamma(3)}\ell_{m_1,m_2,m_3,m_4}\,. \tag{2.158}$$

In summary, Eq. (2.130) reduces to

$$\sum_{n,\text{ব}}c_n^{\text{ব}}(\mathcal{L}c)_n^{\text{ব}} = \frac{10(g^2N_c)^2N_c^2}{\pi^5}\ln\left(\frac{\kappa}{g^2N_c}\right)$$
$$\times\sum_{n,m}\begin{bmatrix}c_n^{\mathrm{g}} & c_n^{\text{৩}}\end{bmatrix}\begin{bmatrix}T^8\mathcal{X}_{nm}^{\mathrm{gg}}+T^6T_d^2\mathcal{X}_{nm}^{\prime\,\mathrm{gg}} & 0\\ 0 & T^4T_d^4\mathcal{X}_{nm}^{\text{৩৩}}+T^6T_d^2\mathcal{X}_{nm}^{\prime\,\text{৩৩}}\end{bmatrix}\begin{bmatrix}c_m^{\mathrm{g}}\\ c_m^{\text{৩}}\end{bmatrix}\,. \tag{2.159}$$

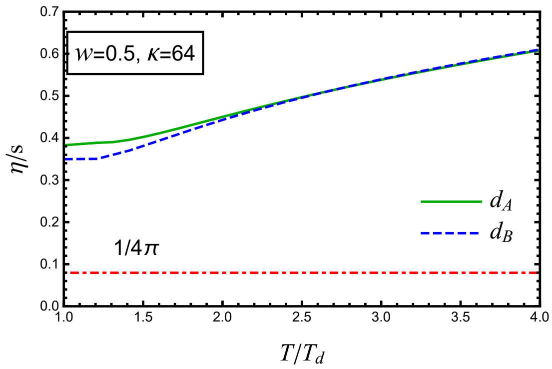

Figure 2.11: Ratio of the shear viscosity to the entropy with the ansatzes of Eq. (2.28). The dash-dot line denotes the value from AdS/CFT, $1/4\pi$.

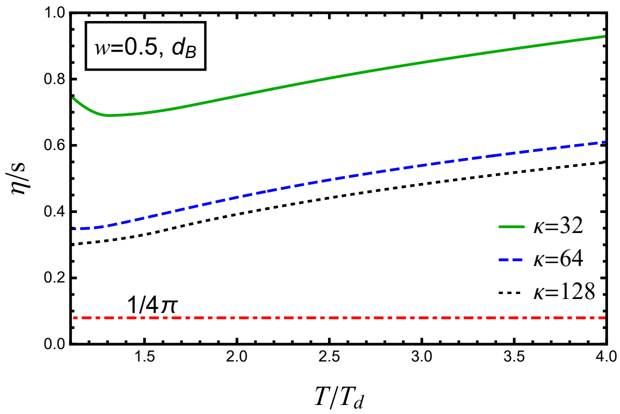

Figure 2.12: Ratio of the shear viscosity to the entropy for different parameter sets of κ. The values of the parameters $\kappa : 32, 64, 128$ are chosen so that η/s is relatively small.

2.5.4 Results for the shear viscosity

We make the extreme approximation of considering only $n = 0$. From Eq. (2.130) we write

$$\eta = \frac{2T}{5} \sum_{ব} c_0^{ব} (\mathcal{L}c)_0^{ব} \,, \tag{2.160}$$

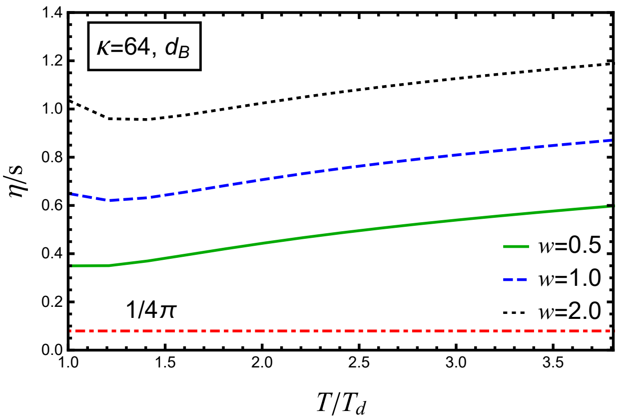

Figure 2.13: Ratio of the shear viscosity to the entropy for different parameter sets of w.

where the sum over ব includes that over gluon and teen fields. The final expression for the shear viscosity becomes

$$\eta = \frac{4\pi^5 T^3}{225(g(T)^2 N_c)^2 N_c^2 \ln(\kappa/g^2 N_c)} \left[\frac{(d_0^{\text{৩}})^2}{\chi_{00}^{\text{৩৩}} + \frac{T^2}{T_d^2}\chi_{00}^{\prime\text{৩৩}}} + \frac{(d_0^{\mathrm{g}})^2}{\chi_{00}^{\mathrm{gg}} + \frac{T_d^2}{T^2}\chi_{00}^{\prime\mathrm{gg}}} \right] . \tag{2.161}$$

Now we estimate the shear viscous coefficient η for the small value of the Polyakov loop. Neglecting higher moments (ℓ_n for $n \geq 2$) and power of ℓ_1,

$$\eta \;=\; \frac{16\pi}{5} \frac{12800T^4 - 3248T^2T_d^2 + 3T_d^2}{64T^4 - 20T^2T_d^2 + T_d^2} \frac{N_c^2 \; T^3}{10(g^2N_c)^2 \ln(\kappa/g^2N_c)} \, \ell_1^2 \, . \tag{2.162}$$

For pure gluonic cases without teen contribution, we have the following expression,

$$\begin{aligned} \eta_{\text{glue}} &= \frac{4\pi^5 T^3}{225(g(T)^2 N_c)^2 N_c^2 \ln(\kappa/g^2 N_c)} \frac{(d_0^{\mathrm{g}})^2}{\chi_{00}^{\mathrm{gg}}} \\ &= \frac{\pi^6}{270\zeta^2(5)} \, \ell_1^2 \, \eta_{\text{pert}} \simeq 3.31 \; \ell_1^2 \; \eta_{\text{pert}} \; , \end{aligned} \tag{2.163}$$

where $\eta_{\rm pert}$ is the shear viscosity at large N_c, in zero background field and given as

$$\eta_{\rm pert} \;=\; 540\zeta^2(5)\left(\frac{2}{\pi}\right)^5 \frac{T^3 N_c^2}{(g^2N_c)^2\ln(\kappa/g^2N_c)}\;, \tag{2.164}$$

which agrees with the previous works in the pure glue theory [86, 98, 122]. At small ℓ_1, the shear viscosity is $\eta\sim\ell_1^2$ for the gluonic medium with and without teens. This can be understood as $\eta\sim d_0^2/\chi_{00}\sim\ell_1^2$, where $d_0\sim\ell_1^2$ and $\chi_{00}\sim\ell_1$.

In Fig 2.11, we plot Eq. (2.161) for two ansatzes mentioned in Eq. (2.28). We adopt the functional form of the one-loop perturbative coupling for zero quark flavors ($N_f = 0$), as presented in Refs. [123, 124], to define a non-perturbative running coupling characterized by a single parameter w. For the running coupling, we take

$$g(T)^2N_c = 4\pi\frac{6\pi}{11\log(w2\pi T/T_d)}\;. \tag{2.165}$$

With the increasing temperature T, the coupling decreases, and the shear viscosity increases. With this form of the coupling constant, taking the values $w = 0.5$ and $\kappa = 64$, at T_d $\eta_{\rm pert}/s\approx 0.55$. We comment that we *choose* rather large values for $\kappa = 32, 64, 128$, so that that η/s is relatively small. Needless to say, it would be useful to compute beyond leading logarithmic order [99] to see if these values are reasonable.

Here and henceforth, to be self-consistent we used the entropy as computed from the matrix model. The difference from the entropy for $N_c = 3$ from the lattice is small.

In the matrix model, even with admittedly large values of κ, the ratio η/s is still well above that in Anti-de Sitter/Conformal Field Theory, AdS/CFT [125] bound. This is illustrated in the figures with a red dash-dotted line.

The dependence of shear viscosity on the parameters κ and w are shown in Figs. 2.12

and 2.13, respectively. The former is obtained by varying κ with a fixed value of energy scale πT i.e., $w = 0.5$. With increasing κ, the value of the viscosity reaches towards the AdS/CFT bound. These results are shown for one ansatz d_B. One will obtain a similar result for another ansatz with a marginal difference. As the QCD coupling is not well-known near the transition, we show the plots varying w. Figure 2.13 shows the results for different energy scales around $2\pi T$, i.e., for $w = 0.5, 1, 2$.

In Fig. 2.14, we compare our results with zero background field case. The green line represents the ratio of shear viscosity accounting for teen-teen, teen-gluon, and gluon-gluon scattering compared to gluon-gluon scattering in zero background field, whereas, the red line indicates the ratio of viscosity only including gluon-gluon scattering in presence and absence of the background fields. In the presence of background fields, these additional contributions, particularly from teens as ghost fields, lead to a rise in the overall viscosity. The inclusion of teen-teen and teen-gluon scattering contributes around 6% to the viscosity near T_d.

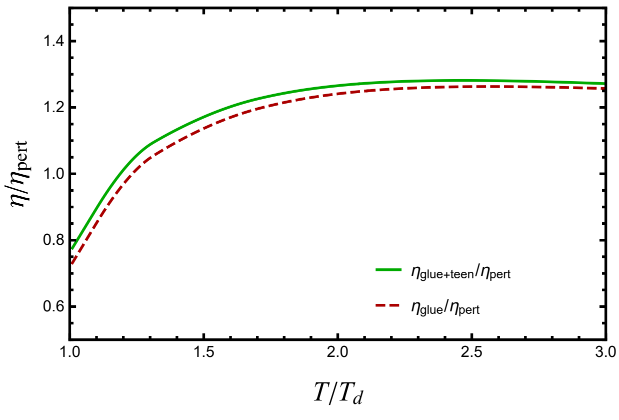

Figure 2.14: The green line denotes the ratio of the shear viscosity including teen-teen, teen-gluon, and gluon-gluon scattering, to that with perturbative gluon-gluon scattering. The red-dashed line indicates the ratio of the shear viscosity including just gluon-gluon scattering, to that with perturbative. As a ghost field, the contribution with teens increases the total shear viscosity.

2.6 Bulk Viscosity

We next compute the bulk viscosity. While of utmost importance for phenomenology, in perturbation theory, it is more difficult to extract. The bulk viscosity vanishes for any conformal theory, so in gauge theory, it is strongly suppressed relative to the shear viscosity. As shown by Arnold, Dugan, and Moore [100], the bulk viscosity only arises because quarks and gluons develop a thermal "mass" $\sim gT$. Even then, it is necessary to include the running of the coupling constant with temperature. Consequently, the bulk viscosity is suppressed by $\sim g^8$ and is $\zeta \sim g^4$, relative to the shear viscosity, $\eta \sim 1/g^4$.

In contrast, in our matrix model the theory is not conformally invariant if the Polyakov loops are less than unity, since then there must be a non-trivial distribution for the eigenvalues of the thermal Wilson line. Thus while in perturbation theory it is involved to measure the deviation from conformality through the bulk viscosity, in our matrix model it is straightforward. In particular, we can compute in precisely the same way as for the shear viscosity, to leading logarithmic order in the coupling constant. As we show, the bulk viscosity is nonzero because the speed of sound squared is not equal to $1/3$; *i.e.*, the theory is not conformal.

For the bulk viscosity, from Eq. (2.104),

$$2P^{\mu,a_1b_1}\partial^{(1)}_\mu f_{\sphericalangle,a_1b_1} = \beta f^0_{a_1b_1}(1+f^0_{a_1b_1})\mathrm{X}q(|\boldsymbol{p}|) \ , \tag{2.166}$$

where

$$\mathrm{X} = \nabla\cdot\boldsymbol{u} \ , \tag{2.167}$$

and

$$q(p) = 2p^2\left(\frac{1}{3} - v_s^2\right) \equiv 2p^2\Delta v_s^2 \ , \tag{2.168}$$

with v_s^2 the speed of sound, squared, Eq. (2.103). In a conformally invariant theory $v_s^2 = 1/3$ and the bulk viscosity vanishes. In our matrix model, the dominant source of conformal symmetry breaking is from $v_s^2 \neq 1/3$ as discussed below.

We expand the statistical distribution functions to linear order,

$$f^{(n)}_{\text{ব},ab} = f^0_{ab}\,(1 + f^0_{ab})\psi^{(n)}_{\text{ব},ab}\ . \tag{2.169}$$

Analogous to Eq. (2.106), then, the Boltzmann equation is written as

$$\beta f^0_{a_1b_1}(1 + f^0_{a_1b_1})\mathrm{X}q(|\boldsymbol{p}|) = -\mathcal{S}_{\text{ব}}(\bar{\mathcal{L}}\psi^{(1)})_{\text{ব},a_1b_1}\ , \tag{2.170}$$

where $\bar{\mathcal{L}}$ is a linear operator,

$$\begin{aligned}
(\bar{\mathcal{L}}\psi^{(n)})_{\text{ব},a_1b_1} &= \frac{1}{2}\sum_{\text{দ},\text{ব}',\text{দ}'} \mathcal{S}_{\text{ব}}\mathcal{S}_{\text{দ}}\int_{\text{দ}} d\Gamma_{a_2b_2}\int_{\text{ব}'} d\Gamma_{a_3b_3}\int_{\text{দ}'} d\Gamma_{a_4b_4}\,(2\pi)^4 \\
\times\ & \delta^{(4)}(P_1^{a_1b_1} + P_2^{a_2b_2} - P_3^{a_3b_3} - P_4^{a_4b_4})|\mathcal{M}_{\text{বদ}\to\text{ব}'\text{দ}'}|^2 \\
\times\ & \left[f^0_{a_1b_1}f^0_{a_2b_2}(1 + f^0_{a_3b_3})(1 + f^0_{a_4b_4})\right]\left(\psi^{(n)}_{\text{ব},a_1b_1} + \psi^{(n)}_{\text{দ},a_2b_2} - \psi^{(n)}_{\text{ব}',a_3b_3} - \psi^{(n)}_{\text{দ}',a_4b_4}\right)\ .
\end{aligned} \tag{2.171}$$

Here, the operator $\bar{\mathcal{L}}$ is the same as $\mathcal{L}$ in Eq. (2.97), with the bar added to emphasize its role in describing the bulk viscosity.

The bulk viscosity is defined by the change in pressure caused by the deviation from equilibrium $\psi_{\text{ব}}$. The bulk viscosity, ζ, is given by [100]

$$\zeta = -\sum_{\text{ব}}\mathcal{S}_{\text{ব}}\int_{\text{ব}} d\Gamma_{a_1b_1}\,q(|\boldsymbol{p}|)f^0_{a_1b_1}(1 + f^0_{a_1b_1})\psi_{\text{ব}}(p)\ . \tag{2.172}$$

The source term, $f^0_{a_1b_1}(1+f^0_{a_1b_1})q(|\boldsymbol{p}|)$, in Eq. (2.170) can be written in terms of an expansion basis as

$$V_{\text{ব},n} = \mathcal{S}_{\text{ব}} \int_{\text{ব}} d\Gamma_{a_1b_1}\, 2p^2 \psi^{\text{ব}}_n \beta f^0_{a_1b_1}(1+f^0_{a_1b_1})\, \Delta v_s^2 \,, \tag{2.173}$$

giving us $V_{\text{ব},n} = -(\bar{\mathcal{L}}\bar{c})^{\text{ব}}_n$. Here, we expanded $\psi^{\text{ব}}$ in an orthogonal basis equivalent to Eq. (2.112) as $\psi^{\text{দ}} = \sum_n \bar{c}^{\text{দ}}_n \psi^{\text{দ}}_n$. Finally, the coefficient of bulk viscosity from Eq. (2.172) becomes

$$\begin{aligned}
\zeta &= T\sum_{\text{ব}} \int_{\text{ব}} d\Gamma_{a_1b_1} \psi_{\text{ব}} (\bar{\mathcal{L}}\psi)_{\text{ব}} \\
&= T\sum_{\text{ব}} \sum_{n=0}^{\infty} V^{\text{ব}}_n \left(\bar{\mathcal{L}}^{-1}V\right)^{\text{ব}}_n = T\sum_{\text{ব}} \sum_{n=0}^{\infty} \bar{c}^{\text{ব}}_n (\bar{\mathcal{L}}\bar{c})^{\text{ব}}_n \,.
\end{aligned} \tag{2.174}$$

In Appendix A.2, we show that if one computes the pressure for a teen field from kinetic theory, then one obtains $\mathscr{P}_{\text{teen}} = -T^2T_d^2/72$, with the energy $\mathscr{E} = -T^2T_d^2/24$. That is, in kinetic theory teen quasiparticles still look three-dimensional, with $\mathscr{E} = 3\mathscr{P}_{\text{teen}}$. In Appendix A.2, we argue how a kinetic theory of two dimensional teen particles can arise, with $\mathscr{E} = \mathscr{P}_{\text{teen}} = -T^2T_d^2/24$ [97], as in thermodynamics.

In practice, we *define* our model such that in Eq. (2.174), the deviation from conformality, Δv_s^2, is computed from *thermodynamics*. After all, in our model the teen fields are not really two-dimensional, but defined with the functions $d_A(T)$ and $d_B(T)$, which are fit to obtain $(\mathscr{E}-3\mathscr{P})/T^4$ from the lattice, Eq. (2.28). Except for the contribution to Δv_s^2, though, we compute Eq. (2.174) using gluon and teen quasiparticles in the semi-QGP. We believe that this ansatz yields a reasonable estimate of the bulk viscosity.

With this assumption, following Ref. [100], we use a simple ansatz for the basis functions, ψ^{g},

$$\psi^{\mathrm{g}}_m = \frac{T}{(1+p/T)^{K-2}} \left(\frac{p}{T}\right)^m , \qquad m = 1, 2, \cdots , K \ . \tag{2.175}$$

Here, the ψ^{g}_m are not necessarily orthogonal. We take a different basis for the $\psi^{\text{৩}}_m$ as

$$\psi^{\text{৩}}_m = \frac{T}{(1+p/T)^{K-4}} \left(\frac{p}{T}\right)^m , \qquad m = 1, 2, \cdots , K \ . \tag{2.176}$$

By trial and error, we found that a different basis for the teen functions, Eq. (2.176), converges more quickly (at $K \sim 30$) than if we take the same basis as for gluons, Eq. (2.175).

For a single order basis, i.e., $K = 1$, we get

$$\begin{aligned} V_{\mathrm{g},1} &= 2(\Delta v_s^2)\, \frac{24T^4}{2\pi^2} \sum_{k=1}^{\infty} \frac{N_c^2 \ell_k^2 - 1}{k^5} (5+k) \ , && (2.177) \\ V_{\text{৩},1} &= -(\Delta v_s^2)\, \frac{T^2 T_d^2}{4\pi^2} \sum_{k=1}^{\infty} \frac{N_c^2 \ell_k^2 - 1}{k^5} (60 + 36k + 9k^2 + k^3) \ . && (2.178) \end{aligned}$$

Equation (2.177) shows the order of temperature V_{g} and $V_{\text{৩}}$ contributes to the bulk viscosity computation. But beyond $K = 1$, it is also necessary to treat the zero modes in the operator for the bulk viscosity. This is discussed in Appendix A.3. In the next section, we have computed bulk viscosity results for $K \sim 20 - 30$, shown in Figs. 2.15, 2.16, and 2.17.

2.6.1 Matrix Elements at Leading logarithmic order

Analogous to Eq. (2.131), the matrix element form for the ব-দ scattering becomes

$$\begin{aligned} \bar{\Lambda}^{\text{ব},\text{দ}}_{mn} &= \left(2\frac{1}{4}\right) \frac{1}{2} \mathcal{S}_{\text{ব}} \mathcal{S}_{\text{দ}} \int_{\text{ব}} d\Gamma_{a_1 b_1} \int_{\text{দ}} d\Gamma_{a_2 b_2} \int_{\text{ব}} d\Gamma_{a_3 b_3} \int_{\text{দ}} d\Gamma_{a_4 b_4}\, (2\pi)^4 \\ &\times \delta^{(4)}(P_1^{a_1 b_1} + P_2^{a_2 b_2} - P_3^{a_3 b_3} - P_4^{a_4 b_4}) |\mathcal{M}_{\text{বদ} \to \text{বদ}}|^2 f^0_{a_1 b_1} f^0_{a_2 b_2} \big(1 + f^0_{a_3 b_3}\big) \big(1 + f^0_{a_4 b_4}\big) \\ &\times \left[(\psi_1^{\text{ব},m} - \psi_3^{\text{ব},m}) \bar{c}^{\text{ব}}_n + (\psi_2^{\text{দ},m} - \psi_4^{\text{দ},m}) \bar{c}^{\text{দ}}_n \right] \left[(\psi_1^{\text{ব},n} - \psi_3^{\text{ব},n}) \bar{c}^{\text{ব}}_m + (\psi_2^{\text{দ},n} - \psi_4^{\text{দ},n}) \bar{c}^{\text{দ}}_m \right] \ . \end{aligned}$$

(2.179)

If the momentum transfer in the scattering process is small, we get

$$\psi_1^{\text{ব}} - \psi_3^{\text{ব}} \simeq \boldsymbol{k} \cdot \partial_{\boldsymbol{p}} \psi^{\text{ব}}(p) \ , \quad \psi_2^{\text{ব}} - \psi_4^{\text{ব}} \simeq -\boldsymbol{k} \cdot \partial_{\boldsymbol{p}'} \psi^{\text{ব}}(p') \ , \tag{2.180}$$

where we have used $\boldsymbol{p} \equiv (\boldsymbol{p}_1 + \boldsymbol{p}_3)/2$ and $\boldsymbol{p}' \equiv (\boldsymbol{p}_2 + \boldsymbol{p}_4)/2$, $x \equiv k_0/k \simeq \cos\theta_{\boldsymbol{pk}} \simeq \cos\theta_{\boldsymbol{p'k}}$ from Eqs. (2.65)-(2.67). In the small momentum transfer limit, the matrix element from Eq. (2.179) becomes

$$\begin{aligned}
\bar{\Lambda}_{mn}^{\text{ব},\text{দ}} &= 2\frac{g^4}{(2\pi)^5}\frac{\sigma_{\text{ব}}\sigma_{\text{দ}}}{4}\mathcal{S}_{\text{ব}}\mathcal{S}_{\text{দ}}\prod_{i=1}^{4}\sum_{a_i,b_i}\sum_{n_1,n_2=1}^{\infty}\sum_{n_3,n_4=0}^{\infty}\mathcal{G}(Q,n_1,\cdots,n_4)t_{13}^{ab}\,t_{24}^{ba}\,t_{13}^{cd}\,t_{24}^{dc} \\
&\times\int_0^\infty dp\,p^2 e^{-\beta p(n_1+n_3)}\int_0^\infty dp'\,p'^2\,e^{-\beta p'(n_2+n_4)}\int_0^{2\pi}\frac{d\phi}{2\pi}\int_{-1}^{1}dx\int_0^\infty dk\,k^3 \\
&\times|D_L^{ab}(K)+(1-x^2)\cos\phi\,D_T^{ab}(K)|^2\left[\bar{c}_m^{\text{ব}}\,\hat{\boldsymbol{k}}\cdot\partial_{\boldsymbol{p}}\psi^{\text{ব},m}(p)-\bar{c}_m^{\text{দ}}\,\hat{\boldsymbol{k}}\cdot\partial_{\boldsymbol{p}'}\psi^{\text{দ},m}(p')\right] \\
&\times\left[\bar{c}_n^{\text{ব}}\,\hat{\boldsymbol{k}}\cdot\partial_{\boldsymbol{p}}\psi^{\text{ব},n}(p)-\bar{c}_n^{\text{দ}}\,\hat{\boldsymbol{k}}\cdot\partial_{\boldsymbol{p}'}\psi^{\text{দ},n}(p')\right] \ .
\end{aligned} \tag{2.181}$$

Here, $\sigma_{\text{ব}}$ represents the spin degeneracy; $\sigma_{\text{g}} = 2$ and $\sigma_{\text{৩}} = 1$. We assume rotational invariance, $\psi^{\text{ব},n}(\boldsymbol{p}) = \psi^{\text{ব},n}(p)$, so that

$$\left[\bar{c}_m^{\text{ব}}\,\hat{\boldsymbol{k}}\cdot\partial_{\boldsymbol{p}}\psi^{\text{ব},m}(p)-\bar{c}_m^{\text{দ}}\,\hat{\boldsymbol{k}}\cdot\partial_{\boldsymbol{p}'}\psi^{\text{দ},m}(p')\right] = x\left[\bar{c}_m^{\text{ব}}\,(\psi_m^{\text{ব}})'(p)-\bar{c}_m^{\text{দ}}\,(\psi_m^{\text{দ}})'(p')\right] \ . \tag{2.182}$$

Hence, using Eq. (2.182) we can rewrite Eq. (2.181) as

$$\begin{aligned}
\bar{\Lambda}_{mn}^{\text{ব},\text{দ}} &= \frac{g^4}{(2\pi)^5}\frac{\sigma_{\text{ব}}\sigma_{\text{দ}}}{4}\log\left(\frac{\kappa}{g^2N_c}\right)\mathcal{S}_{\text{ব}}\mathcal{S}_{\text{দ}}\prod_{i=1}^{4}\sum_{a_i,b_i}\sum_{n_1,n_2=1}^{\infty}\sum_{n_3,n_4=0}^{\infty}\mathcal{G}(Q,n_1,\cdots,n_4)t_{13}^{ab}\,t_{24}^{ba}\,t_{13}^{cd}\,t_{24}^{dc} \\
&\times\int_0^\infty dp\,p^2\,e^{-\beta p(n_1+n_3)}\int_0^\infty dp'\,p'^2\,e^{-\beta p'(n_2+n_4)}\int_0^{2\pi}\frac{d\phi}{2\pi}(1-\cos\phi)^2\int_{-1}^{1}dx\,x^2
\end{aligned}$$

$$
\begin{aligned}
&\times \left[\bar{c}^{\text{ব}}_m\,(\psi^{\text{ব}}_m)'(p) - \bar{c}^{\text{দ}}_m\,(\psi^{\text{দ}}_m)'(p')\right]\left[\bar{c}^{\text{ব}}_n\,(\psi^{\text{ব}}_n)'(p) - \bar{c}^{\text{দ}}_n\,(\psi^{\text{দ}}_n)'(p')\right] \\
= \quad & \frac{g^4}{(2\pi)^5}\frac{\sigma_{\text{ব}}\sigma_{\text{দ}}}{4}\log\left(\frac{\kappa}{g^2 N_c}\right)\mathcal{S}_{\text{ব}}\mathcal{S}_{\text{দ}}\prod_{i=1}^{4}\sum_{a_i,b_i}\sum_{n_1,n_2=1}^{\infty}\sum_{n_3,n_4=0}^{\infty}\mathcal{G}(Q,n_1,\cdots,n_4)t^{ab}_{13}\,t^{ba}_{24}\,t^{cd}_{13}\,t^{dc}_{24} \\
&\times \int_0^\infty dp\,p^2\,e^{-\beta p(n_1+n_3)}\int_0^\infty dp'\,p'^2\,e^{-\beta p'(n_2+n_4)}\left[\bar{c}^{\text{ব}}_m\,(\psi^{\text{ব}}_m)'(p) - \bar{c}^{\text{দ}}_m\,(\psi^{\text{দ}}_m)'(p')\right] \\
&\times \left[\bar{c}^{\text{ব}}_n\,(\psi^{\text{ব}}_n)'(p) - \bar{c}^{\text{দ}}_n\,(\psi^{\text{দ}}_n)'(p')\right] \\
= \quad & \frac{g^4}{(2\pi)^5}\frac{\sigma_{\text{ব}}\sigma_{\text{দ}}}{4}\log\left(\frac{\kappa}{g^2 N_c}\right)\mathcal{S}_{\text{ব}}\mathcal{S}_{\text{দ}}\sum_{m_1,m_2=1}^{\infty}\sum_{m_3=1}^{m_1}\sum_{m_4=1}^{m_2}\frac{N_c^4}{2}\ell_{m_1}\ell_{m_2}(\ell_{m_1-m_2-m_3+m_4}\ell_{m_4-m_3} \\
&+\ell_{m_1-m_3+m_4}\ell_{m_2+m_3-m_4})\int_0^\infty dp\,p^2\,e^{-\beta p m_1}\int_0^\infty dp'\,p'^2\,e^{-\beta p' m_2} \\
&\times \left[\bar{c}^{\text{ব}}_m\,(\psi^{\text{ব}}_m)'(p) - \bar{c}^{\text{দ}}_m\,(\psi^{\text{দ}}_m)'(p')\right]\left[\bar{c}^{\text{ব}}_n\,(\psi^{\text{ব}}_n)'(p) - \bar{c}^{\text{দ}}_n\,(\psi^{\text{দ}}_n)'(p')\right]. \qquad (2.183)
\end{aligned}
$$

Here we have used the color sum in the limit of large N_c and it becomes

$$
\begin{aligned}
&\prod_{i=1}^{4}\sum_{a_i,b_i}t^{ab}_{13}\,t^{ba}_{24}\,t^{cd}_{13}\,t^{dc}_{24}\mathcal{G}(Q,n_1,\cdots,n_4) \\
&= \frac{N_c^4}{2}\ell_{n_1+n_3}\ell_{n_2+n_4}(\ell_{n_2-n_1}\ell_{n_4-n_3}+\ell_{n_1+n_4}\ell_{n_2+n_3})\,, \qquad (2.184)
\end{aligned}
$$

with $m_1 \equiv n_1+n_3$, $m_2 \equiv n_2+n_4$, $m_3 \equiv n_3$, $m_4 \equiv n_4$.

Gluon-gluon scattering

For the gluon-gluon scattering, at nonzero holonomy, the matrix element from Eq. (2.183) becomes

$$
\begin{aligned}
\bar{\Lambda}^{\rm gg}_{mn} \quad = \quad & \frac{g^4 N_c^4}{2(2\pi)^5}\log\left(\frac{\kappa}{g^2 N_c}\right)\sum_{m_1,m_2=1}^{\infty}\sum_{m_3=1}^{m_1}\sum_{m_4=1}^{m_2}\ell_{m_1}\ell_{m_2}\;\ell_{m_1,m_2,m_3,m_4}\int_0^\infty dp\,p^2 \\
&\times\int_0^\infty dp'\,p'^2 \mathrm{e}^{-\beta(m_1 p+m_2 p')}\bar{c}^{\rm g}_m\bar{c}^{\rm g}_n[(\psi^{\rm g}_m(p))'-(\psi^{\rm g}_m(p'))'][(\psi^{\rm g}_n(p))'-(\psi^{\rm g}_n(p'))'] \\
= \quad & \frac{g^4 N_c^4}{2(2\pi)^5}\log\left(\frac{\kappa}{g^2 N_c}\right)\bar{c}^{\rm g}_m\bar{c}^{\rm g}_n T^6\,Y^{\rm gg}_{mn}\,, \qquad (2.185)
\end{aligned}
$$

where, ℓ_{m_1,m_2,m_3,m_4} is defined in Eq. (2.145) and we define

$$
\begin{aligned}
Y^{\mathrm{gg}}_{mn} \;&=\; \frac{1}{T^6}\sum_{m_1,m_2=1}^{\infty}\sum_{m_3=1}^{m_1}\sum_{m_4=1}^{m_2}\ell_{m_1}\ell_{m_2}\,\ell_{m_1,m_2,m_3,m_4}\int_0^{\infty}p^2dp \\
&\times\int_0^{\infty}(p')^2dp'\mathrm{e}^{-\beta(m_1p+m_2p')}[(\psi^{\mathrm{g}}_m(p))'-(\psi^{\mathrm{g}}_m(p'))'][(\psi^{\mathrm{g}}_n(p))'-(\psi^{\mathrm{g}}_n(p'))']\;.
\end{aligned}
\tag{2.186}
$$

The factors related to temperature and the coupling constant remain consistent with those found in the perturbative Quark-Gluon Plasma (QGP) framework. The function Y^{gg}_{nm} encapsulates all the modifications or effects introduced by the background field in the system's behavior or properties. The diagram that plays a role in the contributions to the calculation is shown in Fig. 2.9a.

Gluon-teen scattering

Analogous to the gluon-gluon scattering, the matrix element for gluon-teen scattering at nonzero holonomy is

$$
\begin{aligned}
\bar{\Lambda}^{\mathrm{g}\text{ɞ}}_{mn} \;&=\; -\frac{1}{2}\frac{g^4N_c^4}{2(2\pi)^5}\log\left(\frac{\kappa}{g^2N_c}\right)\sum_{m_1,m_2=1}^{\infty}\sum_{m_3=1}^{m_1}\sum_{m_4=1}^{m_2}\ell_{m_1}\ell_{m_2}\,\ell_{m_1,m_2,m_3,m_4}\frac{T_d^2}{2}\int_0^{\infty}dp \\
&\times\int_0^{\infty}dp'\,p'^2\mathrm{e}^{-\beta(m_1p+m_2p')}[\bar{c}^{\text{ɞ}}_m\,(\psi^{\text{ɞ}}_m(p))'-\bar{c}^{\mathrm{g}}_m(\psi^{\mathrm{g}}_m(p'))'][\bar{c}^{\text{ɞ}}_n(\psi^{\text{ɞ}}_n(p))'-\bar{c}^{\mathrm{g}}_n(\psi^{\mathrm{g}}_n(p'))'] \\
&=\; \frac{g^4N_c^4}{2(2\pi)^5}\log\left(\frac{\kappa}{g^2N_c}\right)T^4T_d^2(\bar{c}^{\mathrm{g}}_m\bar{c}^{\mathrm{g}}_n\overline{Y}^{\mathrm{gg}}_{mn}+\bar{c}^{\text{ɞ}}_m\bar{c}^{\text{ɞ}}_n\overline{Y}^{\text{ɞɞ}}_{mn}-\bar{c}^{\mathrm{g}}_m\bar{c}^{\text{ɞ}}_nY^{\mathrm{g}\text{ɞ}}_{mn}-\bar{c}^{\text{ɞ}}_m\bar{c}^{\mathrm{g}}_nY^{\text{ɞ}\mathrm{g}}_{mn})\;,
\end{aligned}
\tag{2.187}
$$

with ℓ_{m_1,m_2,m_3,m_4} given in Eq. (2.145) and

$$
\overline{Y}^{\mathrm{gg}}_{mn} \;=\; -\frac{1}{2}\frac{1}{T^4}\sum_{m_1,m_2=1}^{\infty}\sum_{m_3=1}^{m_1}\sum_{m_4=1}^{m_2}\ell_{m_1}\ell_{m_2}\,\ell_{m_1,m_2,m_3,m_4}
$$

$$
\begin{aligned}
& \times \quad \frac{1}{2}\int_0^\infty dp \int_0^\infty (p')^2 dp' \mathrm{e}^{-\beta(m_1 p + m_2 p')} (\psi_m^{\mathrm{g}}(p'))' (\psi_n^{\mathrm{g}}(p))' \ , \\
\overline{Y}_{mn}^{\mathrm{g}\circlearrowleft} \quad &= \quad -\frac{1}{2}\frac{1}{T^4} \sum_{m_1,m_2=1}^{\infty} \sum_{m_3=1}^{m_1} \sum_{m_4=1}^{m_2} \ell_{m_1}\ell_{m_2} \ \ell_{m_1,m_2,m_3,m_4} \\
& \times \quad \frac{1}{2}\int_0^\infty dp \int_0^\infty (p')^2 dp' \mathrm{e}^{-\beta(m_1 p + m_2 p')} (\psi_m^{\mathrm{g}}(p'))' (\psi_n^{\circlearrowleft}(p))' \ , \\
\overline{Y}_{mn}^{\circlearrowleft\mathrm{g}} \quad &= \quad -\frac{1}{2}\frac{1}{T^4} \sum_{m_1,m_2=1}^{\infty} \sum_{m_3=1}^{m_1} \sum_{m_4=1}^{m_2} \ell_{m_1}\ell_{m_2} \ \ell_{m_1,m_2,m_3,m_4} \\
& \times \quad \frac{1}{2}\int_0^\infty dp \int_0^\infty (p')^2 dp' \mathrm{e}^{-\beta(m_1 p + m_2 p')} (\psi_m^{\circlearrowleft}(p'))' (\psi_n^{\mathrm{g}}(p))' \ , \\
\overline{Y}_{mn}^{\circlearrowleft\circlearrowleft} \quad &= \quad -\frac{1}{2}\frac{1}{T^4} \sum_{m_1,m_2=1}^{\infty} \sum_{m_3=1}^{m_1} \sum_{m_4=1}^{m_2} \ell_{m_1}\ell_{m_2} \ \ell_{m_1,m_2,m_3,m_4} \\
& \times \quad \frac{1}{2}\int_0^\infty dp \int_0^\infty (p')^2 dp' \mathrm{e}^{-\beta(m_1 p + m_2 p')} (\psi_m^{\circlearrowleft}(p'))' (\psi_n^{\circlearrowleft}(p))' \ . \qquad (2.188)
\end{aligned}
$$

The contributing diagram is presented in Fig. 2.9b.

Teen-Teen scattering

The matrix element for teen-teen scattering is

$$
\begin{aligned}
\bar{\Lambda}_{mn}^{\circlearrowleft\circlearrowleft} \quad &= \quad \frac{1}{4}\frac{g^4 N_c^4}{2(2\pi)^5} \log\left(\frac{\kappa}{g^2 N_c}\right) \sum_{m_1,m_2=1}^{\infty} \sum_{m_3=1}^{m_1} \sum_{m_4=1}^{m_2} \ell_{m_1}\ell_{m_2} \ \ell_{m_1,m_2,m_3,m_4} \frac{T_d^2}{2} \int_0^\infty dp \\
& \times \frac{T_d^2}{2} \int_0^\infty dp' \ e^{-\beta(m_1 p + m_2 p')} \bar{c}_m^{\circlearrowleft} \bar{c}_n^{\circlearrowleft} [(\psi_m^{\circlearrowleft}(p))' - (\psi_m^{\circlearrowleft}(p'))'][(\psi_n^{\circlearrowleft}(p))' - (\psi_n^{\circlearrowleft}(p'))'] \\
&= \quad \frac{g^4 N_c^4}{2(2\pi)^5} \log\left(\frac{\kappa}{g^2 N_c}\right) \bar{c}_m^{\circlearrowleft} \bar{c}_n^{\circlearrowleft} T_d^4 T^2 Y_{mn}^{\circlearrowleft\circlearrowleft} \ , \qquad (2.189)
\end{aligned}
$$

where

$$
\begin{aligned}
Y_{mn}^{\circlearrowleft\circlearrowleft} \quad &= \quad \frac{1}{4}\frac{1}{T^2} \sum_{m_1,m_2=1}^{\infty} \sum_{m_3=1}^{m_1} \sum_{m_4=1}^{m_2} \ell_{m_1}\ell_{m_2} \ \ell_{m_1,m_2,m_3,m_4} \\
& \times \quad \frac{1}{2}\int_0^\infty dp \frac{1}{2} \int_0^\infty dp' \mathrm{e}^{-\beta(m_1 p + m_2 p')} (\psi_m^{\circlearrowleft}(p'))' (\psi_n^{\circlearrowleft}(p))' \ . \qquad (2.190)
\end{aligned}
$$

Adding up the matrix elements from gluon-gluon, gluon-teen, and teen-teen scattering, one can rewrite the total matrix element as

$$\sum_{\text{ব},n} \bar{c}_n^{\text{ব}} (\bar{\mathcal{L}} \bar{c})_n^{\text{ব}} \simeq \frac{g^4 N_c^4}{2(2\pi)^5} \log\left(\frac{\kappa}{g^2 N_c}\right)$$
$$\times \sum_{m,n=1}^{K} \begin{bmatrix} \bar{c}_m^{\text{g}} & \bar{c}_m^{\text{৩}} \end{bmatrix} \begin{bmatrix} T^6 Y_{mn}^{\text{gg}} + T^4\, T_d^2 \overline{Y}_{mn}^{\text{gg}} & -T^4\, T_d^2 Y_{mn}^{\text{g৩}} \\ -T^4\, T_d^2 Y_{mn}^{\text{৩g}} & T_d^4\, T^2 Y_{mn}^{\text{৩৩}} + T^4\, T_d^2 \overline{Y}_{mn}^{\text{৩৩}} \end{bmatrix} \begin{bmatrix} \bar{c}_n^{\text{g}} \\ \bar{c}_n^{\text{৩}} \end{bmatrix} . \tag{2.191}$$

It is worth commenting about the terms from gluon-teen scattering in this expression. Naively, one might expect that the only contribution to the glue-glue term, $\bar{c}_m^{\text{g}} \bar{c}_n^{\text{g}}$, is from glue-glue scattering. This is incorrect, since Eq. (2.183), there are terms $\sim \bar{c}^{\text{ব}} \bar{c}^{\text{দ}}$, where ব and দ can be *either* a gluon or a teen field. Hence gluon-teen scattering contributes to $\bar{c}_m^{\text{g}} \bar{c}_n^{\text{g}}$ term, through the term $\overline{Y}_{mn}^{\text{gg}}$. Similarly, for the $\bar{c}_m^{\text{৩}} \bar{c}_n^{\text{৩}}$ term, there are terms from gluon-teen scattering, $\sim \overline{Y}_{mn}^{\text{৩৩}}$.

Because the scattering kernel in Eq. (2.191) has zero modes, it is necessary to add an additional term to compute the bulk viscosity. We discuss these details in Appendix (A.3).

2.6.2 Results for the Bulk Viscosity

We first compute ζ for small values of the loop. Neglecting higher powers of the first loop, ℓ_1, and higher loops, ℓ_n for $n \geq 2$,

$$\zeta \approx 68.035 \frac{(\Delta v_s^2)^2\, T^3}{g^4 \ln(\kappa / g^2 N_c)} \ell_1^2 \, . \tag{2.192}$$

Note, however, that in the pure glue theory the Polyakov loops are never small: near T_d, $\langle \ell_1 \rangle \approx 0.5$ at $N_c = \infty$, and $\langle \ell_1 \rangle \approx 0.4$ for $N_c = 3$.

Notice that the results with nonzero holonomy are very different from perturbation theory. In perturbation theory, the theory is only nonconformal, with $\Delta v_s^2 = 1/3 - v_s^2 \neq 0$, because of two effects. First, the gluons have a thermal mass, $\sim gT$. Second, the coupling constant runs. With $\eta \sim 1/(g^4 \log(1/g^2))$, this gives $\Delta v_s^2 \sim g^4$, and $\zeta \sim (\Delta v_s^2)^2 \eta \sim g^4$, up to logarithms of $\log(1/g^2)$. In contrast, our model is manifestly non-conformal, with $\Delta v_s^2 = 1/3 - v_s^2 \neq 0$ from the nonperturbative equation of state. Thus our bulk viscosity is $\zeta \sim (\Delta v_s^2)^2/(g^4 \log(1/g^2))$, Eq. (2.192).

The entropy density $s(T)$ and Δv_s^2 are calculated using Eq. (2.27), i.e., lattice pressure for three colors [111]. In Fig. 2.15, we show the ratio of the bulk viscosity to the entropy,

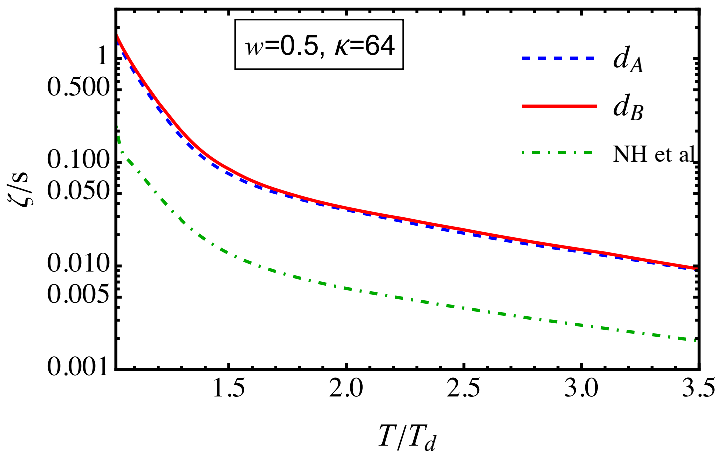

Figure 2.15: Ratio of the bulk viscosity to the entropy density with the ansatz of Eq. (2.28), with the parameters $w = 0.5$ and $\kappa = 64$. The dot-dashed line corresponds to the result in a Gribov-Zwanziger model [126].

versus temperature, for the two ansatzes, d_A and d_B. We choose the parameters to fix the coefficients in the logarithms as $w = 1$ and $\kappa = 64$. We compare our result with the Gribov-Zwanziger model of Ref. [126], and find that our result for ζ/s is much larger, almost an order of magnitude. The value of ζ/s is ~ 1.59 and 1.71 for d_A and d_B.

The dependencies of the parameters κ and w on ζ/s are shown in Fig. 2.16. The left panel of Fig. 2.16 demonstrates a large sensitivity to the value of the parameter κ, which is greatest as $T \to T_d$. Similar to the parameter κ, there is a large uncertainty on w, especially as $T \to T_d$, although it is weaker than for κ. The ratio of bulk viscosity ζ to shear viscosity

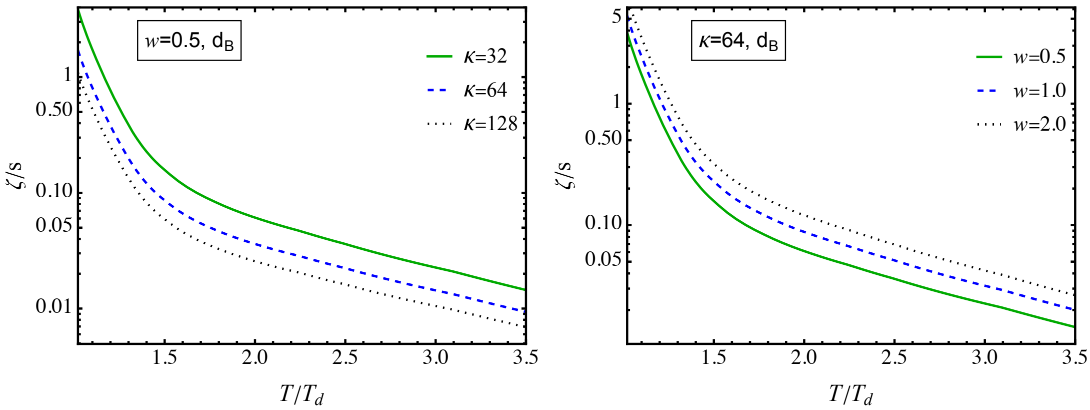

Figure 2.16: *Left*: Ratio of the bulk viscosity to the entropy density for different parameter sets of κ. *Right*: Ratio of the bulk viscosity to the entropy density for different parameter sets of w.

η has a thermodynamic significance as it reflects the type of dissipative response a medium exhibits in nonequilibrium conditions, particularly near phase transitions.

Bulk viscosity, which relates to the resistance to volume changes, tends to increase near phase transitions due to critical slowing down, where the medium struggles to equilibrate under isotropic stress. This increase is tied to the medium's equation of state (EoS), which defines pressure and density relationships that influence the system's relaxation toward equilibrium. Hence, the ratio ζ/η has an important physical significance.

The left panel of Fig. 2.17 suggests a trend where the ratio decreases with increasing temperature. For T/T_d values from around 1.5 to 3.5, ζ/η moves from values closer to 1 to significantly lower values. Lastly, the right panel of Fig. 2.17 shows the temperature

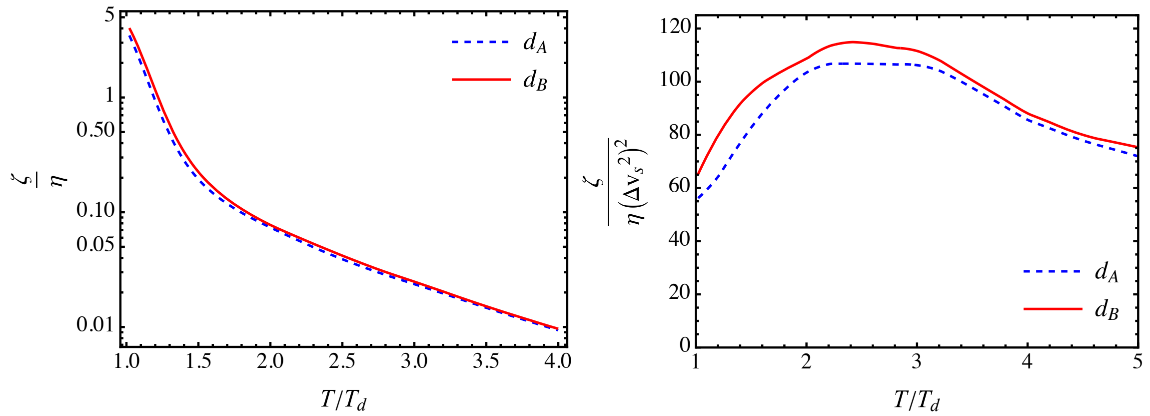

Figure 2.17: *Left*: Ratio of the bulk viscosity to the shear viscosity with the ansatz of Eq. (2.28). *Right*: Ratio of the bulk viscosity to the shear viscosity scaled with the square of the conformality measure (Δv_s^2).

dependence of the ratio of the bulk viscosity to the shear viscosity scaled with the square of the conformality measure (Δv_s^2). We comment on the relationship to other models in Eqs. (2.197) and (2.198).

2.7 Summary

The computation of the shear and bulk viscosities in our matrix model is admittedly involved, so we conclude by summarizing our results, and comparing to those obtained with different methods.

In heavy ion collisions at RHIC and LHC energies, experimentally it is observed that a nearly ideal hydrodynamics works amazingly well [127–131]. The standard paradigm for understanding this is the AdS/CFT correspondence: for a $\mathcal{N}=4$ $SU(N_c)$ gauge theory at $N_c=\infty$ and $g^2N_c=\infty$ [132–134],

$$\frac{\eta}{s}\bigg|^{\mathrm{AdS/CFT}} = \frac{1}{4\pi} \ , \quad \frac{\zeta}{s}\bigg|^{\mathrm{AdS/CFT}} = 0 \ . \tag{2.193}$$

As a conformally invariant theory, the dimensionless ratio η/s is independent of temperature, and the bulk viscosity vanishes identically.

While our understanding of thermodynamics in equilibrium rests upon computations in lattice QCD, measuring transport coefficients is extraordinarily difficult. From the Kubo formula, they depend upon the relevant spectral densities as the frequency $\omega \to 0$. However, this requires analytic continuation from discrete, Euclidean p_0, to the continuous, Minkowski ω. The most recent results from the lattice are from Ref. [135]; at $1.5\,T_d$,

$$\left.\frac{\eta}{s}\right|_{1.5T_d} \approx 0.15 - 0.48 \;\; ; \;\; \left.\frac{\zeta}{s}\right|_{1.5\mathrm{T_d}} \approx 0.017 - 0.059 \; . \tag{2.194}$$

We can then compare results from AdS/CFT, Eq. (2.193), and the lattice, Eq. (2.194), to the results at leading logarithmic order in matrix models. For the shear viscosity, η/s, see Figs. 2.11, 2.12, 2.13, and 2.14; for the bulk viscosity, ζ/s, see Figs. 2.15 and 2.16.

In order to understand results from the lattice, it is essential to be able to model the spectral densities; see Refs. [136–139].

In a matrix model, the results are rather insensitive to which ansatz we use for the eigenvalue density, A or B in Eq. (2.28). They also depend upon the parameter w, which determines the running of the coupling, Eq. (2.165), and the constant κ, which fixes the behavior beyond leading logarithmic order in the coupling, Eq. (2.138). Using what we take as the optimal values of $w = 0.5$ and $\kappa = 64$, at $1.5\,T_d$,from Figs. 2.11 and 2.15 we find

$$\left.\frac{\eta}{s}\right|_{1.5T_d} \approx 0.38 - 0.4 \; ; \; \left.\frac{\zeta}{s}\right|_{1.5T_d} \approx 0.076 - 0.087 \; . \tag{2.195}$$

The value for η/s at $1.5\,T_d$ is consistent with Ref. [135], although at the high end, while the bulk viscosity is somewhat larger than that of Ref. [135]. The matrix model, however, also provides results for the temperature dependence of each quantity.

If the coupling constant runs relatively slowly with temperature, as is true for the moderate values of the coupling constant which we use, then as the temperature $T \to T_d$, the principle way by which η/s decreases is if the expectation value(s) of the Polyakov loops decrease as well. In the pure glue theory, for three colors the decrease in the expectation value of the first Polyakov loop is not very large, though: from $\langle \ell_1 \rangle \to 1.0$ as $T \to \infty$ to $\langle \ell_1 \rangle \approx 0.4$ at the deconfining transition T_d; for $N_c = \infty$, $\langle \ell_1 \rangle \approx 0.5$ at T_d. Thus at T_d, the decrease in the shear viscosity is relatively moderate, as illustrated in Fig. 2.11. The precise temperature dependence is sensitive to varying κ, Fig. 2.12, or w, Fig. 2.13. These changes tend to bring η/s much closer to the perturbative value.

In contrast, for the bulk viscosity, ζ/s increases sharply from $1.5T_d$ to T_d. From Fig. 2.15, with $w = 0.5$ and $\kappa = 64$, at the transition temperature the bulk viscosity is large,

$$\left.\frac{\zeta}{s}\right|_{T_d} \approx 1.6 - 1.7\,. \tag{2.196}$$

The variation with respect to κ and w are shown in Fig. 2.16. Varying κ, at T_d we find that $\zeta/s \approx 1.1 - 4$; varying w, at T_d the matrix model gives $\zeta/s \approx 4 - 7$. The variation in these values and the sensitivity with respect to w and κ, indicate the limitations of our model and the attendant assumptions. However, what is clear is that ζ/s increases *strongly* as $T \to T_d$.

It is also useful to compare our results with those obtained in other effective models.

Corrections to the perturbative results for the shear and bulk viscosity were estimated in Refs. [114–119, 140–143], and do tend to decrease η/s.

Another approach is to use a quasiparticle model, where the gluon masses are $m_{\text{gl}} \sim g(T)T$. Taking $g(T)$ to increase strongly as $T \to T_d$, a small pressure is obtained by letting $g(T)$ become large as $T \to T_d$, so the gluon quasiparticles are (very) heavy. This was done in Refs. [144, 145], with results that depend strongly on temperature. As T decreases, it reaches a minimum at $T_{\text{min}} \approx 1.1\, T_d$, and then increases sharply. The shear viscosity is very small at T_{min}, with $\eta/s(T_{\text{min}}) \approx 0.1$, close to the AdS/CFT bound. For the bulk viscosity, it is extremely small until $\approx 1.2\, T_d$, where it then increases sharply, and is large, $\zeta/s \approx 0.25$ at T_{min}. In contrast to our model, η/s is much smaller at T_{min}, while our values for $\zeta/s \approx 0.76 - 0.81$ at $1.1T_d$ (see Fig. 2.15) is larger than the quasiparticle model. Still, given the assumptions in both the quasiparticle model, and our matrix model, the results are not that far apart.

There are also results for the bulk viscosity from other models. For the bulk viscosity, in $\mathcal{N}^* = 2$ SUSY gauge theories Buchel [146] established the bound

$$\frac{\zeta}{\eta} \times \frac{1}{(1/3 - v_s^2)} \geq 2 \; . \tag{2.197}$$

However, this bound is not exact [147–150].

Bounds on the bulk viscosity were also obtained by Dusling and Schaefer in Ref. [151]. In the relaxation time approximation to kinetic theory,

$$\frac{\zeta}{\eta} \times \frac{1}{(1/3 - v_s^2)^2} \approx 15 \; . \tag{2.198}$$

This is stronger than the bound from $\mathcal{N}^* = 2$ SUSY, in that, it involves the square of the difference in the speed of sound from the conformal limit, where $v_s^2 = 1/3$.

In the right panel of Fig. 2.17 we plot the same quantity as on the left-hand side of Eq. (2.198), ζ/η times $1/(1/3 - v_s^2)^2$. Unlike the relaxation time approximation, unsurprisingly, this is temperature dependent, with a value $\approx 56 - 65$ at T_d. The ratio then increases to a maximum of $\approx 105 - 114$ at $\approx 2.5T_d$, and then it falls off as T increases further. In this ratio, there is sensitivity to which ansatz is used.

Still, the right panel of Fig. 2.17 shows that the relaxation time approximation gives a good rule of thumb, although the matrix model value is about five time larger, with a non-trivial dependence upon temperature.

There are other models to which we can compare. Using a Gribov-Zwanziger model, Refs. [126, 152, 153] find that $\zeta/s \approx 0.2$ at T_d. While large, ours is approximately an order of magnitude larger, $\zeta/s \approx 1.7$ at T_d.

There are also results from holographic models [154]. Anisotropic holographic models find that while the transverse shear viscosity obeys the AdS/CFT bound, that longitudinal to the direction of the anisotropy can be smaller than the bound [150]. Reference [155] also finds that in holographic models, η/s can be below the AdS/CFT bound. Reference [156] finds η/s has a minimum at T_d, with a model dependent value above $1/(4\pi)$. Reference [157] construct a model where η/s is below the AdS/CFT bound, while $\zeta/s \approx 0.12$ at T_d. Reference [158] constructs a bottom-up model where η/s is constant, equal to the AdS/CFT bound, with a small bulk viscosity, $\zeta/s \approx 0.045$ at T_d. Reference [159] found a large value for the bulk viscosity at the transition, $\zeta(T)/T^3 \approx 0.1$ at T_d. Reference [160] finds a violation of the Buchel bound [146], in a model-dependent fashion. Reference [161] find $\zeta/s \approx 0.2$ at T_d. At T_d, Ref. [162] find a small minimum for the shear viscosity, $\eta/s \approx 0.2$, and for the bulk viscosity, $\zeta/s \approx 0.12$.

In all, at T_d holographic models give a value of η/s near the AdS/CFT bound, while ζ/s is larger than that from the lattice, but much smaller than in a matrix model.

Of course, what is relevant to QCD, and real experiments, is the theory with dynamical quarks. In a matrix model, the results for η/s at the chiral phase transition, T_χ will *certainly* be much smaller than in the pure glue theory. This is because while the (first) Polyakov loop is relatively large at T_d, at the chiral phase transition, at T_χ, the expectation value of the (first) Polyakov loop is rather small, $\langle \ell_1 \rangle (T_\chi) \approx 0.04$, Fig. 1 of Ref. [163]; see, also, Ref. [164]. This suggests that QCD enters a regime where, at T_χ, chiral symmetry restoration occurs in a regime with nearly perfect confinement. In a matrix model, inexorably this will generate a *much* smaller value of η/s [95]. The implications for the bulk viscosity are less clear, and can only be determined by computation, which is actively underway.

CHAPTER 3

THE COMPLEX HEAVY QUARKONIUM POTENTIAL WITH THE GRIBOV-ZWANZIGER ACTION

In this chapter heavy quark coulomb potential in a thermal medium within the Gribov-Zwanziger prescription discussed in Chapter 3. This chapter is based on the work presented in the following paper: ***The complex heavy quarkonium potential with the Gribov-Zwanziger action***

Manas Debnath, Ritesh Ghosh, Najmul Haque ***Eur.Phys.J.C 84*** (2024) 3, 313, [arXiv: 2305.16250].

3.1 Introduction

Quarkonium suppression is one of the signatures of the creation of a novel state of quarks and gluons, i.e., quark-gluon plasma (QGP) [165] in relativistic heavy-ion collision experiments at the Large Hadron Collider (LHC) and Relativistic Heavy Ion Collider (RHIC). In 1986, Matsui and Satz [28] suggested that the J/ψ suppression due to Debye screening by color interaction in the medium can play an important role as a QGP formation signature. The heavy quarkonium spectral functions are studied, theoretically, via approaches like Lattice QCD [166–170] and using effective field theories [171–173]. In an EFT, the study of quarkonium potential is not trivial, as the separation of scales is not always obvious. On the other hand, the lattice QCD simulation approach is used where spectral functions are computed from Euclidean meson correlation [174]. As the temporal length at high temperatures decreases, the calculation of spectral functions is not straightforward, and the results highly depend on the discretization effect and have large statistical errors. So, the study of quarkonia at finite temperatures using the potential models [175, 176] are well accepted and has been investigated widely as a complement to lattice studies.

At high temperatures, the perturbative computations indicate that the potential of the quarkonia state is complex [177]. The real part is related to the screening effect of color charges [28], and the imaginary part is used to obtain the thermal width of the resonance [178]. So, it was initially thought that the resonances dissociate when the screening is strong enough; in other words, the real part of the potential is too feeble to bind the $Q\bar{Q}$ pair together. In recent times, the melting of quarkonia is thought to be also because of the broadening of the resonance width occurring either from the gluon-mediated inelastic parton scattering mechanism aka Landau damping [177] or from the hard gluo-dissociation process in which a color octet state is produced from a color singlet state [179]. The latter process is more important when the medium temperature is lesser than the binding energy of the resonance state. As a result, the quarkonium, even at lower temperatures, can be dissociated. Gauge-gravity duality [180, 181] study also shows that the potential develops an imaginary component beyond a critical separation of the quark-antiquark pair. Lattice studies [182, 183] suggest the existence of a finite imaginary part of the potential. Spectral extraction strategy [184, 185] and the machine learning method [186] have been recently used to calculate the heavy quarkonium (HQ) potential, both indicating a larger imaginary part of $Q\bar{Q}$ potential with respect to the pure perturbative QCD calculation. All the studies of heavy quarkonium using potential models have been done within the perturbative resummation framework. In recent times, open quantum systems method [187–191] is drawing more attention to the study of the quarkonium suppression in QGP matter. This method has also been applied to the framework of potential non-relativistic QCD, i.e., pNRQCD [173, 179, 192].

In the study of hot QCD matter, there are three scales of the system: hard scale, i.e., temperature (T), (chromo) electric gT, and (chromo)magnetic scale (g^2T), where g is the QCD coupling. Hard thermal loop (HTL) resummed perturbation theory deals with the hard scale T and the soft scale gT but breaks down at magnetic scale (g^2T), known as Linde problem [68, 193]. The physics in the magnetic scale is related to the nonperturbative nature. LQCD is appropriate to probe the nonperturbative behavior of QCD. Due to the difficulties in the computation of dynamical quantities with LQCD, it is useful to have an alternate technique to incorporate nonperturbative effects, which can be derived in a more analytical way, as in resummed perturbation theory. A formalism has been developed to incorporate the nonperturbative magnetic screening scale by employing the Gribov-Zwanziger (GZ) action [61, 62] and it regulates the magnetic IR behavior of QCD. As discussed in ref. [194], the Gribov parameter is nonzero in the deconfined phase and GZ action relavant in deconfined phase of nuclear matter. Since the gluon propagator with the GZ action is IR improved, this imitates confinement, causing the calculations to be more consistent with the results of functional methods and LQCD. Equation of state of gluon plasma, thermodynamics and kinetic theories are well studied within GZ framework at finite temperature [194, 195]. Heavy quark diffusion coefficients [124], quark number susceptibility and dilepton rate [196], quark dispersion relations [197], quark-antiquark potential [198], correlation length of mesons [199] have been investigated using GZ action. Recent progress can be found in Refs. [200–207].

In this chapter, we study the heavy quarkonium potential at finite temperatures within a non-perturbative resummation considering Gribov-Zwanziger action, which reflects the confining properties. In this direction, the heavy quark-antiquark potential has been studied at zero temperature in recent times [208, 209]. We extend the zero temperature calculation to finite temperatures. This is performed from the Fourier transform of the effective gluon propagator in the static limit. In the current article, we have used the Landau gauge and we consider the contribution from the Gribov-modified gluon loop, Faddeev-Popov ghost loop and quark loop in the gluon propagator. Additionally, the contribution from auxiliary fields to the potential is discussed as a possibile source of the linear term in the potential. The article is organized as follows: The general structure of the gauge-boson propagator within the Gribov prescription has been constructed in Sec. 3.2. The effective gluon propagator is calculated from the one-loop gluon self-energy in Sec. 3.3. In the presence of GZ action, we consider the effect of the Gribov parameter on the gluon and the ghost loop. We compute the real part of potential due to color screening and the imaginary part arising from the Landau damping in Sec. 3.4. We have also evaluated thermal width for J/ψ and Υ. In Sec. 3.5, we discuss the medium effect on a local version of the Gribov action where the new set of auxiliary fields is introduced. In the present study, we have incorporated all those effects. Finally, in Sec. 5.6, we summarize our work.

3.2 Resummed gluon propagator with Gribov parameter

The form of Gribov's gluon propagator in Landau gauge in Euclidean spacetime is given by [61, 62]

$$\Delta^0_{\mu\nu}(P) = \left(\delta_{\mu\nu} - \frac{P_\mu P_\nu}{P^2}\right)\frac{P^2}{P^4+\gamma_G^4}, \tag{3.1}$$

where γ_G is the Gribov parameter and $\delta_{\mu\nu} = (1,1,1,1)$. The appearance of the parameter γ_G in the denominator shifts the pole of the gluon to the unphysical poles i.e. $P^2 = \pm i\gamma_G^2$. This unphysical excitation using the Gribov parameter indicates the effective confinement of gluons. More detailed discussions about Gribov prescription can be found in review papers [200–203].

The Gribov mass parameter can be obtained from the following gap equation at one-loop order, as [201],

$$g^2\frac{(d-1)N_c}{d}\sum\!\!\!\!\!\!\!\int_P \frac{1}{P^4+\gamma_G^4} = 1, \tag{3.2}$$

where N_c is the number of colors, d is the space-time dimension and $\sum\!\!\!\!\!\!\int_P = T\sum_n\int d^3p/(2\pi)^3$. The temporal component of the Euclidean four-momentum possesses discrete bosonic Matsubara frequencies. At asymptotically high temperatures, the form of the Gribov parameter simplifies as [123],

$$\gamma_G = \frac{d-1}{d}\frac{N_c}{4\sqrt{2}\pi}g^2 T. \tag{3.3}$$

In addition to the Gribov parameter, the QCD strong coupling is also needed and we use one-loop running as follows:

$$g^2(T) = 4\pi\alpha_s = \frac{24\pi^2}{11N_c - 2N_f}\frac{1}{\ln(2\pi T/\Lambda_{\overline{\text{MS}}})}, \tag{3.4}$$

where the scale $\Lambda_{\overline{\text{MS}}} = 0.176\text{GeV}$ [50] for $N_f = 3$ QCD.

The ghost propagator in the Landau gauge with no-pole condition reads

$$D_c(P) = \frac{\delta^{ab}}{P^2}\frac{1}{1-\sigma(P)}, \tag{3.5}$$

where, $(1-\sigma(P))^{-1} = Z_G$ is the ghost dressing function with

$$\sigma(P) \quad = \quad g^2 N_c \frac{P_\mu P_\nu}{P^2} \sum\!\!\!\!\!\!\!\int_K \frac{1}{K^4+\gamma_G^4}\frac{K^2}{(K-P)^2}\Big(\delta^{\mu\nu} - \frac{K^\mu K^\nu}{K^2}\Big). \tag{3.6}$$

Equation (3.5) in the infrared limit reduces to [201]

$$D_c(K^2) = \frac{128\pi^2\gamma_G^2}{g^2 N_c}\frac{1}{K^4}, \tag{3.7}$$

indicating that ghost propagator is enhanced for $K \to 0$.

In the vacuum, the gluon self energy can be written as

$$\Pi^{\mu\nu} = \Pi(P^2)\Big(\delta^{\mu\nu} - \frac{P^\mu P^\nu}{P^2}\Big) = \Pi(P^2)V^{\mu\nu}, \tag{3.8}$$

where $P^\mu = (p_0, \mathbf{p})$ is the gluon four momentum and $\Pi(P^2)$ is the Lorentz invariant quantity depending upon P^2.

In a thermal medium, the general structure of gluon self-energy, satisfying tranversality condition $p_\mu \Pi^{\mu\nu} = 0$, can be written in terms of two independent symmetric tensors, as

$$\Pi^{\mu\nu} = \Pi_T A^{\mu\nu} + \Pi_L B^{\mu\nu}, \tag{3.9}$$

where the forms of tensors are $B^{\mu\nu} = \frac{\bar{u}^\mu \bar{u}^\nu}{\bar{u}^2}$ with $\bar{u}^\mu = V^{\mu\nu} u_\nu$ and $A^{\mu\nu} = V^{\mu\nu} - B^{\mu\nu}$. We choose the rest frame of the heat bath *i.e.,* $u^\mu = (1, 0, 0, 0)$. The form factors Π_L and Π_T are functions of two Lorentz scalars p_0 and $p = |\mathbf{p}|$.

The effective gluon propagator can be written using Dyson-Schwinger equation as

$$\Delta^{-1}_{\mu\nu} \;=\; \left(\Delta^0_{\mu\nu}\right)^{-1} + \Pi_{\mu\nu}. \tag{3.10}$$

Here we would use the form of the gluon propagator,

$$\Delta^0_{\mu\nu}(P) = \left(\delta_{\mu\nu} - \frac{P_\mu P_\nu}{P^2}\right) \frac{P^2}{P^4 + \gamma_G^4} + \xi \frac{P_\mu P_\nu}{P^4}, \tag{3.11}$$

where ξ is the gauge parameter. This form is useful to invert the propagator. In the final expression of the effective gluon propagator, we put $\xi = 0$ (Landau gauge). The form of the inverse gluon propagator from Eq. (4.6) reads as

$$\left(\Delta^0_{\mu\nu}\right)^{-1} = \left(\delta_{\mu\nu} - \frac{P_\mu P_\nu}{P^2}\right) \frac{P^4 + \gamma_G^4}{P^2} + \frac{1}{\xi} P_\mu P_\nu. \tag{3.12}$$

Putting the form of $\left(\Delta^0_{\mu\nu}\right)^{-1}$ in eq. (4.5), one gets the expression of inverse effective gluon propagator

$$\Delta^{-1}_{\mu\nu} = \frac{1}{\xi} P_\mu P_\nu + \left(\frac{P^4 + \gamma_G^4}{P^2} + \Pi_T\right) A_{\mu\nu} + \left(\frac{P^4 + \gamma_G^4}{P^2} + \Pi_L\right) B_{\mu\nu}. \tag{3.13}$$

To find the effective gluon propagator, one can write the general structure of gluon propagator in the tensor basis as, $\Delta_{\mu\nu} = \alpha P_\mu P_\nu + \beta A_{\mu\nu} + \gamma B_{\mu\nu}$, where we need to find the coefficients α, β, γ. Then we use the relation $\delta^\nu_\alpha = \Delta^{\mu\nu}\left(\Delta_{\mu\alpha}\right)^{-1}$ to obtaine the coefficients α, β, γ as

$$\begin{aligned} \beta &= \frac{P^2}{P^4 + \gamma_G^4 + P^2\Pi_T}, \\ \gamma &= \frac{P^2}{P^4 + \gamma_G^4 + P^2\Pi_L}, \quad \alpha = \frac{\xi}{P^4}. \end{aligned} \tag{3.14}$$

So, in-medium gluon propagator with Gribov term can be written as

$$\begin{aligned} \Delta_{\mu\nu} &= \frac{\xi P_\mu P_\nu}{P^4} + \frac{P^2 A_{\mu\nu}}{P^4 + \gamma_G^4 + P^2\Pi_T} + \frac{P^2 B_{\mu\nu}}{P^4 + \gamma_G^4 + P^2\Pi_L} \\ &= \frac{\xi P_\mu P_\nu}{P^4} + D_T A_{\mu\nu} + D_L B_{\mu\nu}. \end{aligned} \tag{3.15}$$

One can recover the usual Euclidean Matsubara gluon propagator (without Gribov term) by putting $\gamma_G = 0$, such that

$$\Delta^T_{\mu\nu} = \frac{\xi P_\mu P_\nu}{P^4} + \frac{A_{\mu\nu}}{P^2 + \Pi_T} + \frac{B_{\mu\nu}}{P^2 + \Pi_L}. \tag{3.16}$$

From the pole of the propagator dispersion relation of gluons can be obtained. In the next section we would find Π_L and Π_T from one loop gluon self-energy.

3.3 One-loop gluon self-energy

In this section, we discuss the one-loop gluon self-energy in Quark-Gluon Plasma in the Gribov quantization scheme at finite temperatures. We can obtain Debye screening mass from the static limit of the polarization tensor. There are four contributions to the gluon self-energy: the tadpole diagram ($\Pi^{(a)}$), gluon loop ($\Pi^{(b)}$), quark loop ($\Pi^{(d)}$), and ghost loop ($\Pi^{(c)}$) as shown in fig. 3.1. We note that the quark loop is unaffected by the Gribov parameter.

First, we write down the expression of gluon self-energy from the tadpole diagram

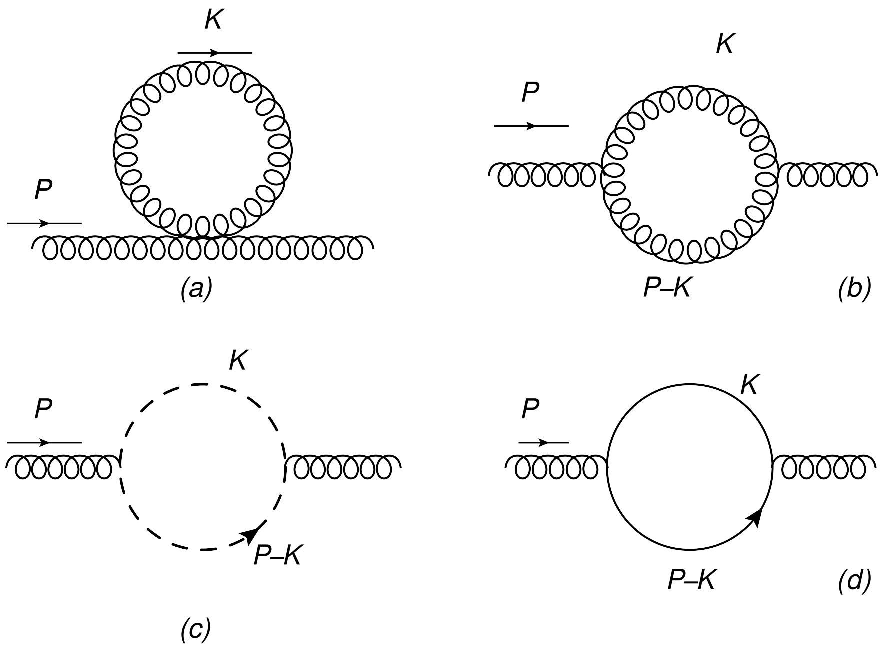

Figure 3.1: Feynman diagrams for gluon self-energy.

$$\Pi^{(a)}_{\mu\nu}(P) = 3\,C_A g^2 \delta_{\mu\nu} \int \frac{d^4K}{(2\pi)^4} \Delta(K) = 3C_A g^2 \delta_{\mu\nu} J_1, \tag{3.17}$$

with $\Delta(K) = \frac{K^2}{K^4+\gamma_G^4}$. $\Pi^{(a)}_{\mu\nu}$ is independent of external momentum (P) and $C_A = 3$. The expression of J_1 are derived in appendix B. The gluon loop contribution in the Landau gauge reads as

$$\Pi^{(b)}_{\mu\nu} = -6g^2 C_A I_{\mu\nu} - \frac{1}{2} g^2 C_A \delta_{\mu\nu} J_1 + \frac{1}{2} g^2 C_A \delta_{\mu\nu} J_2, \tag{3.18}$$

The total contribution from the tadpole and gluon loop can be obtained by adding Eq. (3.17) and Eq. (3.18) as

$$\Pi_{00}^{a+b}(p_0,\mathbf{p}) = g^2C_A\bigg(-\frac{7}{2}J_1+\frac{13}{2}J_2(p_0,\mathbf{p})+6J_3(p_0,\mathbf{p})\bigg), \tag{3.19}$$

where the detailed expressions of J's and $I_{\mu\nu}$, are evaluated in appendix B.

The contribution of the ghost loop to the gluon self-energy can be computed as

$$\begin{aligned}\Pi_{\mu\nu}^{(c)}(P) &= C_Ag^2\int\frac{d^4K}{(2\pi)^4}K_\mu K_\nu D_c(K)D_c(P-K)\\ &= C_Ag^2\left(\frac{128\gamma_G^2\pi^2}{N_cg^2}\right)^2 I_{00}^c(p_0,\mathbf{p})\end{aligned} \tag{3.20}$$

The form of I_{00}^c can be found in appendix B.

Quarks are not affected by the Gribov condition as the path integral over the gauge fields are constrained within the Gribov region. So, the quark-loop contribution to gluon self-energy is the same as of the usual HTL case. In our present case, we only need the temporal component of self-energy. So for N_f number of flavors, we have

$$\Pi_{00}^{(d)}(p_0,\mathbf{p}) = \frac{g^2T^2N_f}{12}\left(1-\frac{p_0}{2p}\log\left[\frac{p_0+p}{p_0-p}\right]\right), \tag{3.21}$$

and in the static limit

$$\Pi_{00}^{(d)}(p_0\to 0,\mathbf{p}) = \frac{g^2T^2}{6}\left(1-\frac{p_0}{2p}i\pi\right). \tag{3.22}$$

Finally, we need to add up all the contributions to get the total self-energy, i.e., $\Pi_{\mu\nu}^{(a+b+c+d)}(P)$.

In a thermal medium, the Debye screening mass (m_D) is an important quantity as this determines how the heavy quarkonium potential gets screened with inter-quark distance.

Debye mass m_D is defined by taking the static limit of '00' component of the gluon self-energy as $m_D^2 = \Pi^{00}(p_0 = 0, \mathbf{p} \to 0)$. Within the one-loop order, the Debye screening mass squared can be computed in thermal medium as [42]

$$(m_D^T)^2 = \left(N_c + \frac{N_f}{2}\right)\frac{g^2T^2}{3}. \tag{3.23}$$

The gluon and ghost loop of the gluon self-energy gets modified in the presence of the Gribov medium. By taking the static limit of $\Pi_{00}^{(a+b+c+d)}(P)$, we get the Debye mass in thermal Gribov plasma. We have compared the Debye masses for perturbative and Gribov cases in fig. 3.2.

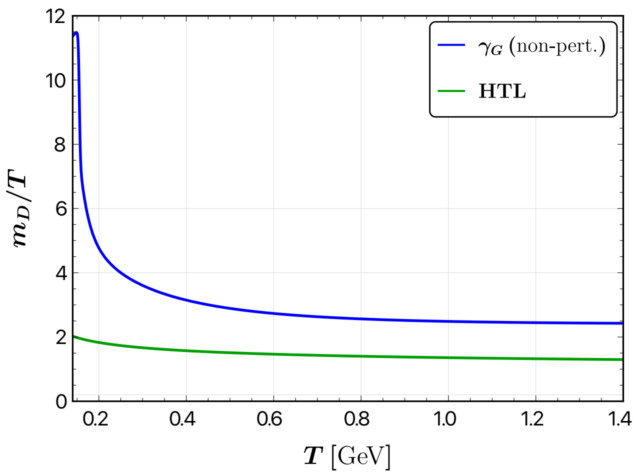

Figure 3.2: Debye mass scaled with temperature is plotted with temperature.

3.4 Heavy quark-antiquark potential

The physics of quarkonium state at zero temperature can be explained in terms of non-relativistic potential models, where the masses of heavy quark (m_Q) are much higher than QCD scale (Λ_{QCD}), and velocity of the quarks in the bound state is small, $v \ll 1$ [171, 210].

Therefore, to realise the binding effects in quarkonia, one generally uses the non-relativistic potential models [211]. In the following subsections, we investigate the effect of the Gribov parameter at finite temperature in the heavy quark-antiquark potential.

3.4.1 Real part of potential

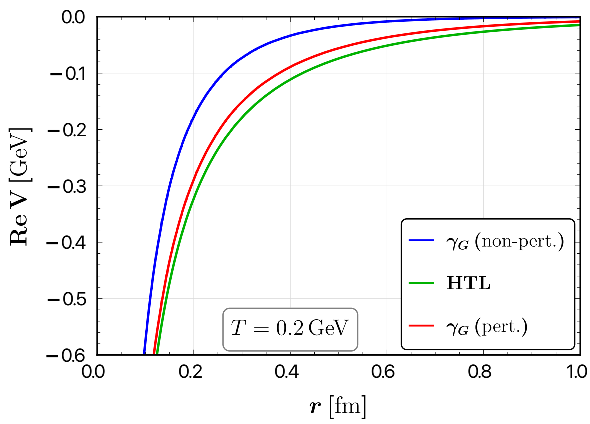

Figure 3.3: Variation of real part of quarkonium potential with distance for fixed temperature $T = 0.2$ GeV.

The real part of the HQ potential gives rise to the Debye screening, and in the non-relativistic limit, it can be determined from the Fourier transform of static gluon Matsubara propagator as

$$V(r) = g^2 C_F \int \frac{d^3p}{(2\pi)^3}\, \Delta_{00}(p_0 = 0, p)\; e^{i\mathbf{p}\cdot\mathbf{r}}. \tag{3.24}$$

For the free case we can write, $\Delta^0_{00}(p_0 = 0, p) = -p^2/(p^4 + \gamma_G^4)$ and after the Fourier transform leads to the expression

$$V_0(r) = -\frac{C_F g^2}{4\pi r} \exp\left[-\gamma_G r/\sqrt{2}\right] \cos\left(\gamma_G r/\sqrt{2}\right). \tag{3.25}$$

To investigate the static potential at finite temperature, we can consider a medium effect to this potential due to thermal bath. In a thermal medium, the effective gluon propagator is given by,

$$\Delta_{00}(p_0=0,p) = -\frac{p^2}{p^4+\gamma_G^4+p^2\Pi_L(p_0=0,p)}. \tag{3.26}$$

In this case, the heavy quarkonium potential in coordinate space can be written as

$$\begin{aligned}
V(r) &= -g^2C_F\int\frac{d^3p}{(2\pi)^3}\;e^{i\mathbf{p}\cdot\mathbf{r}}\;\frac{p^2}{p^4+\gamma_G^4+p^2m_D^2}\\
&= -\frac{g^2C_F}{(2\pi)^3}\int\frac{4\pi p^3\,dp}{p^4+\gamma_G^4+p^2m_D^2}\frac{\sin(p\,r)}{r}\\
&= -\frac{g^2C_F}{8\pi\,r}\frac{1}{\sqrt{m_D^4-4\gamma_G^4}}\\
&\times\;\Bigg[\left(-m_D^2+\sqrt{m_D^4-4\gamma_G^4}\right)e^{-\frac{r}{\sqrt{2}}\sqrt{m_D^2-\sqrt{m_D^4-4\gamma_G^4}}}\\
&+\;\left(m_D^2+\sqrt{m_D^4-4\gamma_G^4}\right)e^{-\frac{r}{\sqrt{2}}\sqrt{m_D^2+\sqrt{m_D^4-4\gamma_G^4}}}\Bigg],
\end{aligned} \tag{3.27}$$

where m_D is the Debye mass. The last line simplification is done by contour integral where $m_D \geq \sqrt{2}\gamma_G$. When the Gribov parameter $\gamma_G = 0$, from Eq. (3.27) we get back the isotropic potential

$$V(r,\gamma_G=0) = -g^2C_F\int\frac{d^3p}{(2\pi)^3}\;e^{i\mathbf{p}\cdot\mathbf{r}}\;\frac{1}{p^2+(m_D^T)^2} = -\frac{g^2C_F}{4\pi r}\exp\left[-r/m_D^T\right], \tag{3.28}$$

where m_D^T is the Debye mass for HTL case without Gribov. For the $r\to 0$ limit, the denominator will be dominated by p^2 as $p\to\infty$ and we recover vacuum Coulomb potential

$$V(r\to 0) = -g^2C_F\int\frac{d^3p}{(2\pi)^3}\;e^{i\mathbf{p}\cdot\mathbf{r}}\;\frac{1}{p^2} = -\frac{g^2C_F}{4\pi r}. \tag{3.29}$$

The real part of the potential is shown in fig. 3.3. We compare the Gribov-modified potential with the usual HTL case. The blue line shows the Gribov result using Gribov parameter of Eq. (3.3) and green line shows the quarkonium potential obtained from the usual HTL calculation. In the presence of the Gribov parameter, the potential value is less negative than the HTL case at fixed r, indicating more screening. This happens because the Debye mass of Gribov plasma is higher than the perturbative medium at a fixed temperature.

3.4.2 Imaginary part of potential

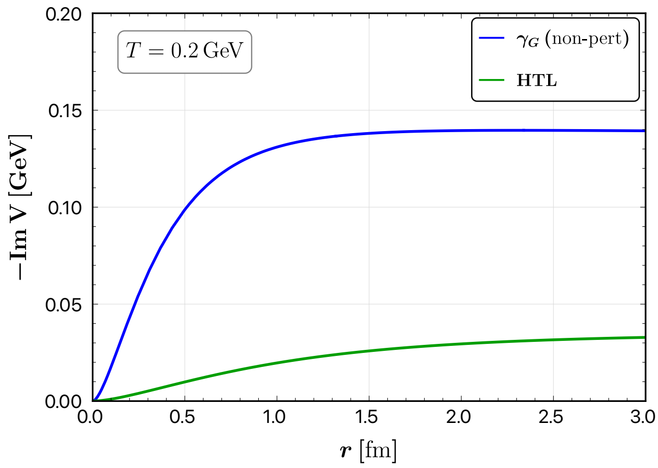

Figure 3.4: The imaginary part of the quarkonium potential as a function of distance for temperature $T = 0.2$ GeV.

The heavy quarkonium is dissociated at finite temperature by color screening and Landau damping. The Landau damping part is related to the imaginary part of the gluon self-energy as initially suggested in Ref. [177]. The imaginary part of the in-medium heavy quark-antiquark potential related to the gluon propagator is written as,

$$\mathrm{Im}\,V(r) = \int \frac{d^3p}{(2\pi)^3}(e^{i\mathbf{p}\cdot\mathbf{r}} - 1)\left[\lim_{p_0\to 0} \mathrm{Im}\,\Delta_{00}(P)\right]. \tag{3.30}$$

Here one should note that, the Matsubara propagator can be expressed in terms of spectral function as,

$$\Delta^{\mu\nu}(p_0, p) = \int_{-\infty}^{\infty} \frac{dp_0'}{2\pi} \frac{\rho_i(p_0', p) P_i^{\mu\nu}}{p_0' - p_0}. \tag{3.31}$$

From which one can express the spectral function as,

$$\operatorname{Im} \Delta^{\mu\nu}(P) = \rho_i P_i^{\mu\nu}, \tag{3.32}$$

where for Gribov-Zwanziger scheme,

$$\rho_i = P^4 \frac{\operatorname{Im} \Pi_i}{(P^4 + \gamma_G^4 + P^2 \operatorname{Re} \Pi_i)^2 + P^4 (\operatorname{Im} \Pi_i)^2}. \tag{3.33}$$

Hence, the imaginary part of the effective gauge boson propagator can be written as,

$$\operatorname{Im} \Delta^{\mu\nu}(P) = \frac{P^4 \ \operatorname{Im} \Pi_i}{(P^4 + \gamma_G^4 + P^2 \operatorname{Re} \Pi_i)^2 + P^4 (\operatorname{Im} \Pi_i)^2} P_i^{\mu\nu}, \tag{3.34}$$

for $i = T, L$. From Eq. (4.10), $P^i_{\mu\nu}$ are the projection operators.

The spectral representation of a quark propagator in GZ scheme within HTL resummation was discussed in [196, 197]. It was shown in [197] that if the Gribov gluon propagator is used to study quark collective behavior, a new space-like mode appears in addition to the two existing HTL modes and sprectral representation is well defined with this new dispersion mode. We believe one can show similar spectral representation for gluon propagator as well.

The imaginary parts are coming from the Landau damping. The contributions appearing from the self-energy diagrams are finally calculated numerically. In the following subsection, calculations of decay width related to the imaginary part of the potential are presented. The variation of the imaginary part of the potential with separation distance r is shown in fig. 3.4. The Gribov part is shown with a blue line, whereas the green line denotes the perturbative part. It can be found from the graph that the magnitude of the imaginary part of potential in Gribov is more significant than in the perturbative case at fixed temperature T. This behavior indicates more contribution to the Landau damping-induced thermal width in Gribov plasma obtained from the imaginary part of the potential.

3.4.3 Decay Width

In the previous subsection, we obtained the imaginary part of the HQ potential by calculating the imaginary part of gluon self-energy. The imaginary part arises due to the interaction occurs between the heavy quarks and particles of momenta $\sim T$, with the exchange of soft space-like gluons, namely, Landau damping. The physics of the finite width emerges from this Landau damping. The imaginary part of the HQ potential plays a crucial role in the dissociation of the HQ-bound state. The formula which gives a good approximation of the decay width (Γ) of $Q\bar{Q}$ states is written as [212],

$$\Gamma(T) = -\int |\psi(\mathbf{r})|^2 \, \mathrm{Im}\, V(\mathbf{r},T) \, d^3\mathbf{r}. \tag{3.35}$$

Here we have used the Coulombic wave function for the ground state of hydrogen like atom which is given by $\psi(r) = \frac{1}{\sqrt{\pi b_0^3}} e^{-r/b_0}$, where $b_0 = \frac{1}{m_Q \alpha_s}$ is the Bohr radius of the heavy quarkonium system and m_Q is the mass of the heavy quark and antiquark. We determine the decay width by substituting the imaginary part of the potential for a given temperature. We evaluate the decay width of the following quarkonia states, J/ψ (the ground state of charmonium, $c\bar{c}$) and Υ (bottomonium, $b\bar{b}$).

Fig. 3.5 displays the variation of decay width with temperature T. In this calculation, we have taken the masses of charmonium (m_c) and bottomonium (m_b) as $m_c = 1.275$ GeV and $m_b = 4.66$ GeV, respectively. The decay width for the charm (left panel) and the bottom (right panel) are shown. As the magnitude of the imaginary part of the potential in Gribov is larger than usual HTL case, we are getting larger decay width for the case of Gribov plasma. For both the bottom and charm, the decay width is increased in the case of Gribov plasma. The thermal width for Υ is lesser than the J/Ψ, as the bottomonium states are smaller in size with larger masses than the charmonium states.

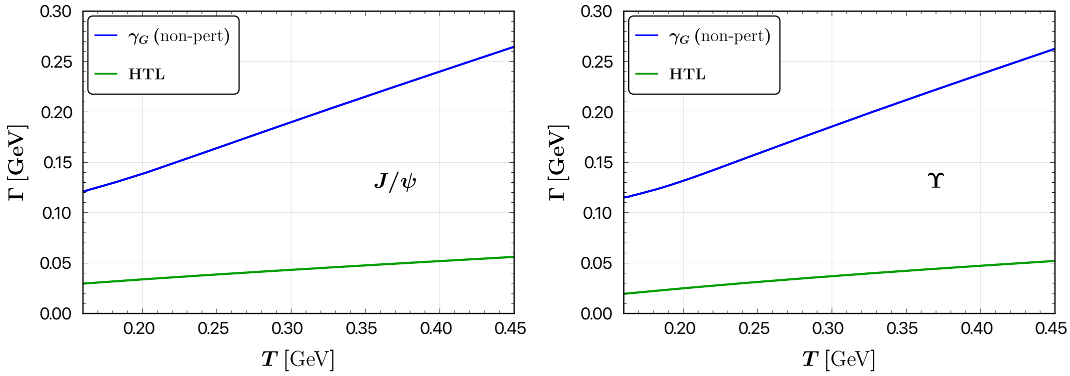

Figure 3.5: The temperature variation of decay for a charmonium (left) and bottomonium (right).

3.5 Effect of Auxilliary fields

In this section, we extend the discussion of heavy quarkonium potential in presence of a localized action and it's medium effect on the potential to check whether the localized action can contribute a linear term in the quarkonium potential. The restriction of the integration domain in the functional integral is realized by adding a non-local horizon term to the Faddeev-Popov action [213, 214]. The localization of the horizon non-locality was introduced in Refs. [62, 213, 215] by introducing Zwanziger ghost fields, $\{\phi_\mu^{ab}, \bar{\phi}_\mu^{ab}\}$, a pair of commuting fields and $\{\omega_\mu^{ab}, \bar{\omega}_\mu^{ab}\}$, a pair of anti-commuting fields. The Lagrangian is

$$
\begin{aligned}
L &= L^{\rm YM} - \bar{c}^a \partial^\mu D_\mu^{ab} c^b + \frac{1}{2}\chi_\mu^{ab}\partial^\nu (D_\nu \chi^\mu)^{ab} + \frac{i}{2}\chi_\mu^{ab}\partial^\nu (D_\nu \xi^\mu)^{ab} - \frac{i}{2}\xi_\mu^{ab}\partial^\nu (D_\nu \chi^\mu)^{ab} \\
&+ \frac{1}{2}\xi_\mu^{ab}\partial^\nu (D_\nu \xi^\mu)^{ab} - \bar{\omega}_\mu^{ab}\partial^\nu (D_\nu \omega^\mu)^{ab} - \frac{1}{\sqrt{2}} g f^{abc}\partial^\nu \bar{\omega}_\mu^{ae}(D_\nu c)^b \chi^{ec\,\mu} - i\gamma_G^2 f^{abc} A^{a\,\mu}\xi_\mu^{bc} \\
&- \frac{i}{\sqrt{2}} g f^{abc}\partial^\nu \bar{\omega}_\mu^{ae}(D_\nu c)^b \xi^{ec\,\mu} - \frac{1}{2g^2} dN\gamma^4,
\end{aligned}
$$

where $\phi_\mu^{ab} = \frac{1}{\sqrt{2}}(\chi_\mu^{ab} + i\xi_\mu^{ab})$. The authors of Ref. [208] have calculated the static potential and discussed the nature of the potential with separation distance. The ghost fields are treated as internal lines in Feynman diagrams. Tree level and one-loop corrections are considered to calculate the static potential. In this work, we have investigated the potential behavior in the presence of a thermal bath. The one loop potential in the Landau gauge is given by (see Ref. [208])

$$
\begin{aligned}
V(p) = -\frac{C_F g^2}{p^2}\Bigg\{ &\left[1 - \frac{C_A\gamma_G^4}{(p^2)^2} + \mathcal{O}\left(\frac{\gamma_G^8}{(p^2)^4}\right)\right] \\
&+ \left[\left(\frac{31}{9} - \frac{11}{3}\log\left(\frac{p^2}{\Lambda^2}\right)\right)C_A + \frac{1}{2}\left(\frac{4}{3}\log\left(\frac{p^2}{\Lambda^2}\right) - \frac{20}{9}\right)N_f \right. \\
&- \frac{2\pi C_A^{3/2}\gamma_G^2}{p^2} + \left[\left(\frac{79}{12}\log\left(\frac{p^2}{\Lambda^2}\right) + \frac{9}{8}\log\left(\frac{C_A\gamma_G^4}{(p^2)^2}\right) - \frac{1315}{72}\right)C_A^2 \right. \\
&\left.\left. + \frac{1}{2}\left(\frac{40}{9} - \frac{8}{3}\log\left(\frac{p^2}{\Lambda^2}\right)\right)N_f\right]\frac{C_A\gamma_G^4}{(p^2)^2} + \mathcal{O}\left(\frac{\gamma_G^6}{(p^2)^3}\right)\right]\frac{g^2}{16} + \mathcal{O}\left(g^4\right)\Bigg\}.
\end{aligned}
\tag{3.36}
$$

At non-zero temperature, we use an ansatz that the thermal-medium effect enters through the dielectric permittivity $\epsilon(p)$ such as [216, 217] $\bar{V}(p) = V(p)/\epsilon(k)$.

The dielectric permittivity, related to the static limit of $\Pi_L(p_0 = 0, p) = m_D^2$, is given by $\epsilon(p) = (1 + m_D^2/p^2)$. So, the in-medium quarkonium potential in real space becomes

$$
\begin{aligned}
V(r) =& \int \frac{d^3p}{(2\pi)^3}\, e^{i\mathbf{p}\cdot\mathbf{r}}\, p^2 \frac{V(p)}{p^2+m_D^2} \\
=& -\frac{C_F g^2}{4\pi}\left[4\pi^2 + \frac{1}{36}(31C_A - 20N_fT_f)g^2\right]\left(\frac{1}{r} + \frac{m_D^2 r}{2}\right) \\
&- \frac{g^2\alpha_s C_F}{72r}(11C_A - 4N_fT_f)\Big[6[2\gamma_E + 2\log(\Lambda r)] \\
&+ 3r^2m_D^2[-3 + 2\gamma_E + 2\log(\Lambda r) + 2r^3m_D^3\log\left(\frac{m_D}{\Lambda}\right)\Big] \\
&+ \frac{\pi r\alpha_s\gamma_G^2}{12m_D^2}\left[g^2m_D^2(-3C_A^{3/2}C_F + rm_D) - 8\pi C_A C_F r\gamma_G^2\right] \\
&+ \frac{C_A C_F g^2\alpha_s\gamma_G^4 r^2}{1728 m_D}\left[19201315C_A^2 + 81C_A^2\log\left(\frac{C_A\gamma_G^4}{m_D^4}\right)\right] \\
&- \frac{C_A C_F g^2\alpha_s\gamma_G^4}{288m_D^4 r}\left[(64 - 79C_A^2)r^3m_D^3 + 384\sinh(m_D r)\right]\log\left(m_D^2/\Lambda^2\right), \qquad (3.37)
\end{aligned}
$$

where $\gamma_E = 0.57721566...$ is the Euler–Mascheroni constant. Equation (3.37) is the medium-modified potential of Gribov plasma with auxiliary fields. It is apparent from Eq. (3.37) that the linearly rising term ($\sim (+ve)r$) in the potential does not emerge with considering auxiliary fields at one loop order even after considering the medium effect.Instead of taking the given intuitive form of the dielectric permittivity, one can systematically calculate the thermal medium effect for these auxilliary fields, but the nature will remain same. One may also consider higher loop contributions to the HQ potential for improved results.

3.6 Discussion

The quarkonium potential and decay width are modified within Gribov scenario. It is clear from Eq. (3.27) that the confining property is still absent in the quarkonium potential. It is evident from the fig. 3.3 that at a fixed temperature, the heavy quarkonium static potential is marginally more screened than that obtained from pure HTL perturbation theory.

In the temperature range we are interested in, the medium is non-perturbative and HTL result may not be appropriate to use. The Gribov parameter increases the debye mass and the potential becomes more screened as the debye radius is inversely proportional to the debye mass.

3.7 Summary and outlook

In the present theoretical study, the real and imaginary parts of heavy quarkonium complex potential have been computed considering both the perturbative resummation using HTLpt and non-perturbative resummation using the Gribov-modified gluon and ghost propagators. We first obtained an effective gluon propagator in the presence of the Gribov parameter. The longitudinal and transverse part (Π_L, Π_T) of the effective propagator is then obtained from the one-loop gluon self-energy. The gluon self-energy gets the contribution from quark, gluon, and ghost loops. The dependence on the Gribov parameter comes from the gluon and ghost loops. Then we plotted the Debye mass. In our work, an asymptotically high-temperature form of the Gribov parameter (γ_G) has been considered. The real part of the potential is obtained from the Fourier transform of the static gluon propagator. The $Q\bar{Q}$ is more screened in the presence of the Gribov parameter. The imaginary part of the potential and the decay width are evaluated in Gribov plasma. The magnitude of the imaginary part of the potential increases with distance. Accordingly, the width increases with temperature. We have also discussed the medium effect on the HQ potential in the presence of auxiliary fields at one loop order. As also discussed in Ref. [208], the linearly increasing potential in coordinate space is missing even with the additional auxiliary fields. The confining term in the quarkonium potential with Gribov action may appear beyond the leading order in the QCD weak-coupling expansion.

CHAPTER 4

ENERGY LOSS OF A FAST MOVING PARTON IN GRIBOV-ZWANZIGER PLASMA

In this chapter heavy quark energy loss in a thermal medium within the Gribov-Zwanziger prescription discussed in Chapter 4. This chapter is based on the work presented in the following paper: ***Energy loss of a fast moving parton in Gribov-Zwanziger plasma***
Manas Debnath, Ritesh Ghosh, Mohammad Yousuf Jamal, Manu Kurian, Jai Prakash
Phys.Rev.D 109 (2024) 1, L011503, [arXiv:2311.16005].

4.1 Introduction

In chapter 1, we discussed that the properties of the QGP can be probed through several direct and indirect observables. Among them, the energy loss of high-momentum partons that originate from the initial hard scatterings of the nuclei serve as *hard probes* and play an efficient role in unraveling the properties of the QGP. They traverse through the QGP while interacting with the medium constituents and leave behind imprints of the QGP on its experimental observables [218–223].

Efforts have been made to study the complex dynamics of pre-equilibrium, unstable, expanding, magnetized, and chiral media by investigating the energy loss of partons within their respective environments [224–235]. The moving parton undergoes interactions with both hard components, arising from elastic collisions with the medium constituents carrying momenta on the order of T (the temperature scale), and soft modes, which encompass the gauge fields within the medium carrying momenta around gT, where g represents the coupling constant. The impact of the soft modes has received comparatively less attention in the literature, which may be due to the fact that the energy loss caused by the hard components is typically more significant. Nevertheless, it is essential to consider that the soft modes, represented by the gauge fields in the medium, play a non-negligible role in the interaction dynamics with the test parton. This is due to the high occupation number of these soft modes within the plasma [236], which leads to a non-trivial interaction frequency between the parton and the classical fields.

A semi-classical approach is employed to analyze the soft contribution of energy loss experienced by an energetic parton that takes into account its interaction with the chromodynamic fields by quantifying the polarization effects of the QCD medium due to the passage of the parton. It is important to highlight that there exists a substantial disparity between the resummed perturbative results and the lattice-based estimations. For instance, a notable discrepancy has been observed in the estimation of the charm quark diffusion coefficient when comparing results from pQCD analysis with the lattice data [237]. In a very recent study [124], the authors have shown a remarkable improvement over the pQCD estimate of diffusion coefficient with the implementation of the Gribov-Zwanziger(GZ) prescription [61, 62] in the analysis. Chapter 3 discusses about the Gribov-Zwanziger(GZ) prescription in detail. Recent progress on the Gribov-Zwanziger approach and its application in various processes in QCD can be found in Refs. [64, 123, 196–199, 201–206, 209, 238].

In this chapter, utilizing the Gribov-Zwanziger prescription for the first time in the analysis of the passage of a fast moving parton, we show that the energy loss is highly influenced by the non-perturbative effects and has an important role in the phenomenological implication within the context of heavy-ion collision. However, one should note that, in general, the medium induced radiation has significant contribution in energy loss phenomena, which has not been addressed in the current thesis. First, We construct the gluon self-energy for the Gribov plasma and determine the effective gluon propagator to quantify the induced current generated by the moving parton in the medium. Further, we formulated the energy loss of parton with the Gribov-Zwanziger approach and studied the momentum evolution and nuclear suppression factor of the test parton in Gribov plasma.

4.2 Energy loss in Gribov plasma

As a high-energy test parton moves through the plasma, it is subject to energy loss stemming from interactions with the color fields. To comprehensively describe the dynamics of a test parton in the presence of these chromodynamic fields, the Wong equations offer a valuable and Lorentz covariant framework as follows [239],

$$\frac{dX^\mu(\tau)}{d\tau} = V^\mu(\tau), \tag{4.1}$$

$$\frac{dQ^\mu(\tau)}{d\tau} = g\tilde{q}^a(\tau)F_a^{\mu\nu}(X(\tau))V_\nu(\tau), \tag{4.2}$$

$$\frac{d\tilde{q}^a(\tau)}{d\tau} = -gf^{abc}V_\mu(\tau)A_b^\mu(X(\tau))\tilde{q}_c(\tau), \tag{4.3}$$

in which τ, $X^\mu(\tau)$, $Q^\mu(\tau)$, and $V^\mu(\tau)$ correspond to the proper time, position, momentum and velocity of the test parton, respectively with a color charge $\tilde{q}_a$. Here, $F^{\mu\nu}$ denotes the chromodynamic field tensor, A^μ represents the gauge potential, f^{abc} is the structure constant of the $SU(N_c)$ group, and a serves as the color index, where $a = 1, 2, \ldots, N_c^2 - 1$. These equations provide a formalism for understanding how the test parton behaves within the intricate interplay of forces and fields, shedding light on the energy loss phenomenon in this context. This energy loss is quantified by examining the work done by retarding forces acting on the parton within the medium. These forces arise from the induction of a chromo-electric field due to the parton's motion. By adopting the well-established formalism described in Refs. [225, 233], Wong equations, along with the linearized Yang-Mills equation, provide the parton energy loss in the Gribov plasma as,

$$\frac{dE}{dx} = i\frac{1}{|\mathbf{v}|}g^2 C_F v^i v^j \int \frac{d^3\mathbf{p}}{(2\pi)^3}\omega\Delta^{ij}, \tag{4.4}$$

with C_F as the Casimir invariant of $SU(N_c)$, $\omega = \mathbf{p}\cdot\mathbf{v}$ where $\mathbf{v} = \frac{\mathbf{q}}{E_q}$ and Δ^{ij} is the IR improved gluon propagator with the Gribov-Zwanziger approach. The properties of Gribov plasma are captured in Δ^{ij} and can be represented by employing the Dyson-Schwinger equation as,

$$\Delta^{-1}_{\mu\nu} \;=\; \left(\Delta^0_{\mu\nu}\right)^{-1} - \Pi_{\mu\nu}. \tag{4.5}$$

The gluon propagator with Gribov term can be described as [197],

$$\Delta^0_{\mu\nu}(P) = \left(\delta_{\mu\nu} - (1-\xi)\frac{P_\mu P_\nu}{P^2}\right)\frac{P^2}{P^4 + \gamma_G^4}, \tag{4.6}$$

where $P^\mu \equiv (p_0 = \omega, \mathbf{p})$, ξ denotes the gauge parameter and $\delta_{\mu\nu} = \text{diag}(1,1,1,1)$. Here, γ_G represents the Gribov parameter. Its temperature dependence can be extracted within the framework of finite-temperature Yang-Mills theory by solving the gap equation. The presence of the parameter γ_G in the denominator has the effect of shifting the pole of the gluon to an unphysical position, specifically $P^2 = \pm i\gamma_G^2$. These unphysical excitations, which emerge when incorporating the Gribov parameter, signify the effective confinement of gluons [201–203]. The gluon self-energy is characterized by two independent symmetric tensors, which can be expressed in terms of form factors Π_L and Π_T as,

$$\Pi^{\mu\nu} = \Pi_T A^{\mu\nu} + \Pi_L B^{\mu\nu}. \tag{4.7}$$

Here, $B^{\mu\nu} = \frac{\bar{u}^\mu \bar{u}^\nu}{\bar{u}^2}$ where $\bar{u}^\mu = G^{\mu\nu}u_\nu$ with $G^{\mu\nu} = \delta^{\mu\nu} - \frac{P^\mu P^\nu}{P^2}$ and $A^{\mu\nu} = G^{\mu\nu} - B^{\mu\nu}$. Employing Eq. (4.6) and Eq. (4.7) in Eq. (4.5), the inverse effective gluon propagator can be expressed as,

$$\Delta^{-1}_{\mu\nu} = \frac{P^4 + \gamma_G^4}{P^2\xi}\delta_{\mu\nu} + \left(\frac{\xi - 1}{\xi}\frac{P^4 + \gamma_G^4}{P^2} - \Pi_T\right) A_{\mu\nu} + \left(\frac{\xi - 1}{\xi}\frac{P^4 + \gamma_G^4}{P^2} - \Pi_L\right) B_{\mu\nu}. \tag{4.8}$$

The general structure of the gluon propagator can be decomposed in the tensor basis as,

$$\Delta_{\mu\nu} = \alpha P_\mu P_\nu + \beta A_{\mu\nu} + \gamma B_{\mu\nu}, \tag{4.9}$$

where the coefficients α, β, γ can be determined from the relation $\delta^\nu_\alpha = \Delta^{\mu\nu}\left(\Delta_{\mu\alpha}\right)^{-1}$. We obtain the gluon propagator in Gribov plasma as,

$$\Delta_{\mu\nu} = \frac{\xi P_\mu P_\nu}{P^4 + \gamma_G^4} + \frac{P^2 A_{\mu\nu}}{P^4 + \gamma_G^4 - P^2\Pi_T} + \frac{P^2 B_{\mu\nu}}{P^4 + \gamma_G^4 - P^2\Pi_L}. \tag{4.10}$$

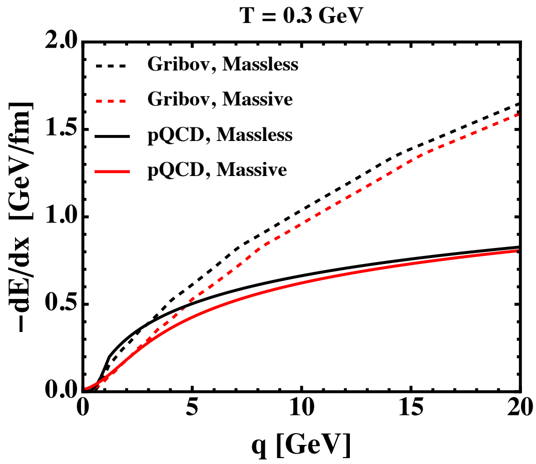

Figure 4.1: Gribov-modified energy loss of massless and massive parton and its comparison with that from the pQCD calculations.

The modified dispersion relation of gluons with the Gribov term can be extracted from the pole of the propagator. It is important to emphasize that in the case $\gamma_G = 0$, Eq. (4.10) reduce back to the form of thermal gluon propagator. The form factors Π_L and Π_T can be obtained from one loop gluon self-energy as,

$$\Pi_L(\omega, p) = -\frac{\omega^2 - p^2}{p^2}\Pi_{00}(\omega, p), \tag{4.11}$$

$$\Pi_T(\omega, p) = \frac{1}{2}[\Pi_{\mu\mu}(\omega, p) - \Pi_L(\omega, p)]. \tag{4.12}$$

One needs to estimate the quark, gluon, and ghost loops contributions to the gluon self-energy. It is important to emphasize that the gluon and ghost loops will be affected by the Gribov-Zwanziger approach. The Gribov constraint does not affect the quark sector, as it only affects the gauge sector of the QCD. We focus on the estimation of $\Pi_{\mu\mu}$ and Π_{00} from each sector to obtain Gribov parameter dependence of Π_T and Π_L.

The contribution of the tadpole diagram and gluon loop to the gluon self-energy can be

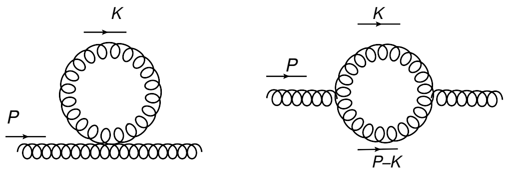

(a) Tadpole diagram (b) Gluon loop

described as,

$$\Pi_{00}^{a+b}(p_0, \mathbf{p}) = -\frac{13}{2} g^2 C_A J_1 + 3g^2 C_A J_4(p_0, \mathbf{p}) + \frac{13}{2} g^2 C_A J_2(p_0, \mathbf{p}) + 6g^2 C_A J_3(p_0, \mathbf{p}), \tag{4.13}$$

$$\Pi_{\mu\mu}^{a+b}(p_0, \mathbf{p}) = \frac{5}{2} g^2 C_A (\delta_{\mu\mu} - 1) J_1 + \frac{1}{2} g^2 C_A \delta_{\mu\mu} J_2(p_0, \mathbf{p}) - 6g^2 C_A \Big(J_1 - J_2(p_0, \mathbf{p}) \Big). \tag{4.14}$$

It is important to note that the $\Pi^a_{\mu\nu}(P)$ is independent of external momentum. A detailed derivation of Eq. (4.13) and Eq. (4.14) along with the functional forms of $J_i (i = 1, .., 4)$ is discussed in Section A of the supplementary material.

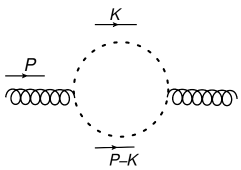

(c) Ghost loop

In the Landau gauge, the ghost propagator in the infrared limit reads as [201],

$$D^c(K^2) = \frac{128\pi^2 \gamma_G^2}{3g^2} \frac{1}{K^4}. \tag{4.15}$$

Employing the form of the ghost propagator, we can define the ghost loop contribution to

$\Pi_{\mu\mu}$ and Π_{00} as,

$$\Pi^c_{\mu\mu} = \left(\frac{128\pi^2\gamma_G^2}{3g^2}\right)^2 I^c_{\mu\mu}, \qquad \Pi^c_{00} = \left(\frac{128\pi^2\gamma_G^2}{3g^2}\right)^2 I^c_{00}, \tag{4.16}$$

where the functional form of $I^c_{\mu\mu}$ and I^c_{00} take the forms as follows,

$$I^c_{\mu\mu} = -\frac{1}{4\pi^2}\frac{7\zeta(3)}{8\pi^2T^2}\left[\frac{1}{4} + \left\{\frac{p_0^2}{p_0^2-p^2} - \frac{p_0}{2p}\log\left(\frac{p_0+p}{p_0-p}\right)\right\}\right], \tag{4.17}$$

$$I^c_{00} = -\frac{1}{8\pi^2}\frac{7\zeta(3)}{8\pi^2T^2} + \frac{1}{(2\pi)^2}\frac{p_0^2}{(p^2-p_0^2)^2} - \frac{2}{(2\pi)^2}\frac{7\zeta(3)}{8\pi^2T^2}\left\{\frac{p_0^2}{p_0^2-p^2} - \frac{p_0}{2p}\log\left(\frac{p_0+p}{p_0-p}\right)\right\}. \tag{4.18}$$

The derivation of Eq. (4.17) and Eq. (4.18) is presented in Section B of the supplementary material.

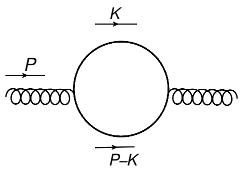

(d) Quark loop

Quark loop contribution to the gluon self-energy $\Pi^d_{\mu\nu}$ remains the same as it is in the usual perturbative case. Similar to the thermal case, we have

$$\Pi^d_{\mu\nu}(p_0,\mathbf{p}) \quad = \quad \frac{g^2T^2}{6}N_f\int\frac{d\Omega}{4\pi}\left(\delta_{\mu0}\delta_{\nu0} + \frac{i\omega}{P\cdot\hat{K}}\hat{K}_\mu\hat{K}_\nu\right),$$

with N_f as the number of flavors. Hence, we can define

$$\Pi^d_{00}(p_0,\mathbf{p}) = \frac{g^2T^2}{6}N_f\left(1 - \frac{p_0}{p}R_0(p_0,p)\right), \tag{4.19}$$

$$\Pi^d_{\mu\mu}(P) = \frac{g^2T^2}{6}N_f\int\frac{d\Omega}{4\pi}(1) = \frac{g^2T^2}{6}N_f, \tag{4.20}$$

with $R_0(p_0, p) = \frac{1}{2}\ln\left|\frac{\mathrm{p}_0+\mathrm{p}}{\mathrm{p}_0-\mathrm{p}}\right| - \frac{\mathrm{i}\pi}{2}\theta(\mathrm{p}^2 - \mathrm{p}_0^2)$. Gribov parameter-dependent form factors can be obtained by summing up all the contributions from different sectors, and this can be used in the analysis of energy loss formalism as described in Eq. (4.4). For the quantitative estimation of the energy loss of parton in the Gribov plasma, we consider the temperature dependence of the γ_G that can be described from the gap equation as [124],

$$\gamma_G = \frac{d-1}{d}\frac{N_c}{4\sqrt{2}\pi}g^2T. \tag{4.21}$$

Details of the temperature behavior of γ_G are discussed in the supplementary material (Section C).

4.3 Results and discussions

We start with the discussion of momentum dependence of Gribov-modified parton energy loss in the QGP medium. We performed the numerical integration of the integral described in Eq. (4.4) by employing the effective gluon propagator for the Gribov-Zwanziger plasma. The gluon and ghost loops contribution to the gluon self-energy is modified with the Gribov-Zwanziger framework and is reflected in the energy loss of the test parton in the medium. In Fig. 4.1, energy loss experienced by the moving massless and massive parton in the medium is plotted as a function of its momentum at a finite temperature. For the massive case, we chose M=1.25 GeV. The estimations from the Gribov-Zwanziger approach are compared with those from the perturbative calculations in the thermal medium. It is seen that non-perturbative effects incorporated through the Gribov-Zwanziger framework significantly enhance the leading order pQCD estimation of the energy loss pattern of the moving parton. The analysis holds true for both massless and massive cases. This observation is consistent with the result of the heavy quark diffusion coefficient $2\pi DT$ based on

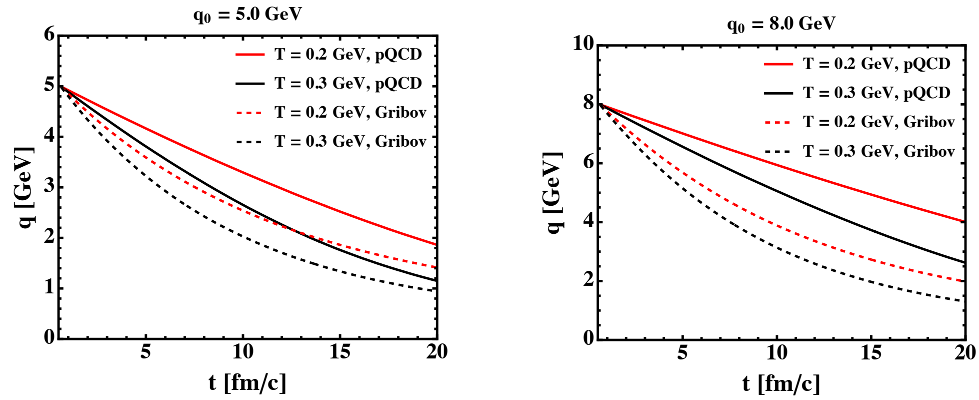

Figure 4.2: Momentum evolution of the massless parton in Gribov plasma with different choices of initial momentum.

the transport theory framework in the Gribov and quasiparticle approaches [124, 240] as $2\pi DT \propto \frac{1}{-dE/dx}$. Notably, the pQCD estimation of energy loss of massless and massive parton converges at a higher momentum regime. However, in Gribov plasma, where the analysis incorporates a temperature-dependent Gribov mass parameter along with the parton mass, we observe that the mass of the parton exerts a more substantial impact on the energy loss even at higher momentum scales.

The impact of the Gribov parameter on the momentum evolution of the massless parton is depicted in Fig.4.2. The proper time evolution of the parton momentum is obtained by solving Langevin equations. Langevin equation [241–243] requires the knowledge of the stochastic force and dissipative force experienced by the energetic parton in the medium. The latter is estimated from the Gribov-modified energy loss, and the random kicks are described by a Gaussian noise with the width related to the momentum diffusion coefficient. We use the fluctuation-dissipation theorem to determine the momentum diffusion in the analysis [244, 245]. We observe that the parton loses a higher fraction of its initial momentum while propagating through the Gribov medium due to the soft interactions in comparison with that in a thermal pQCD medium. Notably, the proper time evolution of the momentum is sensitive to the value of the initial momentum of the parton and the temperature of the medium.

We have considered the static thermal medium by fixing a constant temperature profile. This choice is justified as the focus of the current study is to analyze the non-perturbative effect of the QCD medium by comparing estimations from the Gribov-Zwanziger framework and pQCD results. Importantly, we find that the non-equilibrium corrections to parton energy loss arising due to the medium evolution are negligible when compared to the impact of non-perturbative effects. The gluon self-energy of anisotropic non-equilibrium can be decomposed as $\Pi^{ij} = \alpha A^{ij} + \beta B^{ij} + \gamma Y^{ij} + \delta Z^{ij}$ where $Y^{ij} = \frac{\tilde{a}^i \tilde{a}^j}{\tilde{a}^2}$, $Z^{ij} = p^i \tilde{a}^j + p^j \tilde{a}^i$ with $\tilde{a}^i = A^{ij} a_j$ (**a** is the direction of anisotropy). The structure functions $\alpha, \beta, \gamma, \delta$ for the anisotropic QCD medium are discussed in detail in Refs. [246, 247]. Employing the form of Π^{ij}, parton energy loss in an evolving anisotropic medium can be defined as,

$$
\begin{aligned}
\frac{dE}{dx} &= -i \frac{1}{|\mathbf{v}|} g^2 C_F v^i v^j \int \frac{d^3\mathbf{p}}{(2\pi)^3} \omega \Big[\Delta_1(\omega)(A^{ij} - Y^{ij}) \\
&+ \Delta_2(\omega) \Big((\omega^2 - |\mathbf{p}|^2 - \alpha - \gamma) B^{ij} + (\omega^2 - \beta) Y^{ij} + \delta Z^{ij} \Big) \Big],
\end{aligned} \tag{4.22}
$$

with $\Delta_1 = \omega^2 - |\mathbf{p}|^2 - \alpha$ and $\Delta_2 = (\omega^2 - \beta)(\omega^2 - |\mathbf{p}|^2 - \alpha - \gamma) - |\mathbf{p}|^2 \delta^2 \tilde{a}^2$. We have verified that these non-equilibrium corrections to the energy loss due to the anisotropy of the evolving medium are marginal in comparison with the non-perturbative effect of the QCD medium. This conclusion aligns with the findings of the recent study [248], where it was shown that non-equilibrium corrections play a negligible role in the momentum evolution of charm quarks within a $1 + 3$-dimensional evolving QGP medium.

To quantify the phenomenological implication of the Gribov-modified energy loss of parton in the context of heavy-ion collision experiments, we study the nuclear suppression

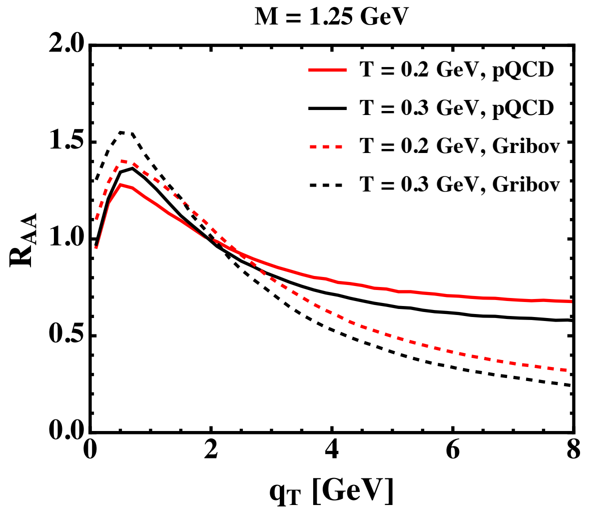

Figure 4.3: R_{AA} in the static Gribov-Zwanziger plasma as a function of transverse momentum.

factor $R_{AA}(q_T)$ in a static medium that can be described as [241],

$$R_{AA}(q_T) = \frac{f_{\tau_f}(q_T)}{f_{\tau_0}(q_T)}, \tag{4.23}$$

where $f_{\tau_0}(q_T)$ and $f_{\tau_f}(q_T)$ represent the initial and final momentum distribution of the parton in the medium at the time evolution period. Here, we consider the case of charm quark with M=1.25 GeV and τ_f=5 fm/c. The initial momentum spectra and f_{τ_0}, have been taken from fixed order + next-to-leading log (FONLL) calculations, as described in Refs. [249, 250]. Final spectra and f_{τ_0} are obtained by solving the stochastic Langevin dynamics with the Gribov-modified transport coefficients in the medium as an essential input parameter to the simulation. We observe a stronger suppression (smaller R_{AA}) upon the inclusion of non-perturbative effects as depicted in Fig. 4.3, and the impact is more pronounced in the higher momentum regimes. This finding is a consequence of the fact that Gribov plasma imposes a greater hindrance for the energetic parton as it traverses through the medium.

4.4 Summary and Outlook

In this work, we studied the energy loss of a test parton, considering the non-perturbative resummation using the Gribov-Zwanziger prescription for the first time. We utilized Wong's equations along with linearized Yang-Mills equations to quantify the back-reaction exerted on the parton. This analysis involves examining the polarization effects of the medium, thereby determining the parton's energy loss as it traverses through the medium. As a first step, we estimated the gluon, quark, and ghost loop contributions to the Gribov-modified gluon self-energy. Notably, gluon and ghost loops are modified with the inclusion of the Gribov parameter, and their effects are reflected in the energy loss pattern of the energetic parton in the medium. We conducted a systematic analysis of the momentum evolution of the massless fast-moving parton by solving the Langevin dynamics. We observe that the Gribov-modified estimation of the energy loss pattern and momentum evolution significantly improves the leading order pQCD results. Moreover, the incorporation of non-perturbative effects is essential for ensuring consistency in the theoretical description of parton energy loss within a realistic QGP medium. Further, we explored the nuclear suppression factor for the charm quark to analyze the phenomenological implication of the present study. It is seen that R_{AA} is highly sensitive to the non-perturbative effects, evidenced by a stronger suppression in the Gribov plasma in comparison with that of the leading order pQCD estimation.

Looking ahead, it will be interesting to extend the energy loss formalism to an evolving medium within the Gribov approach which requires the knowledge of the medium evolution of the Gribov plasma. The thermodynamics and temperature dependence of transport coefficients of the Gribov plasma have recently studied in Ref. [126]. The challenging task ahead lies in obtaining second-order viscous hydrodynamics within the Gribov-Zwanziger framework, which is essential for describing the medium evolution and exploring energy loss phenomena in an expanding medium.

CHAPTER 5

COMPLEX HEAVY QUARKONIUM POTENTIAL IN AN ANISOTROPIC COLLISIONAL QUARK-GLUON PLASMA

In this chapter heavy quark cornell potential in a anisotropic thermal medium with collision present in the system. This chapter is based on the work presented in the following paper: ***Complex Heavy Quarkonium Potential in an Anisotropic Collisional Quark-Gluon Plasma***

Manas Debnath, Lata Thakur, Najmul Haque [arXiv:2504.02802].

5.1 Introduction

Heavy quarkonium suppression is a well-established probe of QGP formation [28]. In a vacuum, quarkonium states are well characterized by non-relativistic potential models, which exhibit a Coulomb-like behavior at short distances and a linear confining potential at larger distances [171, 211, 251–254]. In a thermal medium, color screening modifies this potential and can dissociate bound states once the temperature exceeds the crossover scale. Because different states possess different binding energies, their dissociation occurs sequentially [255], a pattern observed experimentally at RHIC and the LHC [256, 257].

While earlier studies of heavy quarkonium in QGP assume an isotropic medium [216], the early stages of heavy-ion collisions introduce momentum-space anisotropies caused by the rapid expansion of the plasma [246, 258, 259]. Non-central collisions, in particular, generate an anisotropic momentum distribution, leading to differential pressures in longitudinal and transverse directions, resulting in a momentum space anisotropy, and it causes a kinetic instability [260]. The instability has a significant effect on the system's evolution, leading to faster isotropization [260, 261]. This anisotropy influences collective gluon modes [246, 262, 263], which in turn modify the heavy-quark potential [262, 264–270]. In addition to the momentum anisotropy, the collisions among plasma constituents are usually ignored at high temperatures as the hard collision (large momentum exchange) time scale is much longer than the time scale for the soft momentum exchange [271]. When the temperature of the system decreases, it becomes necessary to consider both hard and soft collisions.

The gluon collective modes in an isotropic thermal QGP with collisional effects have been studied using a Bhatnagar-Gross-Krook (BGK) collisional kernel [272], and this formalism has been extended to anisotropic plasmas [273] in which the authors have considered only those modes which are propagating parallel to the anisotropy vector. In Ref. [273], the authors found a single unstable mode and a few other stable modes. Later, in Ref. [274], the authors considered the modes that can propagate in all possible directions with respect to the (small) anisotropy vector, where they considered the interacting medium in terms of the effective quasiparticle model. Recently, in Ref. [271], the authors extended the existing results for the collective modes by incorporating the full angular dependence of gluon propagation while considering general anisotropy strength.

Previous studies have explored quarkonium properties in an anisotropic QGP under collisionless scenarios [262, 264, 267, 275–277], while Ref. [271] examined collective modes with collisions. In a momentum-anisotropic QGP, we extend these efforts by systematically deriving the complex heavy-quark potential with finite collisional effects. Using the collective modes of Ref. [271], for the first time, we compute the real and imaginary components of the potential, incorporating both general anisotropy and the BGK collision kernel. However, one has to be careful in evaluating the imaginary part of the heavy quarkonium potential in a general anisotropic case in collisional plasma. For collisionless plasma with small anisotropy (ξ), one can expand the imaginary part of the potential at small ξ, and it can be calculated at first order of ξ (see [275]). But for general anisotropy strength in collisionless plasma, this is not possible due to the presence of the Pinch singularity, known as Weibel instability as discussed in [276]. However, we show the region, for finite collisional effects, where the imaginary potential is free from such singularities. Our studies reveal how these effects influence quarkonium thermal widths and dissociation rates in a nonequilibrium QGP, providing valuable insights into quarkonium suppression in relativistic heavy-ion collisions.

In addition to the quarkonium potential in an anisotropy system, the quarkonium properties are also studied in various non-trivial situations relevant to HIC. As a strong magnetic field appears in non-central HIC, the heavy quarkonium properties are studied in the presence of an external magnetic field [278, 279]. Additionally, the quarkonium properties are also studied when there is relative motion between the medium and quarkonium [212, 280], in a bulk viscous medium [217, 281, 282] and with the Gribov–Zwanziger action [64].

This chapter is structured as follows: Section 5.2 discusses the gluon propagator in a collisional anisotropic QGP medium. In Section 5.3, we discuss the dielectric permittivity of the collisional anisotropic QGP medium. In section 5.4, we present the derivation of the complex heavy-quark potential and examine the impact of collisions and momentum-anisotropy on the real and imaginary components of the complex static potential. In Section 5.5, we study the thermal width of the ground state of charmonium. Finally, we summarize our results and discuss their implications in Section 5.6.

5.2 Gluon propagator in a collisional anisotropic medium

In this section, we discuss the gluon self-energy and propagator in the presence of a collisional anisotropic QGP medium, which affect the permittivity of the medium and eventually use that to determine the in-medium heavy quark-antiquark potential.

The momentum-space anisotropic correction is introduced by deforming the distribution functions of constituent particles [246]. The deformed distribution function is parametrized in the following spheroidal form

$$f(\boldsymbol{k}) = f_{\text{iso}}\left(\frac{1}{\lambda}\sqrt{k_T^2 + (1+\xi)k_L^2}\right) = f_{\text{iso}}\left(\frac{1}{\lambda}\sqrt{\boldsymbol{k}^2 + \xi(\boldsymbol{k}\cdot\boldsymbol{n})^2}\right), \tag{5.1}$$

where $f(\boldsymbol{k})$ is derived from $f_{iso}(k)$ by filtering out particles with a large momentum component along the anisotropic direction, $\boldsymbol{n}$ [246]. Here, k_T is transverse and k_L is longitudinal components of momentum to a given anisotropy axis $\boldsymbol{n}$ with $k = |\boldsymbol{k}| = \sqrt{k_T^2 + k_L^2}$. Here, in Eq. (5.1), the parameter ξ quantitatively measures the strength of momentum-space anisotropy. The quantity λ serves as a typical characteristic momentum scale of plasma particles. Here, it is relevant as the temperature is only in thermal equilibrium. Considering a spheroidal distortion, only one anisotropy axis is being considered. As a result, the modes of the gluon polarization tensor depend on the propagation angle relative to

$\boldsymbol{n}$. We first calculate the gluon self-energy and propagators in a collisional anisotropic QGP medium. Subsequently, we determine the inverse dielectric permittivity of the anisotropic medium with collision, which will be used to compute the real and imaginary parts of the quarkonium static potential.

5.2.1 Gluon self-energy and resummed propagator

In the collisionless case, the gluon self-energy is typically obtained by the hard thermal loop (HTL) resummation technique from the Feynman diagrams. However, for the collisional QGP, the gluon self-energy is usually obtained using the Kinetic theory [271–273]. In the kinetic theory prescription, the phase-space distribution of partons (viz. gluons, quarks, and antiquarks) in the QCD plasma is characterized using gauge-covariant Wigner functions, $W^i(\boldsymbol{k}, X)$ with $i \in \{g, q, \bar{q}\}$ and $\boldsymbol{k}$ and X denote the three momentum and four position respectively. These particles are considered massless and follow the mass-shell constraint. To obtain the linearized transport equation, we expand $W^i(\boldsymbol{k}, X) = W^i(\boldsymbol{k}) + \delta W^i(\boldsymbol{k}, X)$. After applying a gauge-covariant gradient expansion, the generalized Boltzmann equation governing quarks and gluons takes the form

$$V \cdot \partial_X \delta f^i_a(\boldsymbol{k}, X) + g\theta_i\, V_\mu F^{\mu\nu}_a \partial^{(K)}_\nu f^i(\boldsymbol{k}) = \mathcal{C}^i_a(\boldsymbol{k}, X), \tag{5.2}$$

where $V = (1, \boldsymbol{v})$ with $\boldsymbol{v} \equiv \boldsymbol{k}/k$ and $\theta_g = \theta_q = 1, \theta_{\bar{q}} = -1$. In Eq. (5.2), the weak-coupling limit is taken, and higher order terms of coupling g are neglected. So the field tensor becomes $F^{\mu\nu} = \partial_\mu A_\nu - \partial_\nu A_\mu + \mathcal{O}(g)$. In this limit, the theory becomes effectively Abelian, and one may consider there is no coupling between different color channels. The distribution function $f^i(\boldsymbol{k})$ and its color fluctuations $\delta f^i_a(\boldsymbol{k}, X)$ are related via the Wigner function as

$$f^{q/\bar{q}}(\boldsymbol{k}) = \frac{1}{N_c}\mathrm{Tr}[\mathrm{W}^{\mathrm{q}/\bar{\mathrm{q}}}(\mathrm{k},\mathrm{X})], \quad f^g(\mathrm{k}) = \frac{1}{\mathrm{N_c^2}-1}\mathrm{Tr}[\mathrm{W}^{\mathrm{g}}(\mathrm{k},\mathrm{X})], \tag{5.3}$$

and

$$\delta f_a^{q/\bar{q}}(\boldsymbol{k}, X) = 2\mathrm{Tr}[\mathrm{t_a}\,\delta\mathrm{W}^{\mathrm{q}/\bar{\mathrm{q}}}(\mathrm{k},\mathrm{X})], \quad \delta f_a^g(\mathrm{k},\mathrm{X}) = \frac{1}{\mathrm{N_c}}\mathrm{Tr}[\mathrm{T_a}\,\delta\mathrm{W}^{\mathrm{g}}(\mathrm{k},\mathrm{X})], \tag{5.4}$$

where t_a is the $SU(N_c)$ group generators in the fundamental representation and T_a is the corresponding adjoint representations. Now, for the collisionless case, the right-hand side of Eq. (5.2) is simply zero, that is, $\mathcal{C}_a^i(\boldsymbol{k}, X) = 0$. But when we include collision, $\mathcal{C}_a^i(\boldsymbol{k}, X)$ can be given by a BGK-type collision kernel,

$$\mathcal{C}_a^i(\boldsymbol{k}, X) \;=\; -\nu\left[f_a^i(\boldsymbol{k}, X) - \frac{N_a^i(X)}{N_{eq}^i} f_{eq}^i(k)\right], \tag{5.5}$$

with $f_a^i(\boldsymbol{k}, X) = f^i(\boldsymbol{k}) + \delta f_a^i(\boldsymbol{k}, X)$, and

$$N_a^i(X) = \int_{\boldsymbol{k}} f_a^i(\boldsymbol{k}, X), \qquad N_{eq}^i = \int_{\boldsymbol{k}} f_{eq}^i(k). \tag{5.6}$$

The BGK-type collision term in Eq. (5.5) characterizes the equilibration of the system through collisions, occurring over a timescale inversely proportional to ν. In this work, the collision parameter, ν, is taken to be a free parameter, with no dependence on particle momentum and particle species. The advantage of the BGK kernel is that the particle number conservation is instantaneously followed; that is,

$$\int_{\boldsymbol{k}} \mathcal{C}_a^i(\boldsymbol{k}, X) = 0. \tag{5.7}$$

In Ref. [273], it is estimated that ν lies in the range $\nu \sim 0.1m_D - 0.2m_D$, but it is possible that the collision rate could even be larger than this. However, in this article, we have assumed a small ν [1]. The induced current for each color channel is given by,

$$J^{\mu}_{ind,a} = g\int_{\boldsymbol{k}} V^{\mu}\{2N_c\,\delta f^{g}_{a}(k,X) + N_f[\delta f^{q}_{a}(k,X) - \delta f^{\bar{q}}_{a}(k,X)]\}. \tag{5.8}$$

The gluon self-energy for the collisional case can be obtained following the Ref. [271, 273] as

$$\begin{aligned}
\Pi^{\mu\nu}_{ab}(P) &= \frac{\delta J^{\mu}_{ind,a}(P)}{\delta A^{b}_{\nu}(P)} \\
&= g^2\delta_{ab}\int_{\boldsymbol{k}} V^{\mu}\partial^{\boldsymbol{k}}_{l} f(\boldsymbol{k})\frac{g^{l\nu}(\hat{\omega}-\hat{\boldsymbol{p}}\cdot\boldsymbol{v}) - \hat{P}^{l}V^{\nu}}{\hat{\omega}-\hat{\boldsymbol{p}}\cdot\boldsymbol{v}+i\hat{\nu}} + g^2\delta_{ab}(i\hat{\nu})\int\frac{d\Omega}{4\pi}\frac{V^{\mu}}{\hat{\omega}-\hat{\boldsymbol{p}}\cdot\boldsymbol{v}+i\hat{\nu}} \\
&\times \int_{\boldsymbol{k}'}\partial^{(\boldsymbol{k}')}_{l} f(\boldsymbol{k}')\frac{g^{l\nu}(\hat{\omega}-\hat{\boldsymbol{p}}\cdot\boldsymbol{v}') - \hat{P}^{l}V'^{\nu}}{\hat{\omega}-\hat{\boldsymbol{p}}\cdot\boldsymbol{v}'+i\hat{\nu}}\mathcal{W}^{-1}(\hat{\omega},\hat{\nu}),
\end{aligned} \tag{5.9}$$

where $\int_{\boldsymbol{k}} \equiv \int d^3\boldsymbol{k}/(2\pi)^3$. For convenience, we define the dimensionless collision rate $\hat{\nu} = \nu/p$. $\hat{P} = (\hat{\omega}, \hat{\boldsymbol{p}})$ with $\hat{\omega} = \omega/p$ and $\hat{\boldsymbol{p}} = \boldsymbol{p}/p$. The function $\mathcal{W}(\hat{\omega},\hat{\nu})$ is defined as

$$\mathcal{W}(\hat{\omega},\hat{\nu}) = 1 - \frac{i\hat{\nu}}{2}\int_{-1}^{1}\frac{dy}{\hat{\omega}-y+i\hat{\nu}} = 1 - \frac{i\hat{\nu}}{2}\ln\frac{\hat{\omega}+i\hat{\nu}+1}{\hat{\omega}+i\hat{\nu}-1}. \tag{5.10}$$

In Eq. (5.9), $f(\boldsymbol{k}) = N_f[f^{q}(\boldsymbol{k}) + f^{\bar{q}}(\boldsymbol{k})] + N_c f^{g}(\mathbf{k})$, where the distribution function of partons is anisotropic as defined in eq. (5.1). The gluon self-energy still satisfies the transversality condition even after introducing the collisional term. The spatial component of gluon

[1] For the imaginary part of the potential calculation, we take only $\nu = 0.3m_D, 0.4m_D$ where imaginary part of the potential is well defined because there is a region of singularity for up to $\nu \sim 0.24m_D$ at around $\xi \sim 10$. See Fig. 5.2

self-energy can be obtained after substituting the Eq. (5.1) into Eq. (5.9) as

$$\begin{aligned}\Pi^{ij}(P) &= m_D^2 \int \frac{d\Omega}{4\pi} v^i \frac{v^l + \xi(\boldsymbol{v}\cdot\boldsymbol{n})n^l}{(1+\xi(\boldsymbol{v}\cdot\boldsymbol{n})^2)^2} \frac{\delta^{lj}(\hat{\omega} - \hat{\boldsymbol{p}}\cdot\boldsymbol{v}) + \hat{p}^l v^j}{\hat{\omega} - \hat{\boldsymbol{p}}\cdot\boldsymbol{v} + i\hat{\nu}} + i\hat{\nu} m_D^2 \int \frac{d\Omega'}{4\pi} \\ &\times \frac{v'^i}{\hat{\omega} - \hat{\boldsymbol{p}}\cdot\boldsymbol{v'} + i\hat{\nu}} \int \frac{d\Omega}{4\pi} \frac{v^l + \xi(\boldsymbol{v}\cdot\boldsymbol{n})n^l}{(1+\xi(\boldsymbol{v}\cdot\boldsymbol{n})^2)^2} \frac{\delta^{lj}(\hat{\omega} - \hat{\boldsymbol{p}}\cdot\boldsymbol{v}) + \hat{p}^l v^j}{\hat{\omega} - \hat{\boldsymbol{p}}\cdot\boldsymbol{v} + i\hat{\nu}} \mathcal{W}(\hat{\omega}, \hat{\nu})^{-1},\end{aligned} \tag{5.11}$$

where

$$m_D^2 = -\frac{g^2}{2\pi^2} \int_0^\infty dk\ k^2 \frac{df_{iso}(k)}{dk}. \tag{5.12}$$

The gluon self-energy given in Eq. (5.11) is asymmetric in the Lorentz indices due to the presence of a collision term of BGK-type. This asymmetry is also seen in magnetized plasma because of the lack of time-reversal symmetry [283]. Therefore, the symmetric tensor basis for anisotropic systems in the collisionless limit is unsuitable for the decomposition in Eq. (5.11). Instead, we adopt a more general tensor basis with five structure functions to decompose the gluon self-energy.

$$\Pi^{ij}(P) = \alpha A^{ij} + \beta B^{ij} + \gamma C^{ij} + \delta D^{ij} + \rho E^{ij}, \tag{5.13}$$

with the tensor basis defined as

$$A^{ij} = \delta^{ij} - \hat{p}^i\hat{p}^j, \quad B^{ij} = \hat{p}^i\hat{p}^j, \quad C^{ij} = \frac{\tilde{n}^i\tilde{n}^j}{\tilde{n}^2}, \quad D^{ij} = \tilde{n}^i\hat{p}^j, \quad E^{ij} = \tilde{n}^j\hat{p}^i \tag{5.14}$$

Here, $\tilde{n}^i \equiv A^{ij}n^j$, which is orthogonal to $\hat{p}^i$. Note that the basis functions follow the following orthonormal conditions:

$$A^{ij}A^{ij} = 2,\ B^{ij}B^{ij} = 1,\ C^{ij}C^{ij} = 1,\ D^{ij}D^{ij} = 0,\ E^{ij}E^{ij} = 0, \tag{5.15a}$$

$$\hat{p}^i A^{ij} = 0,\ \hat{p}^i B^{ij} = \hat{p}^j,\ \hat{p}^i C^{ij} = 0,\ \hat{p}^i D^{ij} = 0,\ \hat{p}^i E^{ij} = \tilde{n}^j, \tag{5.15b}$$

$$\tilde{n}^i A^{ij} = \tilde{n}^j,\ \tilde{n}^i B^{ij} = 0,\ \tilde{n}^i C^{ij} = \tilde{n}^j,\ \tilde{n}^i D^{ij} = \tilde{n}^2 \hat{p}^j,\ \tilde{n}^i E^{ij} = 0. \tag{5.15c}$$

Using the orthonormal properties of the tensor basis, the five structure functions can be determined from Eq. (5.13) based on the following contraction as

$$\hat{p}^i \Pi^{ij} \hat{p}^j = \beta, \tag{5.16a}$$

$$\tilde{n}^i \Pi^{ij} \tilde{n}^j = \tilde{n}^2(\alpha + \gamma), \tag{5.16b}$$

$$\tilde{n}^i \Pi^{ij} \hat{p}^j = \tilde{n}^2 \delta, \tag{5.16c}$$

$$\hat{p}^i \Pi^{ij} \tilde{n}^j = \tilde{n}^2 \rho, \tag{5.16d}$$

$$\mathrm{Tr}\Pi^{ij} = 2\alpha + \beta + \gamma. \tag{5.16e}$$

By utilizing gluon self-energy, the inverse of the resummed gluon propagator $\Delta^{ij}(P)$ can be computed in temporal axial gauge using the Dyson-Schwinger equation as

$$(\Delta^{-1})^{ij}(P) = (p^2 - \omega^2 + \alpha)A^{ij} + (\beta - \omega^2)B^{ij} + \gamma C^{ij} + \delta D^{ij} + \rho E^{ij}. \tag{5.17}$$

Upon inversion, the resummed gluon propagator becomes

$$\Delta^{ij}(P) = \Delta_A[A^{ij} - C^{ij}] + \Delta_G[(p^2 - \omega^2 + \alpha + \gamma)B^{ij} + (\beta - \omega^2)C^{ij} - \delta D^{ij} - \rho E^{ij}], \tag{5.18}$$

with

$$
\begin{aligned}
\Delta_A &= \frac{1}{\omega^2 - p^2 - \alpha}, &\text{(5.19a)}\\
\Delta_G &= \frac{1}{(p^2 - \omega^2 + \alpha + \gamma)(\beta - \omega^2) - \tilde{n}^2\delta\rho}. &\text{(5.19b)}
\end{aligned}
$$

The dispersion relation can be determined by finding the poles of the propagator $\Delta^{ij}(P)$, namely,

$$
\begin{aligned}
\Delta_A^{-1} &= \omega^2 - p^2 - \alpha = 0,\\
\Delta_G^{-1} &= (p^2 - \omega^2 + \alpha + \gamma)(\beta - \omega^2) - \tilde{n}^2\delta\rho = (\omega^2 - \Omega_+^2)(\omega^2 - \Omega_-^2) = 0, \quad (5.20)
\end{aligned}
$$

where

$$
2\Omega_\pm^2 = \bar{\Omega}^2 \pm \sqrt{\bar{\Omega}^4 - 4[(\alpha + \gamma + p^2)\beta - \tilde{n}^2\delta\rho]}, \tag{5.21}
$$

with $\bar{\Omega}^2 = \alpha + \beta + \gamma + p^2$. Using Eq. (5.16), we can get the following forms of the structure functions ([271]),

$$
\begin{aligned}
\alpha(\xi,\hat{\omega},t,\hat{\nu}) &= \frac{m_D^2}{2(1-t^2)}\Big[\hat{\omega} z f_0(\xi) - \xi t^2 f_1(\xi) + \hat{\omega}(1-t^2-z^2)\mathcal{I}^{[0]}(\xi,\hat{\omega},t,\hat{\nu})\\
&\quad + t\big\{\xi(1-t^2) + z(2\hat{\omega} - \xi z)\big\}\mathcal{I}^{[1]}(\xi,\hat{\omega},t,\hat{\nu}) - (\hat{\omega} - 2\xi z t^2)\mathcal{I}^{[2]}(\xi,\hat{\omega},t,\hat{\nu})\\
&\quad - \xi t\mathcal{I}^{[3]}(\xi,\hat{\omega},t,\hat{\nu})\Big], &\text{(5.22a)}\\
\beta(\xi,\hat{\omega},t,\hat{\nu}) &= -\frac{\hat{\omega}^2 m_D^2}{2\mathcal{W}(\hat{\omega},\hat{\nu})}\Big[f_0(\xi) - z\mathcal{I}^{[0]}(\xi,\hat{\omega},t,\hat{\nu}) - \xi t\mathcal{I}^{[1]}(\xi,\hat{\omega},t,\hat{\nu})\Big], &\text{(5.22b)}\\
\gamma(\xi,\hat{\omega},t,\hat{\nu}) &= \frac{m_D^2}{2(1-t^2)}\Big[\xi(1+t^2)f_1(\xi) - \hat{\omega} z(1+t^2)f_0(\xi) - \hat{\omega}\left\{(1-t^2) - z^2(1+t^2)\right\}\\
&\quad \times\mathcal{I}^{[0]}(\xi,\hat{\omega},t,\hat{\nu}) - t\left\{4\hat{\omega} z - 2\xi z^2 + \xi(1-t^2)(1+\hat{\omega} z)\right\}\mathcal{I}^{[1]}(\xi,\hat{\omega},t,\hat{\nu})\\
&\quad - \left\{4\xi z - 2\hat{\omega} - \xi(1-t^2)(\hat{\omega} + 3z)\right\}\mathcal{I}^{[2]}(\xi,\hat{\omega},t,\hat{\nu}) + 2\xi t\mathcal{I}^{[3]}\Big], &\text{(5.22c)}
\end{aligned}
$$

$$\delta(\xi,\hat{\omega},t,\hat{\nu}) = \frac{\hat{\omega}m_D^2}{2(1-t^2)}\Big[tzf_0(\xi) - tz^2\mathcal{I}^{[0]}(\xi,\hat{\omega},t,\hat{\nu}) + z(1-\xi t^2)\mathcal{I}^{[1]}(\xi,\hat{\omega},t,\hat{\nu})$$
$$+\xi t\mathcal{I}^{[2]}(\xi,\hat{\omega},t,\hat{\nu})\Big], \qquad (5.22d)$$
$$\rho(\xi,\hat{\omega},t,\hat{\nu}) = \frac{\hat{\omega}m_D^2}{2\mathcal{W}(\hat{\omega},\hat{\nu})(1-t^2)}\Big[\hat{\omega}tf_0(\xi) - \hat{\omega}tz\mathcal{I}^{[0]}(\xi,\hat{\omega},t,\hat{\nu})$$
$$+\left\{\hat{\omega}(1+\xi-\xi t^2) - \xi z\right\}\mathcal{I}^{[1]}(\xi,\hat{\omega},t,\hat{\nu}) + \xi t\mathcal{I}^{[2]}(\xi,\hat{\omega},t,\hat{\nu})\Big], \qquad (5.22e)$$

where $z = \hat{\omega} + i\hat{\nu}$. The master integral, $\mathcal{I}^{[n]}(\xi,\hat{\omega},t,\hat{\nu})$ has the form

$$\begin{aligned}
\mathcal{I}^{[n]}(\xi,\hat{\omega},t,\hat{\nu}) &= \int_{-1}^{1} dy\, \frac{y^n}{(1+\xi y^2)^2}\int_0^{2\pi}\frac{d\phi}{2\pi}\frac{1}{\hat{\omega} - \hat{\boldsymbol{p}}\cdot\boldsymbol{v} + i\hat{\nu}} \\
&= \int_{-1}^{1} dy\, \frac{y^n}{(1+\xi y^2)^2}\frac{\text{sign}(\text{Re}[\hat{\omega}] - \hat{p}_z y)}{\sqrt{(\hat{\omega} - \hat{p}_z y + i\hat{\nu})^2 - \hat{p}_y^2(1-y^2)}}, \\
&= \int_{-1}^{1} dy\, \frac{y^n}{(1+\xi y^2)^2}\frac{\text{sign}(\text{Re}[\hat{\omega}] - ty)}{\sqrt{(\hat{\omega} - ty + i\hat{\nu})^2 - (1-t^2)(1-y^2)}}, \qquad (5.23)
\end{aligned}$$

where $n = 0, 1, 2, 3$ and $t = \cos\theta$, with θ being the angle between $\boldsymbol{p}$ and $\boldsymbol{n}$. It is assumed that $\boldsymbol{p}$ lies in the y-z plane, while $\boldsymbol{n}$ is parallel to the z-axis. The ω generally has a complex value, and the integration variable y represents the cosine of the polar angle between $\boldsymbol{k}$ and $\boldsymbol{n}$. The functions $f_0(\xi)$ and $f_1(\xi)$ are defined as

$$f_0(\xi) = \int_0^1 \frac{2}{(1+\xi y^2)^2}\,dy = \frac{1}{1+\xi} + \frac{\arctan\sqrt{\xi}}{\sqrt{\xi}}, \qquad (5.24a)$$
$$f_1(\xi) = \int_0^1 \frac{2y^2}{(1+\xi y^2)^2}\,dy = -\frac{1}{\xi+\xi^2} + \frac{\arctan\sqrt{\xi}}{\sqrt{\xi^3}}. \qquad (5.24b)$$

Note that, in the collisionless limit, that is, when the collision parameter $\nu = 0$, $\mathcal{W}(\hat{\omega}, 0) = 1$ and $z = \hat{\omega}$ only. Then,

$$\rho(\xi,\hat{\omega},t,0) = \delta(\xi,\hat{\omega},t,0), \qquad (5.25)$$

The above relation implies that in the collisionless limit, we have only four structure functions, and the self-energy is symmetric, i.e., $\Pi^{ij} = \Pi^{ji}$.

As the medium's dielectric permittivity is defined in the static limit ($\omega \to 0$), we can define various mass scales corresponding to the structure functions as

$$m_\alpha^2 = \lim_{\omega\to 0} \alpha, \tag{5.26a}$$
$$m_\beta^2 = -\lim_{\omega\to 0} \frac{\beta}{\hat{\omega}^2}, \tag{5.26b}$$
$$m_\gamma^2 = \lim_{\omega\to 0} \gamma, \tag{5.26c}$$
$$m_\delta^2 = \lim_{\omega\to 0} \frac{\tilde{n}}{\hat{\omega}}\text{Im}[\delta], \tag{5.26d}$$
$$m_\rho^2 = \lim_{\omega\to 0} \frac{\tilde{n}}{\hat{\omega}}\text{Im}[\rho]. \tag{5.26e}$$

After taking the static limit, the master integral $\mathcal{I}^{[n]}(\xi, 0, t, \hat{\nu})$, reduces to

$$\tilde{\mathcal{I}}^{[n]}(\xi, t, \hat{\nu}) = -\int_0^1 dy \; \frac{2}{(1+\xi y^2)^2} f^{[n]}(y, t, \hat{\nu})$$

with

$$f^{[n]}(y,t,\hat{\nu}) = \begin{cases} \frac{\sqrt{s(y,t,\hat{\nu})+y^2-\hat{\nu}^2+t^2-1}}{\sqrt{2}s(y,t,\hat{\nu})} y^n, & n \text{ is odd} \\ i\frac{\sqrt{2}\hat{\nu}t/s(y,t,\hat{\nu})}{\sqrt{s(y,t,\hat{\nu})+y^2-\hat{\nu}^2+t^2-1}} y^{n+1}, & n \text{ is even} \end{cases}, \tag{5.27}$$

where $s(y,t,\hat{\nu}) \equiv \sqrt{\left(y^2-\hat{\nu}^2+t^2-1\right)^2 + 4y^2\hat{\nu}^2t^2}$. So the mass scales become [271]

$$m_\alpha^2 = -\frac{\xi t\, m_D^2}{2(1-t^2)}\Big[t f_1(\xi) - (1-t^2+\hat{\nu}^2)\tilde{\mathcal{I}}^{[1]}(\xi,t,\nu) - 2i\hat{\nu}t\tilde{\mathcal{I}}^{[2]}(\xi,t,\hat{\nu}) + \tilde{\mathcal{I}}^{[3]}(\xi,t,\hat{\nu})\Big], \tag{5.28a}$$

$$m_\beta^2 = \frac{m_D^2}{2\mathcal{W}(0,\hat{\nu})}\Big[f_0(\xi) - i\hat{\nu}\tilde{\mathcal{I}}^{[0]}(\xi,t,\hat{\nu}) - \xi t\tilde{\mathcal{I}}^{[1]}(\xi,t,\hat{\nu})\Big], \tag{5.28b}$$

$$m_\gamma^2 = \frac{\xi\, m_D^2}{2(1-t^2)}\Big[(1+t^2)f_1(\xi) - t(1-t^2+2\hat{\nu}^2)\tilde{\mathcal{I}}^{[1]}(\xi,t,\hat{\nu}) - i\hat{\nu}(1+3t^2)\tilde{\mathcal{I}}^{[2]}(\xi,t,\hat{\nu})$$
$$+ 2t\tilde{\mathcal{I}}^{[3]}(\xi,t,\hat{\nu})\Big], \tag{5.28c}$$
$$m_\delta^2 = \frac{m_D^2}{2\sqrt{1-t^2}}\Big[\hat{\nu}tf_0(\xi) - i\hat{\nu}^2t\tilde{\mathcal{I}}^{[0]}(\xi,t,\hat{\nu}) + \hat{\nu}(1-\xi t^2)\tilde{\mathcal{I}}^{[1]}(\xi,t,\hat{\nu}) - i\xi t\tilde{\mathcal{I}}^{[2]}(\xi,t,\hat{\nu})\Big], \tag{5.28d}$$
$$m_\rho^2 = -\frac{m_D^2}{2\mathcal{W}(0,\hat{\nu})\sqrt{1-t^2}}\Big[\xi\hat{\nu}\tilde{\mathcal{I}}^{[1]}(\xi,t,\hat{\nu}) + i\xi t\tilde{\mathcal{I}}^{[2]}(\xi,t,\hat{\nu})\Big], \tag{5.28e}$$

where the factor $\mathcal{W}(0,\hat{\nu}) = (1-\hat{\nu}\ \mathrm{arccot}\,\hat{\nu})$ is real-valued, and hence, all mass scales are real-valued. It is worth mentioning that the master integrals can be evaluated analytically in the collision-less limit, and the mass scales at $\nu = 0$ become

$$m_{\alpha,0}^2 = -\frac{m_D^2t^2}{2(1-t^2)}\left[f_0(\xi) - \frac{1}{1+\xi(1-t^2)}f_0\left(\frac{\xi t^2}{1+\xi(1-t^2)}\right)\right], \tag{5.29a}$$
$$m_{\beta,0}^2 = \frac{m_D^2}{2}\left[f_0(\xi) + \frac{\xi t^2}{(1+\xi(1-t^2))^2}f_0\left(\frac{\xi t^2}{1+\xi(1-t^2)}\right)\right], \tag{5.29b}$$
$$m_{\gamma,0}^2 = -\frac{m_D^2}{2(1-t^2)}\left[\frac{2(1-t^2)}{1+\xi} - (1+t^2)f_0(\xi)\right.$$
$$\left. + \left(3 - \frac{1}{1+\xi(1-t^2)}\right)\frac{t^2}{1+\xi(1-t^2)}f_0\left(\frac{\xi t^2}{1+\xi(1-t^2)}\right)\right], \tag{5.29c}$$
$$m_{\delta,0}^2 = m_{\rho,0}^2 = -\frac{\pi}{4}\frac{m_D^2\xi t\sqrt{1-t^2}}{[1+\xi(1-t^2]^{3/2}}. \tag{5.29d}$$

5.3 Dielectric Permittivity

In this section, we deduce the complex color dielectric permittivity in a collisional anisotropic QGP medium, which is later used to determine the in-medium heavy quarkonium potential. In the temporal axial gauge, this permittivity can be computed from the gluon propagator in the static limit as [267]

$$\epsilon^{-1}(p) = -\lim_{\omega\to 0}\omega^2\frac{p^ip^j}{p^2}\Delta_{ij}(\omega,p) \;=\; \lim_{\omega\to 0}\omega^2\frac{(p^2-\omega^2+\alpha+\gamma)}{(\omega^2-\Omega_+^2)(\omega^2-\Omega_-^2)}. \tag{5.30}$$

The dielectric permittivity depends on the gluon propagator, which has both the real and imaginary parts. Hence, it is a complex quantity with both real and imaginary parts, which can be written as

$$\text{Re}\,\epsilon^{-1}(p) \;=\; -\lim_{\omega\to 0}\omega^2\frac{p^ip^j}{p^2}\text{Re}\Delta_{ij}(\omega,p). \tag{5.31}$$

In the static limit, the real part of the dielectric permittivity can be written in terms of the mass scales as

$$\begin{aligned}\text{Re}\,\epsilon^{-1}(p) &= \frac{p^2(p^2+m_\alpha^2+m_\gamma^2)}{\left(p^4+p^2\left(m_\alpha^2+m_\beta^2+m_\gamma^2\right)+m_\alpha^2m_\beta^2+m_\beta^2m_\gamma^2-m_\delta^2m_\rho^2\right)},\\ &= \frac{p^2(p^2+m_\alpha^2+m_\gamma^2)}{(p^2+m_+^2)(p^2+m_-^2)},\end{aligned} \tag{5.32}$$

where

$$2m_\pm^2 = \left(m_\alpha^2+m_\beta^2+m_\gamma^2\right) \pm \sqrt{\left(m_\alpha^2+m_\beta^2+m_\gamma^2\right)^2 - 4\left\{m_\beta^2(m_\alpha^2+m_\gamma^2)-m_\delta^2m_\rho^2\right\}}\,. \tag{5.33}$$

Now, from Ref. [277], the imaginary part of the propagator can be obtained as

$$\text{Im}\Delta_{ij}(\omega,p) = -\frac{2\pi i}{\omega}\frac{\int_0^\infty dk k^2 f_F(k)\left[1-f_F(k)\right]}{\int_0^\infty dk k f_F(k)}\sum_m \text{R}_m\mathcal{P}_m^{ij} \tag{5.34}$$

where $\mathcal{P}_m^{ij} = A^{ij}, B^{ij}, C^{ij}, D^{ij}, E^{ij}$ - are the projection operators and

$$\mathrm{R}_m = \frac{1}{\pi}\left(1 + 2f_B(\omega)\right)\rho_m(\omega, p). \tag{5.35}$$

Now,

$$\lim_{\omega\to 0}\left(1 + 2f_B(\mathbf{p})\right)\mathrm{sgn}(\omega) \approx \frac{2T}{\sqrt{1+\xi(\boldsymbol{v}\cdot\boldsymbol{n})^2}}\frac{1}{\omega} + \mathcal{O}\left(\omega^0\right) \tag{5.36}$$

and

$$\frac{\int_0^\infty dk k^2 f_F(k)\left[1 - f_F(k)\right]}{\int_0^\infty dk k f_F(k)} = 2T\frac{\int \frac{d\Omega}{4\pi}\frac{1}{(1+\xi(\boldsymbol{v}\cdot\boldsymbol{n})^2)^{3/2}}}{\int \frac{d\Omega}{4\pi}\frac{1}{(1+\xi(\boldsymbol{v}\cdot\boldsymbol{n})^2)}} \tag{5.37}$$

Additionally, the imaginary part of the dielectric permittivity is given by

$$\mathrm{Im}\,\epsilon^{-1}(p) \quad = \quad -\lim_{\omega\to 0}\omega^2\frac{p^i p^j}{p^2}\mathrm{Im}\Delta_{ij}(\omega, p). \tag{5.38}$$

Based on the spectral function approach [284], the imaginary part of the gluon propagator can be expressed as

$$\mathrm{Im}\Delta^{ij} = -\pi(1 + e^{-\beta\omega})\sum_m \mathrm{R}_m\mathcal{P}_m^{ij}, \tag{5.39}$$

where $\mathcal{P}_m^{ij} = A^{ij}, B^{ij}, C^{ij}, D^{ij}, E^{ij}$ - are the projection operators and

$$\mathrm{R}_m = \frac{1}{\pi}\frac{e^{\beta\omega}}{e^{\beta\omega} - 1}\rho_m(\omega, p), \tag{5.40}$$

where non-vanishing contribution comes from,

$$\rho_m(\omega,p) = \lim_{\omega\to 0} \text{Im}[(p^2-\omega^2+\alpha+\gamma)\Delta_G]. \tag{5.41}$$

In the static limit which implies $\omega \to 0$ limit, the imaginary part of the dielectric permittivity given in Eq. (5.38)) reduces to

$$\begin{aligned}
\text{Im}\,\epsilon^{-1} &= -\lim_{\omega\to 0}\frac{e^{\beta\omega}+1}{e^{\beta\omega}-1}\omega^2\,\text{Im}\left(\frac{p^2-\omega^2+\alpha+\gamma}{(\omega^2-\Omega_+^2)(\omega^2-\Omega_-^2)}\right)\\
&\approx \lim_{\omega\to 0}\frac{2\omega T}{(\text{Re}\,\Omega_+^2)^2\ \left(\omega^2-\text{Re}\,\Omega_-^2\right)^2}\\
&\times \left[\left(p^2+m_\alpha^2+m_\gamma^2\right)\left\{\text{Re}\,\Omega_+^2\ \text{Im}\,\Omega_-^2-\text{Im}\,\Omega_+^2\ (\omega^2-\text{Re}\,\Omega_-^2)\right\}\right.\\
&\qquad\qquad\left.+\,(\text{Im}\,\alpha+\text{Im}\,\gamma)\,\text{Re}\,\Omega_+^2\left(\omega^2-\text{Re}\,\Omega_-^2\right)\right]\\
&= \lim_{\omega\to 0}\frac{2T}{(\text{Re}\,\Omega_+^2)^2\ \left(1-\frac{\text{Re}\,\Omega_-^2}{\omega^2}\right)^2}\left[\left(p^2+m_\alpha^2+m_\gamma^2\right)\right.\\
&\quad\times\left\{\text{Re}\,\Omega_+^2\ \frac{\text{Im}\,\Omega_-^2}{\omega^3}-\frac{\text{Im}\,\Omega_+^2}{\omega}\ \left(1-\frac{\text{Re}\,\Omega_-^2}{\omega^2}\right)\right\}\\
&\qquad\left.+\left(\frac{\text{Im}\,\alpha}{\omega}+\frac{\text{Im}\,\gamma}{\omega}\right)\text{Re}\,\Omega_+^2\left(1-\frac{\text{Re}\,\Omega_-^2}{\omega^2}\right)\right].
\end{aligned} \tag{5.42}$$

To determine $\text{Im}\epsilon^{-1}$, we need to evaluate the following quantities in the static limit as

$$\begin{aligned}
\lim_{\omega\to 0}\text{Re}\,\Omega_+^2 &\approx (p^2+m_\alpha^2+m_\gamma^2)+\mathcal{O}\left(\omega\right),\\
\lim_{\omega\to 0}\text{Re}\,\Omega_-^2 &\approx \frac{\omega^2}{p^2}\left[-m_\beta^2+\frac{2m_\rho^2 m_\delta^2}{p^2+m_\alpha^2+m_\gamma^2}\right]+\mathcal{O}\left(\omega^3\right),\\
\lim_{\omega\to 0}\text{Im}\,\Omega_+^2 &\approx (\text{Im}\,\alpha+\text{Im}\,\gamma)+\mathcal{O}\left(\omega^2\right),\\
\lim_{\omega\to 0}\text{Im}\,\Omega_-^2 &\approx \text{Im}\,\beta+\mathcal{O}\left(\omega^4\right).
\end{aligned} \tag{5.43}$$

Using the static limit from Eq. (5.43) in Eq. (5.42), we get

$$\begin{aligned}
\mathrm{Im}\,\epsilon^{-1}(p,\xi,\nu,t) &= \lim_{\omega\to 0}\frac{2\,\mathrm{Im}\,\beta\, p^4 T\left(p^2+m_\alpha^2+m_\gamma^2\right)^2}{\omega^3\left(p^4+p^2\left(m_\alpha^2+m_\beta^2+m_\gamma^2\right)+m_\alpha^2 m_\beta^2+m_\beta^2 m_\gamma^2-m_\delta^2 m_\rho^2\right)^2} \\
&= -\frac{\pi\, m_{i\beta}^2\, pT\left(p^2+m_\alpha^2+m_\gamma^2\right)^2}{\left(p^4+p^2\left(m_\alpha^2+m_\beta^2+m_\gamma^2\right)+m_\alpha^2 m_\beta^2+m_\beta^2 m_\gamma^2-m_\delta^2 m_\rho^2\right)^2}, \\
&= -\frac{\pi\, m_{i\beta}^2\, pT\left(p^2+m_\alpha^2+m_\gamma^2\right)^2}{\left(p^2+m_+^2\right)^2\left(p^2+m_-^2\right)^2}. \qquad (5.44)
\end{aligned}$$

In Eq. (5.44), we introduce a new mass scale $m_{i\beta}$ as

$$\begin{aligned}
m_{i\beta}^2 &= -\frac{2}{\pi}\lim_{\omega\to 0}\frac{p^3}{\omega^3}\,\mathrm{Im}\,\beta \\
&= \frac{2}{\pi\mathcal{W}\left(0,\hat{\nu}\right)}\left[\frac{\hat{\nu}}{1+\hat{\nu}^2}m_\beta^2-\frac{m_D^2}{2}\left\{\tilde{\mathcal{J}}(\xi,t,\hat{\nu})-i\,\tilde{\mathcal{I}}^{[0]}(\xi,t,\hat{\nu})\right\}\right], \qquad (5.45)
\end{aligned}$$

where

$$\tilde{\mathcal{J}}(\xi,t,\hat{\nu})=\int_{-1}^{1}\frac{(\hat{\nu}+itx)(i\hat{\nu}+\xi tx)\,\mathrm{sgn}(tx)}{\left(1+\xi x^2\right)^2\left[(tx-i\hat{\nu})^2-(1-t^2)(1-x^2)\right]^{3/2}}\,dx. \qquad (5.46)$$

In the collision-less medium ($\nu=0$), the new mass scale $m_{i\beta}$ becomes

$$\begin{aligned}
m_{i\beta,0}^2 &= \lim_{\hat{\nu}\to 0}\frac{m_D^2}{\pi}\left[i\,\tilde{\mathcal{I}}^{[0]}(\xi,t,\hat{\nu})-\tilde{\mathcal{J}}(\xi,t,\hat{\nu})\right] \\
&= \frac{m_D^2}{\left(1+(1-t^2)\,\xi\right)^{3/2}}\left[1+\frac{\xi}{2}\frac{(1+t^2)+\xi\,(1-t^2)\,(1-2t^2)}{1+(1-t^2)\,\xi}\right]. \qquad (5.47)
\end{aligned}$$

With the analytic form of mass scales in Eq. (5.29) and (5.47), one can express the $\mathrm{Im}\epsilon^{-1}(\nu=0)$ in the analytic form using Eq. (5.44). In the earlier literature, the analytic form of $\mathrm{Im}\epsilon^{-1}(\nu=0)$ was never obtained for a collisionless anisotropic medium, in our knowledge.

In the isotropic limit, i.e., $\xi = 0$, the dielectric permittivity in the collisional medium matches with the result obtained in Ref. [272]. Lastly, in the limit $\xi = \nu = 0$, all the mass scales becomes

$$\begin{aligned} m_\alpha^2 &= m_\gamma^2 = m_\delta^2 = m_\rho^2 = m_-^2 = 0, \\ m_\beta^2 &= m_{i\beta}^2 = m_+^2 = m_D^2. \end{aligned} \tag{5.48}$$

The dielectric permittivity will be used to compute the in-medium heavy quark-antiquark potential.

5.4 In-medium heavy quark-antiquark potential

In this section, we investigate the effect of a collisional anisotropic medium on the in-medium heavy quark potential. We compute the in-medium heavy quark-antiquark potential by correcting the Cornell potential in momentum space using the dielectric permittivity (5.30), which accounts for the effects of the collisional anisotropic thermal medium [212, 216, 275]

$$V(\boldsymbol{r}, \xi, \nu, T) = \int \frac{d^3\boldsymbol{p}}{(2\pi)^{3/2}} \left(e^{i\boldsymbol{p}\cdot\boldsymbol{r}} - 1\right) \frac{V_{\rm C}(p)}{\epsilon(p, \xi, \nu)}, \tag{5.49}$$

where $V_{\rm C}(p) = -\sqrt{(2/\pi)}(\alpha/p^2 + 2\sigma/p^4)$ [216] is the Fourier transform of the vacuum Cornell potential $V_{\rm C}(r) = -\alpha/r + \sigma\, r$. Here $\alpha = C_F\, \alpha_s$ with $C_F = 4/3$ being the Casimir fundamental and α_s being the strong coupling constant [50]

$$\alpha_s(\Lambda^2) = \frac{12\pi}{(11N_c - 2N_f)\ln\left(\frac{\Lambda^2}{\Lambda^2_{\overline{\rm MS}}}\right)}, \tag{5.50}$$

In Eq. (5.50), $N_c = 3$ and $\Lambda_{\overline{\rm MS}} = 0.176$ GeV for $N_f = 3$ and $\Lambda = 2\pi T$. Here the string tension, σ, is taken as $(0.44)^2$ GeV^2. After substituting Eq. 5.30 into Eq. 5.49, we obtain the medium-modified complex heavy-quark potential in an anisotropic medium, whose real part reads

$$\begin{aligned}
\mathrm{Re}\,V(r,\xi,\nu,T) &= \int \frac{d^3\boldsymbol{p}}{(2\pi)^{3/2}}\,(e^{i\boldsymbol{p}\cdot\boldsymbol{r}}-1)\,V_{\rm C}(p)\mathrm{Re}\,\epsilon^{-1}(p,\xi,\nu) \\
&= -\frac{1}{2\pi^2}\int d^3\boldsymbol{p}\,\,(e^{i\boldsymbol{p}\cdot\boldsymbol{r}}-1)\frac{(p^2+m_\alpha^2+m_\gamma^2)}{(p^2+m_+^2)(p^2+m_-^2)}\left(\alpha+\frac{2\sigma}{p^2}\right)
\end{aligned} \tag{5.51}$$

For general direction of $\boldsymbol{r}$ with the anisotropy direction, $\hat{\boldsymbol{n}}$, we will have,

$$\boldsymbol{p}\cdot\boldsymbol{r} = rp[\sin\theta\sin\Theta\cos(\phi-\Phi)+\cos\theta\cos\Theta],$$

where $\theta(\Theta)$ and $\phi(\Phi)$ are the polar and the azimuthal angles in momentum (coordinate) space with the anisotropy direction, respectively, since we take $\hat{\boldsymbol{n}} = \hat{z}$. After an integration over the azimuthal angle of the $(\exp\{(i\boldsymbol{p}\cdot r)\}-1)$, Eq. (5.51) becomes

$$\begin{aligned}
\mathrm{Re}\,V(r,\xi,\nu,T) &= -\frac{1}{\pi}\int_{p=0}^{\infty}\int_{\theta=0}^{\pi} p^2\,dp\,\,\sin\theta d\theta\left[e^{ipr\,\cos\theta\cos\Theta}J_0(pr\sin\theta\sin\Theta)-1\right] \\
&\quad\times\frac{(p^2+m_\alpha^2+m_\gamma^2)}{(p^2+m_+^2)(p^2+m_-^2)}\left(\alpha+\frac{2\sigma}{p^2}\right), \\
&= -\frac{2}{\pi}\int_{p=0}^{\infty}\int_{t=0}^{1} p^2\,dp\,dt\left[e^{ipr\,t\cos\Theta}J_0(pr\sqrt{1-t^2}\sin\Theta)-1\right] \\
&\quad\times\frac{(p^2+m_\alpha^2+m_\gamma^2)}{(p^2+m_+^2)(p^2+m_-^2)}\left(\alpha+\frac{2\sigma}{p^2}\right),
\end{aligned} \tag{5.52}$$

where J_0 is the Bessel's function of the first kind. Now, in the Coulomb part of the potential, Eq. (5.52) has a zero-temperature UV divergence, and that is set to zero, giving us

$$\begin{aligned}
\mathrm{Re}\,V(r,\xi,\nu,T) &= -\frac{2}{\pi}\int_{p=0}^{\infty}\int_{t=0}^{1} p^2\,dp\,dt\left[e^{ipr\,t\cos\Theta}J_0(pr\sqrt{1-t^2}\sin\Theta)-1\right] \\
&\quad\times\frac{(p^2+m_\alpha^2+m_\gamma^2)}{(p^2+m_+^2)(p^2+m_-^2)}\left(\alpha+\frac{2\sigma}{p^2}\right)-\frac{2}{\pi}\int_{p=0}^{\infty}dp\,\alpha. \qquad (5.53)
\end{aligned}$$

Note that for a collisionless, isotropy plasma, the real part of the quarkonium potential is

$$\mathrm{Re}\,V_{\mathrm{HTL}}(r,T) = -\alpha m_D\left(1+\frac{e^{-m_D r}}{m_D r}\right)+\frac{2\sigma}{m_D}\left(1+\frac{e^{-m_D r}-1}{m_D r}\right). \qquad (5.54)$$

In Fig. 5.1, we plot the real part of the potential (Eq. (5.53)) as a function of the separation

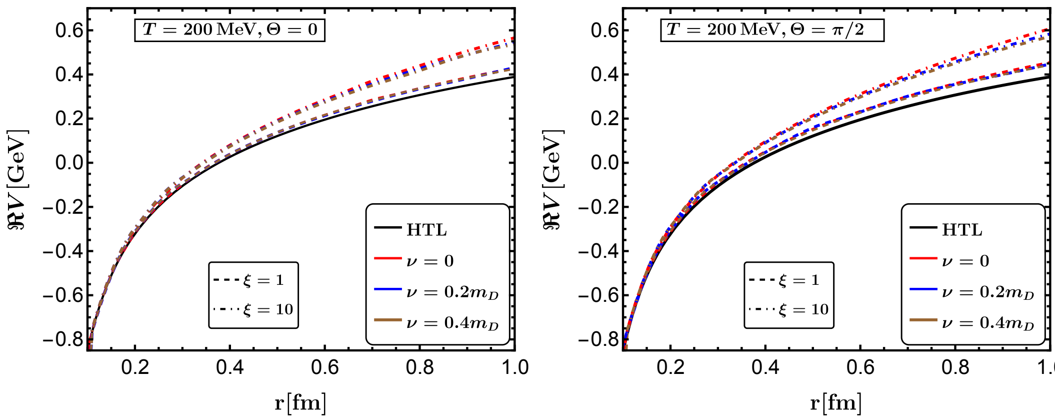

Figure 5.1: Real part of the heavy-quark potential at $T = 0.2$ GeV plotted against the quark-antiquark seperation r. The left panel corresponds to the pair oriented along the anisotropy direction ($\Theta = 0$), while the right panel shows the transverse configuration ($\Theta = \pi/2$). The HTL limit is included for comparison.

distance (r) at temperature $T = 0.2$ GeV. The left panel illustrates the results for various values of the collision parameter, ν, and anisotropy parameter, ξ when the $Q\bar{Q}$ dipole axis is aligned parallel to the anisotropy axis, while the right panel shows the results when the dipole is aligned transverse to the anisotropy axis. Here, the solid black line shows the real part of the potential for the isotropic collisionless plasma (Eq. (5.54)) when $\xi = 0$ and $\nu = 0$, while various colors denote the various values of the collision parameter, ν. We find that the real component of the potential has nominal effects with increasing collisional parameter ν. Notably, the impact of ν on the real part of the potential remains nearly consistent for both parallel and transverse alignments.

The imaginary part of the potential is written as

$$\begin{aligned}
\mathrm{Im}\, V(r,\xi,\nu,T) &= \int \frac{d^3p}{(2\pi)^{3/2}}(e^{i\mathbf{p}\cdot\mathbf{r}}-1)V_C(p)\mathrm{Im}\,\epsilon^{-1}(p,\xi,\nu) \\
&= -\frac{1}{\pi}\int_{p=0}^{\infty}\int_{\theta=0}^{\pi} p^2\,dp\,\sin\theta\,d\theta\,\left[e^{ipr\,\cos\theta\cos\Theta}J_0(pr\sin\theta\sin\Theta)-1\right] \\
&\times\; \frac{1}{p^2}\left(\alpha+\frac{2\sigma}{p^2}\right)\frac{-\pi\, m_{i\beta}^2\,pT\left(p^2+m_\alpha^2+m_\gamma^2\right)^2}{\left(p^2+m_+^2\right)^2\left(p^2+m_-^2\right)^2} \\
&= -\frac{1}{\pi}\int_{p=0}^{\infty}\int_{t=0}^{1} p^2\,dp\;dt\,\left[\cos\left(p\,r\,t\cos\Theta\right)J_0(pr\sqrt{1-t^2}\sin\Theta)-1\right] \\
&\times\; \frac{2}{p^2}\left(\alpha+\frac{2\sigma}{p^2}\right)\frac{-\pi\, m_{i\beta}^2\,pT\left(p^2+m_\alpha^2+m_\gamma^2\right)^2}{\left(p^2+m_+^2\right)^2\left(p^2+m_-^2\right)^2},
\end{aligned} \tag{5.55}$$

where $t = \cos\theta$. Note that for the isotropy case in the absence of the collisional term, the imaginary potential reduces to

$$\mathrm{Im}\, V_{\mathrm{HTL}}(r,T) = -2Tm_D^2\int\frac{p\,dp}{(p^2+m_D^2)^2}\left(\alpha+\frac{2\sigma}{p^2}\right)\left(1-\frac{\sin pr}{pr}\right). \tag{5.56}$$

In Eq. (5.55) the integral has a pinch singularity. This singularity arises from the term $(p^2+m_-^2)^2$ in the denominator of the integrand, which makes the imaginary component of the potential ill-defined. The $(p^2+m_-^2)$ term also appears in the integral of real potential in Eq. (5.51), where it is a simple pole and can be integrated using the Principle part prescription. But for the imaginary potential, $(p^2 + m_-^2)^2$ appears as a double pole, hence it cannot be integrated out using Principle value method. The issue of the pinch singularity was previously discussed in [276] in the collisionless case that is when $\nu = 0$. In Fig. 5.2, we illustrate the region where this singularity occurs for finite collisional effect, which certainly includes the $\nu = 0$ axis as mentioned in [276] for collision-less case. In this way, we identify the region of anisotropic collisional plasma, where the imaginary potential is calculable and the Weibel instability is gone. In our numerical observation, we found that the region of singularity is extending approximately from $\nu = 0$ up to $\nu \sim 0.24 m_D$ for anisotropy parameter $\xi \sim 10$. In this article, we are showing the imaginary part of potential only for the region where the Weibel instability is absent, i.e., for the white colored region in Fig. 5.2. In Fig. 5.2, the right edge can be obtained by reaching closer to $p \to 0$ and $t \to 1$. With increasing p-value and decreasing t-value the singularity move towards $\nu \to 0$ and finally all singularities accumulate at $\nu = 0$ axis. In Fig. 5.3, we plot the

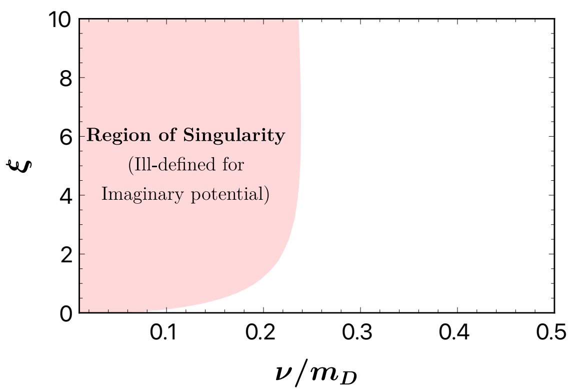

Figure 5.2: Region in anisotropy vs collision parameter plot where integral of Eq. (5.55) has the singularity.

imaginary part of the potential (5.55) as a function of separation distance r at temperature $T = 0.2$ GeV when the dipole axis $Q\bar{Q}$ is aligned parallel to the direction of anisotropy. The left panel shows the results for various values of ν while keeping $\xi = 1$. We find

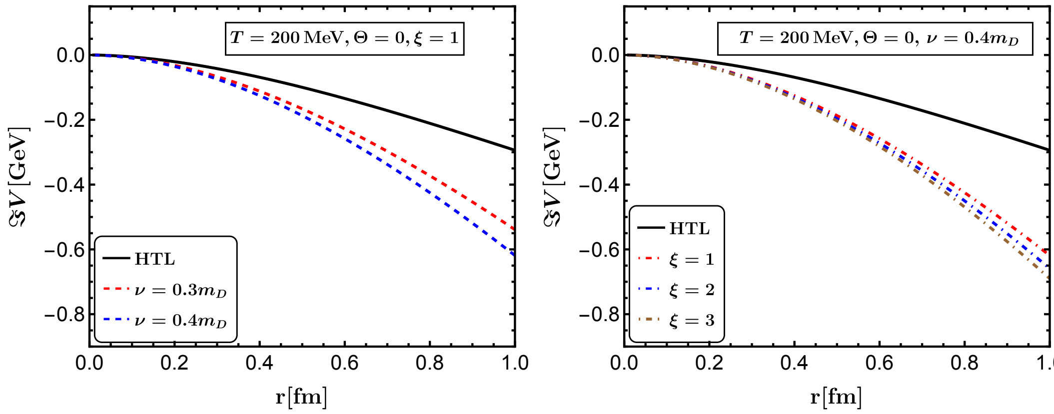

Figure 5.3: The imaginary part of the potential as a function of separation distance r for different values of ν (left) and ξ (right) at $T = 0.2$ GeV and $\Theta = 0$.

that the imaginary part of the potential increases in magnitude as ν increases. The right panel presents the results for the different values of ξ. The dash-dotted lines correspond to $\nu = 0.4m_D$. In this case, the imaginary component of the potential shows a increase in magnitude with the increase in ξ. The solid black line shows the imaginary component of the potential for the isotropic collisionless plasma (5.56).

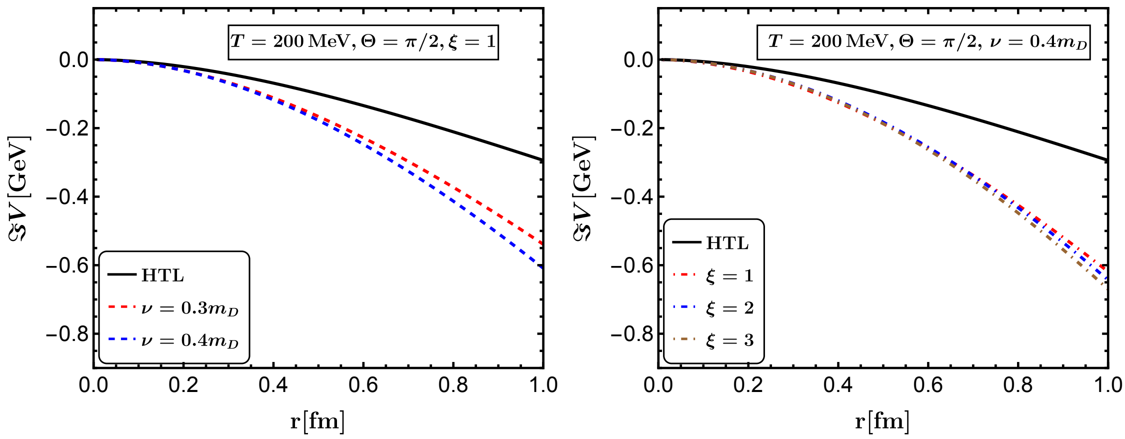

Figure 5.4: The imaginary part of the potential as a function of r for different values of ν (top) and ξ (bottom) at $T = 0.2$ GeV and $\Theta = \pi/2$.

Fig. 5.4 shows a similar plot of the imaginary component of the potential for the perpendicular orientation of the $Q\bar{Q}$ dipole axis relative to the direction of anisotropy. The effect of ν on the imaginary part of the potential is similar for both - the parallel and perpendicular orientations. Notably, the impact of ν is more pronounced on the imaginary part of the potential compared to the real part, where its effect is minimal.

5.5 Decay Width

In this section, we determine the decay width of quarkonium states based on the imaginary part of the potential obtained earlier. Treating this imaginary component as a perturbation to the vacuum potential allows us to estimate the thermal width, Γ, of the quarkonium states as

$$\begin{aligned}
\Gamma(\xi,\nu,T) &= -\int_{\mathbf{r}} |\psi(\mathbf{r},T)|^2 \mathrm{Im}V(\mathbf{r},\xi,\nu,T) \\
&= -2\pi \int_{r=0}^{\infty} dr\, r^2 \int_{\Theta=0}^{\pi} d\Theta\ \sin(\Theta)\, |\psi(r,T)|^2\, \mathrm{Im}V(r,\Theta,\xi,\nu,T) \\
&= -\frac{2}{a_0^3} \int_{r=0}^{\infty} dr\, r^2 \int_{\Theta=0}^{\pi} d\Theta\ \sin(\Theta)\, \mathrm{e}^{-2r/a_0(T)}\, \mathrm{Im}V(r,\Theta,\xi,\nu,T) \\
&= \frac{4}{\pi\, a_0^3} \int_{r=0}^{\infty} dr\, r^2 \int_{\Theta=0}^{\pi} d\Theta\ \sin(\Theta)\, \mathrm{e}^{-2r/a_0(T)} \int_{p=0}^{\infty} \int_{t=0}^{1} dp\ dt \left(\alpha + \frac{2\sigma}{p^2}\right) \\
&\times \left[\cos\left(p\, r\, t \cos\Theta\right) J_0(pr\sqrt{1-t^2}\sin\Theta) - 1\right] \mathrm{Im}\epsilon^{-1}(p,\xi,\nu,T), \qquad (5.57)
\end{aligned}$$

where we have used the Coulombic ground state wave function

$$\psi(r,T) = \frac{1}{\sqrt{\pi\, a_0(T)^3}} \mathrm{e}^{-r/a_0(T)}, \quad \text{and} \quad a_0(T) = \frac{2}{m_0 \alpha(T)} \qquad (5.58)$$

is the Bohr radius of the heavy quarkonium system, and the charm (corresponding to J/ψ) mass is taken as $m_0 = 1.275$ GeV. The primary contribution to the imaginary potential for a deeply bound state involving heavy quarks is Coulombic in nature. This supports the use of Coulomb wave functions for calculating the decay width.

The r-integration in Eq. (5.57) can be computed using the integral

$$\int_0^\infty r^2 e^{-ar} J_0(cr) dr = \frac{2a^2 - c^2}{(a^2 + c^2)^{5/2}}. \tag{5.59}$$

The integral relation in Eq. (5.59) can be used for the following integration as

$$\int_0^\infty r^2 e^{-ar} \cos(br) J_0(cr) dr = \frac{1}{2}\left[\frac{2(a+ib)^2 - c^2}{((a+ib)^2 + c^2)^{5/2}} + \frac{2(a-ib)^2 - c^2}{((a-ib)^2 + c^2)^{5/2}}\right]. \tag{5.60}$$

In Eq. (5.57),

$$\begin{aligned} a &= \frac{2}{a_0}, && (5.61a)\\ b &= p\, r\, t \cos\Theta, && (5.61b)\\ c &= pr\sqrt{1-t^2}\sin\Theta. && (5.61c) \end{aligned}$$

So, Eq. (5.57) becomes

$$\begin{aligned} \Gamma(T,\xi,\nu) &= \int\limits_{p=0}^{\infty}\int\limits_{t=0}^{1}\int\limits_{\Theta=0}^{\pi} \frac{4\sin\Theta}{\pi a_0^3}\left[\frac{\left(\frac{2}{a_0} - ipt\cos\Theta\right)^2 - \frac{1}{2}p^2\left(1-t^2\right)\sin^2\Theta}{\left(\frac{2}{a_0} - ipt\cos\Theta\right)^2 + p^2\left(1-t^2\right)\sin^2\Theta}\right.\\ &+ \left.\frac{\left(\frac{2}{a_0} + ipt\cos\Theta\right)^2 - \frac{1}{2}p^2\left(1-t^2\right)\sin^2\Theta}{\left(\frac{2}{a_0} + ipt\cos\Theta\right)^2 + p^2\left(1-t^2\right)\sin^2\Theta} - \frac{a_0^3}{4}\right]\left(\alpha + \frac{2\sigma}{p^2}\right)\mathrm{Im}\epsilon^{-1} dp\, dt\, d\Theta\\ &= \frac{2}{\pi}\int\limits_{p=0}^{\infty}\int\limits_{t=0}^{1}\left[\frac{16}{\left(a_0^2 p^2 + 4\right)^2} - 1\right]\left(\alpha + \frac{2\sigma}{p^2}\right)\mathrm{Im}\epsilon^{-1}(p,\xi,\nu,t) dp\, dt. \end{aligned} \tag{5.62}$$

For an isotropic, collisionless medium, the decay width of quarkonium can be obtained

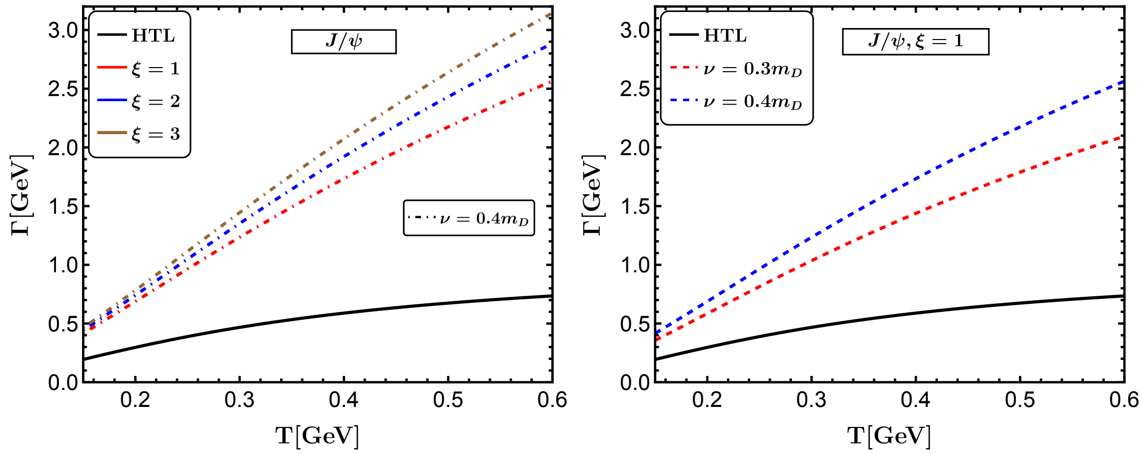

Figure 5.5: Temperature variation of decay width for the ground state of charmonium.

analytically as

$$
\begin{aligned}
\Gamma_{\mathrm{HTL}} &= \frac{2}{\pi}\int\limits_{p=0}^{\infty}\int\limits_{t=0}^{1}\left[\frac{16}{(a_0^2p^2+4)^2}-1\right]\left(\alpha+\frac{2\sigma}{p^2}\right)\frac{-\pi T p m_D^2}{(p^2+m_D^2)^2}\,dp\,dt \\
&= \frac{\alpha m_D^2 a_0^2 T}{(a_0^2m_D^2-4)}\left[1-\frac{8}{(a_0^2m_D^2-4)}+\frac{64}{(a_0^2m_D^2-4)^2}\log\frac{m_D a_0}{2}\right] \\
&\quad+\frac{4\sigma a_0^2 T}{(a_0^2m_D^2-4)^2}\left[4+\frac{a_0^2m_D^2\,(a_0^2m_D^2-12)}{(a_0^2m_D^2-4)}\log\frac{m_D a_0}{2}\right].
\end{aligned}
\tag{5.63}
$$

In Fig.(5.5), we plot the decay width of the ground state of charmonium (J/ψ) as a function of temperature T for the region where the imaginary potential is free from Weibel instabilities. The solid black line represents the decay width calculated for the isotropic, collisionless medium (eq. (5.63)). In the left panel,the dash-dotted lines correspond to the collisional case with $\nu = 0.4m_D$. The different colors represent various values of ξ. In the right panel, the different colored dash-dotted lines indicate various values of ν for $\xi = 1$. We observe that the decay width increases with both temperature and the collisional parameter. In the collisional case as well, the enhancement of ξ also increases the magnitude of the decay width. This behavior is related to the characteristics of the imaginary part discussed in the previous section.

5.6 Summary and discussions

In this article, we studied the complex heavy quarkonium potential in a QGP medium in the presence of a momentum-space anisotropy, considering the effect of collisions among the plasma constituents. The anisotropic correction in momentum space is applied by considering the Romatschke-Strickland anisotropy distribution function of the thermal partons. Consequently, the gluon self-energy is rederived by solving kinetic equations of the Boltzmann-Vlasov type in its linearized approximation, incorporating the BGK collision kernel. We further computed the resummed gluon propagator, based on which we calculated the real and imaginary parts of the dielectric permittivity of the medium in the static limit. Using this dielectric permittivity, we derived the complex potential for heavy quarkonia and analyzed how this potential is affected in the presence of a collisional anisotropic medium. We observed that the momentum-space anisotropic correction, parameterized by ξ, reduces the screening effect. The anisotropy in momentum space makes the potential anisotropic that depends on the angle Θ between the $Q\bar{Q}$ dipole axis and the direction of anisotropy. Though the momentum-space anisotropy reduces the screening, the effect of the collision in the real part of the potential is nominal. We observe that in an anisotropic medium, for a finite range of the collision parameter, the imaginary part of the complex potential is ill-defined due to the presence of a pinch-singularity. The magnitude of the imaginary part of the potential is enhanced with the collisional parameter ν. Further, we calculated the decay width of J/ψ. Our qualitative study of decay width with coulombic wave function shows that the decay width increases with the increase of anisotropy in the presence of the collision among the plasma constituents. So, the charmonium dissociates faster in a collisional plasma.One can try to solve the Schrödinger equation with the complex HQ potential to obtain the wave function and get a more quantitatively accurate decay width. Additionally, further research is needed to determine the appropriate non-equilibrium anisotropic distribution functions and real and imaginary dielectric permittivity.

CHAPTER 6

CONCLUSIONS

In this thesis, I have primarily focused on various non-perturbative aspects of Quark-gluon plasma (QGP) medium. The usual perturbative approach of QCD at finite temperature and density to study QGP has serious limitations in the low temperature and low baryon chemical potential, since that region is highly non-perturbative in nature. The coupling constant α_s is large in this region, so we cannot perform the perturbative expansion. To study this non-perturbative region, I have employed the Hard Thermal Loop resummation technique for the Gribov-Zwanziger prescription, which introduces a lower cut off mass scale, $\sim g^2 T$, which reaches a lower mass scale than the usual HTL perturbation theory, which has a cut off mass scale $\sim gT$. Using this treatment, this thesis shows in in chapter 3, that real part of the static coulomb potential between two heavy quarks becomes more suppressed due to medium effect than the HTL calculation shows but the imaginary potential shows significant increase implying much faster decay of Quarkonium state. In chapter 4, I also showed that when passing through the Gribov plasma, a parton losses more energy.

In chapter 2, where I considered a far more lower temperature- near the deconfinement temperature, T_d , I used an effective field theory - effective matrix model, which considers a background field which is characterized by the order parameter of the confinement deconfinement phase transition, the Polyakov loop. Taking the background field charactised by the Polyakov loop was not enough to give correct equation of state for the gluonic plasma. To reproduce the correct EoS, we needed to consider a ghost field ("Teen") , which is two dimensional in nature, that means its momentum is suppressed in two transverse direction, so we are left with one longitudinal direction and one temporal direction. With the consideration of teen field, I calculated the shear and bulk viscosity for the pure gluonic plasma. One of the major findings from this study is that, our prediction for bulk viscosity is much higher at the deconfinement temperature than the other non-perturbative studies.

In chapter 5, I considered the system to be in anisotropic in momentum space with collisions present in the system. Such a configuration characterizes a non-equilibrium state of the quark–gluon plasma. In this chapter, I have shown that, real part of the static Quarkonium potential has no effect due to collision present in the system, however, collision significantly affect the imaginary potential, which eventually causes the decay width of quarkonium as well.

Overall, the studies presented in this thesis form a cohesive understanding of the QGP that discusses its non-perturbative equilibrium properties and its non-equilibrium properties as well. This thesis highlights the confinement deconfinement phase transition and motivates to my future work to explore the semi-QGP region extensively.

As a future prospect of this current thesis work, I want to extend the matrix model with the adding the quark in the system. Since, in the quark present in the system, the Polyakov loop behavior changes, it no longer shows any first order phase transition, there is a crossover from QGP phase to hadronic phase. We expect that effect will show in the shear and bulk viscosity as well. Future work can also extend towards finite chemical potential near the crossover region. One should explore the real time method to study heavy quarkonium potential for non-equilibrium plasma, manifested through the anisotropic plasma.

APPENDIX A

IMPORTANT NOTES FOR CALCULATIONS IN MATRIX MODEL

A.1 Sign in the Boltzmann equation with teen ghosts

The sign of the Boltzmann equation with teen ghosts is a bit non-trivial. Here we explain how to obtain the sign in Eqs. (2.90) and (2.91). The point is that the teen ghost is equivalent to a fermion with periodic boundary conditions. In other words, it is equivalent to a fermion with an imaginary chemical potential $i\pi T$, which corresponds to the replacement of the fermion distribution function f_f with $-f_{\circlearrowleft}$. This correspondence is more obvious in the case of equilibrium systems:

$$\frac{1}{\mathrm{e}^{(E_p - i(Q^a - Q^b + \pi T))/T} + 1} = -\frac{1}{\mathrm{e}^{(E_p - i(Q^a - Q^b))/T} - 1} = -f^0_{ab} \ . \tag{A.1}$$

From this correspondence, the sign of the left-hand side of the Boltzmann equation in Eq. (2.90) should be obvious. Let us see what happens to the sign of the collision term.

In gluon-fermion scattering, we have a combination of distribution functions, $f_{\mathrm{g}} f_f (1 + f_{\mathrm{g}})(1 - f_f) - (1 + f_{\mathrm{g}})(1 - f_f) f_{\mathrm{g}} f_f$. This turns to

$$
\begin{aligned}
& f_{\mathrm{g}} f_f (1 + f_{\mathrm{g}})(1 - f_f) - (1 + f_{\mathrm{g}})(1 - f_f) f_{\mathrm{g}} f_f \\
& \to (-) \Big[f_{\mathrm{g}} f_{\text{৯}} (1 + f_{\mathrm{g}})(1 + f_{\text{৯}}) - (1 + f_{\mathrm{g}})(1 + f_{\text{৯}}) f_{\mathrm{g}} f_{\text{৯}} \Big]
\end{aligned}
\tag{A.2}
$$

in the gluon-teen scattering. We obtain the negative overall sign $(-)$. Similarly, for teen-teen scattering, we have

$$
\begin{aligned}
& f_f f_f (1 - f_f)(1 - f_f) - (1 - f_f)(1 - f_f) f_f f_f \\
& \to (+) \Big[f_{\text{৯}} f_{\text{৯}} (1 + f_{\text{৯}})(1 + f_{\text{৯}}) - (1 + f_{\text{৯}})(1 + f_{\text{৯}}) f_{\text{৯}} f_{\text{৯}} \Big] .
\end{aligned}
\tag{A.3}
$$

The sign is positive. These considerations show that the sign is determined by the evenness of the incoming ghost number, which corresponds to $\mathcal{S}_{\text{ব}} \mathcal{S}_{\text{দ}}$ in Eq. (2.91).

A.2 Energy and pressure for teen particles

In kinetic theory, the energy-momentum tensor for teen ghost is given by

$$
T^{\mu\nu} = - \int \frac{d\Omega}{4\pi} \int \frac{d^3 p}{(2\pi)^3} \frac{p^\mu p^\nu}{E_p} \frac{1}{e^{\beta E_p} - 1} .
\tag{A.4}
$$

Now,

$$
\begin{aligned}
T^{00} &= - \int \frac{d\Omega}{4\pi} \int \frac{d^3 p}{(2\pi)^3} \frac{p^0 p^0}{E_p} \frac{1}{e^{\beta E_p} - 1} , \\
\mathscr{E}^{\mathrm{kt}} &\simeq -2 \int_0^\infty \frac{dp_\parallel}{2\pi} \int \frac{p_\perp dp_\perp}{2\pi} |p_\parallel| \frac{1}{e^{\beta |p_\parallel|} - 1} , \\
\mathscr{E}^{\mathrm{kt}} &= - \frac{T^2 T_d^2}{24} .
\end{aligned}
\tag{A.5}
$$

Take $\hat{n} \equiv \hat{z}$ and $p_\perp \sim T_d \ll p_\parallel$. The longitudinal pressure along the z-direction is

$$\begin{aligned} T^{33} &= -\int \frac{d\Omega}{4\pi} \int \frac{d^3p}{(2\pi)^3} \frac{p^3 p^3}{E_p} \frac{1}{e^{\beta E_p}-1} \\ &\simeq -2\int_0^\infty \frac{dp_\parallel}{2\pi} \int \frac{p_\perp dp_\perp}{2\pi} |p_\parallel| \frac{1}{e^{\beta |p_\parallel|}-1}\,, \\ \mathscr{P}^{\rm kt}_z &= -\frac{T^2 T_d^2}{24}\,. \end{aligned} \tag{A.6}$$

The perpendicular pressure is

$$\begin{aligned} T^{11} = T^{22} &= -\int \frac{d\Omega}{4\pi} \int \frac{d^3p}{(2\pi)^3} \frac{p_\perp^2}{E_p} \frac{1}{e^{\beta E_p}-1}\,, \\ \mathscr{P}^{\rm kt}_\perp &\simeq 0\,. \end{aligned} \tag{A.7}$$

The difficulty is that in Eq. (A.6), one should average over the direction of the teen field, which gives $\mathscr{P}^{\rm kt} = -T^2T_d^2/72$, so that in kinetic theory, the teen field looks three dimensional, with $\mathscr{E}^{\rm kt} = 3\mathscr{P}^{\rm kt}$. If we compute directly from thermodynamics, though, we obtain $\mathscr{P}^{\rm th} = \mathscr{E}^{\rm th} = -T^2T_d^2/24$, as expected for a two dimensional field.

Thus, as noted in Sec. (2.6), kinetic theory gives the wrong pressure for a teen field. In computing the bulk viscosity, we avoided this by taking Δv_s^2 from thermodynamics. In turn this is fit to the lattice results, through the functions $d_A(T)$ and $d_B(T)$, Eq. 2.28.

We next discuss how to obtain a kinetic theory for teen particles which is consistent with a direct computation in thermodynamics. This considers the analogy to a magnetic field, where there is a difference between computing at constant magnetic field or constant flux.

We start with the energy density and pressure, defined from the partition function $\mathcal{Z}$, as

$$\mathscr{E} = -\frac{1}{V}\frac{\mathrm{d}\log\mathcal{Z}}{\mathrm{d}(1/T)}\,, \qquad \mathscr{P}_i = \frac{T}{V}L_i\frac{\mathrm{d}\log\mathcal{Z}}{\mathrm{d}L_i}\,, \tag{A.8}$$

where L_i is the length of the system along i-th direction. The energy density in Eq. (A.8) becomes

$$\begin{aligned}\mathscr{E} &= (2-1)T\int\frac{d\Omega_n}{4\pi}\int\frac{dp_\parallel}{2\pi}\int\frac{d^2p_\perp}{(2\pi)^2}\ln\left(1-e^{-\beta|p_\parallel|}\right)\\ &= T\frac{1}{4\pi^2}\int_0^{T_d}dp_\perp p_\perp\int_{-\infty}^{\infty}dp_\parallel\ln\left(1-e^{-\beta|p_\parallel|}\right)\\ &= -\frac{1}{24}T_d^2T^2\,. \end{aligned}\tag{A.9}$$

Note that the energy density is the same, whether computed in kinetic theory, or from the partition function.

For the pressure $\mathscr{P}_i$, one can calculate the derivatives of the partition function in in two ways:

1. Keeping the energy density $\mathscr{E}$ constant, analogous to constant magnetic field B.

2. Keeping the longitudinal energy density $\mathscr{E}L_xL_y$ constant, which is analogous to constant magnetic flux Φ.

In the first case, at constant $\mathscr{E}$, the pressure is

$$\mathscr{P}_i^{\mathrm{th}} = \frac{T}{V}\frac{\partial\log\mathcal{Z}}{\partial\log L_i} = -\frac{1}{24}T_d^2T^2\,. \tag{A.10}$$

The second case, with constant longitudinal energy density, corresponds to the conventional energy momentum tensor, in which the pressure is given by Eqs. (A.6) and (A.7). To see this, note that

$$\begin{aligned}\mathscr{P}_i^{\text{kt}} &= \frac{T}{V}\frac{\partial \log \mathcal{Z}}{\partial \log L_i} + \frac{T}{V}\frac{\partial \log \mathcal{Z}}{\partial \mathscr{E}} \cdot \frac{\partial \mathscr{E}}{\partial \log L_i}\bigg|_{\text{kt}} \\ &= \mathscr{P}_i^{\text{th}} + \frac{T}{V}\frac{\partial \log \mathcal{Z}}{\partial \mathscr{E}} \cdot \frac{\partial \mathscr{E}}{\partial \log L_i}\bigg|_{\text{kt}} . \end{aligned} \tag{A.11}$$

Since $\mathscr{E}$ decreases with L_x and L_y,

$$\begin{aligned}\mathscr{P}_z^{\text{kt}} &= \mathscr{P}_z^{\text{th}} = -\frac{1}{24}T^2T_d^2 \qquad \text{and} \\ \mathscr{P}_\perp^{\text{kt}} &= \mathscr{P}_\perp^{\text{th}} + \frac{\partial \mathscr{P}_\perp^{\text{th}}}{\partial \mathscr{E}}(-\mathscr{E}) = \mathscr{P}_\perp^{\text{th}} + (1)(-\mathscr{P}_\perp^{\text{th}}) = \mathscr{P}_\perp^{\text{th}} - \mathscr{P}_\perp^{\text{th}} = 0 .\end{aligned}$$

Thus, the results from $T^{\mu\nu}$ and thermodynamics are consistent with each other, whether one computes at constant longitudinal energy density, or at constant energy density.

A.3 Zero mode

The analysis of the collision kernel for the bulk viscosity, Eq. (2.191), involves zero modes that do not arrive for the shear viscosity. Since only $2 \leftrightarrow 2$ scattering processes are considered, there are zero modes for the conservation of particle number. There are also zero modes for energy conservation. Because of this, finding the inverse of the $\bar{\mathcal{L}}$ matrix is ill-defined.

If only gluons scatter, in Eq. (2.191) only the term $\sim Y_{mn}^{\text{gg}}$ contributes, and has zero modes. Reference [100] adds a term to lift this degeneracy and computes the inverse of $\bar{\mathcal{L}}$, proportional to a parameter λ. They then check, numerically, that the result is independent of λ.

Adding teen fields complicates the analysis, as teens contribute to a variety of processes. The scattering of gluons into themselves, $\text{gg} \to \text{gg}$, gives a term $\sim T^6 Y_{mn}^{\text{gg}}$; that from teens with themselves, $\text{৩৩} \to \text{৩৩}$, gives a term $T_d^4 T^2 Y_{mn}^{\text{৩৩}}$. These contributions have zero modes.

However, there are additional scattering from glue teen scattering, $\text{৩g} \to \text{৩g}$. For the glue-glue term in the upper left hand corner of Eq. (2.191), the total is $T^6\, Y_{mn}^{\rm gg} + T^4\, T_d^2 \overline{Y}_{mn}^{\rm gg}$. Similarly, for the teen-teen term in the lower right hand corner, the total is $T_d^4\, T^2 Y_{mn}^{\text{৩৩}} + T^4\, T_d^2 \overline{Y}_{mn}^{\text{৩৩}}$. Because of the additional contributions, these terms no longer have zero modes.

However, there are also off-diagonal terms in Eq. (2.191). These are $T^4 T_d^2 Y_{mn}^{\text{g৩}}$ and $T^4 T_d^2 Y_{mn}^{\text{৩g}}$, and each has zero modes. By trial and error, we find that a term which lifts the degeneracy of the scattering kernel in Eq. (2.191) is

$$\begin{aligned}\bar{\Lambda}_{mn}^{\text{ব},\text{দ}} \to \bar{\Lambda}_{mn}^{\text{ব},\text{দ}} \quad + \quad & (1 - \delta^{\text{ব},\text{দ}})\, \frac{\lambda g^4 N_c^4}{2(2\pi)^5}\, \log\left(\frac{\kappa}{g^2 N_c}\right) \\ & \times \left(\int \frac{d^3 p}{(2\pi)^3} p^2 \frac{\partial \psi_{\text{ব},m}}{\partial p} \right) \left(\int \frac{d^3 k}{(2\pi)^3} k^2 \frac{\partial \psi_{\text{দ},m}}{\partial k} \right). \end{aligned} \tag{A.12}$$

We checked numerically that for any positive λ, $T \sum_{\text{ব}} \sum_{n=0}^{\infty} V_n^{\text{ব}} \left(\bar{\mathcal{L}}^{-1} V\right)_n^{\text{ব}}$ is independent of λ. In Fig. A.1 we illustrate the convergence of bulk viscosity versus K, the dimension

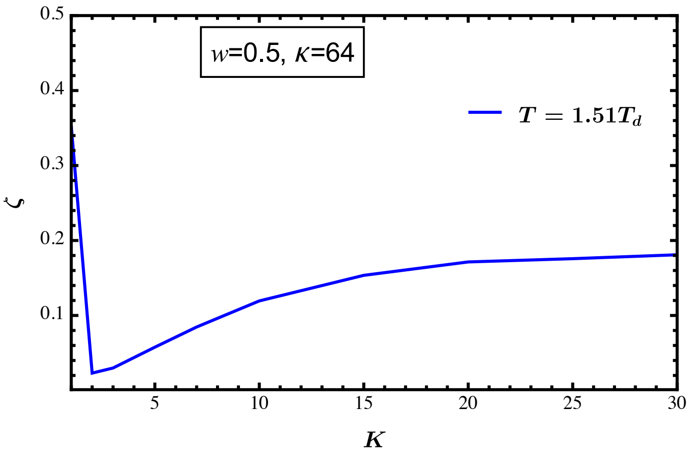

Figure A.1: Variation of bulk viscosity with increasing basis number at $T/T_d = 1.51$, with $w = 0.5$ and $\kappa = 64$.

of the basis functions, for one typical value of the temperature and other parameters. The convergence for other values was consistently similar. While K is in principle infinite, in Ref. [100] they found good convergence for small values of $K \leq 5$. In contrast, we uniformly found convergence by values of $K \sim 20 - 30$, and we computed using $K = 30$.

APPENDIX B

IMPORTANT CALCULATIONS FOR GZ PRESCRIPTION

B.1 Tadpole and gluon loop contribution $\Pi_{\mu\mu}$ and Π_{00}

The Contribution of the tadpole diagram and gluon loop to the gluon self-energy can be respectively described as,

$$\Pi^a_{\mu\nu}(P) = 3C_A g^2 \int \frac{d^4K}{(2\pi)^4}\left(\delta_{\mu\nu} - \frac{K_\mu K_\nu}{K^2}\right)\Delta(K), \tag{B.1}$$

$$\Pi^b_{\mu\nu}(P) = -6g^2 C_A I^b_{\mu\nu} - \frac{1}{2}g^2 C_A \delta_{\mu\nu} J_1 + \frac{1}{2}g^2 C_A \delta_{\mu\nu} J_2, \tag{B.2}$$

with $C_A = N_c = 3$. In Euclidean space $K^2 = \omega_n^2 + k^2$. The expression of $I_{\mu\nu}$, J_1 and J_2 can be defined as [64],

$$I^b_{\mu\nu}(P) = \int \frac{d^4K}{(2\pi)^4} K_\mu K_\nu \Delta(K)\Delta(P-K), \tag{B.3}$$

$$J_1 = \int \frac{d^4K}{(2\pi)^4}\Delta(K) = \frac{1}{4\pi^2}\sum_{a=\pm 1}\int_0^\infty \frac{k^2 dk}{E_a(k)} n_B(E_a(k)), \tag{B.4}$$

$$\begin{aligned}
J_2(P) &= \sum\!\!\!\!\!\!\!\int \frac{d^4K}{(2\pi)^4}\, i\gamma_G^2\, \Delta(K)\Delta(P-K) \\
&= \frac{i\gamma_G^2}{4}\sum_{a,b=\pm 1}\int \frac{d^4K}{(2\pi)^4}\frac{a}{[\omega_n^2 + E_a^2(k)]}\frac{1}{[(\omega-\omega_n)^2 + E_b^2(|\mathbf{p}-\mathbf{k}|)]} \\
&= -\frac{i\gamma_G^2}{16}\int \frac{d^3k}{(2\pi)^3}k^2 \sum_{a,b=\pm} a\frac{n_B(E_a(k)) + n_B(E_b(k))}{E_a(k)\,E_b(k)}\left(-\frac{2}{E_a(k)+E_b(k)}\right) \\
&+ \frac{i\gamma_G^2}{16}\int \frac{dk}{(2\pi)^2}k^2 \sum_{a,b=\pm 1} a\frac{n_B(E_a(k)) - n_B(E_b(k))}{kE_a(k)}\frac{1}{p}\left[Q_0(i\omega_1,p) - Q_0(i\omega_2,p)\right] \\
&- \frac{i\gamma_G^2}{16T}\int \frac{dk}{(2\pi)^2}k^2 \sum_{a,b=\pm 1} a\frac{n_B(E_b(k))(1+n_B(E_b(k)))}{E_a(k)E_b(k)} 2\left[Q_1(i\omega_1,p) + Q_1(i\omega_2,p)\right],
\end{aligned} \tag{B.5}$$

with $E_a(k) = \sqrt{k^2 + ia\gamma_G^2}$. The net contribution from the tadpole and gluon loop for the longitudinal and transverse parts can be expressed as,

$$\Pi_{00}^{a+b}(p_0,\mathbf{p}) = -\frac{13}{2}g^2C_AJ_1 + 3g^2C_AJ_4(p_0,\mathbf{p}) + \frac{13}{2}g^2C_AJ_2(p_0,\mathbf{p}) + 6g^2C_AJ_3(p_0,\mathbf{p}), \tag{B.6}$$

$$\Pi_{\mu\mu}^{a+b}(p_0,\mathbf{p}) = \frac{5}{2}g^2C_A(\delta_{\mu\mu}-1)J_1 + \frac{1}{2}g^2C_A\delta_{\mu\mu}J_2(p_0,\mathbf{p}) - 6g^2C_AI_{\mu\mu}^b(p_0,\mathbf{p}), \tag{B.7}$$

where $I_{\mu\mu}^b = J_1 - J_2$ and $I_{00}^b = J_1 - J_2 - J_3$.

The term J_3 and J_4 can be defined as,

$$\begin{aligned}
J_3(p_0,\mathbf{p}) &= \sum\!\!\!\!\!\!\!\int \frac{d^4K}{(2\pi)^4}k^2\Delta(K)\Delta(P-K) \\
&= -\frac{1}{16}\int \frac{d^3k}{(2\pi)^3}k^2\sum_{a,b=\pm}\frac{n_B(E_a(k)) + n_B(E_b(k))}{E_a(k)\,E_b(k)}\left(-\frac{2}{E_a(k)+E_b(k)}\right)
\end{aligned} \tag{B.8}$$

$$+\frac{1}{16}\int\frac{dk}{(2\pi)^2}k^4\sum_{a,b=\pm1}\frac{n_B(E_a(k))-n_B(E_b(k))}{kE_a(k)}\frac{1}{p}\left[Q_0(i\omega_1,p)-Q_0(i\omega_2,p)\right]$$
$$-\frac{1}{16T}\int\frac{dk}{(2\pi)^2}k^4\sum_{a,b=\pm1}\frac{n_B(E_b(k))(1+n_B(E_b(k)))}{E_a(k)E_b(k)}2\left[Q_1(i\omega_1,p)+Q_1(i\omega_2,p)\right],$$
(B.9)

$$J_4(p_0,\mathbf{p}) \;=\; \sum\!\!\!\!\!\!\!\int\frac{d^4K}{(2\pi)^4}k^2\sum_{a=\pm}\frac{1}{K^2(K^2+ia\gamma_G^2)}=\frac{1}{4\pi^2}\sum_{a=\pm1}\int_0^\infty dk\frac{k^4\,n_B(E_a(k))}{E_a(k)(-ai\gamma_G^2)}. \quad \text{(B.10)}$$

After analytic continuation and taking the static limit i.e. $i\omega\to p_0=0$ limit, we get,

$$\text{Im}[J_3(p_0,\mathbf{p})]=-i\pi\frac{p_0}{p}\frac{1}{8T(2\pi)^2}\int dk\,k^4\sum_{a,b=\pm1}\frac{n_B(E_b(k))[1+n_B(E_b(k))]}{E_a(k)E_b(k)}. \quad \text{(B.11)}$$

Similarly for $J_2(p_0,\mathbf{p})$,

$$\text{Im}[J_2(p_0,\mathbf{p})]=-i\pi\frac{p_0}{p}\frac{i\gamma_G^2}{8T(2\pi)^2}\int dk\,k^2\sum_{a,b=\pm1}\frac{n_B(E_b(k))[1+n_B(E_b(k))]}{E_a(k)E_b(k)}. \quad \text{(B.12)}$$

B.2 Ghost loop contribution of $I^c_{\mu\mu}$ and I^c_{00}

We can express $I^c_{\mu\mu}$ as,

$$I^c_{\mu\mu}=\sum\!\!\!\!\!\!\!\int\frac{d^4K}{(2\pi)^4}\frac{K^2}{K^4(P-K)^4}$$
$$=\frac{\partial}{\partial a}\left[\int\frac{d^3k}{(2\pi)^3}\frac{1}{4E_1E_2}\Big(1-n_f(E_1)-n_f(E_2)\Big)\left(\frac{1}{i\omega-E_1-E_2}-\frac{1}{i\omega+E_1+E_2}\right)\right]$$
$$-\frac{\partial}{\partial a}\left[\int\frac{d^3k}{(2\pi)^3}\frac{1}{4E_1E_2}\Big(n_f(E_1)-n_f(E_2)\Big)\left(\frac{1}{i\omega+E_1-E_2}-\frac{1}{i\omega-E_1+E_2}\right)\right],$$
(B.13)

with $E_1=k$, $E_2=\sqrt{(p-k)^2+a}\approx\sqrt{k^2+a}-\frac{\mathbf{p}\cdot\hat{\mathbf{k}}}{\sqrt{k^2+a}}$. Here, $n_f(E_1)=\frac{1}{e^{k/T}+1}$ and employing the definition of E_2, we can express $n_f(E_2)=n_f(\sqrt{k^2+a})-\mathbf{p}\cdot\hat{\mathbf{k}}\frac{\partial}{\partial k}n_f(\sqrt{k^2+a})$.

We have,

$$I^c_{\mu\mu} = \mathcal{J}_1 + \mathcal{J}_2. \tag{B.14}$$

Employing the definition of E_1, E_2, $n_f(E_1)$, and $n_f(E_2)$ we have,

$$\begin{aligned}
\mathcal{J}_1 &= \frac{\partial}{\partial a}\Big[\int \frac{d^3k}{(2\pi)^3}\frac{1}{4E_1E_2}(-n_f(E_1)-n_f(E_2))\Big(\frac{1}{i\omega-E_1-E_2}-\frac{1}{i\omega+E_1+E_2}\Big)\Big]\\
&= \frac{\partial}{\partial a}\Big[\int dk\,\frac{4\pi k^2}{(2\pi)^3}\frac{1}{4k\sqrt{k^2+a}}\frac{2(n_f(k)+n_f(\sqrt{k^2+a}))}{k+\sqrt{k^2+a}}\Big]\\
&= -\frac{1}{4\pi^2}\int dk\,\frac{e^{k/T}k+3T(1+e^{k/T})}{4(1+e^{k/T})^3k^3T}\\
&= \frac{1}{4\pi^2}\int dk\,\Big[\frac{1}{4k^2}\frac{\partial n_f(k)}{\partial k}-\frac{3n_f(k)}{4k^3}\Big]\\
&= -\frac{1}{16\pi^2}\frac{7\zeta(3)}{8\pi^2T^2},
\end{aligned} \tag{B.15}$$

$$\begin{aligned}
\mathcal{J}_2 &= -\frac{\partial}{\partial a}\Big[\int \frac{d^3k}{(2\pi)^3}\frac{1}{4E_1E_2}(n_f(E_1)-n_f(E_2))\Big(\frac{1}{i\omega+E_1-E_2}-\frac{1}{i\omega-E_1+E_2}\Big)\Big]\\
&= -\frac{\partial}{\partial a}\int dk\,\frac{2\pi k^2}{(2\pi)^3}d(\cos\theta)\,\frac{1}{4k\sqrt{k^2+a}}\Big(n_f(k)-n_f(\sqrt{k^2+a})+p\cos\theta\frac{\partial n_f(\sqrt{k^2+a})}{\partial k}\Big)\\
&\times\Big(\frac{1}{i\omega+k-\sqrt{k^2+a}+\frac{pk\cos\theta}{\sqrt{k^2+a}}}-\frac{1}{i\omega-k+\sqrt{k^2+a}-\frac{pk\cos\theta}{\sqrt{k^2+a}}}\Big)\\
&= -\frac{\partial}{\partial a}\int\frac{dk\,d\cos\theta\,k^2}{(2\pi)^2}\frac{1}{4k\sqrt{k^2+a}}(n_f(k)-n_f(\sqrt{k^2+a}))\\
&\times\frac{\sqrt{k^2+a}}{k}\Big(\frac{1}{\frac{\sqrt{k^2+a}}{k}(i\omega+k-\sqrt{k^2+a})+p\cos\theta}-\frac{1}{\frac{\sqrt{k^2+a}}{k}(i\omega-k+\sqrt{k^2+a})-p\cos\theta}\Big)\\
&-\frac{\partial}{\partial a}\int\frac{dk\,d\cos\theta\,k^2}{(2\pi)^2}\frac{1}{4k\sqrt{k^2+a}}p\cos\theta\frac{\partial n_f(\sqrt{k^2+a})}{\partial a}\frac{\sqrt{k^2+a}}{k}\\
&\times\Big(\frac{1}{\frac{\sqrt{k^2+a}}{k}(i\omega+k-\sqrt{k^2+a})+p\cos\theta}-\frac{1}{\frac{\sqrt{k^2+a}}{k}(i\omega-k+\sqrt{k^2+a})-p\cos\theta}\Big)\\
&= -\frac{\partial}{\partial a}\Big[\int\frac{dk\,k^2}{(2\pi)^2}d\cos\theta\,\frac{n_f(k)-n_f(\sqrt{k^2+a})}{4(k^2)}\Big(\frac{1}{i\omega^1+p\cos\theta}-\frac{1}{i\omega^2-p\cos\theta}\Big)\Big]
\end{aligned}$$

$$
\begin{aligned}
&-\frac{\partial}{\partial a}\Big[\int\frac{dk\,d\cos\theta}{(2\pi)^2}\frac{k^2}{4(k^2)}\,p\cos\theta\frac{\partial n_f(\sqrt{k^2+a})}{\partial k}\Big(\frac{1}{i\omega^1+p\cos\theta}-\frac{1}{i\omega^2-p\cos\theta}\Big)\Big]\\
&\approx-\frac{\partial}{\partial a}\Big[\int\frac{d\cos\theta\,dk}{(2\pi)^2}\frac{e^{k/T}a}{8k^3T(1+e^{k/T})^2}\Big(\frac{1}{p_0+p\cos\theta}-\frac{1}{p_0-p\cos\theta}\Big)\Big]\\
&-\frac{\partial}{\partial a}\int\frac{dk\,d\cos\theta\,k^2}{(2\pi)^2}\frac{1}{4k^2}p\cos\theta\frac{\partial}{\partial k}\Big(n_f(k)-\frac{a}{2kT}n_f(k)(1-n_f(k))\Big)\\
&\times\Big(\frac{1}{p_0+p\cos\theta}-\frac{1}{p_0-p\cos\theta}+a\Big[\frac{k-p_0}{2k^2(p_0+p\cos\theta)^2}+\frac{k+p_0}{2k^2(p_0-p\cos\theta)^2}\Big]\Big)\\
&\approx 0-\frac{\partial}{\partial a}\Big[\int\frac{dk}{(2\pi)^2}k^2\frac{a}{4}\Big(-\frac{1}{k^2}\frac{\partial}{\partial k}\Big(\frac{n_f(k)(1-n_f(k))}{2kT}\Big)\Big)d(\cos\theta)\Big(\frac{1}{p_0+p\cos\theta}-\frac{1}{p_0-p\cos\theta}\Big)\Big]\\
&-\frac{\partial}{\partial a}\Big(\int\frac{dk\,k^2}{(2\pi)^2}p\cos\theta\,d(\cos\theta)\,\frac{a}{4k^2}\frac{\partial n_f(k)}{\partial k}\Big[\frac{k-p_0}{2k^2(p_0+p\cos\theta)^2}+\frac{k+p_0}{2k^2(p_0-p\cos\theta)^2}\Big]\Big).
\end{aligned}
\tag{B.16}
$$

Hence, we obtain

$$
\mathcal{J}_2=-\frac{1}{4\pi^2}\frac{7\zeta(3)}{8\pi^2T^2}\Big(\frac{p_0^2}{p_0^2-p^2}-\frac{p_0}{2p}\log\Big(\frac{p_0+p}{p_0-p}\Big)\Big). \tag{B.17}
$$

Utilizing Eq. (B.15) and Eq. (B.17) in Eq. (B.14), we obtain

$$
I^c_{\mu\mu}=-\frac{1}{16\pi^2}\frac{7\zeta(3)}{8\pi^2T^2}-\frac{1}{4\pi^2}\frac{7\zeta(3)}{8\pi^2T^2}\left(\frac{p_0^2}{p_0^2-p^2}-\frac{p_0}{2p}\log\left(\frac{p_0+p}{p_0-p}\right)\right). \tag{B.18}
$$

Now, we compute the ghost loop contribution of I_{00}. We have,

$$
\begin{aligned}
I^c_{00} &= \int\frac{d^4K}{(2\pi)^4}\frac{k_0^2}{(K^2+a)^2((P-K)^2+b)^2}\\
&= \lim_{a,b\to0}\frac{\partial^2}{\partial a\partial b}\Big(\frac{k_0^2}{(k_0^2+k^2+a)((p_0-k_0)^2+(p-k)^2+b)}\Big)\\
&= \lim_{a,b\to0}\frac{\partial^2}{\partial a\partial b}\Big(\frac{1}{(P-K)^2+b}-\frac{k^2+a}{(k_0^2+k^2+a)((p_0-k_0)^2+(p-k)^2+b)}\Big)\\
&= \lim_{a,b\to0}\frac{\partial}{\partial a}\frac{\partial}{\partial b}\int\frac{d^3K}{(2\pi)^3}\frac{k^2+a}{E_aE_b}(1-n_f(E_a)-n_f(E_b))\Big(\frac{1}{i\omega-E_a-E_b}-\frac{1}{i\omega+E_a+E_b}\Big)
\end{aligned}
$$

$$
\begin{aligned}
& -(n_f(E_a)-n_f(E_b))\Big(\frac{1}{i\omega+E_a-E_b}-\frac{1}{i\omega-E_a+E_b}\Big) \\
=\;& \mathcal{T}_1+\mathcal{T}_2. \qquad \text{(B.19)}
\end{aligned}
$$

Employing the forms $E_a=\sqrt{k^2+a}$, $E_b=\sqrt{(p-k)^2+b}\approx\sqrt{k^2+b}-\frac{pk\cos\theta}{\sqrt{k^2+b}}$, $\mathcal{T}_1$ and $\mathcal{T}_2$ can be further simplified as,

$$
\begin{aligned}
\mathcal{T}_1 &= \lim_{a,b\to 0}\frac{\partial^2}{\partial a\partial b}\left[\int\frac{d^3k}{(2\pi)^3}\frac{k^2+a}{E_aE_b}\frac{2(n_f(E_a)+n_f(E_b))}{E_a+E_b}\right] \\
&= \lim_{a,b\to 0}\frac{\partial^2}{\partial a\partial b}\int\frac{4\pi k^2\,dk}{(2\pi)^3}\frac{\sqrt{k^2+a}}{\sqrt{k^2+b}}2\frac{n_f(\sqrt{k^2+a})+n_f(\sqrt{k^2+b})}{\sqrt{k^2+a}+\sqrt{k^2+b}} \\
&= \int\frac{dk}{\pi^2}k^2\frac{e^{k/T}-T-Te^{k/T}}{8(1+e^{k/T})^2k^5T}=\int_0^\infty\frac{dk}{\pi^2}\frac{1}{8k^3}\left[k\frac{\partial n_f(k)}{\partial k}-n_f(k)\right] \\
&= -\frac{1}{8\pi^2}\frac{7\zeta(3)}{8\pi^2T^2}, \qquad \text{(B.20)}
\end{aligned}
$$

$$
\begin{aligned}
\mathcal{T}_2 &= -\lim_{a,b\to 0}\frac{\partial^2}{\partial a\partial b}\int\frac{d^3k}{(2\pi)^3}\frac{k^2+a}{\sqrt{k^2+a}\sqrt{k^2+b}}\Big(n_f(\sqrt{k^2+a})-n_f(\sqrt{k^2+b}) \\
&\qquad +p\cos\theta\frac{\partial n_f(\sqrt{k^2+b})}{\partial k}\Big) \\
&\times\Big(\frac{1}{i\omega+\sqrt{k^2+a}-\sqrt{k^2+b}+\frac{p\,k\cos\theta}{\sqrt{k^2+b}}}-\frac{1}{i\omega-\sqrt{k^2+a}+\sqrt{k^2+b}-\frac{pk\cos\theta}{\sqrt{k^2+b}}}\Big) \\
&= \mathcal{T}_{21}+\mathcal{T}_{22}, \qquad \text{(B.21)}
\end{aligned}
$$

where

$$
\begin{aligned}
\mathcal{T}_{21} &= -\lim_{a,b\to 0}\frac{\partial^2}{\partial a\partial b}\int\frac{d^3k}{(2\pi)^3}\frac{k^2+a}{\sqrt{k^2+a}\sqrt{k^2+b}}\Big(n_f(\sqrt{k^2+a})-n_f(\sqrt{k^2+b})\Big) \\
&\times\left(\frac{1}{i\omega+\sqrt{k^2+a}-\sqrt{k^2+b}+\frac{pk\cos\theta}{\sqrt{k^2+b}}}-\frac{1}{i\omega-\sqrt{k^2+a}+\sqrt{k^2+b}-\frac{pk\cos\theta}{\sqrt{k^2+b}}}\right) \\
&= \frac{1}{(2\pi)^2}\frac{1}{p_0^2-p^2}, \qquad \text{(B.22)}
\end{aligned}
$$

and

$$
\begin{aligned}
\mathcal{T}_{22} &= -\lim_{a,b\to 0}\frac{\partial^2}{\partial a\partial b}\int\frac{d^3k}{(2\pi)^3}\frac{k^2+a}{\sqrt{k^2+a}\sqrt{k^2+b}}p\cos\theta\frac{\partial n_f(\sqrt{k^2+b})}{\partial k}\\
&\times\left(\frac{1}{i\omega+\sqrt{k^2+a}-\sqrt{k^2+b}+\frac{pk\cos\theta}{\sqrt{k^2+b}}}-\frac{1}{i\omega-\sqrt{k^2+a}+\sqrt{k^2+b}-\frac{pk\cos\theta}{\sqrt{k^2+b}}}\right)\\
&\approx \frac{1}{(2\pi)^2}\frac{p^2}{(p^2-p_0^2)^2}-\frac{2}{(2\pi)^2}\frac{7\zeta(3)}{8\pi^2T^2}\left(\frac{p_0^2}{p_0^2-p^2}-\frac{p_0}{2p}\log\left(\frac{p_0+p}{p_0-p}\right)\right). \qquad \text{(B.23)}
\end{aligned}
$$

The real part contributes to the Debye mass. We also get the imaginary part from the Landau damping part,

$$
\begin{aligned}
\lim_{p_0\to 0}\mathrm{Im}[I^c_{00}(p_0,p)] &= i\frac{\pi p_0}{p}\int_0^\infty\frac{dk}{(2\pi)^2}\frac{n_F(k)}{k^3}\\
&= \frac{\pi p_0}{p}\frac{7\zeta(3)}{8\pi^2T^2}. \qquad \text{(B.24)}
\end{aligned}
$$

Hence, from Eq. (3.20) imaginary part of the self-energy from ghost loop looks like

$$
\lim_{p_0\to 0}\mathrm{Im}[\Pi^{(c)}_{00}(p_0,p)] = i\frac{\pi p_0}{p}C_A\frac{128^2\gamma_G^4}{32N_c^2g^2T^2}7\zeta(3). \qquad \text{(B.25)}
$$

B.3 Extracting the Gribov parameter

The Gribov-modified parton energy loss in the medium has a dependence on the temperature behaviour of the Gribov parameter. The Gribov approach modifies the partion function and thereby improves the Faddeev-Popov quantization procedure as,

$$
\begin{aligned}
\mathcal{Z} &= \int\mathcal{D}A\,\mathcal{D}\bar{c}\,\mathcal{D}c\,\det[-\partial\cdot A]\,\delta(\partial\cdot A)\,V(\Omega)\\
&\times\exp\left[-S_{\mathrm{YM}}-\int d^4x\,\bar{c}^a(x)\partial_\mu D^{ab}_\mu c^b(x)\right], \qquad \text{(B.26)}
\end{aligned}
$$

where c and $\bar{c}$ represent the ghost and anti-ghost fields, respectively. Here, D_μ^{ab} is the covariant derivative and $S_{\rm YM}$ denotes the Yang-Mills action. The no pole condition which prohibits the path integral over field configurations from extending beyond the Gribov horizon $\Omega = \{A : \partial \cdot A = 0, -\partial \cdot D \geq 0\}$ is enforced with the inclusion of the step function $V(\Omega)$ with the form as follows [123, 201],

$$V(\Omega) \;=\; \theta[1 - \sigma(P = 0)] = \int_{-i\infty+\epsilon}^{+i\infty+\epsilon} \frac{e^{s(1-\sigma[0])}}{2\pi i s} ds. \tag{B.27}$$

Introducing the mass parameter γ_G that minimizes the exponent of the integral Eq. (B.26) at specific value of s, one can obtain gap equation at finite temperature for Gribov mass parameter as [201],

$$g^2 \frac{(d-1)N_c}{d} \sum\!\!\!\!\!\!\!\int_P \frac{1}{P^4 + \gamma_G^4} = 1, \tag{B.28}$$

with d as the space-time dimension and Euclidean four-momentum P temporal component exhibits discrete bosonic Matsubara frequencies. In the asymptotic limit ($T \to \infty$), temperature dependence of the γ_G can be described from the gap equation as [124],

$$\gamma_G = \frac{d-1}{d} \frac{N_c}{4\sqrt{2}\pi} g^2 T. \tag{B.29}$$

It is important to emphasize that the temperature behaviour of the Gribov parameter is critically depending on the running coupling constant. The running coupling is taken as,

$$g^2(T) = \frac{48\pi^2}{11N_c - 2N_f} \frac{1}{\ln\left(\Lambda^2/\Lambda_{\overline{\rm MS}}^2\right)}, \tag{B.30}$$

where $\Lambda_{\overline{\text{MS}}}$ is extracted from the lattice estimation $\alpha_s(\Lambda = 1.5\,\text{GeV}, N_f = 3) = 0.326$ [285].
We consider $T_c = 160$ MeV for the quantitative estimations in the analysis.

BIBLIOGRAPHY

[1] T. Muta, *Foundations of Quantum Chromodynamics: An Introduction to Perturbative Methods in Gauge Theories, (3rd ed.)*, vol. 78 of *World scientific Lecture Notes in Physics*. World Scientific, Hackensack, N.J., 3rd ed., 2010.

[2] U. Mosel, *The Path Integral in Quantum Theory*. Springer Berlin, Heidelberg, 2004.

[3] F. Halzen and A. D. Martin, *QUARKS AND LEPTONS: AN INTRODUCTORY COURSE IN MODERN PARTICLE PHYSICS*. John Wiley and Sons, 1984.

[4] D. J. Gross and F. Wilczek, "Asymptotically Free Gauge Theories - I," *Phys. Rev. D* **8** (1973) 3633–3652.

[5] S. Bethke, "Experimental tests of asymptotic freedom," *Prog. Part. Nucl. Phys.* **58** (2007) 351–386, `arXiv:hep-ex/0606035`.

[6] C. Shen, Z. Qiu, H. Song, J. Bernhard, S. Bass, and U. Heinz, "The iEBE-VISHNU code package for relativistic heavy-ion collisions," *Comput. Phys. Commun.* **199** (2016) 61–85, `arXiv:1409.8164 [nucl-th]`.

[7] **PHENIX** Collaboration, N. J. Abdulameer *et al.*, "Disentangling Centrality Bias and Final-State Effects in the Production of High-pT Neutral Pions Using Direct Photon in d+Au Collisions at sNN=200 GeV," *Phys. Rev. Lett.* **134** no. 2, (2025) 022302, `arXiv:2303.12899 [nucl-ex]`.

[8] **BRAHMS** Collaboration, I. Arsene *et al.*, "Quark gluon plasma and color glass condensate at RHIC? The Perspective from the BRAHMS experiment," *Nucl. Phys. A* **757** (2005) 1–27, `arXiv:nucl-ex/0410020`.

[9] **STAR** Collaboration, J. Adams *et al.*, "Experimental and theoretical challenges in the search for the quark gluon plasma: The STAR Collaboration's critical assessment of the evidence from RHIC collisions," *Nucl. Phys. A* **757** (2005) 102–183, `arXiv:nucl-ex/0501009`.

[10] **PHENIX** Collaboration, K. Adcox *et al.*, "Formation of dense partonic matter in relativistic nucleus-nucleus collisions at RHIC: Experimental evaluation by the PHENIX collaboration," *Nucl. Phys. A* **757** (2005) 184–283, `arXiv:nucl-ex/0410003`.

[11] J. Rafelski and B. Muller, "Strangeness Production in the Quark - Gluon Plasma," *Phys. Rev. Lett.* **48** (1982) 1066. [Erratum: Phys.Rev.Lett. 56, 2334 (1986)].

[12] **NA49** Collaboration, C. Alt *et al.*, "Energy dependence of Lambda and Xi production in central Pb+Pb collisions at A-20, A-30, A-40, A-80, and A-158 GeV measured at the CERN Super Proton Synchrotron," *Phys. Rev. C* **78** (2008) 034918, `arXiv:0804.3770 [nucl-ex]`.

[13] **ALICE** Collaboration, P. Cortese *et al.*, "ALICE: Physics performance report, volume I," *J. Phys. G* **30** (2004) 1517–1763.

[14] **ALICE** Collaboration, C. W. Fabjan *et al.*, "ALICE: Physics performance report, volume II," *J. Phys. G* **32** (2006) 1295–2040.

[15] G. Aarts *et al.*, "Phase Transitions in Particle Physics: Results and Perspectives from Lattice Quantum Chromo-Dynamics," *Prog. Part. Nucl. Phys.* **133** (2023) 104070, arXiv:2301.04382 [hep-lat].

[16] S. Borsanyi, Z. Fodor, C. Hoelbling, S. D. Katz, S. Krieg, and K. K. Szabo, "Full result for the QCD equation of state with 2+1 flavors," *Phys. Lett. B* **730** (2014) 99–104, arXiv:1309.5258 [hep-lat].

[17] S. Borsanyi, G. Endrodi, Z. Fodor, S. D. Katz, and K. K. Szabo, "Precision SU(3) lattice thermodynamics for a large temperature range," *JHEP* **07** (2012) 056, arXiv:1204.6184 [hep-lat].

[18] H. Stoecker, "Collective flow signals the quark gluon plasma," *Nucl. Phys. A* **750** (2005) 121–147, arXiv:nucl-th/0406018.

[19] C. Gale, S. Jeon, B. Schenke, P. Tribedy, and R. Venugopalan, "Event-by-event anisotropic flow in heavy-ion collisions from combined Yang-Mills and viscous fluid dynamics," *Phys. Rev. Lett.* **110** no. 1, (2013) 012302, arXiv:1209.6330 [nucl-th].

[20] U. W. Heinz, "'RHIC serves the perfect fluid': Hydrodynamic flow of the QGP," in *Workshop on Extreme QCD*, pp. 3–12. 12, 2005. arXiv:nucl-th/0512051.

[21] H. Niemi, G. S. Denicol, P. Huovinen, E. Molnar, and D. H. Rischke, "Influence of the shear viscosity of the quark-gluon plasma on elliptic flow in ultrarelativistic

heavy-ion collisions," *Phys. Rev. Lett.* **106** (2011) 212302, arXiv:1101.2442 [nucl-th].

[22] C. Shen, "Studying QGP with flow: A theory overview," *Nucl. Phys. A* **1005** (2021) 121788, arXiv:2001.11858 [nucl-th].

[23] **ALICE** Collaboration, K. Aamodt *et al.*, "Higher harmonic anisotropic flow measurements of charged particles in Pb-Pb collisions at $\sqrt{s_{NN}}$=2.76 TeV," *Phys. Rev. Lett.* **107** (2011) 032301, arXiv:1105.3865 [nucl-ex].

[24] A. Majumder and M. Van Leeuwen, "The Theory and Phenomenology of Perturbative QCD Based Jet Quenching," *Prog. Part. Nucl. Phys.* **66** (2011) 41–92, arXiv:1002.2206 [hep-ph].

[25] G.-Y. Qin and X.-N. Wang, "Jet quenching in high-energy heavy-ion collisions," *Int. J. Mod. Phys. E* **24** no. 11, (2015) 1530014, arXiv:1511.00790 [hep-ph].

[26] F. D'Eramo, H. Liu, and K. Rajagopal, "Transverse Momentum Broadening and the Jet Quenching Parameter, Redux," *Phys. Rev. D* **84** (2011) 065015, arXiv:1006.1367 [hep-ph].

[27] CMS Collaboration, "CMS studies the quark–gluon plasma," https://cerncourier.com/a/cms-studies-the-quark-gluon-plasma/, Sept. 26, 2021. [Online; accessed 28-October-2025].

[28] T. Matsui and H. Satz, "J/ψ Suppression by Quark-Gluon Plasma Formation," *Phys. Lett. B* **178** (1986) 416–422.

[29] **ALICE** Collaboration, J. Adam *et al.*, "Enhanced production of multi-strange hadrons in high-multiplicity proton-proton collisions," *Nature Phys.* **13** (2017) 535–539, arXiv:1606.07424 [nucl-ex].

[30] L. D. McLerran and T. Toimela, "Photon and Dilepton Emission from the Quark - Gluon Plasma: Some General Considerations," *Phys. Rev. D* **31** (1985) 545.

[31] Y. Hidaka, S. Lin, R. D. Pisarski, and D. Satow, "Dilepton and photon production in the presence of a nontrivial Polyakov loop," *JHEP* **10** (2015) 005, arXiv:1504.01770 [hep-ph].

[32] C. Gale and K. L. Haglin, "Electromagnetic radiation from relativistic nuclear collisions," arXiv:hep-ph/0306098.

[33] P. Braun-Munzinger and J. Stachel, "The quest for the quark-gluon plasma," *Nature* **448** (2007) 302–309.

[34] **HotQCD** Collaboration, A. Bazavov *et al.*, "Equation of state in (2+1)-flavor QCD," *Phys. Rev. D* **90** (2014) 094503, arXiv:1407.6387 [hep-lat].

[35] **Wuppertal-Budapest** Collaboration, S. Borsanyi, Z. Fodor, C. Hoelbling, S. D. Katz, S. Krieg, C. Ratti, and K. K. Szabo, "Is there still any T_c mystery in lattice QCD? Results with physical masses in the continuum limit III," *JHEP* **09** (2010) 073, arXiv:1005.3508 [hep-lat].

[36] H. Caines, "The Search for Critical Behavior and Other Features of the QCD Phase Diagram – Current Status and Future Prospects," *Nucl. Phys. A* **967** (2017) 121–128.

[37] M. G. Mustafa, "An introduction to thermal field theory and some of its application," *Eur. Phys. J. ST* **232** no. 9, (2023) 1369–1457, arXiv:2207.00534 [hep-ph].

[38] N. Haque and M. G. Mustafa, "Hard Thermal Loop—Theory and applications," *Prog. Part. Nucl. Phys.* **140** (2025) 104136, arXiv:2404.08734 [hep-ph].

[39] M. Strickland, "Relativistic Quantum Field Theory, Volume 1,".

[40] M. Strickland, "Relativistic Quantum Field Theory, Volume 2,".

[41] M. Strickland, *Relativistic Quantum Field Theory, Volume 3*. IOP, 11, 2019.

[42] M. L. Bellac, *Thermal Field Theory*. Cambridge Monographs on Mathematical Physics. Cambridge University Press, 3, 2011.

[43] J. I. Kapusta and C. Gale, *Finite-temperature field theory: Principles and applications*. Cambridge Monographs on Mathematical Physics. Cambridge University Press, 2011.

[44] M. Laine and A. Vuorinen, *Basics of Thermal Field Theory*, vol. 925. Springer, 2016. arXiv:1701.01554 [hep-ph].

[45] J. I. Kapusta, "Quantum Chromodynamics at High Temperature," *Nucl. Phys. B* **148** (1979) 461–498.

[46] E. Braaten and R. D. Pisarski, "Soft Amplitudes in Hot Gauge Theories: A General Analysis," *Nucl. Phys. B* **337** (1990) 569–634.

[47] E. Braaten and R. D. Pisarski, "Deducing Hard Thermal Loops From Ward Identities," *Nucl. Phys. B* **339** (1990) 310–324.

[48] J. O. Andersen, E. Braaten, and M. Strickland, "Hard thermal loop resummation of the free energy of a hot gluon plasma," *Phys. Rev. Lett.* **83** (1999) 2139–2142, arXiv:hep-ph/9902327.

[49] J.-P. Blaizot and E. Iancu, "The Quark gluon plasma: Collective dynamics and hard thermal loops," *Phys. Rept.* **359** (2002) 355–528, arXiv:hep-ph/0101103.

[50] N. Haque, A. Bandyopadhyay, J. O. Andersen, M. G. Mustafa, M. Strickland, and N. Su, "Three-loop HTLpt thermodynamics at finite temperature and chemical potential," *JHEP* **05** (2014) 027, arXiv:1402.6907 [hep-ph].

[51] N. Haque, J. O. Andersen, M. G. Mustafa, M. Strickland, and N. Su, "Three-loop pressure and susceptibility at finite temperature and density from hard-thermal-loop perturbation theory," *Phys. Rev. D* **89** no. 6, (2014) 061701, arXiv:1309.3968 [hep-ph].

[52] P. N. Meisinger, T. R. Miller, and M. C. Ogilvie, "Phenomenological equations of state for the quark gluon plasma," *Phys. Rev. D* **65** (2002) 034009, arXiv:hep-ph/0108009.

[53] A. Dumitru, Y. Hatta, J. Lenaghan, K. Orginos, and R. D. Pisarski, "Deconfining phase transition as a matrix model of renormalized Polyakov loops," *Phys. Rev. D* **70** (2004) 034511, arXiv:hep-th/0311223.

[54] A. Dumitru, J. Lenaghan, and R. D. Pisarski, "Deconfinement in matrix models about the Gross-Witten point," *Phys. Rev. D* **71** (2005) 074004, arXiv:hep-ph/0410294.

[55] Y. Hidaka and R. D. Pisarski, "Suppression of the Shear Viscosity in a "semi" Quark Gluon Plasma," *Phys. Rev. D* **78** (2008) 071501, arXiv:0803.0453 [hep-ph].

[56] Y. Hidaka and R. D. Pisarski, "Hard thermal loops, to quadratic order, in the background of a spatial 't Hooft loop," *Phys. Rev. D* **80** no. 3, (2009) 036004, arXiv:0906.1751 [hep-ph]. [Erratum: Phys.Rev.D 102, 059902 (2020)].

[57] A. Dumitru, Y. Guo, Y. Hidaka, C. P. K. Altes, and R. D. Pisarski, "How Wide is the Transition to Deconfinement?," *Phys. Rev. D* **83** (2011) 034022, arXiv:1011.3820 [hep-ph].

[58] K. Kashiwa, R. D. Pisarski, and V. V. Skokov, "Critical endpoint for deconfinement in matrix and other effective models," *Phys. Rev. D* **85** (2012) 114029, arXiv:1205.0545 [hep-ph].

[59] A. Dumitru, Y. Guo, Y. Hidaka, C. P. K. Altes, and R. D. Pisarski, "Effective Matrix Model for Deconfinement in Pure Gauge Theories," *Phys. Rev. D* **86** (2012) 105017, arXiv:1205.0137 [hep-ph].

[60] R. D. Pisarski and V. V. Skokov, "Gross-Witten-Wadia transition in a matrix model of deconfinement," *Phys. Rev. D* **86** (2012) 081701, arXiv:1206.1329 [hep-th].

[61] V. N. Gribov, "Quantization of Nonabelian Gauge Theories," *Nucl. Phys. B* **139** (1978) 1.

[62] D. Zwanziger, "Local and Renormalizable Action From the Gribov Horizon," *Nucl. Phys. B* **323** (1989) 513–544.

[63] M. Debnath, R. Ghosh, N. Haque, Y. Hidaka, and R. D. Pisarski, "Shear and bulk viscosity for a pure glue theory using an effective matrix model," *Phys. Rev. D* **112** no. 1, (2025) 014040, arXiv:2504.20138 [hep-ph].

[64] M. Debnath, R. Ghosh, and N. Haque, "The complex heavy quarkonium potential with the Gribov–Zwanziger action," *Eur. Phys. J. C* **84** no. 3, (2024) 313, arXiv:2305.16250 [hep-ph].

[65] M. Debnath, R. Ghosh, M. Y. Jamal, M. Kurian, and J. Prakash, "Energy loss of a fast moving parton in Gribov-Zwanziger plasma," *Phys. Rev. D* **109** no. 1, (2024) L011503, arXiv:2311.16005 [hep-ph].

[66] M. Debnath, L. Thakur, and N. Haque, "Complex Heavy Quarkonium Potential in an Anisotropic Collisional Quark-Gluon Plasma," arXiv:2504.02802 [hep-ph].

[67] D. Banerjee, S. Datta, R. V. Gavai, and P. Majumdar, "Temperature dependence of the static quark diffusion coefficient," *Nucl. Phys. A* **1038** (2023) 122721, arXiv:2206.15471 [hep-ph].

[68] D. J. Gross, R. D. Pisarski, and L. G. Yaffe, "QCD and Instantons at Finite Temperature," *Rev. Mod. Phys.* **53** (1981) 43.

[69] N. Weiss, "The Effective Potential for the Order Parameter of Gauge Theories at Finite Temperature," *Phys. Rev. D* **24** (1981) 475.

[70] K. Enqvist, K. Kajantie, L. Karkkainen, and K. Rummukainen, "Constant field modes in lattice SU(3) gauge theory at large T," *Phys. Lett. B* **249** (1990) 107–113.

[71] T. Bhattacharya, A. Gocksch, C. P. Korthals Altes, and R. D. Pisarski, "Interface tension in an SU(N) gauge theory at high temperature," *Phys.Rev.Lett.* **66** (1991) 998–1000.

[72] T. Bhattacharya, A. Gocksch, C. Korthals Altes, and R. D. Pisarski, "Z(N) interface tension in a hot SU(N) gauge theory," *Nucl. Phys. B* **383** (1992) 497–524, arXiv:hep-ph/9205231.

[73] A. Gocksch and R. D. Pisarski, "Partition function for the eigenvalues of the Wilson line," *Nucl. Phys. B* **402** (1993) 657–668, arXiv:hep-ph/9302233.

[74] C. P. Korthals Altes, R. D. Pisarski, and A. Sinkovics, "The Potential for the phase of the Wilson line at nonzero quark density," *Phys. Rev. D* **61** (2000) 056007, arXiv:hep-ph/9904305.

[75] R. D. Pisarski, "Quark gluon plasma as a condensate of SU(3) Wilson lines," *Phys.Rev.* **D62** (2000) 111501, arXiv:hep-ph/0006205 [hep-ph].

[76] A. Dumitru and R. D. Pisarski, "Two point functions for SU(3) Polyakov loops near T(c)," *Phys. Rev. D* **66** (2002) 096003, arXiv:hep-ph/0204223.

[77] A. Dumitru, R. D. Pisarski, and D. Zschiesche, "Dense quarks, and the fermion sign problem, in a SU(N) matrix model," *Phys. Rev. D* **72** (2005) 065008, arXiv:hep-ph/0505256.

[78] M. Oswald and R. D. Pisarski, "Beta-functions for a SU(2) matrix model in 2 + epsilon dimensions," *Phys. Rev. D* **74** (2006) 045029, arXiv:hep-ph/0512245.

[79] R. D. Pisarski, "Effective Theory of Wilson Lines and Deconfinement," *Phys.Rev.* **D74** (2006) 121703, `arXiv:hep-ph/0608242 [hep-ph]`.

[80] R. D. Pisarski, "Scattering Amplitudes in Hot Gauge Theories," *Phys. Rev. Lett.* **63** (1989) 1129.

[81] E. Braaten and R. D. Pisarski, "Resummation and Gauge Invariance of the Gluon Damping Rate in Hot QCD," *Phys. Rev. Lett.* **64** (1990) 1338.

[82] E. Braaten and R. D. Pisarski, "Calculation of the gluon damping rate in hot QCD," *Phys. Rev. D* **42** (1990) 2156–2160.

[83] E. Braaten and R. D. Pisarski, "Simple effective Lagrangian for hard thermal loops," *Phys. Rev. D* **45** no. 6, (1992) R1827.

[84] P. F. Kelly, Q. Liu, C. Lucchesi, and C. Manuel, "Deriving the hard thermal loops of QCD from classical transport theory," *Phys. Rev. Lett.* **72** (1994) 3461–3463, `arXiv:hep-ph/9403403`.

[85] P. F. Kelly, Q. Liu, C. Lucchesi, and C. Manuel, "Classical transport theory and hard thermal loops in the quark - gluon plasma," *Phys. Rev. D* **50** (1994) 4209–4218, `arXiv:hep-ph/9406285`.

[86] Y. Hidaka and R. D. Pisarski, "Small shear viscosity in the semi quark gluon plasma," *Phys. Rev. D* **81** (2010) 076002, `arXiv:0912.0940 [hep-ph]`.

[87] Y. Hidaka and R. D. Pisarski, "Zero Point Energy of Renormalized Wilson Loops," *Phys. Rev. D* **80** (2009) 074504, `arXiv:0907.4609 [hep-ph]`.

[88] P. Bicudo, R. D. Pisarski, and E. Seel, "Matrix model for deconfinement in a SU(2) gauge theory in 2+1 dimensions," *Phys. Rev. D* **88** no. 3, (2013) 034007, arXiv:1306.2943 [hep-ph].

[89] K. Kashiwa and R. D. Pisarski, "Roberge-Weiss transition and 't Hooft loops," *Phys. Rev. D* **87** no. 9, (2013) 096009, arXiv:1301.5344 [hep-ph].

[90] S. Lin, R. D. Pisarski, and V. V. Skokov, "Collisional energy loss above the critical temperature in QCD," *Phys. Lett. B* **730** (2014) 236–242, arXiv:1312.3340 [hep-ph].

[91] S. Lin, R. D. Pisarski, and V. V. Skokov, "Zero interface tension at the deconfining phase transition for a matrix model of a $SU(\infty)$ gauge theory," *Phys. Rev. D* **87** no. 10, (2013) 105002, arXiv:1301.7432 [hep-ph].

[92] D. Smith, A. Dumitru, R. Pisarski, and L. von Smekal, "Effective potential for SU(2) Polyakov loops and Wilson loop eigenvalues," *Phys. Rev. D* **88** no. 5, (2013) 054020, arXiv:1307.6339 [hep-lat].

[93] P. Bicudo, R. D. Pisarski, and E. Seel, "Matrix model for deconfinement in a SU(Nc) gauge theory in 2+1 dimensions," *Phys. Rev. D* **89** no. 8, (2014) 085020, arXiv:1402.5137 [hep-ph].

[94] C. Gale, Y. Hidaka, S. Jeon, S. Lin, J.-F. Paquet, R. D. Pisarski, D. Satow, V. V. Skokov, and G. Vujanovic, "Production and Elliptic Flow of Dileptons and Photons in a Matrix Model of the Quark-Gluon Plasma," *Phys. Rev. Lett.* **114** (2015) 072301, arXiv:1409.4778 [hep-ph].

[95] R. D. Pisarski and V. V. Skokov, "Chiral matrix model of the semi-QGP in QCD," *Phys. Rev. D* **94** no. 3, (2016) 034015, arXiv:1604.00022 [hep-ph].

[96] C. P. Korthals Altes, H. Nishimura, R. D. Pisarski, and V. V. Skokov, "Free energy of a Holonomous Plasma," *Phys. Rev. D* **101** no. 9, (2020) 094025, arXiv:2002.00968 [hep-ph].

[97] Y. Hidaka and R. D. Pisarski, "Effective models of a semi-quark-gluon plasma," *Phys. Rev. D* **104** no. 7, (2021) 074036, arXiv:2009.03903 [hep-ph].

[98] P. B. Arnold, G. D. Moore, and L. G. Yaffe, "Transport coefficients in high temperature gauge theories. 1. Leading log results," *JHEP* **11** (2000) 001, arXiv:hep-ph/0010177.

[99] P. B. Arnold, G. D. Moore, and L. G. Yaffe, "Transport coefficients in high temperature gauge theories. 2. Beyond leading log," *JHEP* **05** (2003) 051, arXiv:hep-ph/0302165.

[100] P. B. Arnold, C. Dogan, and G. D. Moore, "The Bulk Viscosity of High-Temperature QCD," *Phys. Rev. D* **74** (2006) 085021, arXiv:hep-ph/0608012.

[101] E. Braaten and A. Nieto, "Free energy of QCD at high temperature," *Phys. Rev. D* **53** (1996) 3421–3437, arXiv:hep-ph/9510408.

[102] M. Laine and Y. Schroder, "Two-loop QCD gauge coupling at high temperatures," *JHEP* **03** (2005) 067, arXiv:hep-ph/0503061.

[103] A. Ghosh, "pdfLaTeX Bengali." 6, 2022. https://github.com/aritraghsh09/pdflatex_bengali.

[104] H. Nishimura, R. D. Pisarski, and V. V. Skokov, "Finite-temperature phase transitions of third and higher order in gauge theories at large N," *Phys. Rev.* **D97** no. 3, (2018) 036014, arXiv:1712.04465 [hep-th].

[105] C. P. Korthals Altes, H. Nishimura, R. D. Pisarski, and V. V. Skokov, "Conundrum for the free energy of a holonomous gluonic plasma at cubic order," *Phys. Lett. B* **803** (2020) 135336, arXiv:1911.10209 [hep-th].

[106] D. Gaiotto, A. Kapustin, N. Seiberg, and B. Willett, "Generalized Global Symmetries," *JHEP* **02** (2015) 172, arXiv:1412.5148 [hep-th].

[107] S. Gupta, K. Huebner, and O. Kaczmarek, "Renormalized Polyakov loops in many representations," *Phys. Rev. D* **77** (2008) 034503, arXiv:0711.2251 [hep-lat].

[108] K. Fukushima, "Chiral effective model with the Polyakov loop," *Phys. Lett. B* **591** (2004) 277–284, arXiv:hep-ph/0310121.

[109] C. Korthals-Altes, A. Kovner, and M. A. Stephanov, "Spatial 't Hooft loop, hot QCD and Z(N) domain walls," *Phys. Lett. B* **469** (1999) 205–212, arXiv:hep-ph/9909516.

[110] A. Mykkanen, M. Panero, and K. Rummukainen, "Casimir scaling and renormalization of Polyakov loops in large-N gauge theories," *JHEP* **05** (2012) 069, arXiv:1202.2762 [hep-lat].

[111] M. Caselle, A. Nada, and M. Panero, "QCD thermodynamics from lattice calculations with nonequilibrium methods: The SU(3) equation of state," *Phys. Rev. D* **98** no. 5, (2018) 054513, arXiv:1801.03110 [hep-lat].

[112] S. Datta and S. Gupta, "Continuum Thermodynamics of the GluoN_c Plasma," *Phys.Rev.* **D82** (2010) 114505, arXiv:1006.0938 [hep-lat].

[113] L. Giusti, M. Hirasawa, M. Pepe, and L. Virzì, "A precise study of the SU(3) Yang-Mills theory across the deconfinement transition," (1, 2025) , arXiv:2501.10284 [hep-lat].

[114] G. Jackson and A. Peshier, "Re-running the QCD shear viscosity," *J. Phys. G* **45** no. 9, (2018) 095001, arXiv:1711.02119 [hep-ph].

[115] J. Ghiglieri, G. D. Moore, and D. Teaney, "QCD Shear Viscosity at (almost) NLO," *JHEP* **03** (2018) 179, arXiv:1802.09535 [hep-ph].

[116] G. D. Moore, "Shear viscosity in QCD and why it's hard to calculate," in *Criticality in QCD and the Hadron Resonance Gas*. 10, 2020. arXiv:2010.15704 [hep-ph].

[117] I. Danhoni and G. D. Moore, "Hot and dense QCD shear viscosity at leading log," *JHEP* **02** (2023) 124, arXiv:2212.02325 [hep-ph].

[118] I. Danhoni and G. D. Moore, "Hot and dense QCD shear viscosity at (almost) NLO," *JHEP* **09** (2024) 075, arXiv:2408.00524 [hep-ph].

[119] N. M. MacKay, "Shear Viscosity of Collider-Produced QCD Matter I: AMY Formalism vs. A Modified Relaxation Time Approximation in 0-flavor SU(3) Theory," (7, 2024) , arXiv:2407.16856 [nucl-th].

[120] P. B. Arnold and C.-X. Zhai, "The Three loop free energy for pure gauge QCD," *Phys. Rev.* **D50** (1994) 7603–7623, arXiv:hep-ph/9408276 [hep-ph].

[121] P. B. Arnold and L. G. Yaffe, "The NonAbelian Debye screening length beyond leading order," *Phys. Rev. D* **52** (1995) 7208–7219, arXiv:hep-ph/9508280.

[122] G. Baym, H. Monien, C. J. Pethick, and D. G. Ravenhall, "Transverse Interactions and Transport in Relativistic Quark - Gluon and Electromagnetic Plasmas," *Phys. Rev. Lett.* **64** (1990) 1867–1870.

[123] K. Fukushima and N. Su, "Stabilizing perturbative Yang-Mills thermodynamics with Gribov quantization," *Phys. Rev. D* **88** (2013) 076008, arXiv:1304.8004 [hep-ph].

[124] S. Madni, A. Mukherjee, A. Bandyopadhyay, and N. Haque, "Estimation of the diffusion coefficient of heavy quarks in light of Gribov-Zwanziger action," *Phys. Lett. B* **838** (2023) 137714, arXiv:2210.03076 [hep-ph].

[125] P. Kovtun, D. T. Son, and A. O. Starinets, "Holography and hydrodynamics: Diffusion on stretched horizons," *JHEP* **10** (2003) 064, arXiv:hep-th/0309213.

[126] A. Jaiswal and N. Haque, "Covariant kinetic theory and transport coefficients for Gribov plasma," *Phys. Lett. B* **811** (2020) 135936, arXiv:2005.01303 [hep-ph].

[127] M. Luzum and P. Romatschke, "Conformal Relativistic Viscous Hydrodynamics: Applications to RHIC results at s(NN)**(1/2) = 200-GeV," *Phys. Rev. C* **78** (2008) 034915, arXiv:0804.4015 [nucl-th]. [Erratum: Phys.Rev.C 79, 039903 (2009)].

[128] J. Casalderrey-Solana, H. Liu, D. Mateos, K. Rajagopal, and U. A. Wiedemann, *Gauge/String Duality, Hot QCD and Heavy Ion Collisions*. Cambridge University Press, 2014. arXiv:1101.0618 [hep-th].

[129] C. Gale, S. Jeon, and B. Schenke, "Hydrodynamic Modeling of Heavy-Ion Collisions," *Int. J. Mod. Phys. A* **28** (2013) 1340011, arXiv:1301.5893 [nucl-th].

[130] P. Romatschke and U. Romatschke, *Relativistic Fluid Dynamics In and Out of Equilibrium*. Cambridge Monographs on Mathematical Physics. Cambridge University Press, 5, 2019. arXiv:1712.05815 [nucl-th].

[131] J. L. Nagle and W. A. Zajc, "Small System Collectivity in Relativistic Hadronic and Nuclear Collisions," *Ann. Rev. Nucl. Part. Sci.* **68** (2018) 211–235, arXiv:1801.03477 [nucl-ex].

[132] G. Policastro, D. T. Son, and A. O. Starinets, "The Shear viscosity of strongly coupled N=4 supersymmetric Yang-Mills plasma," *Phys. Rev. Lett.* **87** (2001) 081601, arXiv:hep-th/0104066.

[133] P. Kovtun, D. T. Son, and A. O. Starinets, "Viscosity in strongly interacting quantum field theories from black hole physics," *Phys. Rev. Lett.* **94** (2005) 111601, arXiv:hep-th/0405231.

[134] D. T. Son and A. O. Starinets, "Viscosity, Black Holes, and Quantum Field Theory," *Ann. Rev. Nucl. Part. Sci.* **57** (2007) 95–118, arXiv:0704.0240 [hep-th].

[135] L. Altenkort, A. M. Eller, A. Francis, O. Kaczmarek, L. Mazur, G. D. Moore, and H.-T. Shu, "Viscosity of pure-glue QCD from the lattice," *Phys. Rev. D* **108** no. 1, (2023) 014503, arXiv:2211.08230 [hep-lat].

[136] G. D. Moore and O. Saremi, "Bulk viscosity and spectral functions in QCD," *JHEP* **09** (2008) 015, arXiv:0805.4201 [hep-ph].

[137] H. B. Meyer, "Energy-momentum tensor correlators and spectral functions," *JHEP* **08** (2008) 031, arXiv:0806.3914 [hep-lat].

[138] J. Hong and D. Teaney, "Spectral densities for hot QCD plasmas in a leading log approximation," *Phys. Rev. C* **82** (2010) 044908, arXiv:1003.0699 [nucl-th].

[139] Y. Akamatsu, A. Mazeliauskas, and D. Teaney, "Bulk viscosity from hydrodynamic fluctuations with relativistic hydrokinetic theory," *Phys. Rev. C* **97** no. 2, (2018) 024902, arXiv:1708.05657 [nucl-th].

[140] Z. Xu, C. Greiner, and H. Stocker, "PQCD calculations of elliptic flow and shear viscosity at RHIC," *Phys. Rev. Lett.* **101** (2008) 082302, arXiv:0711.0961 [nucl-th].

[141] M. E. Carrington and E. Kovalchuk, "Leading order QCD shear viscosity from the three-particle irreducible effective action," *Phys. Rev. D* **80** (2009) 085013, arXiv:0906.1140 [hep-ph].

[142] J.-W. Chen, H. Dong, K. Ohnishi, and Q. Wang, "Shear Viscosity of a Gluon Plasma in Perturbative QCD," *Phys. Lett. B* **685** (2010) 277–282, arXiv:0907.2486 [nucl-th].

[143] J.-W. Chen, J. Deng, H. Dong, and Q. Wang, “Shear and bulk viscosities of a gluon plasma in perturbative QCD: Comparison of different treatments for the gg↔ggg process,” *Phys. Rev. C* **87** (2013) 024910, arXiv:1107.0522 [hep-ph].

[144] M. Bluhm, B. Kampfer, and K. Redlich, “Viscosities in the Gluon-Plasma within a Quasiparticle Model,” *Nucl. Phys. A* **830** (2009) 737C–740C, arXiv:0907.3841 [hep-ph].

[145] M. Bluhm, B. Kampfer, and K. Redlich, “Bulk and shear viscosities of the gluon plasma in a quasiparticle description,” *Phys. Rev. C* **84** (2011) 025201, arXiv:1011.5634 [hep-ph].

[146] A. Buchel, “Bulk viscosity of gauge theory plasma at strong coupling,” *Phys. Lett. B* **663** (2008) 286–289, arXiv:0708.3459 [hep-th].

[147] A. Yarom, “Notes on the bulk viscosity of holographic gauge theory plasmas,” *JHEP* **04** (2010) 024, arXiv:0912.2100 [hep-th].

[148] A. Buchel, “Violation of the holographic bulk viscosity bound,” *Phys. Rev. D* **85** (2012) 066004, arXiv:1110.0063 [hep-th].

[149] A. Buchel, U. Gursoy, and E. Kiritsis, “Holographic bulk viscosity: GPR versus EO,” *JHEP* **09** (2011) 095, arXiv:1104.2058 [hep-th].

[150] A. Rebhan and D. Steineder, “Violation of the Holographic Viscosity Bound in a Strongly Coupled Anisotropic Plasma,” *Phys. Rev. Lett.* **108** (2012) 021601, arXiv:1110.6825 [hep-th].

[151] K. Dusling and T. Schäfer, “Bulk viscosity, particle spectra and flow in heavy-ion collisions,” *Phys. Rev. C* **85** (2012) 044909, arXiv:1109.5181 [hep-ph].

[152] W. Florkowski, R. Ryblewski, N. Su, and K. Tywoniuk, "Bulk viscosity in a plasma of Gribov-Zwanziger gluons," *Acta Phys. Polon. B* **47** (2016) 1833, arXiv:1504.03176 [hep-ph].

[153] S. Madni, A. Mukherjee, A. Jaiswal, and N. Haque, "Shear and bulk viscosity of the quark-gluon plasma with Gribov gluons and quasiparticle quarks," *Phys. Rev. D* **110** no. 11, (2024) 116035, arXiv:2401.08384 [hep-ph].

[154] O. DeWolfe, "TASI Lectures on Applications of Gauge/Gravity Duality," *PoS* **TASI2017** (2018) 014, arXiv:1802.08267 [hep-th].

[155] K. A. Mamo, "Holographic RG flow of the shear viscosity to entropy density ratio in strongly coupled anisotropic plasma," *JHEP* **10** (2012) 070, arXiv:1205.1797 [hep-th].

[156] S. Cremonini, U. Gursoy, and P. Szepietowski, "On the Temperature Dependence of the Shear Viscosity and Holography," *JHEP* **08** (2012) 167, arXiv:1206.3581 [hep-th].

[157] D. Li, S. He, and M. Huang, "Temperature dependent transport coefficients in a dynamical holographic QCD model," *JHEP* **06** (2015) 046, arXiv:1411.5332 [hep-ph].

[158] S. I. Finazzo, R. Rougemont, H. Marrochio, and J. Noronha, "Hydrodynamic transport coefficients for the non-conformal quark-gluon plasma from holography," *JHEP* **02** (2015) 051, arXiv:1412.2968 [hep-ph].

[159] R. Yaresko and B. Kampfer, "Bulk viscosity of the gluon plasma in a holographic

approach," *Acta Phys. Polon. Supp.* **7** no. 1, (2014) 137–144, arXiv:1403.3581 [hep-ph].

[160] M. Attems, J. Casalderrey-Solana, D. Mateos, I. Papadimitriou, D. Santos-Oliván, C. F. Sopuerta, M. Triana, and M. Zilhão, "Thermodynamics, transport and relaxation in non-conformal theories," *JHEP* **10** (2016) 155, arXiv:1603.01254 [hep-th].

[161] K. A. Mamo, "Strongly coupled $\mathcal{N} = 4$ supersymmetric Yang-Mills plasma on the Coulomb branch. II. Transport coefficients and hard probe parameters," *Phys. Rev. D* **100** no. 6, (2019) 066011, arXiv:1610.09793 [hep-th].

[162] A. Ballon-Bayona, L. A. H. Mamani, A. S. Miranda, and V. T. Zanchin, "Effective holographic models for QCD: Thermodynamics and viscosity coefficients," *Phys. Rev. D* **104** no. 4, (2021) 046013, arXiv:2103.14188 [hep-th].

[163] P. Petreczky and H. P. Schadler, "Renormalization of the Polyakov loop with gradient flow," *Phys. Rev. D* **92** no. 9, (2015) 094517, arXiv:1509.07874 [hep-lat].

[164] A. Bazavov, N. Brambilla, H. T. Ding, P. Petreczky, H. P. Schadler, A. Vairo, and J. H. Weber, "Polyakov loop in 2+1 flavor QCD from low to high temperatures," *Phys. Rev. D* **93** no. 11, (2016) 114502, arXiv:1603.06637 [hep-lat].

[165] B. Muller, "THE PHYSICS OF THE QUARK - GLUON PLASMA," *Lect. Notes Phys.* **225** (1985) 1.

[166] H. Satz, "Quarkonium Binding and Dissociation: The Spectral Analysis of the QGP," *Nucl. Phys. A* **783** (2007) 249–260, arXiv:hep-ph/0609197.

[167] S. Datta, F. Karsch, P. Petreczky, and I. Wetzorke, "Behavior of charmonium systems after deconfinement," *Phys. Rev. D* **69** (2004) 094507, arXiv:hep-lat/0312037.

[168] H. T. Ding, A. Francis, O. Kaczmarek, F. Karsch, H. Satz, and W. Soeldner, "Charmonium properties in hot quenched lattice QCD," *Phys. Rev. D* **86** (2012) 014509, arXiv:1204.4945 [hep-lat].

[169] G. Aarts, C. Allton, S. Kim, M. P. Lombardo, M. B. Oktay, S. M. Ryan, D. K. Sinclair, and J.-I. Skullerud, "S wave bottomonium states moving in a quark-gluon plasma from lattice NRQCD," *JHEP* **03** (2013) 084, arXiv:1210.2903 [hep-lat].

[170] G. Aarts, C. Allton, S. Kim, M. P. Lombardo, S. M. Ryan, and J. I. Skullerud, "Melting of P wave bottomonium states in the quark-gluon plasma from lattice NRQCD," *JHEP* **12** (2013) 064, arXiv:1310.5467 [hep-lat].

[171] N. Brambilla, A. Pineda, J. Soto, and A. Vairo, "Effective Field Theories for Heavy Quarkonium," *Rev. Mod. Phys.* **77** (2005) 1423, arXiv:hep-ph/0410047.

[172] G. T. Bodwin, E. Braaten, and G. P. Lepage, "Rigorous QCD analysis of inclusive annihilation and production of heavy quarkonium," *Phys. Rev. D* **51** (1995) 1125–1171, arXiv:hep-ph/9407339. [Erratum: Phys.Rev.D 55, 5853 (1997)].

[173] N. Brambilla, J. Ghiglieri, A. Vairo, and P. Petreczky, "Static quark-antiquark pairs at finite temperature," *Phys. Rev. D* **78** (2008) 014017, arXiv:0804.0993 [hep-ph].

[174] W. M. Alberico, A. Beraudo, A. De Pace, and A. Molinari, "Potential models and lattice correlators for quarkonia at finite temperature," *Phys. Rev. D* **77** (2008) 017502, arXiv:0706.2846 [hep-ph].

[175] A. Mocsy, "Potential Models for Quarkonia," *Eur. Phys. J. C* **61** (2009) 705–710, arXiv:0811.0337 [hep-ph].

[176] C.-Y. Wong, "Heavy quarkonia in quark-gluon plasma," *Phys. Rev. C* **72** (2005) 034906, arXiv:hep-ph/0408020.

[177] M. Laine, O. Philipsen, P. Romatschke, and M. Tassler, "Real-time static potential in hot QCD," *JHEP* **03** (2007) 054, arXiv:hep-ph/0611300.

[178] A. Beraudo, J. P. Blaizot, and C. Ratti, "Real and imaginary-time Q anti-Q correlators in a thermal medium," *Nucl. Phys. A* **806** (2008) 312–338, arXiv:0712.4394 [nucl-th].

[179] N. Brambilla, M. A. Escobedo, J. Ghiglieri, and A. Vairo, "Thermal width and quarkonium dissociation by inelastic parton scattering," *JHEP* **05** (2013) 130, arXiv:1303.6097 [hep-ph].

[180] T. Hayata, K. Nawa, and T. Hatsuda, "Time-dependent heavy-quark potential at finite temperature from gauge-gravity duality," *Phys. Rev. D* **87** no. 10, (2013) 101901, arXiv:1211.4942 [hep-ph].

[181] J. L. Albacete, Y. V. Kovchegov, and A. Taliotis, "Heavy Quark Potential at Finite Temperature in AdS/CFT Revisited," *Phys. Rev. D* **78** (2008) 115007, arXiv:0807.4747 [hep-th].

[182] A. Rothkopf, T. Hatsuda, and S. Sasaki, "Complex Heavy-Quark Potential at Finite Temperature from Lattice QCD," *Phys. Rev. Lett.* **108** (2012) 162001, arXiv:1108.1579 [hep-lat].

[183] D. Bala and S. Datta, "Nonperturbative potential for the study of quarkonia in QGP," *Phys. Rev. D* **101** no. 3, (2020) 034507, arXiv:1909.10548 [hep-lat].

[184] R. Larsen, S. Meinel, S. Mukherjee, and P. Petreczky, "Excited bottomonia in quark-gluon plasma from lattice QCD," *Phys. Lett. B* **800** (2020) 135119, arXiv:1910.07374 [hep-lat].

[185] **HotQCD** Collaboration, D. Bala, O. Kaczmarek, R. Larsen, S. Mukherjee, G. Parkar, P. Petreczky, A. Rothkopf, and J. H. Weber, "Static quark-antiquark interactions at nonzero temperature from lattice QCD," *Phys. Rev. D* **105** no. 5, (2022) 054513, arXiv:2110.11659 [hep-lat].

[186] S. Shi, K. Zhou, J. Zhao, S. Mukherjee, and P. Zhuang, "Heavy quark potential in the quark-gluon plasma: Deep neural network meets lattice quantum chromodynamics," *Phys. Rev. D* **105** no. 1, (2022) 014017, arXiv:2105.07862 [hep-ph].

[187] N. Brambilla, M. A. Escobedo, M. Strickland, A. Vairo, P. Vander Griend, and J. H. Weber, "Bottomonium suppression in an open quantum system using the quantum trajectories method," *JHEP* **05** (2021) 136, arXiv:2012.01240 [hep-ph].

[188] Y. Akamatsu, "Quarkonium in quark–gluon plasma: Open quantum system approaches re-examined," *Prog. Part. Nucl. Phys.* **123** (2022) 103932, arXiv:2009.10559 [nucl-th].

[189] J.-P. Blaizot, D. De Boni, P. Faccioli, and G. Garberoglio, "Heavy quark bound states in a quark–gluon plasma: Dissociation and recombination," *Nucl. Phys. A* **946** (2016) 49–88, arXiv:1503.03857 [nucl-th].

[190] N. Brambilla, M. A. Escobedo, J. Soto, and A. Vairo, "Heavy quarkonium suppression in a fireball," *Phys. Rev. D* **97** no. 7, (2018) 074009, arXiv:1711.04515 [hep-ph].

[191] R. Sharma and A. Tiwari, "Quantum evolution of quarkonia with correlated and uncorrelated noise," *Phys. Rev. D* **101** no. 7, (2020) 074004, arXiv:1912.07036 [hep-ph].

[192] M. A. Escobedo and J. Soto, "Non-relativistic bound states at finite temperature (I): The Hydrogen atom," *Phys. Rev. A* **78** (2008) 032520, arXiv:0804.0691 [hep-ph].

[193] A. D. Linde, "Infrared Problem in Thermodynamics of the Yang-Mills Gas," *Phys. Lett. B* **96** (1980) 289–292.

[194] D. Zwanziger, "Equation of State of Gluon Plasma from Local Action," *Phys. Rev. D* **76** (2007) 125014, arXiv:hep-ph/0610021.

[195] V. Begun, W. Florkowski, and R. Ryblewski, "Thermodynamics and kinetics of Gribov-Zwanziger plasma with temperature dependent Gribov parameter," *Acta Phys. Polon. B* **48** (2017) 125, arXiv:1602.08308 [nucl-th].

[196] A. Bandyopadhyay, N. Haque, M. G. Mustafa, and M. Strickland, "Dilepton rate and quark number susceptibility with the Gribov action," *Phys. Rev. D* **93** no. 6, (2016) 065004, arXiv:1508.06249 [hep-ph].

[197] N. Su and K. Tywoniuk, "Massless Mode and Positivity Violation in Hot QCD," *Phys. Rev. Lett.* **114** no. 16, (2015) 161601, arXiv:1409.3203 [hep-ph].

[198] W. Wu, G. Huang, J. Zhao, and P. Zhuang, "Heavy-quark potential in Gribov-Zwanziger approach around deconfinement phase transition," arXiv:2207.05402 [hep-ph].

[199] Sumit, N. Haque, and B. K. Patra, "QCD mesonic screening masses using Gribov quantization," *Phys. Lett. B* **845** (2023) 138143, arXiv:2305.08525 [hep-ph].

[200] R. F. Sobreiro and S. P. Sorella, "Introduction to the Gribov ambiguities in Euclidean Yang-Mills theories," in *13th Jorge Andre Swieca Summer School on Particle and Fields*. 4, 2005. arXiv:hep-th/0504095.

[201] N. Vandersickel and D. Zwanziger, "The Gribov problem and QCD dynamics," *Phys. Rept.* **520** (2012) 175–251, arXiv:1202.1491 [hep-th].

[202] D. Dudal, J. A. Gracey, S. P. Sorella, N. Vandersickel, and H. Verschelde, "A Refinement of the Gribov-Zwanziger approach in the Landau gauge: Infrared propagators in harmony with the lattice results," *Phys. Rev. D* **78** (2008) 065047, arXiv:0806.4348 [hep-th].

[203] M. A. L. Capri, D. Dudal, D. Fiorentini, M. S. Guimaraes, I. F. Justo, A. D. Pereira, B. W. Mintz, L. F. Palhares, R. F. Sobreiro, and S. P. Sorella, "Local and BRST-invariant Yang-Mills theory within the Gribov horizon," *Phys. Rev. D* **94** no. 2, (2016) 025035, arXiv:1605.02610 [hep-th].

[204] E. Gotsman, Y. Ivanov, and E. Levin, "High energy evolution for Gribov-Zwanziger confinement: Solution to the equation," *Phys. Rev. D* **103** no. 9, (2021) 096017, arXiv:2012.14139 [hep-ph].

[205] I. F. Justo, A. D. Pereira, and R. F. Sobreiro, "Toward background field independence within the Gribov horizon," *Phys. Rev. D* **106** no. 2, (2022) 025015, arXiv:2206.04103 [hep-th].

[206] F. Canfora, P. Pais, and P. Salgado-Rebolledo, "Gribov gap equation at finite temperature," *Eur. Phys. J. C* **74** (2014) 2855, arXiv:1311.7074 [hep-th].

[207] D. Dudal, C. P. Felix, L. F. Palhares, F. Rondeau, and D. Vercauteren, "The BRST-invariant vacuum state of the Gribov–Zwanziger theory," *Eur. Phys. J. C* **79** no. 9, (2019) 731, arXiv:1901.11264 [hep-th].

[208] J. A. Gracey, "The One loop anti-MS static potential in the Gribov-Zwanziger Lagrangian," *JHEP* **02** (2010) 009, arXiv:0909.3411 [hep-th].

[209] M. Golterman, J. Greensite, S. Peris, and A. P. Szczepaniak, "The Gribov horizon and the one-loop color-Coulomb potential," *Phys. Rev. D* **85** (2012) 085016, arXiv:1201.4590 [hep-th].

[210] W. Lucha, F. F. Schoberl, and D. Gromes, "Bound states of quarks," *Phys. Rept.* **200** (1991) 127–240.

[211] E. Eichten, K. Gottfried, T. Kinoshita, K. D. Lane, and T.-M. Yan, "Charmonium: Comparison with Experiment," *Phys. Rev. D* **21** (1980) 203.

[212] L. Thakur, N. Haque, and H. Mishra, "Heavy quarkonium moving in hot and dense deconfined nuclear matter," *Phys. Rev. D* **95** no. 3, (2017) 036014, `arXiv:1611.04568 [hep-ph]`.

[213] D. Zwanziger, "Action From the Gribov Horizon," *Nucl. Phys. B* **321** (1989) 591–604.

[214] F. E. Canfora, D. Dudal, I. F. Justo, P. Pais, L. Rosa, and D. Vercauteren, "Effect of the Gribov horizon on the Polyakov loop and vice versa," *Eur. Phys. J. C* **75** no. 7, (2015) 326, `arXiv:1505.02287 [hep-th]`.

[215] D. Zwanziger, "Renormalizability of the critical limit of lattice gauge theory by BRS invariance," *Nucl. Phys. B* **399** (1993) 477–513.

[216] V. Agotiya, V. Chandra, and B. K. Patra, "Dissociation of quarkonium in hot QCD medium: Modification of the inter-quark potential," *Phys. Rev. C* **80** (2009) 025210, `arXiv:0808.2699 [hep-ph]`.

[217] L. Thakur, N. Haque, and Y. Hirono, "Heavy quarkonia in a bulk viscous medium," *JHEP* **06** (2020) 071, `arXiv:2004.03426 [hep-ph]`.

[218] H. van Hees, V. Greco, and R. Rapp, "Heavy-quark probes of the quark-gluon plasma at RHIC," *Phys. Rev. C* **73** (2006) 034913, `arXiv:nucl-th/0508055`.

[219] **JETSCAPE** Collaboration, S. Cao *et al.*, "Multistage Monte-Carlo simulation of jet modification in a static medium," *Phys. Rev. C* **96** no. 2, (2017) 024909, `arXiv:1705.00050 [nucl-th]`.

[220] S. K. Das, J.-e. Alam, and P. Mohanty, "Probing quark gluon plasma properties by heavy flavours," *Phys. Rev. C* **80** (2009) 054916, arXiv:0908.4194 [nucl-th].

[221] S. Cao *et al.*, "Toward the determination of heavy-quark transport coefficients in quark-gluon plasma," *Phys. Rev. C* **99** no. 5, (2019) 054907, arXiv:1809.07894 [nucl-th].

[222] T. Song, P. Moreau, Y. Xu, V. Ozvenchuk, E. Bratkovskaya, J. Aichelin, S. A. Bass, P. B. Gossiaux, and M. Nahrgang, "Traces of nonequilibrium effects, initial condition, bulk dynamics, and elementary collisions in the charm observables," *Phys. Rev. C* **101** no. 4, (2020) 044903, arXiv:2001.07951 [nucl-th].

[223] M. Singh, M. Kurian, S. Jeon, and C. Gale, "Open charm phenomenology with a multistage approach to relativistic heavy-ion collisions," *Phys. Rev. C* **108** no. 5, (2023) 054901, arXiv:2306.09514 [nucl-th].

[224] A. Dumitru, Y. Nara, B. Schenke, and M. Strickland, "Jet broadening in unstable non-Abelian plasmas," *Phys. Rev. C* **78** (2008) 024909, arXiv:0710.1223 [hep-ph].

[225] M. E. Carrington, K. Deja, and S. Mrowczynski, "Energy Loss in Unstable Quark-Gluon Plasma," *Phys. Rev. C* **92** no. 4, (2015) 044914, arXiv:1506.09082 [hep-ph].

[226] J. Prakash, M. Kurian, S. K. Das, and V. Chandra, "Heavy quark transport in an anisotropic hot QCD medium: Collisional and Radiative processes," *Phys. Rev. D* **103** no. 9, (2021) 094009, arXiv:2102.07082 [hep-ph].

[227] J. Prakash, V. Chandra, and S. K. Das, "Heavy quark radiation in an anisotropic hot QCD medium," *Phys. Rev. D* **108** no. 9, (2023) 096016, arXiv:2306.07966 [hep-ph].

[228] M. Kurian, S. K. Das, and V. Chandra, "Heavy quark dynamics in a hot magnetized QCD medium," *Phys. Rev. D* **100** no. 7, (2019) 074003, arXiv:1907.09556 [nucl-th].

[229] S. Hauksson, S. Jeon, and C. Gale, "Momentum broadening of energetic partons in an anisotropic plasma," *Phys. Rev. C* **105** no. 1, (2022) 014914, arXiv:2109.04575 [hep-ph].

[230] A. Shaikh, M. Kurian, S. K. Das, V. Chandra, S. Dash, and B. K. Nandi, "Heavy quark transport coefficients in a viscous QCD medium with collisional and radiative processes," *Phys. Rev. D* **104** no. 3, (2021) 034017, arXiv:2105.14296 [hep-ph].

[231] M. Ruggieri, Pooja, J. Prakash, and S. K. Das, "Memory effects on energy loss and diffusion of heavy quarks in the quark-gluon plasma," *Phys. Rev. D* **106** no. 3, (2022) 034032, arXiv:2203.06712 [hep-ph].

[232] M. E. Carrington, A. Czajka, and S. Mrowczynski, "Transport of hard probes through glasma," *Phys. Rev. C* **105** no. 6, (2022) 064910, arXiv:2202.00357 [nucl-th].

[233] R. Ghosh, M. Y. Jamal, and M. Kurian, "Impact of the chiral asymmetry and a magnetic field on the passage of an energetic test parton in a QCD medium," *Phys. Rev. D* **108** no. 5, (2023) 054035, arXiv:2306.10247 [hep-ph].

[234] J. Prakash and M. Y. Jamal, "Heavy quark energy loss through polarization and radiation in the hot qcd medium," *Journal of Physics G: Nuclear and Particle Physics* (2023) . http://iopscience.iop.org/article/10.1088/1361-6471/ad10c9.

[235] S. Carignano and C. Manuel, "Measuring chiral imbalance with collisional energy loss," *Phys. Rev. D* **103** no. 11, (2021) 116002, arXiv:2103.02491 [hep-ph].

[236] M. E. Carrington, S. Mrówczyński, and B. Schenke, "Momentum broadening in unstable quark-gluon plasma," *Phys. Rev. C* **95** no. 2, (2017) 024906, arXiv:1607.02359 [hep-ph].

[237] X. Dong, Y.-J. Lee, and R. Rapp, "Open Heavy-Flavor Production in Heavy-Ion Collisions," *Ann. Rev. Nucl. Part. Sci.* **69** (2019) 417–445, arXiv:1903.07709 [nucl-ex].

[238] A. Bandyopadhyay, "Electromagnetic Debye mass within Gribov-Zwanziger action," arXiv:2307.09656 [hep-ph].

[239] S. K. Wong, "Field and particle equations for the classical Yang-Mills field and particles with isotopic spin," *Nuovo Cim. A* **65** (1970) 689–694.

[240] F. Scardina, S. K. Das, V. Minissale, S. Plumari, and V. Greco, "Estimating the charm quark diffusion coefficient and thermalization time from D meson spectra at energies available at the BNL Relativistic Heavy Ion Collider and the CERN Large Hadron Collider," *Phys. Rev. C* **96** no. 4, (2017) 044905, arXiv:1707.05452 [nucl-th].

[241] G. D. Moore and D. Teaney, "How much do heavy quarks thermalize in a heavy ion collision?," *Phys. Rev. C* **71** (2005) 064904, `arXiv:hep-ph/0412346`.

[242] A. Beraudo *et al.*, "Extraction of Heavy-Flavor Transport Coefficients in QCD Matter," *Nucl. Phys. A* **979** (2018) 21–86, `arXiv:1803.03824 [nucl-th]`.

[243] S. K. Das, F. Scardina, S. Plumari, and V. Greco, "Heavy-flavor in-medium momentum evolution: Langevin versus Boltzmann approach," *Phys. Rev. C* **90** (2014) 044901, `arXiv:1312.6857 [nucl-th]`.

[244] S. Mazumder, T. Bhattacharyya, and J.-e. Alam, "Gluon bremsstrahlung by heavy quarks - its effects on transport coefficients and equilibrium distribution," *Phys. Rev. D* **89** no. 1, (2014) 014002, `arXiv:1305.6445 [nucl-th]`.

[245] D. B. Walton and J. Rafelski, "Equilibrium distribution of heavy quarks in Fokker-Planck dynamics," *Phys. Rev. Lett.* **84** (2000) 31–34, `arXiv:hep-ph/9907273`.

[246] P. Romatschke and M. Strickland, "Collective modes of an anisotropic quark gluon plasma," *Phys. Rev. D* **68** (2003) 036004, `arXiv:hep-ph/0304092`.

[247] M. Y. Jamal, S. Mitra, and V. Chandra, "Collective excitations of hot QCD medium in a quasiparticle description," *Phys. Rev. D* **95** no. 9, (2017) 094022, `arXiv:1701.06162 [nucl-th]`.

[248] M. Kurian, M. Singh, V. Chandra, S. Jeon, and C. Gale, "Charm quark dynamics in quark-gluon plasma with 3 + 1D viscous hydrodynamics," *Phys. Rev. C* **102** no. 4, (2020) 044907, `arXiv:2007.07705 [hep-ph]`.

[249] M. Cacciari, P. Nason, and R. Vogt, "QCD predictions for charm and bottom production at RHIC," *Phys. Rev. Lett.* **95** (2005) 122001, arXiv:hep-ph/0502203.

[250] M. Cacciari, S. Frixione, N. Houdeau, M. L. Mangano, P. Nason, and G. Ridolfi, "Theoretical predictions for charm and bottom production at the LHC," *JHEP* **10** (2012) 137, arXiv:1205.6344 [hep-ph].

[251] E. Eichten, K. Gottfried, T. Kinoshita, J. B. Kogut, K. D. Lane, and T.-M. Yan, "The Spectrum of Charmonium," *Phys. Rev. Lett.* **34** (1975) 369–372. [Erratum: Phys.Rev.Lett. 36, 1276 (1976)].

[252] E. Eichten, K. Gottfried, T. Kinoshita, K. D. Lane, and T.-M. Yan, "Charmonium: The Model," *Phys. Rev. D* **17** (1978) 3090. [Erratum: Phys.Rev.D 21, 313 (1980)].

[253] W. Buchmuller and S. H. H. Tye, "Quarkonia and Quantum Chromodynamics," *Phys. Rev. D* **24** (1981) 132.

[254] Y. Koma, M. Koma, and H. Wittig, "Nonperturbative determination of the QCD potential at O(1/m)," *Phys. Rev. Lett.* **97** (2006) 122003, arXiv:hep-lat/0607009.

[255] F. Karsch, D. Kharzeev, and H. Satz, "Sequential charmonium dissociation," *Phys. Lett. B* **637** (2006) 75–80, arXiv:hep-ph/0512239.

[256] **CMS** Collaboration, S. Chatrchyan *et al.*, "Indications of suppression of excited Υ states in PbPb collisions at $\sqrt{S_{NN}}$ = 2.76 TeV," *Phys. Rev. Lett.* **107** (2011) 052302, arXiv:1105.4894 [nucl-ex].

[257] **CMS** Collaboration, S. Chatrchyan *et al.*, "Observation of Sequential Upsilon Suppression in PbPb Collisions," *Phys. Rev. Lett.* **109** (2012) 222301, arXiv:1208.2826 [nucl-ex]. [Erratum: Phys.Rev.Lett. 120, 199903 (2018)].

[258] P. Romatschke and M. Strickland, "Collective modes of an anisotropic quark-gluon plasma II," *Phys. Rev. D* **70** (2004) 116006, arXiv:hep-ph/0406188.

[259] S. Mrowczynski, A. Rebhan, and M. Strickland, "Hard loop effective action for anisotropic plasmas," *Phys. Rev. D* **70** (2004) 025004, arXiv:hep-ph/0403256.

[260] S. Mrowczynski, B. Schenke, and M. Strickland, "Color instabilities in the quark–gluon plasma," *Phys. Rept.* **682** (2017) 1–97, arXiv:1603.08946 [hep-ph].

[261] P. Romatschke and A. Rebhan, "Plasma Instabilities in an Anisotropically Expanding Geometry," *Phys. Rev. Lett.* **97** (2006) 252301, arXiv:hep-ph/0605064.

[262] A. Dumitru, Y. Guo, and M. Strickland, "The Imaginary part of the static gluon propagator in an anisotropic (viscous) QCD plasma," *Phys. Rev. D* **79** (2009) 114003, arXiv:0903.4703 [hep-ph].

[263] B. Karmakar, R. Ghosh, and A. Mukherjee, "Collective modes of gluons in an anisotropic thermomagnetic medium," *Phys. Rev. D* **106** no. 11, (2022) 116006, arXiv:2204.09646 [hep-ph].

[264] A. Dumitru, Y. Guo, and M. Strickland, “The Heavy-quark potential in an anisotropic (viscous) plasma,” *Phys. Lett. B* **662** (2008) 37–42, arXiv:0711.4722 [hep-ph].

[265] Y. Burnier, M. Laine, and M. Vepsalainen, “Quarkonium dissociation in the presence of a small momentum space anisotropy,” *Phys. Lett. B* **678** (2009) 86–89, arXiv:0903.3467 [hep-ph].

[266] A. Dumitru, Y. Guo, A. Mocsy, and M. Strickland, “Quarkonium states in an anisotropic QCD plasma,” *Phys. Rev. D* **79** (2009) 054019, arXiv:0901.1998 [hep-ph].

[267] L. Thakur, N. Haque, U. Kakade, and B. K. Patra, “Dissociation of quarkonium in an anisotropic hot QCD medium,” *Phys. Rev. D* **88** no. 5, (2013) 054022, arXiv:1212.2803 [hep-ph].

[268] L. Dong, Y. Guo, A. Islam, A. Rothkopf, and M. Strickland, “The complex heavy-quark potential in an anisotropic quark-gluon plasma — Statics and dynamics,” *JHEP* **09** (2022) 200, arXiv:2205.10349 [hep-ph].

[269] R. Ghosh, A. Bandyopadhyay, I. Nilima, and S. Ghosh, “Anisotropic tomography of heavy quark dissociation by using the general propagator structure in a finite magnetic field,” *Phys. Rev. D* **106** no. 5, (2022) 054010, arXiv:2204.02312 [hep-ph].

[270] M. E. Carrington, G. Kunstatter, and A. Mukherjee, “Effect of anisotropy on the formation of heavy quarkonium bound states,” *Phys. Rev. C* **110** no. 3, (2024) 035203, arXiv:2405.05622 [hep-ph].

[271] R. Zhao, L. Qiu, Y. Guo, and M. Strickland, "Collective modes of a collisional anisotropic quark-gluon plasma," *Phys. Rev. D* **108** no. 3, (2023) 034023, arXiv:2306.12851 [hep-ph].

[272] M. E. Carrington, T. Fugleberg, D. Pickering, and M. H. Thoma, "Dielectric functions and dispersion relations of ultrarelativistic plasmas with collisions," *Can. J. Phys.* **82** (2004) 671–678, arXiv:hep-ph/0312103.

[273] B. Schenke, M. Strickland, C. Greiner, and M. H. Thoma, "A Model of the effect of collisions on QCD plasma instabilities," *Phys. Rev. D* **73** (2006) 125004, arXiv:hep-ph/0603029.

[274] A. Kumar, M. Y. Jamal, V. Chandra, and J. R. Bhatt, "Collective excitations of a hot anisotropic QCD medium with the Bhatnagar-Gross-Krook collisional kernel within an effective description," *Phys. Rev. D* **97** no. 3, (2018) 034007, arXiv:1709.01032 [nucl-th].

[275] L. Thakur, U. Kakade, and B. K. Patra, "Dissociation of Quarkonium in a Complex Potential," *Phys. Rev. D* **89** no. 9, (2014) 094020, arXiv:1401.0172 [hep-ph].

[276] M. Nopoush, Y. Guo, and M. Strickland, "The static hard-loop gluon propagator to all orders in anisotropy," *JHEP* **09** (2017) 063, arXiv:1706.08091 [hep-ph].

[277] M. E. Carrington, D.-f. Hou, and M. H. Thoma, "Equilibrium and nonequilibrium hard thermal loop resummation in the real time formalism," *Eur. Phys. J. C* **7** (1999) 347–354, arXiv:hep-ph/9708363.

[278] J. Sebastian, L. Thakur, H. Mishra, and N. Haque, "Heavy quarkonia in QGP medium in an arbitrary magnetic field," *Phys. Rev. D* **108** no. 9, (2023) 094001, arXiv:2308.04410 [hep-ph].

[279] B. Singh, L. Thakur, and H. Mishra, "Heavy quark complex potential in a strongly magnetized hot QGP medium," *Phys. Rev. D* **97** no. 9, (2018) 096011, arXiv:1711.03071 [hep-ph].

[280] J. Sebastian, M. Y. Jamal, and N. Haque, "Liénard-Wiechert potential of a heavy quarkonium moving in QGP medium," *Phys. Rev. D* **107** no. 5, (2023) 054040, arXiv:2207.08510 [hep-ph].

[281] Q. Du, A. Dumitru, Y. Guo, and M. Strickland, "Bulk viscous corrections to screening and damping in QCD at high temperatures," *JHEP* **01** (2017) 123, arXiv:1611.08379 [hep-ph].

[282] L. Thakur and Y. Hirono, "Spectral functions of heavy quarkonia in a bulk-viscous quark gluon plasma," *JHEP* **02** (2022) 207, arXiv:2111.08225 [hep-ph].

[283] X. Wang and I. Shovkovy, "Photon polarization tensor in a magnetized plasma: Absorptive part," *Phys. Rev. D* **104** no. 5, (2021) 056017, arXiv:2103.01967 [nucl-th].

[284] H. A. Weldon, "Reformulation of finite temperature dilepton production," *Phys. Rev. D* **42** (1990) 2384–2387.

[285] A. Bazavov, N. Brambilla, X. Garcia i Tormo, P. Petreczky, J. Soto, and A. Vairo, "Determination of α_s from the QCD static energy," *Phys. Rev. D* **86** (2012) 114031, arXiv:1205.6155 [hep-ph].